Improved methodologies for evaluation of severe transient conditions of sodium-cooled fast systems

Zur Erlangung des akademischen Grades

Doktor der Ingenieurwissenschaften (Dr.-Ing.)

der Fakultät für Maschinenbau

Karlsruhe Institut für Technologie

genehmigte

Dissertation

von

Alexander Ponomarev

Hauptreferent:	Prof. Dr.-Ing. Robert Stieglitz Karlsruhe Institut für Technologie
Korreferent:	Priv.-Doz. Dr. Konstantin Mikityuk Paul Scherrer Institute
Tag der Einreichung:	18.01.2017
Tag der mündlichen Prüfung:	21.03.2017

Hiermit erkläre ich, dass ich die vorliegende Arbeit selbständig angefertigt und keine anderen als die angegebenen Quellen und Hilfsmittel benutzt sowie die wörtlich und inhaltlich übernommenen Stellen als solche kenntlich gemacht und die Satzung des KIT zur Sicherung guter wissenschaftlicher Praxis in der jeweils gültigen Fassung beachtet habe.

_____ _____

/Alexander Ponomarev/

ACKNOWLEDGEMENTS

This thesis work was done during the last three years of my employment as a researcher at the Institute for Neutron Physics and Reactor Technology (INR) of the Karlsruhe Institute of Technology. I am grateful to have been a part of the INR team working on SFR safety analysis, an opportunity which advanced my knowledge and enabled me to perform this work.

First and foremost, I would like to express my gratitude to the supervisor of the thesis, Prof. Dr. Robert Stieglitz, for his outstanding support and for the detailed proofreading of this thesis.

I am sincerely thankful to Dr. Konstantin Mikityuk, co-supervisor of my work, for his strong support and for the productive technical discussions we had.

The preparation of this work would have been not possible without the continued support of my INR advisor Dr. Dankward Struwe. I appreciate greatly his availability for discussions, forthright remarks, and valuable review, which helped to carry out and structure the work.

I am also very grateful to Dr. Michael Schikorr for his extraordinary efforts to motivate and encourage me during the different stages of my work.

I would like to thank Werner Pfrang, an expert of the SAS-SFR code, whose brilliant knowledge of the code contributed greatly to the new code developments done as part of this work.

Furthermore, I express my gratitude to Dr. Victor Sanchez for his technical support during the preparation of this work and for his important remarks and proposals for structuring the thesis.

Last but not least, I would like to thank my INR colleague and former roommate Dr. Anton Travleev for the fruitful discussions we had and his valuable advice on programming issues.

ABSTRACT

The work is dedicated to the analysis and improvements of methodologies of safety evaluations of Sodium-cooled Fast Reactor (SFR) systems. In particular, the work is built around the SAS-SFR code which is primarily used for the deterministic analysis of the Initiation Phase (IP) of severe accidents in SFRs. It provides comprehensive thermal hydraulics and fuel pin mechanics simulation models for the prediction of steady state characterization of fuel pin configuration during fuel pin burnup cycle and subsequent accident transient behaviour of the entire SFR core including core material melting and relocation phenomena should the fuel pin configuration fail.

Based on existing well-validated computational tools and models for neutron physics, the work aims to improve the existing SAS-SFR capabilities by the application of advanced neutron physics simulation approaches. With regard to the modelling of the IP phenomenology, one important limitation of the currently applied SAS-SFR code is the use of the Point Kinetics (PK) model which considers fixed normalised spatial shape of the core power and neutron flux for the whole range of the simulation time. This work aims to overcome this drawback by coupled simulations and application of spatial kinetics neutron physics solution using the PARCS code, which provides spatially dependent power distributions and feedback effects, in particular, for the transient time period characterized by fuel and clad material motion. It is a first of a kind implementation of the spatial kinetics for SAS-SFR which has been practically applied for comprehensive analysis of an Unprotected Loss Of Flow (ULOF) transient of a large commercial SFR core. For the steady state core characterization, a coupled simulation with Monte Carlo neutron physics solution using the MCNP code has been evaluated additionally. Both coupled solutions employ a newly developed methodology for the transfer of the relevant thermal hydraulics core state parameters to the neutron physics evaluation tools, providing an effective basis for comparisons and analysis.

The analysis performed for the SFR core considered in the CP ESFR project and the evaluation of the respective results obtained with the developed numerical tools, demonstrated the extended capability of the improved coupled codes to describe the core behaviour under both steady state and transient conditions with great detail. In addition, the investigations contributed to better understand model limitations and to identify sources of uncertainties related to the complicated calculation routes necessary to be followed during safety evaluations of sodium cooled nuclear reactors.

Keywords: Sodium-cooled Fast Reactor (SFR), Generation IV, ESFR, SAS-SFR, PARCS, MCNP, coupled thermal-hydraulics and neutron physics simulations, Monte Carlo neutron transport, spatial kinetics, safety analysis, ULOF, Initiation Phase, fuel and clad relocation

CONTENTS

LIST OF ACRONYMS AND ABBREVIATIONS

3D	three-dimensional
ACS	Above Core Structure
BOL	Beginning Of Life
BDBA	Beyond Design Basis Accident
CDA	Core Disruptive Analysis
CEA	Comissiariat à l'énergie atomique (France)
CFD	Computational Fluid Dynamics
CG	cooling group
CR	control rod
CRDL	control rod drive line
CSD	control and shutdown device
DBA	Design Basis Accident
DHR	Decay Heat Removal
DHX	Decay Heat Exchanger
DSD	Diverse Shutdown Device
EDF	Electricité de France
EFR	European Fast Reactor
EOC	End Of Cycle
EOEC	End Of Equilibrium Cycle
ESFR	European Sodium Fast Reactor
FBR	Fast Breeder Reactor
GIF	Generation IV International Forum
GFR	Gas-cooled Fast Reactor
KIT	Karlsruhe Institute of Technology
IAEA	International Atomic Energy Agency
PK	Point Kinetics
IHX	intermediate heat exchanger
IP	Initiation Phase
IPPE	Institute of Physics and Power Engineering (Russia)
JAEA	Japan Atomic Energy Agency (Japan)
LIPOSO	direct pump-diagrid connection with pipes (LIaison POmpe-SOmmier)

LMFBR	Liquid-Metal Fast Breeder Reactor
LWR	Light Water Reactor
MA	minor actinides
MC	Monte Carlo
MOX	Mixed Oxide
PSI	Paul Scherrer Institute (Switzerland)
SFR	Sodium-cooled Fast Reactor
SG	Steam Generator
SS	steady state
TH	thermal hydraulics
TOP	Transient Over-Power
TP	Transition Phase
TPEN	Triangular Polynomial Expansion Nodal Method
TS	transient simulations
ULOF	Unprotected Loss Of Flow
ULOHS	Unprotected Loss Of Heat Sink
UTOP	Unprotected Transient Over-Power
XS	macroscopic neutron cross sections

1 NUCLEAR REACTORS AND SAFETY ASPECTS

1.1 CONTEXT OF SODIUM-COOLED FAST REACTORS AND THEIR SAFETY

The nuclear industry has worldwide accumulated a significant knowledge in physics, technology and safety resulting in more than 50 years' building and operating nuclear power plants for electricity generation safely and economically. Already in the early years of the nuclear industry development it became evident that combining different fuels, coolants and structural materials more than hundred different reactor types could be conceived, while somewhat less could be practically constructed [1]. However, only a few tens of reactor concepts have been realized, including concepts employing liquid fuel. The characteristics of the fuel consumption can be significantly influenced by varying the neutron spectrum in the core of the nuclear reactors.

Nuclear energy aims to complement other energy sources as a significant contributor to a sustainable energy supply for the next hundreds of years. To meet the target it needs to ensure the safety of its main elements, which are the power generation and the corresponding fuel cycle. The first and most important goal is to guarantee the operational safety of nuclear plants especially in case of a large-scale deployment, while secondly one needs to ensure the safety of nuclear materials and waste management and to minimize consequences to the environment, i.e. to ensure the confinement of radionuclide inventory in case of all conceivable both internal and external events. More details on the recent developments may be taken from [2].

Within this long-term perspective, nuclear energy today, having potentially a leadership among other energy technologies, is in its initial phase of application, characterized by a fuel cycle not closed as of today and a relatively low fraction of the total energy production. The worldwide nuclear power production is estimated to about 386 GW_e (about 11% of total) by the end of 2015 generated by the operation of 448 units [3]. The current balance of different reactor types in the nuclear energy system will not allow reaching the goal of sustainability, since the system is characterized by an ineffective use of natural fissile uranium and, in conjunction, an associated high radioactivity level of nuclear wastes disposal. The vast majority of about 90% of the reactor units operated are thermal reactors, which were operated in an open fuel cycle during the first 50 years of nuclear energy. Further development has always been considered as focused on both aspects i.e. an increase of safety during power generation and improvements of the fuel cycle. Accounting for the available technology and experience, only a few reactor types have been selected for further development and they are considered to have a perspective, at least for the next several tens of years. These are systems using thermal neutrons (using either light and heavy water and high-temperature gas as coolant), fast neutrons (using light and heavy metals or gas as coolant) and, probably somewhat later, even more advanced molten salt reactors (using liquid nuclear fuel), as a viable choice for a closed fuel cycle and an effective minor actinides utilization.

The current work is devoted to the first element of the nuclear energy development, in particular, to the safety evaluation of Sodium-cooled Fast Reactor (SFR) under both normal and accidental conditions. One of the main driving forces for designing this innovative reactor concept is its potential to contribute to the second element of nuclear energy production: efficiency and safety of the fuel cycle. It allows a considerable increase of an efficient use of natural nuclear fuel, which is one important target of a sustainable energy supply, and additionally aiming at minimizing the production of nuclear waste by the use of a closed fuel cycle and the capability of the transmutation of minor actinides.

The main objectives of this work were established in the framework of an evolutionary approach for the SAS-SFR code, which was developed and validated in the past decades to analyse SFRs. More in particular, the code is aiming to simulate unprotected transient reactor scenarios like an Unprotected Loss Of Flow accident (ULOF) or an unprotected transient over-power accident (UTOP), which have been identified as the most crucial safety relevant incidents occurring in a SFR. Alternatively to the conventional approaches an alternative projection has been developed considering a coupled simulation framework as basis for an improvement of steady state and transient simulations. The approach relies on an operator splitting coupling technique, in which the neutron physics solution algorithms are considered as one domain and the solution algorithms treating the thermal-hydraulics and fuel pin mechanics are in another domain. Both domains are coupled via appropriate interfaces allowing for the exchange of relevant data. The approach provides a high flexibility using different solutions techniques within the individual domains and characterized by a specific concept elaborated and realized to establish a clearly defined coupled calculation route and data transfer between the two domains.

In order to provide a powerful tool capable to handle most modern SFR designs (ideally, with minimal approximations of the real design details), a new “high-fidelity coupling” approach is proposed for simulation of SFR core steady state. In this approach, the core state parameters determined by SAS-SFR can be transferred directly to the Monte Carlo neutron transport code MCNP core model, including specific phenomena such as non-uniform pin subassembly (SA) thermal expansion. In this case the neutron physics model of MCNP supplied with appropriate neutron cross sections libraries provides significantly reduced approximations for the neutron transport solution. The advantage of such a coupled methodological approach is the capability to predict the reactivity transition between two “quasi” steady state core states (e.g. different power levels) resulting in a change of the reactivity level due to the altered reactivity feedback components (such as Doppler or core expansion) as the core parameters like power level, temperatures and material densities vary. Thereby, the newly developed tool can serve as a reference solution for evaluation of individual reactivity components and allows for comparison with other lower order neutron physics solutions or simplified approximations of the geometry representation.

The major advantage, however, is the capability to conduct transient simulations. In this context a new coupled system consisting of SAS-SFR and PARCS has been developed to depict a more realistic simulation of the initial phase of SFR severe accident scenarios by replacing the neutron physics Point Kinetics (PK) solution by the three-dimensional (3D) spatial kinetics (SK) capability of the PARCS code. Especially in the early phase of a severe

accident potentially accompanied by sodium boiling it is important to predict accurately the reactivity and core power level determined by a strongly interrelated sodium two-phase thermal-hydraulics and sodium-related neutron physics reactivity feedback. In the later phase it is important to predict the reactivity response related to material relocation phenomena (e.g. molten fuel and clad motion), where the framework of PK, strictly speaking, is not valid.

In order to account for the reactivity feedbacks caused by the transient thermal-hydraulic core state, essentially the neutron cross sections need to be modified in a SK solution. The effective macroscopic cross sections (XS) generation model, named "Sigma-zero", which is based on the background σ_0 cross section method, has been evaluated as very much appropriate to describe the different neutron physics feedback effects of a SFR. Such model has been recently implemented in the frame of the FAST code system development for the calculation option of PARCS code. The ability of the "Sigma-zero" model to derive XS for core regions with considerable changes in material content such as molten fuel and clad relocation and successful its application for some transient simulations of fast reactors in conjunction with the PARCS code has been one of the main reasons for the selection of the PARCS code to be coupled with the SAS-SFR code.

Hence, technical goals of the work are formulated within evolutionary approach for the SAS-SFR code development as follows:

1) Implementation of the coupled simulation scheme for more accurate analysis of SFR steady state using Monte Carlo code MCNP
2) Implementation of the coupled transient simulation scheme with spatial kinetics solver of the PARCS code and time-dependant "on-the-fly" cross sections generation system based on background σ_0 cross section method
3) Demonstration of the capabilities of new tools by simulating the steady state and a ULOF transient of the ESFR Reference Oxide core

Additionally, for the needs of coupling of the SAS-SFR code with neutron physics solutions, a specific data transfer approach is required and has been elaborated in this work.

1.2 REVIEW OF REACTOR ANALYSIS METHODS AND TOOLS

1.2.1 SODIUM-COOLED FAST REACTORS

Sodium cooled reactors are studied since the early fifties for potential large scale deployment. The worldwide operational experience accumulated during this time interval is more than 300 reactor-years, including experimental facilities and few industrial prototype reactors located in various countries [4]. A comprehensive overview of designs of the liquid metal cooled fast reactors (LMFR), mainly operating using sodium as coolant is given in [5].

The SFR reactor has been selected within the discussions of the Generation IV International Forum (GIF), [6] and [7], matching currently the GIF requirements in terms of safety and sustainability. The initially defined targets for the SFR development were the use of high thermal-hydraulics parameters of the reactor design, such as power density and coolant heat-up along core height, and the achievement of a high fuel burnup along with the breeding capability. This presumes development of closed uranium and thorium fuel cycles.

In the frame of this thesis, a SFR reactor type has been chosen as reference to compare the attained simulation results, for which validated data are widely and publically available. This reactor has been developed as part of the EU collaborative project (CP ESFR). The Reference Oxide core has been used in this work as a basis for study [8].

Short descriptions of the ESFR pool design reactor components, which are relevant for analysis in this work, are given hereafter. An overview of the reactor vessel and its components is given in Fig. 1. The scheme of primary, secondary and energy conversion circuits is shown in Fig. 2. The reactor vessel has a diameter of 17 m and a height of 17 m and comprises the core, three mechanical vertical shaft primary pumps connected to the strongback by short pipe connections, and six intermediate heat exchangers (IHX). The strongback is a stainless steel box-type structure, which rests on the vessel bottom and transfers the total core weight. The core is supported by a diagrid, which is mounted on the strongback and provides high thermal and mechanical stability to avoid changes in core geometry, which may cause excursions of the reactivity. The diagrid is a stainless steel cylindrical structure of about 7.5 m in diameter containing a number of vertical circular slots with triangular arrangement, which provide positioning and support of the subassemblies and allow the sodium feed from the strongback. Subassemblies are inserted with their lower thimbles in the diagrid, while their upper ends are free. An Above Core Structure (ACS) is intended for support of control rod drive mechanisms and core instrumentation and for control of the primary sodium flow distribution into the hot pool to achieve the required thermal-hydraulic conditions and quality of the sodium free surface. Six decay heat exchangers (DHX) are envisaged to ensure the decay heat removal from the core; each removes up to 50% of total residual power.

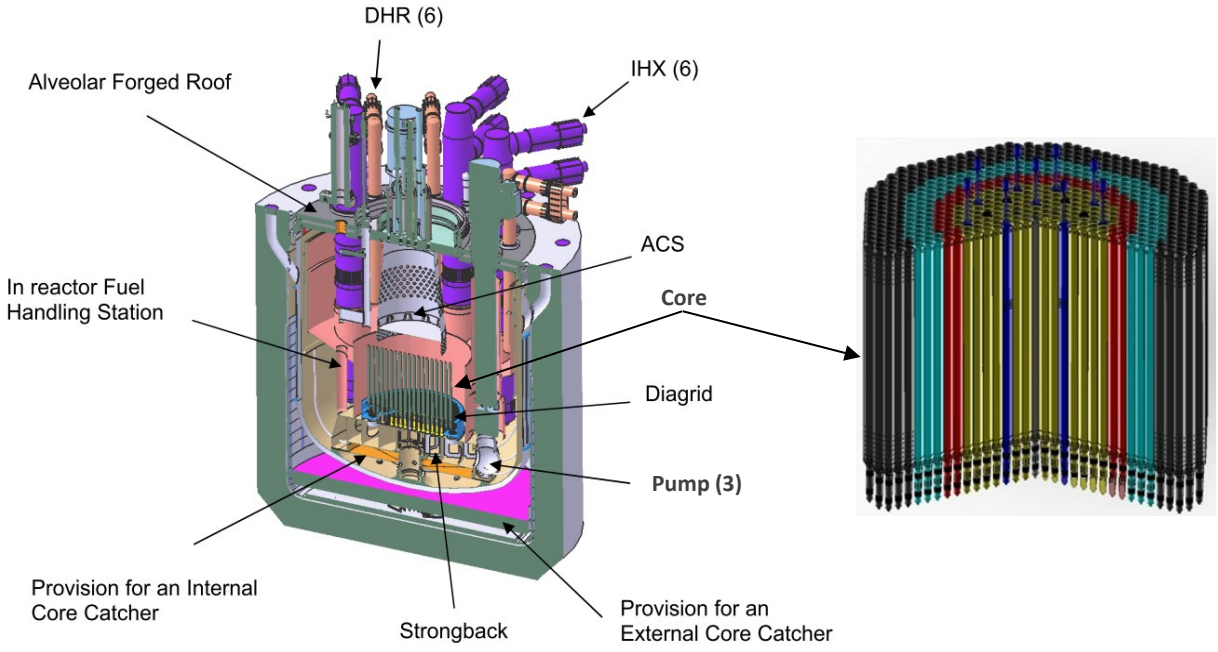

Fig. 1. Overview of ESFR reactor and its components with pool design (left) [8] and sketch of the hexagonal subassembly arrangement of the core (right)

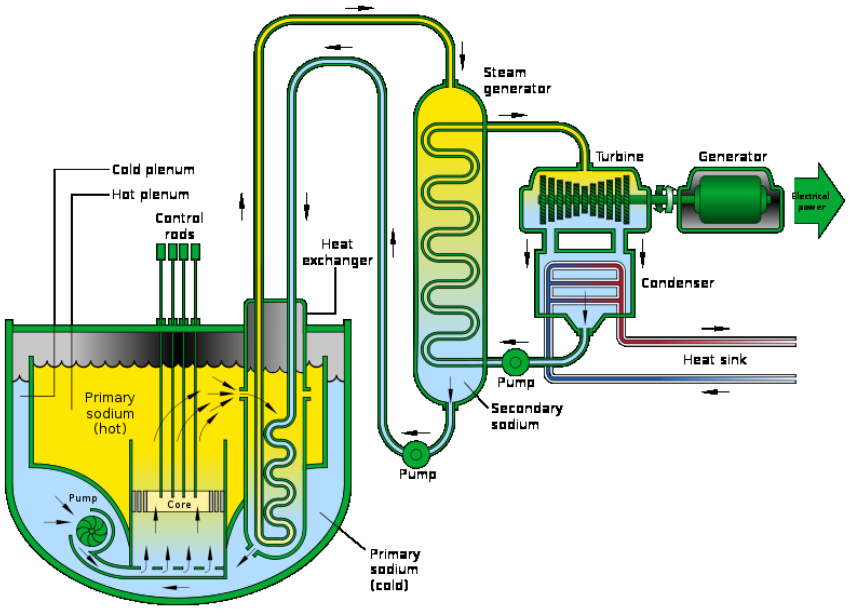

Fig. 2. Principal scheme of SFR plant primary, secondary and energy conversion circuits for pool design [6]

An overview of the SFR subassembly (SA) and its axial structure are given in Fig. 3. The SA is composed of steel shroud with hexagonal cross-section (hexcan) and lower and upper thimbles and contains fuel pin bundle with triangular pin arrangement. The pitch of the subassembly arrangement in the diagrid ensures a distance between hexcan outer flats of neighbour SAs, while marginal part of the sodium flow is directed to the inter-subassembly space. Following axial sections are typically present in the design:

- SA lower thimble, inserted in diagrid;
- Transition section from thimble to lower fuel pin support plate;
- Fuel pin bundle;
- Sodium plenum between the upper pin heads (plugs) and lower heads of the thick pins of upper neutron shielding;
- Upper neutron shielding pins; and
- Outlet section.

The fuel pin includes different axial sections, i.e. fissile height, breeder or steel blanket, lower and/or upper gas expansion plena.

The analysis conducted in the subsequent chapters is aiming to demonstrate the capabilities of the newly developed coupled neutron physics/thermal hydraulic simulation tools for safety analyses and also illustrating its limitations. As the thermal hydraulic and pin mechanics solver, the validated and widely used SAS-SFR code was selected. It provides a detailed core representation, based on parallel channels formulation, for different MOX-fuelled SFR pin and SA designs and ample representation of the primary circuit. Therefore, evaluation results related to the CP ESFR project design provide a consistent basis for comparison of different analysis options.

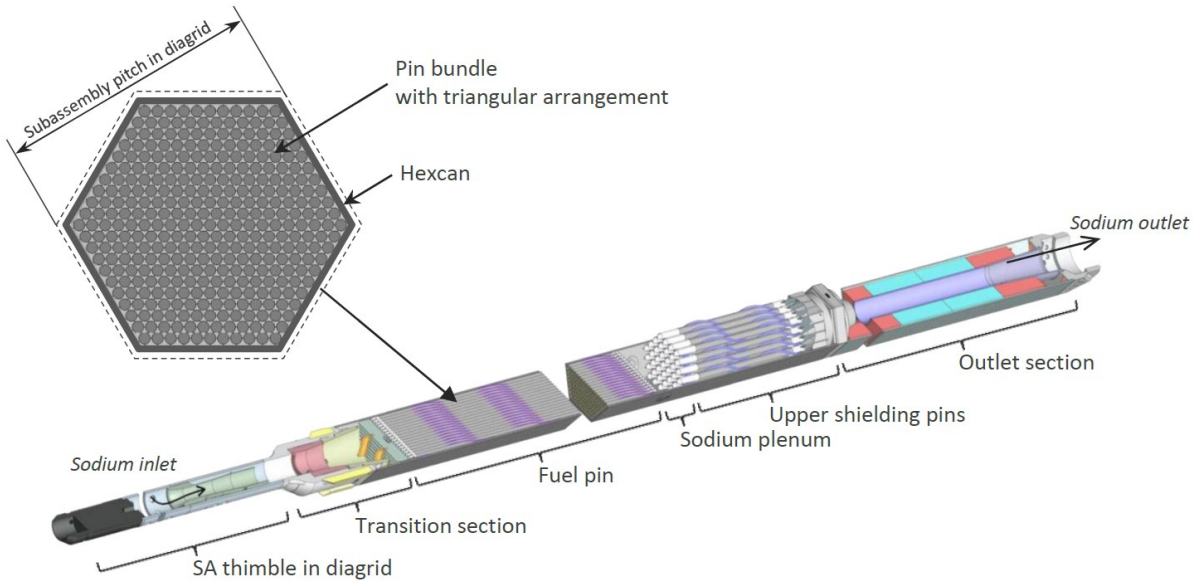

Fig. 3. Sketch of SFR subassembly design with its axial sections

1.2.2 "STATE-OF-THE-ART" OF SAFETY ANALYSIS OF SFR

Unlike conventional thermal neutron spectrum Light Water Reactor (LWR), a neutron moderation, e.g. on the light nuclides of the coolant or fuel, is relegated to undesired effects in fast reactor core, which deteriorate the nuclear fuel breeding capabilities as result of neutron spectrum softening. In reverse, increase of the number of neutrons in a high-energy part of spectrum improves the neutron multiplication and corresponding breeding capability of the system. With regard to SFR, a certain moderation of the neutrons on the light sodium nuclides at nominal operating conditions results in an increase of the multiplicative capabilities of the core at sodium voided conditions. This major neutron physics drawback of SFR systems – the positive sodium-related reactivity feedback effect – is discussed extensively in the literature.

For a large conventional SFR core design, the reactivity feedback effect is typically strongly positive in the core centre [9]. In some loss of flow transients the insertion of a strong positive reactivity may occur after sodium boiling onset and boiling front propagation towards to the core centre[1]. This in turn may lead to a strong power excursion when the net reactivity reaches a nearly prompt-critical level and core disintegration. Inherently to any SFR design, transients characterized by a considerable mismatch of power production and heat removal lead to a coolant heat-up and potentially followed by sodium voiding (such as Unprotected Transient Over-Power (UTOP) or Unprotected Loss Of Flow (ULOF) accidents). Such conditions are to

[1] Downward propagation of the lower limit of the two phase flow region is dominantly not influenced by the direction of the gravity vector, but may be driven either by the vapour pressure at the lower vapour–liquid slug interface when the local vapour pressure becomes considerably higher than the pressure at the lower end of the lower liquid slug and thus ejects the liquid slug into the downward direction, or the lower interface moves downward by the formation of new vapour bubbles in the lower liquid slug when the continuous heat-up of the lower liquid slug leads to sodium temperatures close to the upper end of the lower slug exceeding the local saturation temperature by a specified temperature difference i.e. a superheat of a few Kelvin.

be avoided as they result in sensitive transient scenarios for a large-scale SFR. Therefore, these types of transients are analysed already at the level of the conceptual SFR design phase for an initial assessment of the response of the particular design followed by a search for different design options to improve the safety characteristics of the plant.

Generally an accident scenario initiated by the above mentioned events and resulting in Core Disruptive Accident (CDA) may be partitioned into three subsequent phases according to the core disruption status: the Initiation Phase, the Transition Phase and the post-accidental core material relocation/decay heat-removal phase, [10] and [11]. The outline and progression of these phases are illustrated in Fig. 4.

- The Initiation Phase (IP) is characterized by fuel pin damages and disruption, while the SA steel shrouds (called hexcans as having an hexagonal cross-section) keep their integrity. In this phase the mismatch between power production and heat removal leads to an overheating of the pin and a melting of fuel and clad, which allows for a mobility of the core materials, in particular the axial fuel dispersion within a subassembly [12]. During this phase the thermal hydraulics and dynamic material behaviour are primarily one-dimensional, governed by the hexcan as a physical border. This in turn defines the specific features of the simulation tools used for IP. Basically, the SAS-SFR and SAS4A codes are available for modelling of this phase of the transient.

- The Transition Phase (TP) is characterized by a core-wide three-dimensional material motion and formation of molten core pool, initiated by rupture or at least melting of parts of hexcans. Hence, it requires sophisticated and detailed models of interaction and dynamic motion of core materials in a transient multiphase and multicomponent formulation. This phase of the transient is modelled by code family SIMMER-III/IV. In particular, a specific interface allows SIMMER-III/IV evaluations with the calculation geometry constructed by connecting the material distribution and core status evaluated by SAS4A/SAS-SFR for the Initiation Phase [10].

During these first two phases the main mechanism of mitigating of the core reactivity is fuel discharge out of the fissile core region, what becomes possible for disrupted and molten fuel. Further increases in power will lead to a considerable fraction of molten fuel and steel components of the core and determines then the further development of the CDA.

The safety aspects of fast reactors (FRs), in particular the consideration of Design Basis and Beyond Design Basis Accidents (DBA and BDBA) caused by internal and external events, have been reviewed in representative countries which have developed or have a plan to develop FRs in near future, especially after the Fukushima accident on March 11, 2011. These countries are improving the safety of SFRs by considering the *Defence in Depth* principles [13], [14].

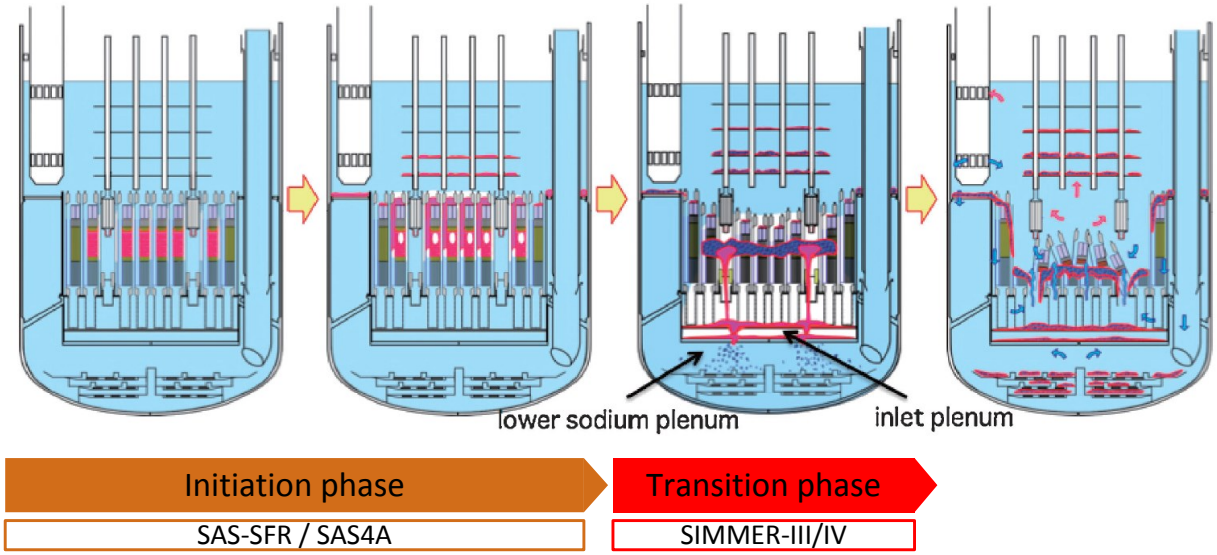

Fig. 4. Categorization of Unprotected Loss Of Flow (ULOF) accident sequence in SFR and outline of event progression, from [11]

In this work the analysis and improvements are considered for modelling of the Initiation Phase of the above mentioned SFR transients, such as ULOF and UTOP. The demonstration of improvements focuses primarily on a ULOF scenario, which has been identified as one of the most sensitive and undesired operational scenarios in terms of a potential core destruction. Its phenomenology is summarized below in more details providing a framework of the simulation modelling challenges being addressed in this work.

1.2.2.1 Overview of ULOF transient in SFR

An Unprotected Loss Of Flow (ULOF) is a transient event characterized by a combination of several failures occurring simultaneously, namely an unintended trip of the primary pumps followed by a failure of reactor shutdown via the insertion of the control and/or shutdown rods. This sequence of events could be initiated, for example, in case of a loss of offsite power event.

The initiating event frequency of an unintended pumps trip is judged to be relatively high, namely in the range between 0.08 and 0.3 times per year. The probability of a reactor trip failure on demand on other hand is judged to be extremely low, namely around 10^{-7} per demand due to two largely independent reactor shutdown systems, implying that the

combined frequency of a ULOF initiator event is judged to be very unlikely and of the order of less than 10^{-8} per year [15].

The ULOF event is essentially characterized by a mismatch between the production of nuclear power and removal of the heating power from the reactor core region by a convective fluid flow, which experiences a transition from forced convective flow to mixed or even natural convection only. Tripping the primary pumps will lead to a continuous decrease of the coolant mass flow rate through the reactor core during the coast-down phase, until the natural convection process takes over. Hence, a limited fraction of the nominal coolant mass flow rate is provided, in which density driven buoyancy forces are balanced by the friction forces in the coolant flow paths. Those friction forces are largely determined by the chosen design and layout characteristics of the primary system. During the flow coast-down transient, the power level should favourably decrease proportional to the decrease of the coolant mass flow rate to prevent a serious mismatch between power produced and heat removed from the core region and to keep the temperatures of the fuel and structures within sustainable limits. However, the coolant mass flow rate during a ULOF decreases usually faster than the power level, leading to a temperature rise of the core materials.

In case the power level does not decrease proportional to the reduction of the coolant flowrate, this will then lead to a rise of the temperature difference across the core $\Delta T_{core} = T_{outlet} - T_{inlet}$ (according to $P = w \cdot c_p \cdot \Delta T_{core}$). As coolant mass flow rate w decreases, ΔT_{core} must therefore increase for a constant power level P. The sensitive parameter that is mostly impacted first by the ULOF is the coolant core outlet temperature T_{outlet} as the core coolant inlet temperature T_{inlet} remains largely unchanged during the initial phase of the pump coast-down process. In large Sodium-cooled Fast Reactor of the 3000 MW_{th} class, extensive boiling of sodium ($T_{boil} \sim$ 880°C at 1 bar, and 937°C at 1.57 bars) in the central core region will most likely insert a significant positive reactivity in excess of the order of one dollar, leading potentially to a power excursion. Conditions that could lead to boiling of sodium in the central core region are thus to be avoided under all conceivable internal and external events in large SFRs [15].

A local pin clad dry-out in case of intensive boiling leads to quick overheating of pin clad and fuel. Local melting processes may occur potentially followed by pin failures, which are realized by different scenarios, depending on the individual pin power and on fuel burnup conditions.

Once the pin structural integrity is lost, fuel and clad material motion strongly influences the core neutron physics. This is expressed by reactivity feedbacks acting on the very small time scales of the material motion dynamics. Typically prior to the moment of materials relocation onset the reactivity of the core increases enormously (up to 50 \$/s) mainly driven by the sodium void reactivity. The material relocation starts at a nearly prompt-critical core configuration depending on the particular core conditions, and results in an insertion of a negative reactivity exceeding 1 \$ within a very short period of time (below 0.1 s), due to fuel ejection out of the fissile core region. Within this phase – Initiation Phase – these material melting and relocation phenomena are considered to occur localized at pin and subassembly level, what allows to study this phenomena confined to the subassembly hexcan physical boundaries.

In case a further core heat-up occurs, the hexcan of the subassembly may fail either by a rupture or melting. Then a three-dimensional core material motion phase starts, which is termed to as Transition Phase.

1.2.2.2 SIMULATION TOOLS FOR ULOF TRANSIENT

There is a large variety of simulation tools available for the transient analysis of the postulated incidents and/or accidents in SFRs. In recent EU collaborative projects on ESFR [8] and ASTRID [16] core physics analysis a number of codes (SAS4A [17], SAS-SFR [18], CATHARE [19], RELAP5 [20], TRACE [21], FAST [22], SIM-SFR [23], MAT4-DYN [24], SPECTRA [25]) have been successfully used to evaluate the transient core behaviour for pre-boiling conditions phase. Some of the codes, which were originally developed for LWR, have been adapted recently capable to depict sodium as coolant. This scopes also the modelling of two-phase sodium boiling (for instance, FAST [26]). A comprehensive presentation and review of capabilities of the codes available for modelling of pre-boiling conditions is given in [27].

For the Initiation Phase (IP), the number of rigorously validated codes available is rather sparse. The most noteworthy development has been initiated by ANL (USA) in the 1960's and 70's, developing the SAS-family codes; this resulted in 1988 in the SAS4A code [17]. The code SAS-SFR used in this work has been developed on the basis of the SAS4A code in close cooperation between KIT, JAEA, IRSN and CEA [18]. Currently the project JASMIN [28] is ongoing with the objective to develop a new European simulation code, ASTEC-Na [29], with improved physical models, accounting for results of recent LWR research, with modern software architecture and high flexibility to account for innovative SFR designs.

For the simulation of the Transition Phase (TP) the SIMMER code family was developed [30] and [31]. Late applications of the code include stand-alone simulation for both IP and TP, as well as the simulation of TP based on the core state provided by the SAS-SFR code at the time of hexcan failure onset [32].

The Russian multi-physics code UNICO [33] is designed to analyse in detail the temperature and velocity fields in a fast reactor core under transient conditions. The code is meant to make 3D coupled computation of neutron physics, thermal-hydraulic and thermal-mechanic characteristics to the accuracy of each individual core fuel assembly. The COREMELT-2D code is developed for the simulation of severe accidents of BN-type SFRs. The code is composed of two coupled modules, namely a two-dimensional dynamic thermal hydraulics module COREMELT and a 3D dynamic neutron physics module RADAR [34].

1.3 SAS-SFR CODE OVERVIEW

The SAS-SFR code is a deterministic code for the analysis of the initial steady state core conditions and severe accident transient conditions of SFRs e.g. caused by a protected or an unprotected loss of coolant flow or reactivity insertions. The current code version is a product of a long-term international cooperation over more than 30 years between scientists from KIT (FZK), CEA, IRSN (IPSN) and JAEA (PNC) [18]. The development of SAS-SFR

has been initiated in the late eighties on basis of the SAS4A code [17] while in the meantime existing models were extended as well as new ones have been introduced. In parallel to the model development the SAS-SFR code has been extensively qualified based on a wide range of experimental data. Additional code qualification was performed in the frame of international benchmarks and by means of code-to-code comparisons. The experimental test programmes covered a wide range of pin designs and test conditions, in particular, pre-irradiation fuel conditions from 0 to 12 at% fuel burn-up, solid and hollow fuel pellets pin designs, transient power insertion with different power ramps either leaving the test pins intact or initiating different types of fuel and clad melting phenomena. Intensive work for model improvement has been conducted for SAS-SFR on basis of the experimental data from the CABRI programs [35]-[39].

1.3.1 SAS-SFR MODELS

The SAS-SFR code provides a multi-channel core thermal-hydraulics treatment, in which each channel represents a number of subassemblies (SAs) with similar thermal hydraulic properties, pin mechanics conditions as well as reactivity feedbacks.

A channel represents the whole length of the subassembly, from coolant inlet to coolant outlet. A number of axial zones are used, as indicated in Fig. 5. One zone represents the fuel pin section, which includes the fissile core height, axial blankets, and gas plenums. Other zones represent so-called reflector regions above and below the pin section which may have different geometry and sodium flow cross-sections in accord to given SA design, e.g. a SA specific sodium plenum and upper neutron shielding sections. The pin section is treated separately in considerably more detail than reflector zones. It is represented by a single fuel pin, its associated coolant flow cross-section and inventory and the respective fraction of the subassembly wrapper (hexcan). Wire wraps or grid spacers are volumetrically considered as lumped into the clad or hexcan steel fraction. The transient behavior of the inter-wrapper sodium is not evaluated explicitly[2].

An appropriate number of channels should be selected to represent the different power levels, coolant flow rates, burn-up levels and operational power history of the core SAs conditions in different positions across the core cross section. A channel can also represent blanket or control subassemblies. Different number of channels – from a few to a few hundred – can be employed to depict the core depending on the design details and/or the desired resolution. In typical applications the core is represented by 10-30 channels to allow for a reasonably accurate prediction of the transient behaviour and its phenomenology [40].

SAS-SFR contains a large variety of models to simulate the steady state and transient thermal-hydraulic and fuel pin mechanical effects and to compute the fuel, cladding and coolant temperatures, coolant boiling, a cladding failure, fuel and cladding melting and their

[2] It would need to simulate transiently in three dimensions the inter-relation of the inter-wrapper sodium for all core subassemblies and their flow connections to the upper and lower sodium pools within the reactor vessel. With the objective of a conservative approach with regard to the reactivity feedback effect of the transient heat-up of the inter-wrapper sodium it is therefore assumed that the inter-wrapper sodium contribution to the reactivity feedback follows the one of the sodium within the subassembly hexcan without time delay. The associated reactivity feedback contribution is defined by multiplication coefficient to node sodium material worth value, given in the input.

relocation. Some of the specific models and approaches integrated in SAS-SFR are briefly presented below.

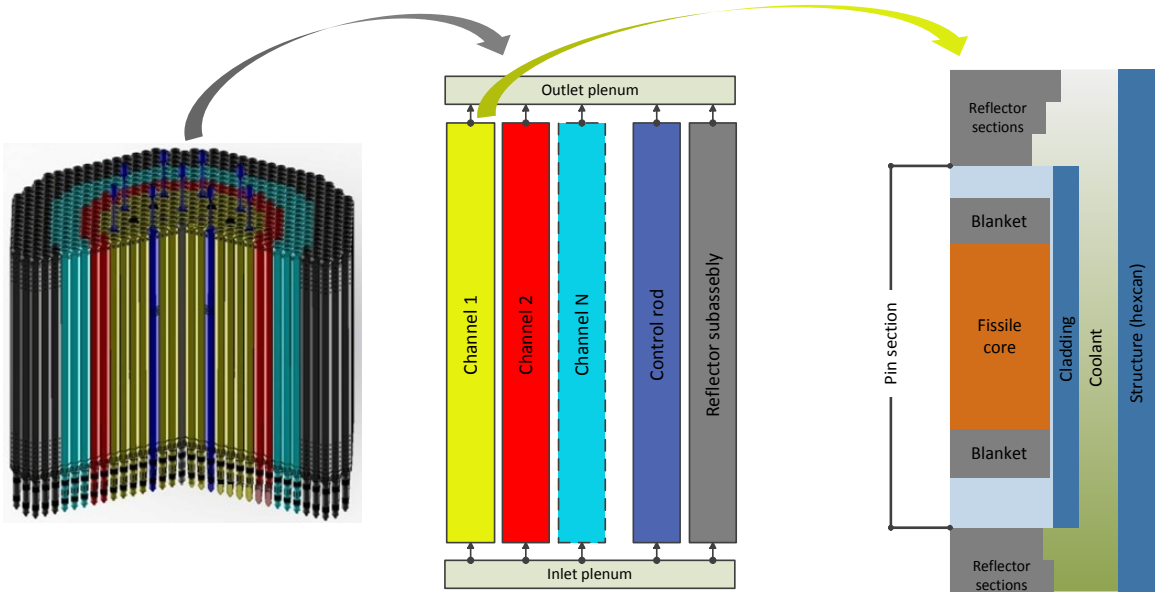

Fig. 5. Channel approach representation of the SFR core (left and centre) and sketch of the axial sectioning structure of one core channel in the SAS-SFR code (right)

The primary circuit model (PRIMAR-4) is intended to model relatively fast transients (ULOF, UTOP) and provides all necessary options for the description of the primary and intermediate circuit conditions: coolant and fission gas temperatures and pressures, coolant flow rates and component temperatures.

A simplified approach (such as a look-up table) or a detailed modelling of the IHX tube and shell side geometries and heat transfer can be applied as boundary condition for the heat sink during transient calculations to solve the momentum, energy and mass conservation equations. In Fig. 6 the example of split-up of the coolant primary loop into blocks as it has been used for simulation of a ULOF of the ESFR core is shown. Each block demands as input a specification of its geometry and its position in the pool vessel. Therein, each component is described by its masses and volumes of steel and of sodium and its thermal characteristics (values for density ρ and specific heat c_p)[3]. Liquid flow elements are characterized by incompressible single-phase flow, with the possible exception of the core element. The hydraulic equations for the primary and intermediate heat-transport loops are solved by a semi-implicit or fully implicit time differencing scheme in which the pressures and flows for all connected compressible volumes and segments are solved simultaneously. This is a rather simplified representation of the primary circuit but appears sufficient for the purpose of considering transient responses of the primary circuit in case of a ULOF accident with a coolant mass flow halving time constant of 5 up to about 50 s.

[3] Pressure drop calculations use user specified Reynolds number dependent correlations for forced convection flow and laminar flow conditions. A similar discrimination is done for heat transfer correlations mainly dependent from the Péclet number.

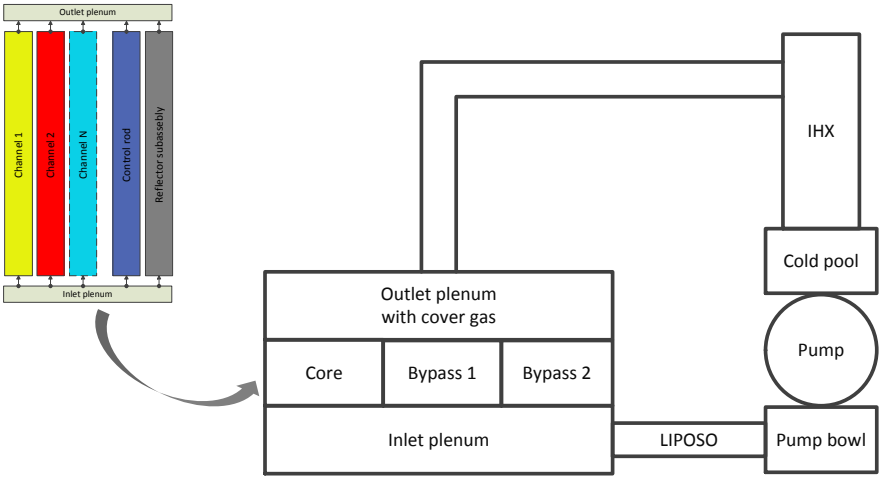

Fig. 6. The scheme of the primary circuit model of a pool configuration SFR in the PRIMAR-4 model of SAS-SFR

The axial and radial dimensions of pin elements are calculated individually for every axial node in each channel depending on the SA power and its axial profile and cooling conditions during both nominal operating and transient conditions. One key issue for steady state and transient simulations is the well-validated fuel pin mechanics model, which is of importance for an accurate prediction of the materials content of an axial node of a SA unit cell with appropriate assumptions what is relevant for establishing of a consistent neutron physics model.

Fuel pin heat transfer model integrated in the SAS-SFR code uses the URGAP model to calculate the gap heat transfer coefficient. Fuel pin behaviour model DEFORM-IVC predicts the fuel-pin characterization at both pre-irradiation phase and transient conditions. In particular, the outer radii of the fuel pin are obtained by the fuel pin behaviour model. In this model the fuel-pin phenomenology is described and it covers:

- grain growth dependent on fuel temperature;
- pore migration and restructuring;
- O/M ratio redistribution;
- solid fission product and fission gas induced fuel swelling;
- fuel pellet cracking and crack healing;
- fission gas release;
- porosity-dependent fuel thermal conductivity calculation;
- irradiation-induced cladding swelling and
- fuel pin expansion.

Before onset of sodium boiling, the coolant is treated as incompressible. The basic momentum conservation equation is solved for the coolant flow rate using a finite difference method. To decrease computational costs and allow a large heat transfer time step, the coolant temperatures are computed implicitly by the fuel-pin heat transfer model in non-voided conditions, thereby fuel, clad, coolant and structure temperatures at an axial node are computed simultaneously [53]. A switch to the boiling module is made before the formation of the first bubble. The two-phase flow conditions are simulated in SAS-SFR on basis of a

multi-bubble slug ejection model. From that moment on, coolant temperatures calculation is explicitly coupled to the fuel-pin heat transfer calculation in a forward marching technique[4].

Once fuel melting has begun, the subsequent formation of the molten cavity is modelled and DEFORM-IVC calculates the molten cavity pressure. A fuel-pin failure can be initiated once a certain criterion or set of criteria are exceeded, which are the melt fraction, the fuel temperature, the molten cavity pressure or dedicated cladding stress/strain conditions. After fuel-pin breakup the multi-component, multi-phase post fuel-pin failure model describes fuel and clad relocation. Two different models are present in SAS-SFR to be selected dependent on the coolant channel state. The PLUTO-2 model is used for non-voided fuel motion and the LEVITATE model describes the failure at voided conditions.

A Point Kinetics (PK) model employed in SAS-SFR uses the net reactivity value calculated as the sum of the following components:

- Doppler reactivity;
- coolant density and void reactivity;
- axial core expansion reactivity;
- radial core expansion (or diagrid expansion) reactivity;
- control rod drive lines expansion reactivity;
- scram/control rods reactivity;
- fuel and clad motion/relocation reactivity; and
- user programmed external reactivity.

The material worth map approach is employed to calculate the expansion and density effects in the core, such as fuel and clad expansion and sodium heat-up and boiling. Every component is calculated as a sum through all calculation nodes, derived on the basis of the actual mass of material component in the node and the worth map as updated in accordance with the axial core expansion. The Doppler reactivity is calculated in a similar way on the basis of the Doppler constant and its normalised spatial distribution given by input. The rest components are defined on the basis of coefficients corresponding to a core state parameter, characterising e.g. the control rod drive lines expansion or the diagrid expansion effect. An example of material reactivity worth coefficients for fuel and sodium is illustrated in Fig. 7, which has been calculated for the ESFR “Reference Oxide” core [41].

The worth value for fuel and clad in the first node above the fissile height is mandatory in SAS-SFR for the correct prediction of pin expansion reactivity and required by the worth map approach. With regard to fuel relocation the described material worth map may scope all nodes of the pin section below and above the fissile height. The associated fuel motion

[4] Boiling onset is defined when somewhere along the coolant channel height the sodium temperature exceeds the pressure dependent local saturation temperature by a user-specified superheat of typically 1 to 3 K. When the onset condition is met a vapour bubble of finite axial extension is assumed to be formed covering the whole coolant flow cross-section but leaving a liquid film of a user specified thickness on clad and structure surfaces. Thus the geometry conditions for heat transfer and pressure drop in the bubble region are defined. On basis of the pressure boundary conditions for the liquid slugs above and below the vapour bubble movements of the liquid slugs are determined and heat-transfer to the liquid slugs and the vapour bubble calculated. When the heat-up in the liquid slugs leads to sodium temperatures again exceeding the local saturation temperatures by a pre-specified super-heat at a pre-specified small distance from the slug interfaces another vapour bubble is formed. Thus the boiling model is a quasi-1D representation of two phase flow conditions in a sodium environment.

reactivity is derived as result of cumulative fuel reactivity along the map incorporating the fuel reactivity response of fuel, relocated outside the fissile core. As shown in the map of Fig. 7, the positive values are considered for two axial nodes above the fissile height, and thus the relocation of some fuel mass to this region contribute with positive value to the fuel motion reactivity component. Since the fuel and clad relocation may cause a considerable distortion of the neutron flux altering the power generation spatial distribution, the use of a PK model and one set of pre-calculated reactivity worth maps for the transient phase of material relocation may lead to doubtful results of motion-related reactivity feedback effects and thereby to non-conservative predictions of the core behaviour and of the sequence of transient phenomena.

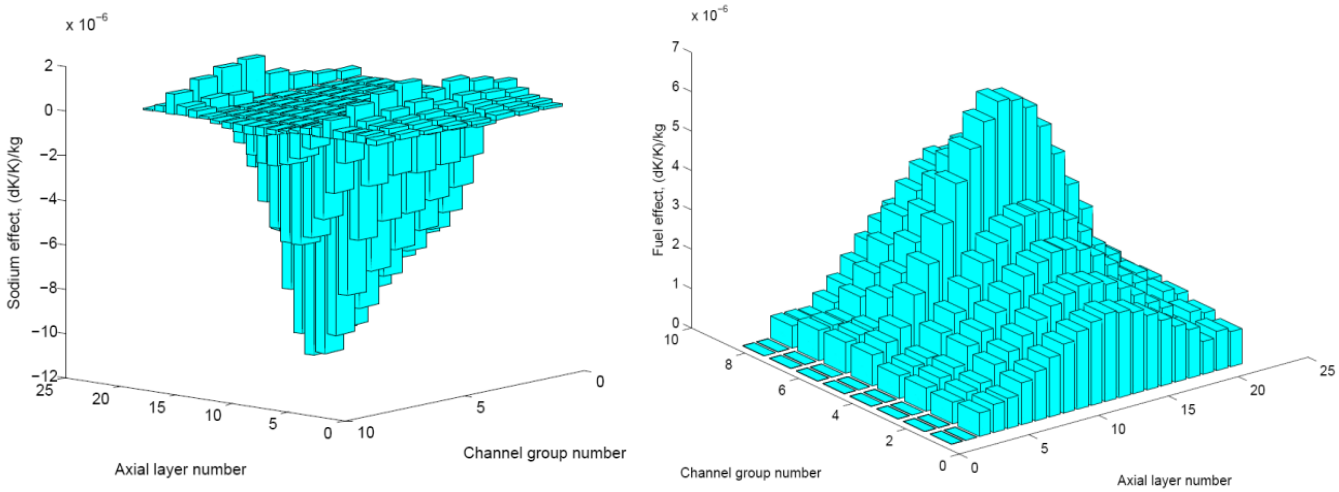

Fig. 7. Computed spatial distribution of the material worth reactivity coefficient for sodium (left) and fuel (right) as calculated for the ESFR "Reference Oxide" core, from [41]

1.3.2 LATEST SAS-SFR IMPROVEMENTS FOR SIMULATION OF INNOVATIVE SFR DESIGNS

Recent investigations with the SAS-SFR code performed for innovative SFR designs revealed significant drawbacks of the pre-calculated worth map approach to evaluate the sodium-related reactivity component adequately, [43]. Those innovative designs are essentially characterized by the introduction of a large sodium plenum axial section of the SA above the fissile core height to mitigate a positive sodium-related reactivity of the fissile core.

The concept of a so-called "sodium plenum" above the fissile core has been proposed already more than 20 years ago by IPPE (Obninsk, Russia) for the BN type reactor designs of a SFR [44]. A SA-specific sodium plenum is foreseen in the upper region of the core above the pin section by a hexcan shroud filled with sodium. In case of a transient associated with boiling, immediately after the boiling onset occurring at top of the fissile height, the sodium steam bubbles can propagate quickly upwards above the pin section into the sodium plenum. In terms of reactor neutron physics this causes an insertion of a considerable negative reactivity (of up to -2 $ depending on the individual design). Physically this negative value

originates from an enhanced axial neutron leakage towards the top of the core and increase of neutron absorption in the upper shielding. Before voiding, the temperature related variations of the sodium density in the upper regions of the core provide a rather limited negative response due to density variation, thus a strong non-linearity on sodium mass variation is observed for these upper regions.

In SAS-SFR the sodium reactivity effect is derived as a linear dependence on the sodium mass variation. Thus for the upper regions an application of the material worth map, obtained with the use of the density variation as a type of perturbation, lead to an underestimation of the plenum voiding "efficiency", while for the map, based on voiding, the plenum "efficiency" is overestimated noticeably at pre-boiling conditions. The latter leads to a non-conservative estimation of the grace time to boiling onset, as it has been clearly demonstrated in [43] for an innovative "low-void" SFR core design. There it was concluded that the original approach is not suitable for such innovative core designs. Hence, an improved method was realised within SAS-SFR, based on the use of two pre-calculated maps (one obtained on basis of coolant density variations and the second one on basis of complete core voiding). The actually used reactivity coefficient is derived based on the actually achieved local void fraction and thus superimposing two reactivity worth values.

1.4 MOTIVATION OF THIS WORK

This work is built around the code SAS-SFR used for deterministic analysis of the Initiation Phase (IP) of severe accident transients in SFRs. The code has been recently applied in KIT (Germany) and EDF (France) for the transient analysis of several innovative SFR core designs. In [45] the different core designs are presented along with the detailed analysis of transient results and a discussion of the underlying phenomenology. Some of the code applications [46] can be considered as a comprehensive comparison of the core behaviour during the pre-boiling phase with other thermal-hydraulic codes. Considerable experience was accumulated with regard to practical application of the code and interpretation of results as well as their dependence on initial assumptions employed in the core model specifications.

Generally, the code input requires the description of the core configuration for the thermal-hydraulics and fuel pin mechanics evaluation and neutron physics core characterization for use by the PK model. The latter typically includes also a burnup history for different core subassemblies, what influences the mechanical and thermal-hydraulic pin state at the start of the transient. The neutron physics core characterization of SAS-SFR includes three main parts, which are the power spatial distribution, the reactivity feedback data and the kinetics parameters, which are obtained by a calculation on the basis of the core model at steady state conditions. The spatial power distribution is obtained as result of the neutron physics simulation, which can employ different methods to solve the neutron transport equation. The latter can be realized by deterministic transport or diffusion, or Monte Carlo method and via different approximations with respect to the description of the core geometry and material content, depending on the calculation methods utilized.

The neutron physics procedure typically assumes two subsequent iterations. The power distribution obtained for the core model with the "as-fabricated" geometry is used as a first

iteration input for the SAS-SFR code to predict the expanded core conditions and the corresponding spatial distributions of core state parameters. Next, the latter are used for setting-up some averaged "expanded" core neutron physics model, which corresponds to the core steady state. Mainly deterministic neutron physics codes as e.g. KANEXT/VARIANT or KANEXT/CITATION [47] and [48] have been employed recently. Further, the described steady state core model is used to prepare the reactivity feedback data for the PK model, which is typically done by means of dedicated modules on the basis of the perturbation theory or based on direct K-effective differences for perturbed and unperturbed core states [41], [49].

The thermal-hydraulics model of the code employs a single (or average) pin approach to represent one or a group of SAs, which are assumed to have a coherent behaviour during the transient. Thus the power gradient within the SAs and the corresponding pin-to-pin power variations are neglected. The power gradients in SFR's are mainly caused by the SA neighbourhood (SA with different burnup and initial fissile isotopes content, control rod channel, steel dummy sub-assembly) and depend on radial SA position. The resulting SA power peaking factors in a conventional SFR, which is characterized by a high fissile fuel breeding ratio, is rather small for SAs located around the centre of the core, while closer to the core boundary the power gradient may result in SA peaking factors of about 1.05-1.10 [50]. The SA power level at the core boundary is by a factor of 1.5-2 lower than that of the core-average value, and thus inaccuracies caused by a single pin approach does not impact to the leading order the temporal evolution of a ULOF transient.

In order to predict local thermal-hydraulics e.g. pin-bundle incoherency a sub-channel level simulation of the SAs is required. The implementation of a sub-channel SA treatment can be of importance to minimize the biases in simulations as well as for safety analysis. Recently a multiple pin option has been implemented (for single phase thermal hydraulics) in SAS4A-family codes at ANL [53]. This especially holds for SFR core designs characterized by a specific SA heterogeneity such as moderator pins [51] or unusual pin arrangement [52].

Another limitation of SAS-SFR is related to the treatment of axially heterogeneous cores, which are currently subject of some innovative SFR designs [49], [54] and [55]. There, the insertion of a fertile fuel zone in-between the upper and lower fissile fuel sections is intended to mitigate the consequences of the ULOF by the decrease of the total core sodium void effect. Such a core with internal axial breeder zone can be treated in SAS-SFR models with potential limitations in the simulation of fuel and clad relocation models.

With regard to the modelling of IP phenomenology, one important drawback of the actual SAS-SFR code is the use of a PK model employed for the entire simulation time of the transient. The importance of spatial kinetics (SK) was studied for different transient phases in detail [56]. The SK is the main option used for the evaluation of the Transition Phase (or secondary phase) but not yet for the Initiation Phase. A brief review of the scope of SFR relevant studies will be given to demonstrate the importance of the use of SK solution for the analysis of the IP, starting at least from the onset of the material relocation phase. This is one of the major goals of this thesis i.e. to considerably improve the neutron physics models of SAS-SFR by coupling it with a SK model.

A comparison of PK and SK results, even employing relatively simple models and core representation details, exhibited significant differences with respect to the core power and reactivity prediction during the transient phase characterized by a spatial flux distortion. The main reason for such a flux distortion occurring first in the IP is given typically by a fuel motion, which follows after a fuel pin failure. In the PK model assumption the flux and power spatial shapes variations are neglected. However, this constant-shape approximation becomes questionable in the transient phase, in which a physical material relocation is associated with considerable changes of spatial flux and power distribution. For the SFR model in [42] with relatively simple approach for the core representation the reactivity effect predicted as result of fuel relocation towards the upper fissile core boundary and beyond is overestimated using a PK neutron physics approach for a ULOF calculation.

In one of the recent studies a comprehensive analysis of the spatial effects for SFR occurring in the Initiation Phase (IP) is performed [58]. There within a coupled neutron physics and thermal-hydraulic simulation using SIMMER-III/SNATCH demonstrated that the PK solution reproduces quite accurately the transient evolution up to the onset of boiling with respect to total power and reactivity. Radial distortions of the power distribution observed in the calculations [42] remain less than to 1%.

For the transient analysis including sodium voiding a multi-group accident analysis model was developed in the frame of a Doctoral thesis [57], targeting to catch the fast reactor's spatial effects. Based on simple models for two-phase sodium and a two-dimensional neutron kinetics code, sodium voiding effects were calculated for a medium-size SFR. The core design considered in [57] exhibits a strong positive sodium void effect leading to prompt critical conditions during the voiding phase. The application of the method was limited to the accidental phase up to pin failure, because the reactivity effects related to the subsequent fuel and clad material relocation has not been considered.

Similar conclusions are drawn in [59], where space-dependent effects are analysed using the three-dimensional kinetics computer code WIN-3D. A ULOF is calculated up to the boiling point showing no significant neutron flux distortions for a medium-size SFR. For the pre-boiling phase of the transient, the results show a close agreement between SK and PK models and are consistent with the analysis conducted in [57]. In another publication [60] similar conclusions are drawn for an approximate calculation model for a long period reactor power excursion, followed by sodium boiling. It has been demonstrated, that axial power distribution is only slightly distorted at the inlet side as compared with the one for steady state.

The normalized power and reactivity evolution as calculated in [42] for pre-boiling phase of ULOF predicted by PK and SK solutions is given in Fig. 8. For the particular ULOF transient calculated in [42] the conventional PK approach using pre-calculated feedback coefficients may produce an acceptable simulation of the boiling and voiding process.

On the basis of fuel and cladding motion model implemented in code SIMMER-III, it is demonstrated in [42] that spatial distortion of original power profile in given channel starts with clad relocation, while a considerable flux profile deformation is only observed after the occurrence of a fuel motion. The normalized power and reactivity evolution as calculated in [42] for the phase of a ULOF after boiling onset predicted by PK and SK solutions is given

in Fig. 9. With regard to the sodium boiling phase, the maximal variation of the channel power fraction is evaluated to amount to 8% at the time of cladding melting at $t = 32.5$ s. This behaviour confirms the analysis made in [57]. After the fuel-pin breakup predicted shortly after fuel melting onset at $t = 35.0$ s after the initiation of the transient, an increase of the shape distortion is observed together with reactivity spikes induced by these three-dimensional effects as illustrated by the computational results in Fig. 9.

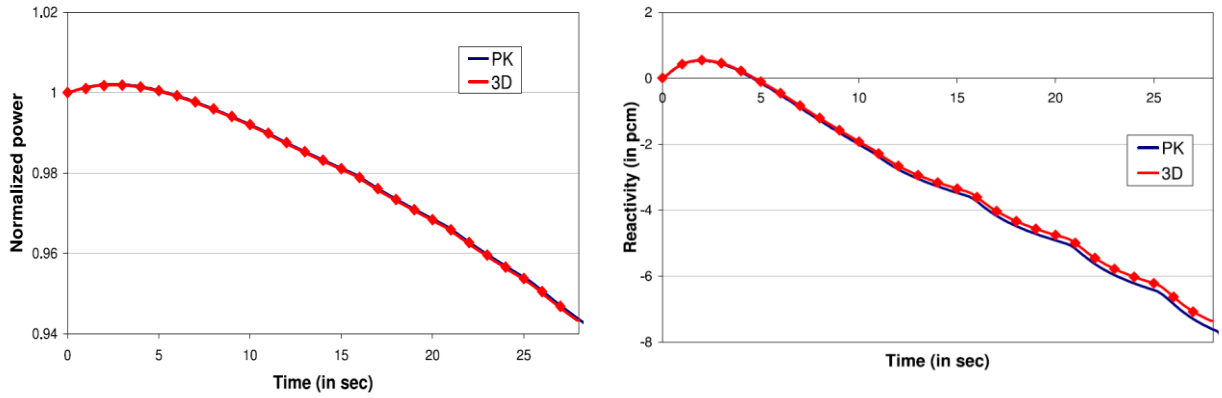

Fig. 8. Comparison of computed normalized power (left) and reactivity (right) versus time for a PK and SK simulation of a ULOF with 15 s flow halving time constant at pre-boiling phase for a large oxide fuelled SFR core, from [42]

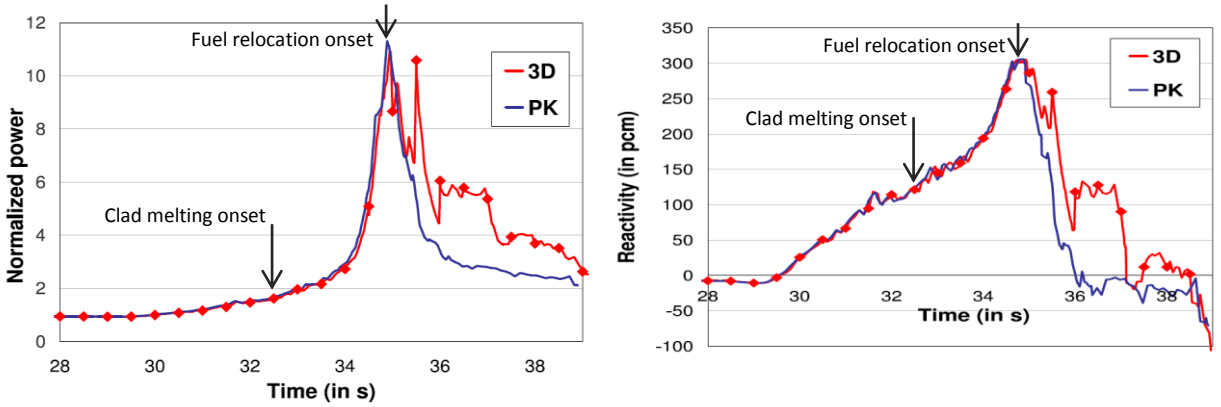

Fig. 9. Comparison of computed normalized power (left) and reactivity (right) versus time at transient phase after boiling onset (at $t = 28.5$ s) for a PK and SK simulation of a ULOF with 15 s flow halving time constant for a large oxide fuel SFR core, from [42]

According to this calculation the PK model predicts a strong negative reactivity insertion after fuel pin breakup at $t > 35.5$ s caused by a fuel dispersal toward less active parts of the core. In contrast to this the SK solution predicts rather noticeable positive reactivity jumps during the same period. From this analysis, it seems that the PK calculation does not represent appropriately the reactivity in this case when fuel dispersal starts. Generally, the conclusion is formulated in [42] that the non-conservative evaluation with use of the PK model at fuel motion conditions for the ULOF accident require further analysis to confirm this trend for different types of accidents and designs.

The study on the preparation of reactivity coefficients (used in the Adiabatic Method) given in [58] is also of interest with regard to the comparison of PK and SK solutions. The potential error of PK model originates mainly from two aspects: the pre-calculated reactivity coefficients, which can be under- or overestimated for the considered time point of the transient, and flux and power spatial shape distortion, which defines the spatial distribution of prompt and delayed neutrons sources. With regard to the latter, the error in node power predicted based on initial shape function with respect to the one obtained in SK solution may be significant in the fuel motion phase, what influences the local phenomenology as well.

A number of early studies were devoted also to application of SK for reactivity-initiated transients, such as [61] and [62]. In [61] on the basis of a two-dimensional model for fast reactor kinetics the study is performed of a small 300 MW_e SFR core transient behaviour after a strong power excursion, caused by successive replacement of control material (absorber) with sodium. It is there demonstrated, that SK model predicts a more rapid power excursion than by PK approach since first one allows to account for an increase of neutron flux in regions from which the absorber is removed. This leads to a significantly earlier fuel melting. In [62] the development, capabilities and some applications of one-, two- and three-dimensional SK diffusion code SPARK are introduced. With the use of an Improved-Quasi-Static method in the SPARK code the comprehensive study of different transients (reactivity ramp insertion, control rod ejection, channel voiding) on the basis of few different SFR core sizes is finalised concluding that spatial effects can be significant in a large commercial fast reactor with power of 1000-2000 MW_e. In addition it is stated, that although an improved PK model, in which the reactivity input is pre-calculated can be used to obtain accurate results for the actual power level. However, detailed temperature distributions cannot be well predicted without renouncing the use of a SK model. It is noticed, that the inclusion of SPARK into a whole core accident code is regarded as important in order to be able to cope with the reactivity and flux shape changes which are associated with events such as coolant voiding and fuel motion which occur under whole core accident conditions. Another study conducted by coupled simulations based on the SAS4A-code in [63] concluded that phenomena as cladding and fuel melting and subsequent relocation could have significant localized neutron physics and thus reactivity effects[5].

1.5 AIM AND SCOPE OF THE WORK

Based on the major conclusion of the previously discussed studies it can be concluded that the implementation of a SK solution for the SAS-SFR code to obtain an accurate prediction of the material relocation reactivity is of high importance. The investigations performed in [42] strongly emphasize to complement the SAS-SFR code with an SK neutron physics model, since the main advantage of the code's sophisticated and well validated models is "localized" in the simulation of the fuel and material motion phase and the

[5] The work is not directly related to the SFR transient analysis but rather presents an overview of approaches available in literature, where the SAS4A-family codes are coupled with SK solutions. The work is dedicated to use of different SK solutions for the analysis of a core benchmark proposed for a minor actinide-burning, subcritical reactor cooled by heavy liquid metal (Pb-Bi eutectic), and driven by a proton accelerator. The analyses focused on the impact of neutron transport and spatial effects by comparing the DIF3D-K nodal diffusion theory results with VARIANT-K P_1 and P_3 nodal transport theory results.

corresponding mechanics, thermal-hydraulics and material dynamics phenomena expected to happen in fast over-power scenarios.

It is of importance to demonstrate and analyse for currently considered commercial SFR designs quantitatively the limitation of the PK model and reactivity worth map approach. The implementation of a SK solution can be identified as a considerable improvement, which is aimed at decreasing bias and the level of uncertainties in the results, to avoid a non-conservative assessment and thus to provide a more reliable basis for a credible safety analysis.

The alternative transient simulations with SAS-SFR can consider application of different SK solvers (direct, quasi-static, adiabatic etc.). The detailed evaluation of errors, which appears as result of the PK approach, is nevertheless a relatively complicated task. But on the basis of one design using best-estimate calculation routes for both PK and SK solutions one can demonstrate quantitatively the differences between both simulation results. There are certain improvements considered in this work in comparison to the study in [58]. Limitation of the work [58] at that time is due to a relatively simple approach in accounting for distributed core parameters. For instance, the axial and radial expansion of the core and its elements were modelled in a simplified manner, what is insufficient for a detailed ULOF analysis presented hereafter in this work.

The work presented is a first of a kind implementation of a spatial kinetics for the SAS-SFR code. It has been applied for a comprehensive analysis of a ULOF transient in a SFR elucidating improvements on the prediction of core transient behaviour prior and during the material melting and relocation phase. The importance of the work is also pointed out by the fact that recently targets of safety considerations for SFRs in many countries have been reconsidered with the focus on the development of overall plant design solutions, which allow a practical elimination of the consideration of core disruptive accidents with fuel melting, even in case of very low probability events in the Beyond Design Basis accident domain. Another goal of the coupling of a spatial kinetics solver with SAS-SFR is envisaged in capability of the improved simulation of non-symmetrical transients (i.e. for Design Basis transients with asymmetrical control rod trip, in addition to the classical “symmetrical” transients).

The implementation of the SK solution requires accounting for distributed core state parameters in the neutron physics core simulation in the steady state, since it poses the starting point of a transient simulation. The analysis of resulting state parameters at steady state with regard to different level of core details representation in the neutron physics is also of interest. The second main goal is devoted to a more accurate prediction of steady state core characteristics. For practical application, a coupled scheme, supplied with the most accurate neutron physics solution, for instance, with the one based on the Monte Carlo method, provides an efficient comparison basis for other systems, which employ other models in thermal-hydraulic and pin mechanics, other level of core details and neutron transport solution (usually, deterministic). One major advantage of this approach arises at the beginning of the design evaluation study, where different partners provide their own solutions to simulate the steady state of the core. Use of different models often leads to considerable differences in the steady state characterization. The coupled simulation scheme to be developed will help to

identify the sources of deviations in the prediction of the spatial power or temperatures distribution, and therefore will provide the basis for minimizing errors, as it will be fully based on well-validated SAS-SFR models, which are fed by power data obtained from the high-fidelity neutron physics solution of Monte Carlo code.

All goals described above result in the minimization of errors and uncertainties during simulation of a complex system like a SFR using validated models coupled to advanced neutron physics solvers. Finally, the improved coupled methods will be developed in a modern informatics platform based on Python that represents an efficient way of assembling different coupled solutions including pre- and post-processing and effective features for the mapping between the involved domains and the definition of data flow.

1.6 STRUCTURE OF THE THESIS

The thesis is structured in five content chapters followed by summary and conclusive remarks. After spanning the background and deficits of the current approaches to describe SFR accidents using the SAS-SFR code complemented by a description of a characteristic ULOF transient to study and formulating the aim and scope of this work in chapter 1, the chapter 2 provides a description of the general background and the methodology selected. Therein at first the different reactivity feedbacks potentially occurring in a SFR transient are qualitatively discussed necessitating a data transfer to a more advanced neutron physics model solution. In a next steps selection of the neutron physics solutions is briefly discussed and the reactor is defined which forms the reference for all simulation studies conducted in this work.

In chapter 3 the developed coupled SAS-SFR/MCNP scheme is presented and application results for the evaluation of core characteristics at steady state conditions using the new tool are shown and discussed.

Chapter 4 is concentrated on the description of the extensions of the SAS-SFR capabilities for transient analyses coupled with the selected spatial kinetics solver of the PARCS code. The chapter provides description of the solution, in particular, additional approaches used for geometry representation and nodes mapping between neutron physics and thermal hydraulics domains, as well as logical schemes of data flow in the new system and codes modifications required.

In chapter 5 applications of the solutions, methodology of data transfer, coupling schemes and convergence mechanisms implemented in new tools for steady state and transient calculations for a variety of cases on the basis of the ESFR Reference Oxide core are presented and discussed along with number of test calculations.

Finally in chapter 6 the major results are summarized, which demonstrate new evaluation capabilities and the major conclusions are drawn. Additionally, an outlook formulating further steps necessary to attain an even more accurate solutions and realistic safety analyses is given.

2 GENERAL BACKGROUND AND SELECTED METHODOLOGY

2.1 REACTIVITY EFFECTS IN SFRS

The formulation of the coupled simulation approach aims to predict realistic core configuration and the power evolution by accounting for changes in relevant core materials properties and geometry parameters caused by the neutron physics and thermal-hydraulics inter-dependency. Therefore, it is important to identify and classify those changes in a generalized manner and to quantify their impact (feedback) on the net core reactivity translated into the power generation.

2.1.1 OVERVIEW OF REACTIVITY EFFECTS IN SFR

Geometry changes in core elements and surrounding structures as well as changes in material temperatures lead to a change of the ability of the system to "feed" chain fission reactions. Firstly these effects lead to a change of the probability of neutrons to interact with given nuclides (named as neutron cross section) due temperature dependence, resulting in a change of the balance of the different reaction rates. Secondly, redistribution of material and density changes lead to a change of the probability of neutrons to meet fissile isotopes, on the one side, and to leak from the core on the other side, and thus, influences the net neutron production rate.

The resulting response of the core multiplicity properties due to the change of some core parameters, for instance, element dimensions, density or temperature, is named reactivity feedback effect. Reactivity feedback effects are also related to changes of reactivity control device position (i.e. control rod absorber or control subassembly), addition or removal of materials, fuel isotopic composition changes with burnup and to some integral plant parameters, as thermal power level.

For the safe operation of a plant the core has to be designed in such a manner, that deviations from nominal operating conditions cause mitigating reactivity feedback effects, which are essentially expressed by a negative value. This either may be realized on a "naturally inherent" level, which is defined by neutron transport peculiarities of the core and response via neutron cross sections and flux changes, or on the level of a dedicated design, where active and/or passive systems are designed in order to influence the core reactivity in an appropriate manner and, if needed, to shut down the chain reaction or to bring it to an acceptably low level.

Irrespective of the reactor design, the reactivity effects have to be considered for the whole life time cycle i.e. from core loading with fresh fuel and start-up up to end of life core and all different conceivable plant operational conditions. At different time scales of reactor operation, different reactivity effects are of importance. But the most demanding tasks, from a safety point of view, are the ones where the reactor is operated close to and around nominal power level.

In case of accidental transients, reactivity effects are typically grouped into components, which are treated independently from each other, while the net reactivity is calculated as a sum of these components. However, in accidents different components may play a significant role with different time scales.

This work is based on the approach to handle the core materials properties in neutron physics as precise as possible, and thus it becomes necessary to identify different phenomena, which cause changes of multiplication capabilities of the core, i.e. reactivity variations. Different ways to group the reactivity components can be found in literature, [15] and [64]. Nevertheless it is indispensable to formulate them in this context again to link them to the phenomenology depicted in the SAS-SFR models. The characteristics of reactivity effects of SFRs exhibit distinct differences to other fast reactor and deviate substantially from those of e.g. LWR reactor types. Firstly, thermal expansion effects in SFRs play a significant role, and thus their inaccurate prediction may lead to serious inaccuracies. Secondly, the sodium coolant, along with its specific features and thermal-hydraulics, provides positive density and void reactivity feedback effects. Additionally it is worth to mention that modelling of structure thermal expansions typically causes uncertainties of results, due the complicated movement of core structures relative to each other.

The description of reactivity effects in a SFR core at nominal operating and transient conditions is given below, followed by the definition of other reactivity effects, which have to be accounted for in the late phase of a ULOF transient and deals with the loss of the core elements integrity as result of thermal and mechanical loads.

2.1.2 DEFINITION OF REACTIVITY EFFECTS CONSIDERED FOR SFR TRANSIENT ANALYSIS

The importance of different reactivity effects is discussed in [15]. Some of the thermal feedback effects are fast acting in time, such as the Doppler feedback effect, some are slow acting as they are driven by temperature changes of in-vessel structures. Core temperature changes provide relatively “fast” acting thermal feedbacks, since core temperatures change relatively rapid. Changes in primary system structural temperatures are delayed in time because due to the thermal inertia it takes several tens of seconds before materials outside the core region heat up or cool down. The most important negative reactivity feedback effects are all driven by primary system structural temperatures, thus acting only on a delayed time scale. Table 1 provides an example of the summary of important reactivity components occurring during an ULOF transient and the corresponding reactivity coefficients for a large scale SFR.

Fuel Doppler effect

The fastest reacting reactivity feedback effect is the Doppler effect related to heavy nuclides which acts instantaneously upon fuel temperature changes. It deals with the temperature broadening of the neutron cross section resonances and changes of the self-shielding effect. For the fertile heavy nuclides, like U-238, it respond with a negative reactivity variation as consequence of a temperature increase, due to an increase of the neutron absorption rate in the resonance energy part of the neutron spectrum. For a SFR operating with U-Pu ceramic fuel, the Doppler effect is negative and rather large, due to the

fact that a certain part of the neutron spectrum is located in the low energy range as result of the neutron scattering on oxide or carbide nuclides of the fuel.

Table 1. Summary of important SFR safety parameters relevant for ULOF, from [15]

Reactivity effect	Reactivity sign	Reactivity magnitude	Reactivity coefficient value for SFR (v2b-ST)	Response time of reactivity to become effective	Comment / Importance during ULOF
Doppler	Negative	Medium	-881 pcm (Doppler constant)	Immediate	Positive reactivity insertion during ULOF due to decreasing power and thus temperature level
Sodium temperature	Positive	Medium/large	0.45 pcm/K	Fast	Significant as it is ULOF's driving positive reactivity insertion
Axial fuel pin expansion	Negative	Small	-0.19 pcm/K*	Very fast	Negative during ULOF
Radial core expansion (diagrid)	Negative	Small	-0.78 pcm/K	Delayed	Diagrid plate needs to change in temperature to become effective
Control rod drive line axial expansion	Negative	Large	-0.86/-1.16 pcm/K (rod position at 25/50 cm)	Delayed	Upper plenum region needs change in temperature before it becomes effective

* This corresponds to a combined, or "linked" fuel-clad reactivity feedback coefficient that is applicable at EOEC core conditions as calculated with ERANOS code

For MOX-fuelled SFR the following correlation is deduced for the temperature dependence of the Doppler effect:

$$\frac{d\rho}{dT} = \frac{K_D}{T},$$

where ρ is the reactivity of the core and K_D – the Doppler constant, which characterizes a given core design and fuel composition for the whole range of fuel temperature T. The Doppler constant is usually derived for a given core design on the basis of two static neutron physics calculations: one is with an average nominal fuel temperature, while a second one employs an increased temperature level, for instance, by 1000 K value. It reads as follows:

$$K_D = \frac{\rho_1 - \rho_0}{\ln(\frac{T_1}{T_0})},$$

where ρ_0, ρ_1– are the core reactivity values for the nominal and the increased fuel temperature (T_0 and T_1), respectively.

In practical transient simulations with multi-node core representation for neutron physics with the PK model, the Doppler constant and its spatial distribution are used to derive the local Doppler effect based on node-averaged fuel temperature variations, while the total effect is derived as a sum of all local (node) values. There is a strong radial gradient of temperature in a fuel pellet of a SFR pin, while in order to obtain the average value for derivation of the Doppler effect in a given calculation node the averaging of the data from several radial calculation meshes within a pellet is taken. For SK simulation, the average node fuel temperature is used in direct XS calculations for this node or XS are calculated via their derivatives with respect to the node averaged fuel temperature.

A certain deterioration of the Doppler effect occurs in accident conditions with sodium voiding, due to spectrum hardening and a decrease of the neutron flux in the resonance energy range. For the sodium voided conditions, the temperature dependence of the Doppler effect has the same shape of $1/T$ and is described by Doppler constant calculated at fully voided conditions, which is about 20% smaller than the one at nominal conditions[6].

Sodium temperature expansion reactivity effect and void effect (SVE)

The sodium-related reactivity depends strongly on the considered core design options, namely:

- type of fuel,
- pin dimensions,
- core power and size,
- overall arrangement of core elements and
- its structure,

It is described typically by two values:

- sodium density reactivity coefficient, given in units of *pcm/K* or *pcm*/(*%of density*),
- and Sodium Void reactivity Effect (SVE), given in *pcm*.

The sodium density coefficient is calculated as a ratio of corresponding reactivity changes to relatively small variations of the density around the nominal value, while the SVE value is evaluated assuming sodium voiding in the whole core or of parts of it, such as the inventory in the sodium plenum.

The decomposition in few components, e.g. [51] and [50], is typically considered for the understanding of the nature of sodium-related reactivity. In particular, for a large SFR core, the reduction of the sodium density leads to insertion of a positive reactivity due to the action of two main contributions – decrease of neutron absorption and hardening of neutron spectrum. The latter spectral component is proportional to the product of the flux and neutron importance function and typically has its maximum in the centre of the core, where the level of flux is higher. This component defines the strong spatial dependency of the sodium reactivity in a large SFR core. The third component – neutron leakage – acts with a negative contribution to the net effect. The neutron leakage term is more effective near core boundaries, and thus the sodium heat-up or voiding in these regions results in a negative local contribution, while the sodium effect demonstrates non-linear dependency on density. The last component which deals with the change of the self-shielding effect is positive but relatively small.

With an increase of the SFR core size the SVE effect increases as result of a decrease of the role of neutron leakage. Thus the design optimization of a large SFR core with regard to the value of the sodium reactivity is a high priority task. The comprehensive analysis of different design options, for instance, has been performed for the ESFR core in [45]. The spectral component is defined primarily by the given fuel type and sodium volumetric

[6] For the ESFR Reference Oxide Core at BOL configuration the Doppler constants for normal and voided conditions are equal to -1100 and -860 pcm respectively.

fraction, which equals to about 25-30% for most of designs. A further decrease of the latter value is practically of marginal interest, since optimal thermal hydraulic parameters of the SA are to be considered as well. Thus optimization of the SVE deals mainly with design options, which influence the leakage component by introducing an upper sodium plenum above the core, which facilitates neutron leakage in case of sodium voiding in this region.

In order to illustrate the non-linearity of the effect on design aspects the sodium reactivity characteristics for a few SFR designs at the End Of Cycle (EOC) conditions are listed in Table 2. For the large SFR core without an upper sodium plenum (or with a relatively small one) the dependence of the reactivity on sodium density is almost linear. Thus for the given example of SFR v2b-ST design it results in a good correspondence of the total SVE value of 2060 pcm and the density coefficient of 0.544 pcm/K. The introduction of a large sodium plenum, as in the SFR v2b-PL design (with sodium plenum height of 30 cm), leads to a considerable decrease of the total SVE, while a considerably smaller relative change is observed with respect to the sodium density coefficient. For the last design considered here, proposed by EDF [65], the SVE in fissile height is slightly lower (1448 pcm), while the total SVE is evaluated to amount to a negative value of (-238 pcm). This is due to the innovative core arrangement with axial heterogeneous fissile and fertile fuel arrangement and application of a large upper sodium plenum. Nevertheless, the plenum does not provide the same "efficiency" for neutron leakage in non-voided conditions. The fissile core region contributes with a still high positive value of the density coefficient, thus resulting in a positive cumulative sodium density effect. It has already been mentioned above in §1.3.2, that neglecting of this effect of a non-linearity in a large sodium plenum may lead to a non-conservative evaluation of the transient behaviour.

Table 2. Sodium void and density reactivity for different SFR designs

Parameter	SFR design		
	SFR v2b-ST [45] (3600 MW_{th})	SFR v2b-PL [45] (3600 MW_{th})	SFR design EDF [65] (2880 MW_{th})
SVE in fissile height, pcm	2060	1969	1448
SVE in sodium plenum, pcm	-100*	-470	-1687
Total SVE, pcm	2060	1499	-238
Sodium density coefficient, pcm/K	0.544	0.458	0.150

* not accounted in simulations in [45]

Thermal expansion reactivity effects of core, SA and fuel pin

Prediction of the thermal expansion of core elements in a SFR is an important and sensitive issue, since the corresponding reactivity effects are relatively large and cannot be neglected in the overall reactivity balance. The main mechanism of expansion effects is the change of the neutron leakage, as result of changes in core radial and axial dimensions, while additionally the mutual expansion of different core elements influences reactivity due changes in neutron absorption and scattering.

The change of the core axial dimension is defined by the axial expansion of the fuel pin and is characterized by the updated fissile height, which is defined by the height of the fissile fuel pellet stack.

The change of the radial dimension deals with the radial thermal expansion of the core supporting structure – diagrid plate, which host all SA foots of the core. This expansion is essentially driven by sodium inlet temperature.

The individual thermal expansion components act practically on different time scales, from almost instantaneous response up to minutes. The individual components of reactivity and their corresponding specificities to account for in the reactivity balance are subsequently discussed. The microscopic cross sections temperature dependence of the structure material and the sodium is usually not accounted for, as it is relatively small in comparison to the reactivity changes due to their local density variations.

a) Fuel pellet thermal expansion:

Upon a temperature rise the fuel pellet expands radially and axially. The axial expansion introduces a significant negative reactivity in conditions of a rapid power increase, due to the increase of radial neutron leakage. The key issue of evaluation of fuel expansion reactivity is the prediction of the relevant local fuel conditions, which are characterized by such parameters as fuel burnup level and fuel-clad gap size (both have considerable variations radially and along the axial core height).

Two main approaches are applied practically to predict the fuel expansion: “free” and “linked” fuel expansion. The first approach is suitable, for instance, for the fresh fuel loaded core (BOL conditions), since typically no fuel-clad mechanical interaction is established for fresh fuel at nominal operation conditions. It means that fuel axial expansion is defined by the local fuel temperature and the fuel thermal expansion coefficient, while axial expansion of the cladding tube is considered separately. The second approach is applied for cores with a significant fuel burnup level. In case of a high fuel burnup and porosity the fuel-clad gap is closed for most of the SAs practically along the whole fissile core height. Thus the character of pin temperature expansion is often assumed to be defined by the local clad temperature due to the limited mobility of pellets relative to the clad. It is important to mention that none of these two approaches is valid for all local conditions of the SFR core. Since the transient analysis typically assumes burnt core configurations, such as EOEC, the assumption on the fuel expansion coefficient is taken on basis of available experimental data or just postulated for the given transient exercise.

Alternatively fuel and clad axial expansion is to be determined as result of an integral simulation of the fuel pin mechanics transient behaviour. This approach allows simulating the detailed differences of the fuel pin behaviour in dependence of the burn-up history, the local position of the SA within the core cross section and the transient integral core behaviour. Such an approach is adopted within the SAS-SFR code by the use of the DEFORM-IVC model.

The integral reactivity coefficient of the simplifying analysis approach in accord to the selected assumption – free or linked fuel expansion – is evaluated usually on the basis of calculations for two core states, which are characterized by a change of the average core fuel

temperature only and the corresponding fuel fissile height change. To account for the spatial distribution of the temperature variations and the related thermal expansion reactivity effect contributions is a more complicated issue. Practically the "local" fissile heights of individual SAs may vary, due to different SA power levels. The treatment of the non-uniformity of the upper core boundary in neutron physics models is discussed in section 2.2 below in more detail.

b) Clad thermal expansion:

The individual treatment of clad expansion reactivity is usually not considered. Only one coefficient for pin expansion is typically used, which accounts for different fuel-clad gap conditions. Nevertheless, the data, provided by the SAS-SFR code, for instance, may serve as basis for a precise treatment of the clad material and thus for prediction of the related reactivity response. Axial and radial cladding expansion provides different reactivity contributions. Heat-up of the cladding leads to an axial expansion, which is strongly defined by the pin state, as mentioned above, including pin and pellet design, its burnup history and power level. In case of a reduction of cladding steel mass within the corresponding expanded fissile height it leads to an introduction of a positive reactivity, mainly due to the reduced neutron absorption in steel. Such a clad behaviour may be observed for transients in the core with fresh fuel (at BOL conditions). In case of burnt fuel, the cladding becomes typically expanded simultaneously with the fuel, while the cladding mass is rather conserved within the pellet stack height. In such a situation a relatively small positive reactivity component is introduced due to decrease of neutron absorption in the core.

Radial expansion and the related reactivity effect is typically not modelled individually until the other important issue is not considered, which deals with decrease of coolant cross section caused by radial thermal expansion of the clad. The coolant flow cross section reduction leads to a decrease of the coolant mass within the core, and thus causes additional components of coolant-related reactivity (generally, a positive reactivity contribution).

c) Hexcan thermal expansion:

A similar behaviour as the clad exhibits the hexcan with respect to the reactivity variation in case of a change of the temperature. It also leads to a change of the hexcan mass within the fissile height (which is defined by the fissile fuel pellet stack height). During the transient the state of the hexcan is defined primarily by the coolant parameters, while the larger thermal inertia of hexcan provides slightly larger time scales for variations of hexcan parameters during a ULOF transient compared to the cladding. Considering a fast fuel expansion, a not negligible negative reactivity may be inserted due a relative increase of the mass of the hexcan within the fissile core height, while the hexcan expansion due to heat-up correlated with the sodium heat-up may introduce an additional positive reactivity, similar to the one of clad expansion. An individual radial expansion of the hexcan shroud is typically neglected. It is simplified considered at some averaged expanded dimensions corresponding to the nominal operating conditions of the core. These dimensions along with expanded pin clad dimension and subassembly pitch in the diagrid define the coolant flow cross-section for

both in-pin-bundle and inter-subassembly gap sodium. The influence of the hexcan-related reactivity is described in more detail in the transient exercise discussed below.

d) Diagrid expansion:

The diagrid related reactivity feedback contribution during a ULOF is primarily determined by the change in the core inlet temperature. The large diagrid plate will adjust only slowly to temperature changes due to its relatively large mass and relatively small heat transfer surface. Considering a core inlet temperature rise caused by an ULOF transient, as in case of a simultaneous trip of primary and secondary pump, the diagrid will expand radially inserting a negative reactivity. However, this insertion is considerably delayed in time. Adversely, a proper function of the secondary pump at an ULOF initiation could yield a core inlet temperature decrease leading to an additional positive reactivity feedback contribution. Hence, the status of the secondary pump (trip or no trip) is an important parameter determining the ULOF event sequence, as it determines the sign of the contribution of the radial diagrid expansion reactivity feedback (positive or negative).

The control rod drive lines expansion reactivity effect

The control rod drive lines (CRDL) expansion reactivity feedback effect is considered in most of the SFR designs due to the specific design of the upper core structure of this type of reactor. The structural elements temperatures above the core outlet are primarily defined by the sodium temperature in the sodium outlet pool (see Fig. 2), thus defining the temperature expansion of CRDLs. With an increase of the sodium outlet pool temperature the corresponding axial expansion of drive lines leads to a movement of the absorber part of control rods towards core mid-plane, what in most of the accident scenarios favourably causes insertion of an important negative reactivity (see Table 1). In a ULOF, this is one of the major negative reactivity feedback effects which may essentially determine the sequence of the transient dependent on the time constant of the coolant flow halving time.

Modelling of this effect is a relatively delicate issue, which deals with the prediction of mutual thermo-mechanical behaviour of following elements: reactor vessel wall, drive lines themselves, pin and SA, while all of them act on a different time scale. The time delay before this reactivity becomes effective is governed by the thermal inertia of the upper sodium pool. The other temperature influencing the CRDL expansion effect is the vessel wall temperature. An expansion of the vessel wall has the effect of withdrawing the control rod absorber from the core region, thus adding positive reactivity into the core. The effect of vessel wall temperature changes are however delayed by 200–400 s due to the nature of the tortuous paths of the vessel wall cooling system. Since a part of the core inlet flow is diverted to cool the vessel walls, the temperatures there only gradually adapt the temperatures of the core inlet flow, or primary outlet flow of the heat exchanger. Therefore, changes of vessel wall temperature are with respect to their large time scales so slow that they have hardly any influence during ULOF transients in reactor designs with a reasonably small coolant flow halving time constant of 5 to 15 s [15].

For practical simulations, the approaches to account for this effect are different for PK and SK simulations. To derive the related reactivity component for a PK model a specific

correlation is usually proposed, which provides the reactivity as function of relevant parameters. In a simple case, the effect can be defined as follows:

$$\Delta\rho_{CRDL} = c_{CRDL} \cdot \Delta T_{CRDL},$$

where c_{CRDL} is the corresponding reactivity coefficient, $\Delta T_{CRDL} = T_{CRDL} - T_{CRDL}^{(0)}$ is the change of the average CRDL steel material temperature from the value $T_{CRDL}^{(0)}$, corresponding to beginning of the transient ($t = 0\ s$) to the actual value T_{CRDL}.

The SK solution does not operate in terms of reactivities. Here, the definition of the CRs axial position is the only parameter, which allows accounting for this effect. Practically, the mechanism should be introduced in the model, which accounts for mutual movement of the fissile core and CR absorbers.

Materials relocation reactivity effects

If the core heat-up leads to a state, where the fuel or clad temperature exceeds the melting temperature, parts of the core material becomes mobile. The molten materials dynamics is an extremely complicated issue for modelling. Depending on design and pin state different accidental sequences may be observed, while the corresponding reactivity feedback may become considerably higher, than any other effect before the start of the core material relocation phase.

After clad dry-out further heat-up of pin leads to a clad melting and a removal of the molten fraction by shear forces imposed by the two-phase coolant flow towards the core boundaries. The resulting reactivity introduced is positive, due to the reduction of neutron absorption and neutron spectrum hardening. A hypothetical positive reactivity due to the removal of all clad material is evaluated to amount to a value of about 9 $ for large SFR core designs [45].

In addition to the clad material, a hexcan melting also may occur later, while the complete melting of part of hexcan defines the beginning of the Transition Phase. As it is observed in the experiments (and modelled in SAS-SFR), the molten clad freezing may occur at core axial boundaries, typically in regions of the upper and the lower gas plenums or reflectors, what may lead to introduction of additional positive reactivity due to the influence on the neutron leakage out of the core region.

The fuel material motion starts typically shortly after clad motion and may result in reactivity feedback effects with different sign during this phase. Fuel melting occurs initially in the most powerful SA at an axial node with the highest fuel temperature. The resulting reactivity feedback due to fuel relocation from the core centre to its boundaries is strongly negative, due to spatial distribution of the fuel worth with its maximum at core mid-plane. The hypothetical negative reactivity correlated to the removal of all fuel is evaluated to amount to a value of about 70 $ for a large SFR core [45]. However, fuel relocation may include a positive contribution, if molten fuel is frozen close to core boundaries, because additional neutron reflection is introduced.

For both clad and fuel relocation effect the relocation of the material out of the pin section is typically considered as a loss of material for the reactivity balance and no reactivity response is calculated. Practically, for a core state characterized by only few percent of the

total material mass becoming mobile, the total reactivity may become negative during the Initiation Phase at fully voided conditions, mainly because of the fuel ejection out of the fissile core height.

Reactivity effects balance

Depending on the reactor core and the primary system design different assumptions are taken into account for the different reactivity effects. Three main reactivity feedbacks define the ULOF development in its initial phase before core damages occur, which are:

- the Doppler effect,
- the sodium density variation and
- the thermal axial and radial expansion of pin and SA elements.

The latter is typically represented by a few components of axial expansion effects, for instance a pin axial expansion, which accounts for the expansion of both fuel and clad, and hexcan axial expansion.

Other negative reactivity effects essentially determining the course of the ULOF transient are reactivity feedback effects associated with the expansion of CRDLs, and the radial diagrid expansion, while both effects are relatively slow with respect to their response time, since they demand a significant change of the temperatures outside the core domain to become effective. Practically, for a SFR ULOF driven by pump coast down with half-time constants of the order of 10s these two effects can be excluded from the reactivity balance due to their large time delay. The corresponding IP is characterized by a relatively quick start of the boiling phase, while the material relocation may start after only few seconds of boiling. For this work, the following reactivity feedback effects are considered in detail:

- the Doppler effect;
- the sodium density and void effect;
- the fuel, clad and hexcan thermal expansion effects;
- the fuel and clad relocation effects.

2.2 DEVELOPMENT OF DATA TRANSFER METHODOLOGY

In this section an overview of the methodology and approaches is given, in a rather general form, providing the basis for organization of the data management in coupled neutron physics and thermal hydraulics simulations. The practical implementation, which deals with more details and peculiarities of neutron physics models, is described in chapters 3 and 4.

One can allocate data transfer problems for coupled simulations to the following main tasks:

(1) transfer of three-dimensional power data from neutron physics calculations to thermal hydraulics calculations;
(2) transfer of relevant thermal hydraulics core state parameters to neutron physics calculations and
(3) exchange of other data important for calculation control and specification of selected model assumptions.

For the first and second task the data exchange for steady state and transient simulations are naturally similar. The neutron physics solution is obtained taking into account local core state parameters. The peculiarity of this work is that one relies on results of thermal hydraulics and pin mechanics models of SAS-SFR for modelling of core neutron physics responses.

Following the given generalization of data transfer, the methodology presented is mainly devoted to the second task aimed to represent the core state parameters for the neutron physics calculations with only a few approximations. All relevant reactivity effects considered above in §2.1.2 are taken into account in the neutron physics calculations via:

(1) variations of the local core conditions (state parameters) and corresponding neutron cross sections changes and
(2) consistent variation of the core geometry.

Particular differences with regard to corresponding reactivity components in the original SAS-SFR PK feedback model are pointed out.

2.2.1 TRANSFER OF CORE STATE PARAMETERS TO NEUTRON PHYSICS MODEL

Five components have been selected as representative for local core state parameters of one calculation node. The calculation node representation in SAS-SFR and the corresponding calculated core state parameters have been taken as a basis for the nodal representation in the neutron physics calculation. Within the SFR framework, it is logical to represent a calculation node with a given axial height as follows:

(1) fuel;
(2) cladding;
(3) sodium within hexcan ("inner sodium");
(4) hexcan and
(5) sodium in one half of the inter-subassembly gap ("outer sodium").

This general formulation, given for an axial node of fissile height is simplified for other core regions of importance[7]. For these five components one needs to determine the corresponding masses, temperatures as well as information on geometrical arrangement and dimensions (for the treatment of the heterogeneity and self-shielding effects). The data can be either used directly in the neutron physics model for the Monte Carlo method or for preparation of the node dependent XS for the multi-group deterministic method. The physical definition of the core for the neutron physics is complete, when the actual core geometry is provided as well.

A general overview of the pin modelled in SAS-SFR is given in Fig. 10. SAS-SFR starts from the as fabricated geometry conditions given for the pin and calculates the axial and radial expansions based on the specified power. SA diagrid pitch is also input parameter which is pre-calculated and should correspond to expansion of the diagrid plate with the nominal sodium temperature at core inlet. The correct input of this value results in a more accurate value of the sodium flow cross-section. Hexcan thickness is modelled explicitly whereas the heat transfer area of the hexcan with the sodium within the hexcan wrapper is

[7] For instance: upper gas plenum zone is composed of the same pin bundle, but doesn't contain fuel, while upper sodium plenum, in accord to the design, is composed of inner sodium, hexcan and outer sodium.

only simulated to that amount correlated with one pin out of the total number of pins within a SA. Thus it is ensured to represent the thermal inertia of the hexcan appropriately. A similar approach has been selected to account for the wires. The sodium outside the hexcan (outer sodium) is modelled implicitly, assuming the same thermal hydraulic state parameters as sodium inside the hexcan.

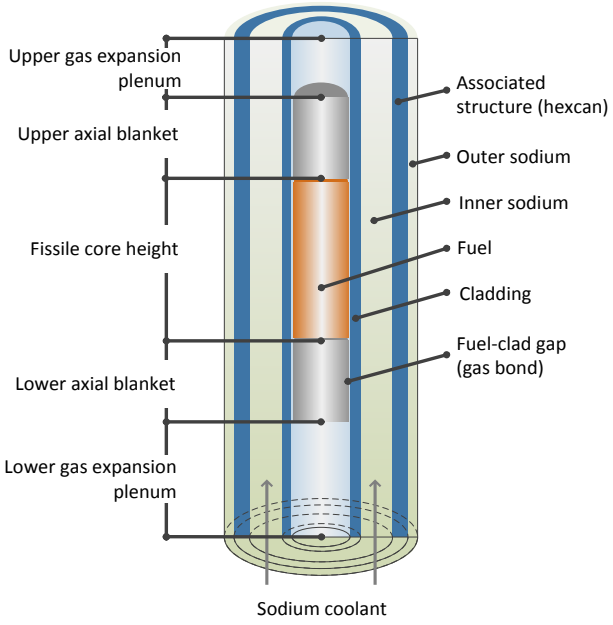

Fig. 10. The overview of SAS-SFR pin model

Thus for the pin fissile section the SAS-SFR node models employ explicit treatment of four main components: (1) fuel, (2) pin cladding (3) sodium within pin bundle and (4) hexcan material. For both steady state and transient simulation SAS-SFR provides actual masses and temperatures for the given four components[8], as well as the node height and relevant dimensions of the fuel pellet and pin cladding. The thermal-hydraulic behavior of the inter-wrapper sodium is not at all considered in the frame of the SAS-SFR simulation approach. For the other component – the inter-subassembly, or "outer" sodium – additional assumptions have been selected. General formulations are given below which are valid for all core states before onset of the material relocation phase, while corresponding assumptions for treating the materials motion phase are mentioned separately.

1) Fuel:

Fuel mass conservation for a thermally expanded node height is guaranteed in the fuel expansion model of SAS-SFR, which employs a Lagrange-type calculation mesh. Thus the height for every node is calculated independently. Fuel expansion is predicted by sophisticated pin thermal and mechanics models[9], which account for fuel-cladding gap

[8] Generally, it is not always true in point of availability of the data within the code and additional calculations are required and have been implemented for some state parameters of interest.
[9] Fuel expansion is calculated in DEFORM-IVC for pre-irradiation phase, steady state and transient conditions.

conditions defined by thermal and mechanical interaction of fuel pellet and cladding, burnup level and pre-irradiation history, while the expanded node height is derived considering mass conservation. The mass is not conserved for the node after the start of the fuel motion. For this phase of the transient the node expansion is not calculated and the channel fissile height is fixed, since pin integrity is lost after fuel pin failure or brake-up. With regard to the node fuel temperature, the enthalpy-averaged fuel temperature is used in the original SAS-SFR PK model for calculation of Doppler feedback and has been considered in this work as well.

2) Cladding:

The cladding axial expansion and the corresponding nodal mass variation are connected to the fuel expansion, defined by the same phenomena of pin thermo-mechanical conditions. In the SAS-SFR models the cladding can expand axially "free", as in case of fresh fuel, or partially "linked" to the fuel, as for high burnup level. The cladding mass and temperature are calculated for each node of the pin section. The radial pin expansion influences another component – the inner sodium inventory – due to a corresponding variation of the available coolant flow cross section within the pin bundle.

3) Inner sodium:

The inner sodium mass is calculated in SAS-SFR for a given core state (temperature, pressure, single or two-phase) and the associated volume, defined by the node height and flow cross section. The latter is derived by accounting for the pin radial expansion; while the assumption is used, that the inner hexcan perimeter is only varying marginally. By this assumption the input value corresponding to the steady state conditions can be considered constant for the whole transient time scale. For all nodes within and outside (i.e. sodium plenum) the pin section the predicted inner sodium mass, for both single and two-phase flow, and its average temperature are considered in this work.

Not all information necessary for the performance of neutron physics calculations can be deduced from information provided by SAS-SFR. In order to accomplish the formulation of data transfer to the neutron physics model the following assumptions have been taken into account within the framework of the reactivity effects selected for modelling of a ULOF in section 2.1:

Subassembly diagrid pitch size:

The diagrid pitch size of SA defines the size of corresponding neutron physics nodes in a plane. It is calculated for the nominal operating conditions as result of diagrid plate expansion as function of inlet sodium temperature. For the fast ULOF transients the reactivity effect related to potential inlet temperature variations acts on a time scale of a minute. For the actual data exchange it is assumed that the SA pitch does not vary during the considered time scale. Hence, the pre-calculated value referring to the steady state conditions has been used.

Hexcan treatment:

For both steady state and transient conditions the treatment of "free" expansion driven by node hexcan temperature has been assumed in this work. Steel mass of the hexcan within a node is calculated as a function of the average nodal temperature. In the SAS-SFR PK feedback model the hexcan is accounted in the reactivity balance only after a material

relocation takes place. In this case the hexcan-related reactivity is calculated in a similar way to clad motion reactivity, assuming corresponding reactivity effect from the molten hexcan material motion.

Outer sodium (inter-subassembly sodium):

In the SAS-SFR PK feedback model the outer sodium inventory is respected only implicitly, considering the same transient state of the sodium and its associated reactivity contribution according to its volumetric fraction, which is prescribed by the input. The outer sodium volume fraction doesn't vary significantly, because the hexcan radial expansion after transient start is very moderate within the considered ULOF time scale. Therefore, here it is assumed that the outer sodium volumetric fraction remains constant during both steady state and transient simulations, while the mass is calculated as function of the temperature of the inner sodium before boiling onset. After boiling onset of the inner sodium different strategies have been considered for handling the outer sodium mass in the calculation[10].

The component masses of a node have been used to calculate the isotopic number densities for a given isotopic vector. It is important that the same component treatment is effectively employed in the material relocation phase, because additionally to the sodium voiding a significant mass variation of fuel and cladding occurs. The remark here should be made with regard to the treatment of a partial or complete loss of the pin structure integrity yielding a loss of heterogeneity of the corresponding unit cell. This "hypothetical" negative reactivity effect is evaluated for the SFR core at a level of about 2-3 β_{eff}[11]. If the core fraction represented by the disrupted nodes and amount of relocated fuel and clad materials is relatively low, this effect of the loss of the heterogeneity can be excluded from further considerations.

2.2.2 PECULIARITIES OF GEOMETRY MODELLING FOR DIFFERENT NEUTRON PHYSICS SOLUTIONS

With regard to core geometry, the nodal axial expansion translates into a change of the fissile core height. Using the Monte Carlo (MC) method to compute the neutron transport the core can be modelled with minor approximations, accounting for the structure, dimensions and content of every node. The microscopic cross sections libraries of the core comprising nuclides are prepared for a given temperature based on continuous energy libraries, such as JEFF31 [66] or ENDF-B [67]. Currently MC methods do not provide an effective time dependent solution and are still extremely time consuming (for steady state simulations) compared to deterministic methods. Nevertheless, the availability of MC neutron physics solutions coupled to SAS-SFR can provide a powerful basis to obtain a reference solution for the steady state. In this work the coupled solution with the MC code MCNP [69] has been realized to obtain a precise steady state solution. In more details the approach and the practical implementation are discussed in chapter 3.

[10] Basically, the strategies can be assumed from one of a simultaneous boiling of the inner and outer sodium to one of no boiling occurred at all, while an "intermediate" case assumes a slight delay in time of the boiling of the outer sodium. In the approach currently implemented the boiling of outer sodium occurs, if the inner sodium void fraction exceeds some value, prescribed by the input, while further simultaneous boiling is considered for a higher void fraction of the inner sodium. The value of 0.5 has been considered as a default parameter.

[11] For ESFR Reference Oxide core it is evaluated by about -800 pcm (with β_{eff} equal to 390 pcm) [68].

With regard to deterministic methods, the individual channel expansion calculated by SAS-SFR has to be treated in conjunction with some assumptions, because most of the appropriate deterministic codes employ identical axial mesh sizes in a plane. Typically an averaged core height and updated axial mesh is derived as result of an average core expansion on the basis of a core wide averaged fuel temperature. A new approach, named here "smeared-out geometry"[12] model, has been analysed and further developed in this work [70]. It includes all advantages of the individual thermal expansion modelling of the SAS-SFR code while it allows simultaneously for a "decoupled" axial node representation with respect to neutron physics and thermal-hydraulics calculations.

Different code options have been evaluated as potential candidates to implement the envisaged approach in a coupled multi-physics simulation. Transport solutions are more time consuming, as compared to diffusion ones. Some transport codes employ square geometry, what defines additional peculiarities of the coupling related to the mapping of the calculation nodes in plane. On the other side, diffusion solutions have been used effectively for SFR neutron physics evaluations although they are accompanied by some drawbacks.

A key point for the deterministic neutron physics analysis is the XS feedback model. The calculation of the nodal XS using lattice neutron physics codes for representative material zones of the core "on-line" is rather time consuming. The alternative methods include XS look-up tables or parametrization with regard to core state parameters, [71] and [72]. Nevertheless, both of them exhibit drawbacks especially if large variations of the state parameters of the unit cell material components are to be modelled[13].

One of the other sophisticated approaches is the background cross section method. In this case, the XS are derived for a given unit cell composition based on a pre-calculated library of self-shielded microscopic cross sections. This approach has recently been adopted in the FAST code for the PARCS neutron physics solver [73]. The potential of this method to account for a significant variation of the material content within a unit cell has been pointed out as an advantage for the modelling of the material relocation phase. The PARCS solution supplied with the XS calculated by "Sigma-zero" model has been tested for SFR and GFR reactor transients [73]. Further applications of PARCS with this XS model for SFR have been reported [74], where sodium boiling has been considered. The experience accumulated with the code PARCS for the SFR modelling, along with all considered drawbacks and advantages facilitated the choice of this code for the coupled simulation in this work. Within the scope of a close cooperation of KIT and PSI, Switzerland, the "Sigma-zero" model with dedicated libraries has been provided for implementation and use in this work. The improvements provided within this work refer to a more accurate neutron physics data preparation for the calculation nodes of PARCS and the corresponding XS.

[12] Later on named as "smeared geometry"

[13] Essentially during material relocation phase a considerable change of component mass e.g. fuel or clad mass, should be treated in preparation of XS, what can be hardly modelled via XS parameterization as typically used for LWRs.

2.3 SELECTED NEUTRON PHYSICS SOLUTIONS

2.3.1 DETERMINISTIC SPATIAL KINETICS SOLUTION: PARCS

The PARCS code – Purdue Advanced Reactor Core Simulator – is a reactor core simulator, which has been developed at the Purdue University [75]. It is originally intended to simulate LWRs transients and solves the steady state and time-dependent multi-group neutron nodal diffusion or simplified P_3 (SP_3) transport equations in square and hexagonal (only diffusion) geometries. With regard to fast reactor applications, PARCS was integrated into the FAST code system for the purpose of spatial kinetics calculations of SFR.

The spatial kinetics solution of PARCS involves different computational methods integrated into PARCS in a modular form. The temporal discretization employs the theta-method with an exponential transformation and a second-order analytic precursor integration technique. The temporal discretization scheme allows sufficiently large time step sizes even in severe transients involving super-prompt critical reactivity insertion. With regard to the SFR relevant hexagonal geometry PARCS provides the multi-group nodal diffusion kernel based on the Triangular Polynomial Expansion Method (TPEN).

In a typical calculation procedure of PARCS, the macroscopic cross sections (XS) are used to compute the reference state, while their derivatives with respect to state variables (assuming a linear dependency of the different effects) are used to account for the reactivity feedbacks. The XS parameterization has been modified within the framework of PSI's FAST project in order to enable a fast spectrum reactor analysis [22]. Lately PARCS is successfully applied for transient simulations of GFR and SFR with TRACE as part of the FAST code system, [80] and [51][14].

Recently the TRACE models were extended for sodium coolant [26] and for simulation of two-phase sodium flow (sodium boiling phenomena). Its application together with the PARCS spatial kinetics was reported in [81] for the Initiation Phase of a ULOF transient with boiling up to the onset of clad melting. For this studies, the FAST code system version with a new XS generation model – background cross section σ_0 [73] – has been used.

2.3.2 MONTE CARLO SOLUTION FOR STEADY STATE: MCNP

The Monte Carlo neutron transport simulation code MCNP6 [69] has been used for three dimensional neutron physics calculations coupled with SAS-SFR. The Monte Carlo method allows a simulation with only a minimum of assumptions, because the code offers the capability to model almost any detail of a core with respect to the SA and the fuel pin design. The JEFF3.1 neutron cross section library has been used in the simulations in this work [66]. Monte Carlo codes have been extensively used to analyse core designs of fast reactors without taking into account local feedbacks between neutron physics and thermal hydraulics, see e.g. [49] and [82].

[14] One of the earliest applications of the coupled PARCS and TRACE codes to a fast-spectrum system is reported in [76]. A modified model of the CAPRA-CADRA gas-cooled core has been used for test calculations of steady state and transient behaviour, while the results have been compared with the ERANOS [77], [78] and KIN3D [79] codes.

2.4 SFR DESIGN FOR STUDY AND ULOF CASE SET-UP

2.4.1 ESFR REFERENCE OXIDE CORE

To demonstrate the capabilities of the new coupled simulations the Reference Oxide core of the CP ESFR project is taken as basis [55]. The ESFR core general data are listed in Table 3. It is a core for a large 3600 MW_{th} power reactor with an equivalent radius of about 250 cm and an active fissile core height of 100 cm. The fissile core consists of inner and outer sub-cores with different Pu content (225 SAs with 14.1% and 228 SAs with 16.4%) to flatten the radial power distribution. It is surrounded by rows of steel reflector subassemblies, while no fertile breeder zones are considered. The SA of a conventional design contains 271 MOX fuel pin bundle with the triangular arrangement within a hexagonal wrapper tube (hexcan), where the pins are separated by helically arranged wire wraps. A so called "sodium plenum" of 15 cm height is located in each SA above the pin section. A cross sectional cut in the core mid-plane illustrating the core SA arrangement of the inner and outer sub-cores and control rods positions as well as the power distribution in one third of the core is illustrated in Fig. 11 (left). The corresponding axial structure of the fissile core SA is depicted in Fig. 11 (right). The Reference Oxide core differs from the "Working Horse" design by a modified upper SA part representation and includes the regions of upper gas plenum, upper reflector and sodium plenum above the pin section.

Table 3. General data on ESFR Reference Oxide core design

Parameter	Unit	Value
Total reactor power	MW_{th}	3600
Nominal operating conditions:		
Core-average fuel temperature	ºC	1227
Core-average structural materials temperature	ºC	470
Sodium inlet/outlet temperature	ºC	395 / 545
Core fuel:	-	$(U, Pu)O_2$
Fuel average density*	%TD	88.8
O/M ratio	-	1.98
Pu content in fresh fuel:		
Inner core	mass%	14.05
Outer core	mass%	16.35
Volume of the core	m^3	18.70
Equivalent core radius	m	2.44
Height of the core	m	1.00
Volume fractions in the core:		
Fuel fraction	%	52.36
Sodium fraction	%	27.60
Structure steel	%	20.04
Number of SAs:		
Inner core	-	225
Outer core	-	228
Number of control rods (CSD/DSD)	-	24 / 9
SA external across flat size/pitch	mm	206.3 /210.8
Number of pins in SA	-	271
Pin parameters:		
Pin outer diameter	mm	10.73
Pellet outer diameter	mm	9.43
Clad thickness	mm	0.50

*Fuel average density accounts for both the porosity of the fuel pellet and also the central helium hole and is normalized to the fuel pellet diameter

The Beginning Of Life (BOL) core state is selected for the simulations. The core state is characterized by a strong radial non-uniformity with the peak power subassembly located in the outer sub-core on the boundary between the two sub-cores (see SA power map in Fig. 11 (left) as calculated using the KANEXT code system within the CP-ESFR project [41]. Important safety parameters calculated for the Reference Oxide core at BOL conditions are given in Table 4. The kinetics parameters of the ESFR core at BOL conditions are listed in Table 5, as evaluated in the CP-ESFR project.

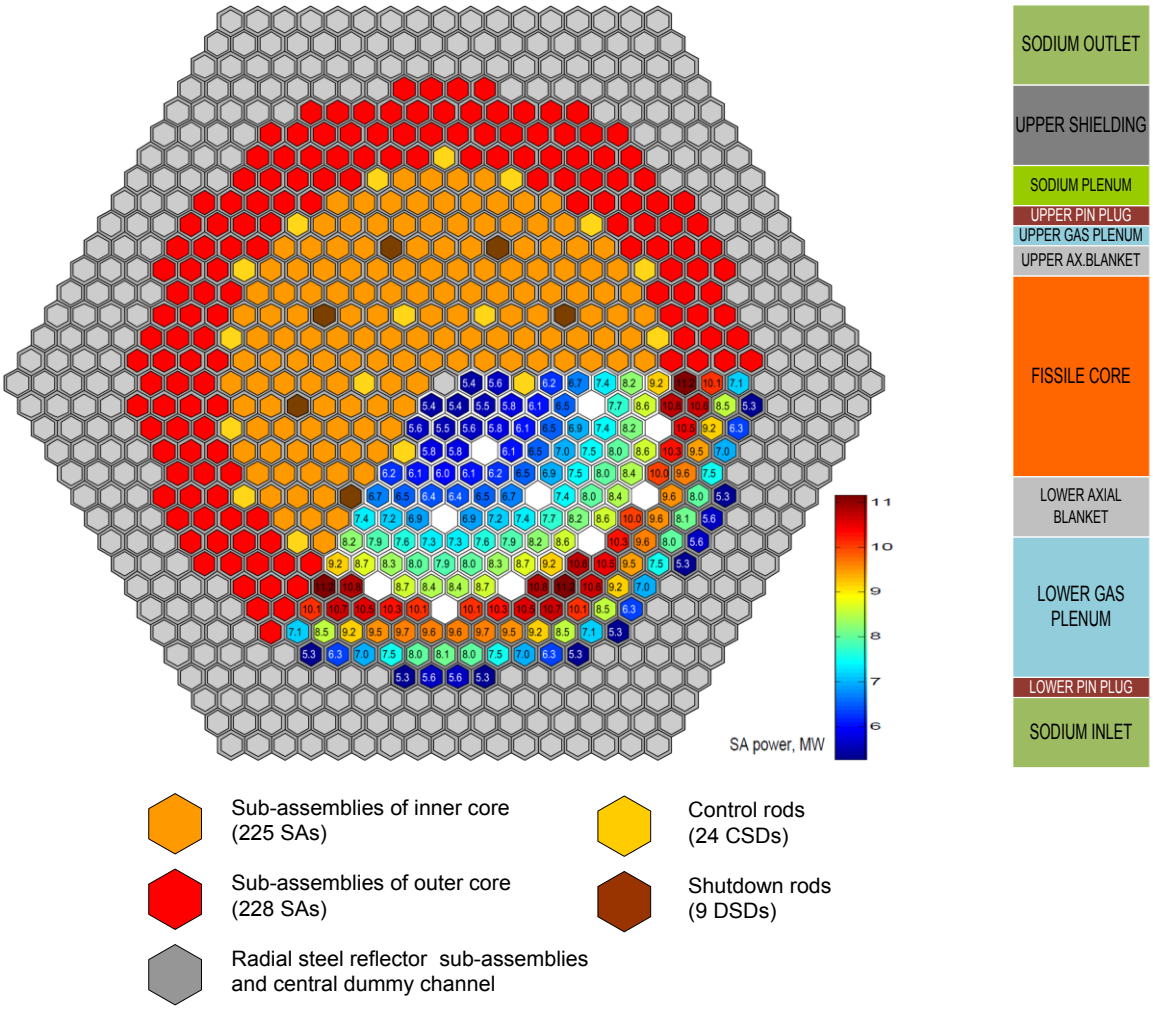

Fig. 11. Cross sectional cut at the core mid-plane of the ESFR "Reference Oxide" core and corresponding nominal power radial distribution (left) and axial structure of a SA (right)

Table 4. Safety parameters of ESFR Reference Oxide core at BOL state calculated at nominal operating conditions

Safety parameter	Calculation tool		
	ERANOS	KANEXT [41]	MCNP
Doppler constant, pcm	-1150	-1094	-1115
Doppler constant at "voided" conditions[15], pcm	-	-860	-858
SVE in fissile core, pcm	1750	1784	1600
SVE in fissile core and upper core regions, pcm	-	1656	1510
Sodium density effect, pcm/K	-	0.448	0.498

Table 5. Kinetics data of ESFR Reference Oxide core at BOL state [41]

Parameter		Value					
Effective delayed neutron fraction β, pcm		389.0					
Prompt neutron generation time Λ, 1/s		$4.95 \cdot 10^{-7}$					
Group parameters	Yield β_i	Group i					
		1	2	3	4	5	6
		$8.169 \cdot 10^{-5}$	$7.313 \cdot 10^{-4}$	$6.224 \cdot 10^{-4}$	$1.443 \cdot 10^{-3}$	$7.547 \cdot 10^{-4}$	$2.567 \cdot 10^{-4}$
	Relative yield β_i/β	0.021	0.188	0.160	0.371	0.194	0.066
	Decay constant λ_i, 1/s	0.013	0.031	0.119	0.319	0.954	3.015

2.4.2 CHANNEL REPRESENTATION OF ESFR CORE

The accurate allocation of SAs into groups – channels – allows simplifying the modelling of a core design. Usually the core is adequately represented by 10 to 30 channels in analysis with SAS-SFR, depending on the specific characteristics of the considered problem, though the current version of the code allows to consider up to 200 channels for the fissile core. A larger number of channels become necessary for a more accurate prediction of boiling and material relocation phases, while few channels representation is typically appropriate to depict the pre-boiling phase.

The allocation of channels takes into account the following aspects:

(1) fuel composition (fertile or fissile, different initial fissile fraction);
(2) sodium coolant mass flow rate;
(3) burn-up history;
(4) subassembly design;
(5) transient conditions;
(6) position within the core cross section.

The last criterion is practically not of interest for the PK model. The SAs with almost identical power and power-to-flow ratio can be treated as one channel, providing one cumulative reactivity response. Power in every channel, defined by the initial radial power shape in the PK model, will increase or decrease also simultaneously, according to the normalized power

[15] "Voided" core conditions are considered as all sodium is removed from core fissile height region.

amplitude predicted by the PK solution. It results in an identical transient phenomenology with no specific consideration of the SA position.

In contrast to this, for the spatial kinetics, which evaluates changes in the spatial power distributions, the individual SA position is of significant importance when determining the channel allocation scheme.

The coherent transient behaviour of subassemblies with a similar burn-up history is mainly defined by the ratio of SA power to the coolant mass flow at steady state conditions. Simultaneous events, such as sodium boiling, should be expected in all SA's of a given group (one channel). The study on different channel representations of the SFR core and its impact on the transient phenomenology progression can be found in [40]. The optimization of the SA arrangement into representative channels is code-specific, because the main issue is minimising of the consequences of the SA grouping on the prediction of a generalized phenomenology of the transient with appropriate calculation costs. Hence, a scheme optimized for one power distribution map may be not fully suitable for another one, obtained with different neutron physics (and TH) solutions, especially in case of modelling of a burnt core configuration with reloading scheme.

For this work, the 10 channels allocation scheme for the BOL core configuration has been selected for the analyses as proposed for ULOF simulations in the ESFR project with the original version of SAS-SFR. The channel allocation maps assuming a 120°- and the 60°-symmetry of the core are illustrated in Fig. 12.

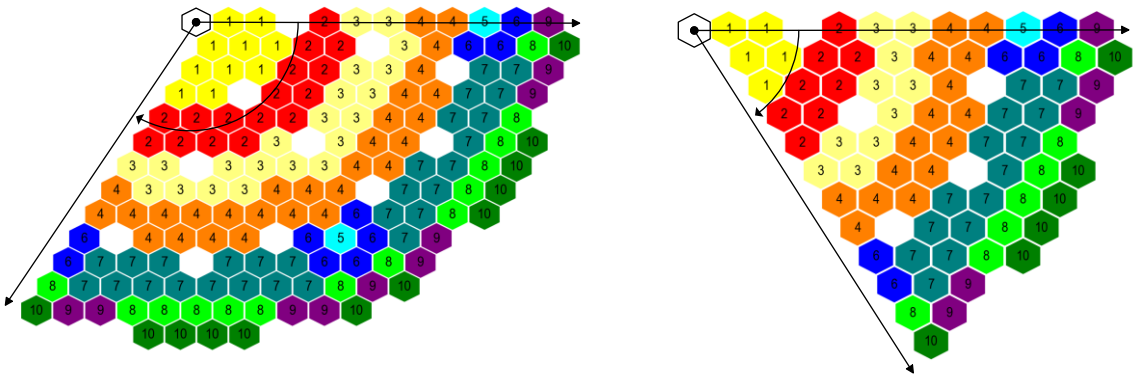

Fig. 12. Channel allocation maps for the ESFR core at BOL state assuming a 120°- (left) and 60°-degree (right) symmetry in model (numbers denote channel type, open hexagons correspond to the control and safety rods positions)

The 10 channel core representation provides the option to evaluate appropriately the important phenomenology of a ULOF transient studied in the CP-ESFR project. The channel allocation scheme has been selected on basis of the following criteria:

- two core sub-zones with different initial plutonium content (inner and outer sub-core);

- three cooling groups with different coolant mass flow rates as optimized for EOEC core conditions;
- individual SA power differences within one group from the average value of the channel are minimized;
- SAs with the highest power are grouped into one channel.

For the given channel allocation scheme two coolant flow gagging schemes have been considered in this study (see Table 6):

- First option is a configuration with 9 different cooling groups (CG) which considers an identical sodium heat-up of 150 K for all channels except the channel #5 with the highest power. For this work it has been taken as an effective basis for comparison evaluations.
- The second option considers only 3 cooling groups: one is applied in the inner sub-core and two are applied in the outer sub-core, as it was proposed as a realistic configuration for the ESFR core at EOEC. Considerable differences in the individual power-to-flow ratios of the ten channels for the two gagging schemes lead to a different transient behaviour of the core.

Highest values of the power-to-flow ratio in Table 6 are marked by red colour (channels #8 and #5 for 3 CG and 9 CG configurations, respectively).

Table 6. Channel parameters for two different coolant flow gagging schemes

Ch. #	Number of SAs		Position in core	Fraction of total thermal power [%]	Average SA power [MW]	Average SA mass flow [kg/s]		Power-to-flow ratio [MW/(kg/s)]	
	120*	60*				3 CG	9 CG	3 CG	9 CG
1	30	30	Inner	5.57	6.64	47.7	34.2	0.139	0.194
2	48	48		9.46	7.04	47.7	36.3	0.148	0.194
3	63	60		13.31	7.56	47.7	39.0	0.159	0.194
4	84	90		18.84	8.02	47.7	41.4	0.168	0.194
5	6	6	Outer	1.85	11.00	44.2	53.4	0.249	0.206
6	30	30		8.68	10.34	44.2	53.4	0.234	0.194
7	84	84		21.91	9.33	44.2	48.1	0.211	0.194
8	42	42		9.28	7.90	26.8	40.8	0.295	0.194
9	30	30		5.70	6.79	26.8	35.1	0.254	0.194
10	36	36		5.41	5.38	26.8	27.7	0.201	0.194

* core model symmetry representation

2.4.3 ULOF CASE SET-UP

Results of transient analyses are determined to a large extent by the core and primary system design characteristics, the steady state power operation history and the neutron physics characteristics of the different core configurations. For simulation of the ULOF, a coherent primary pumps coast down is assumed[16]. This is modelled on the basis of the specified coolant mass flow halving time constant $t_{1/2}$ as follows:

[16] The primary sodium circuit consists of three to four branches with three to four primary pumps. All primary pumps fail simultaneously according to the same time dependence.

$$\frac{m_c(t)}{m_c(t=0)} = \frac{t_{1/2}}{t+t_{1/2}},$$

where m_c is the coolant mass flow in *kg/s*, *t* – time and $t_{1/2}$ – the coolant mass flow halving time constant in *s*, which is defined equal 10 s, according to the ESFR primary circuit design data.

The primary system has been modelled within the capabilities of the PRIMAR-4 model of SAS-SFR according to the model description (see §1.3.1). In SAS-SFR the reduction of the primary coolant flow rate is explicitly calculated by specifying the reduction of the pump head as a function of time. The reduction of flow in the secondary circuit and the feed-water flow-rate (heat sink-ternary system) is not simulated explicitly. For the short time period of the considered transient it is assumed, that the temperature drop along the IHX is not significantly modified [41]. This approximation has been selected on basis of a more detailed analyses by means of the SIM-SFR code system for the ESFR and similar core cases [15]. The imposed temporal change of the pump head results in a transient variation of pressures in both the core coolant inlet and the core outlet plenum, which in turn yields a pressure difference variation between the plena. Respective transient variations, primarily dictated by the characteristics of the pump head up to boiling onset are illustrated in Fig. 13.

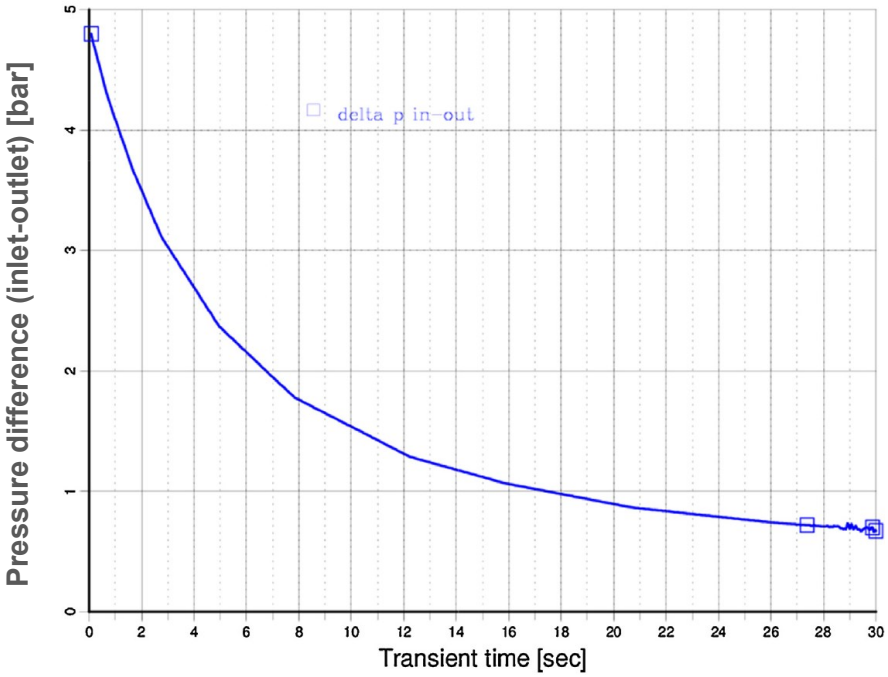

Fig. 13. Transient variation of the pressure difference between inlet and outlet plena of the ESFR core assuming a 10 s coolant mass flow halving time constant [41]

3 EXTENSION OF SAS-SFR CODE CAPABILITIES FOR STATIONARY CONDITIONS AND APPLICATION

This chapter describes the coupled simulation methodology for the steady state SFR core using SAS-SFR and the MCNP codes and its application. The coupled simulations for core stationary conditions are broadly presented in literature for different neutron spectrum reactor types. Considerable increase of computational capabilities nowadays allows to establish "high-fidelity" coupled solutions on the basis of sub-channel and CFD thermal hydraulics and Monte Carlo neutron physics which demonstrate advanced capabilities for the core representation, [83] and [84]. The coupled code systems Serpent 2/SUBCHANFLOW [85], ATHLET-MCNP [86], TRIPOLI/SUBCHANFLOW [87] and MCNP/StarCD [88] have been developed and applied exclusively to LWR core analyses.

With regard to SFR the steady state core characterization is given, for instance, in [89], where the Monte Carlo code MCNP and the sub-channel code COBRA-IV [90] have been applied. In [91] the coupled multi-physics simulation tool FRENETIC is presented for the quasi-3D analysis of a Lead-cooled Fast Reactor core with a hexagonal SA geometry. Within the FAST code system [22] the core steady state characterization is prepared for different fast reactor types (SFR, GFR, LFR) using for TH the advanced code TRACE extended by options allowing the use for different coolants and fuels and spatial kinetics code PARCS for neutron physics. On basis of different methods of the XS generation with the help of the deterministic code system ERANOS and the MC code SERPENT [92], different options are available in FAST for core neutron physics representation.

3.1 COUPLED NEUTRON PHYSICS, THERMAL HYDRAULICS AND PIN MECHANICS CODE SYSTEM SAS-SFR/MCNP

Alternatively to the approaches mentioned above, this work uses the two codes SAS-SFR and MCNP to establish a reliable characterisation of the steady state (SS) condition of the SFR design. Herein, an "explicit" coupling scheme is employed for the coupled simulations of the steady state (SS) core conditions by considering the operator splitting technique. Both of the codes – SAS-SFR and MCNP – perform the calculations starting from input data based on design specifications. With regard to practical implementation, the coupled calculation route is defined as external coupling performed in a straight forward manner, where the codes exchange information via data files after the end of each iteration step controlled by a driver program. All data processing is developed in a Python platform allowing compatibility with existing Python-based tools used (TSP [93] and PIRS [94], which are discussed hereafter).

3.1.1 OVERVIEW OF THE COUPLED CODE SYSTEM

The coupled calculation scheme and data flow of new code system is shown schematically in Fig. 14. The coupled simulation is initialized by a SAS-SFR run. To calculate accurately the SS parameters the SAS-SFR code requires power data as input for

each calculation node, which is assumed unchanged during one SAS-SFR run[17]. Predicted thermal hydraulics (TH) parameters are passed to the neutron physics solver, i.e. MCNP, for the accurate prediction of the three-dimensional power distribution taking into account local feedback effects typical for SFR. In this way, the output data of one code should be provided as input to the other one. Finally, the iteration loop will be stopped if all convergence criteria defined in the driver program for both neutron physics and TH parameters are fulfilled, i.e. no further changes observed of the power values supplied to SAS-SFR code and no changes in resulting core parameters and expanded geometry transferred to the MCNP calculation.

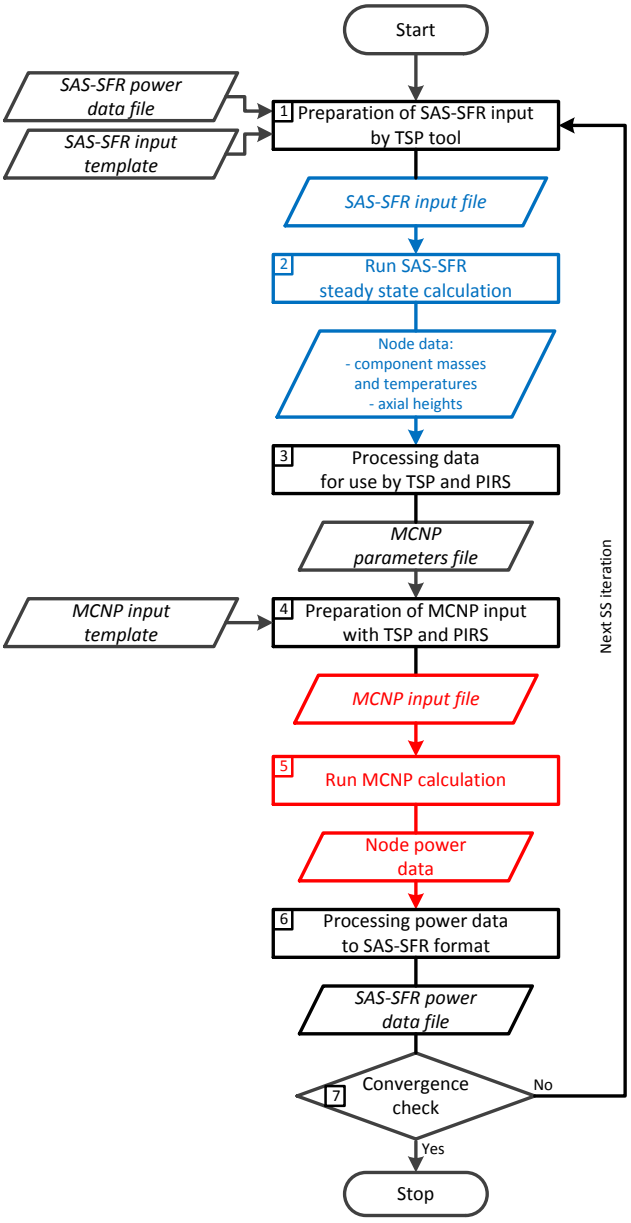

Fig. 14. SAS-SFR/MCNP coupled calculation scheme and data flow

The application of the methodology given in §2.2.1 for the transfer of relevant information from SAS-SFR to MCNP is described in more details in Appendix I. The information

[17] Update of power data during one steady state run is not possible without noticeable modification of the actual structure of the code

exchange between the two domains is performed according to a mapping of the neutron physics and TH spatial resolutions, which is organized in a straight-forward manner, as follows:

- Radial mapping: Sub-assemblies are allocated to channels corresponding to the input map given by MCNP input. The map defines associated channel number for subassemblies in a similar way, as given in Fig. 12 above. This input is supported by the original MCNP input deck defining the subassembly type (i.e. channel type) in core cross-section and corresponding material content.
- Axial mapping: For coupled nodes, in accord with formulations of §2.2.1, the approach provides the equivalence of nodes in TH and neutron physics models, respecting the peculiarities of the code input. For instance, the same number of nodes and identical node heights are considered for representation of the fissile height pin section.

3.1.2 IMPLEMENTATION OF THE COUPLED CALCULATION

In current implementation the driver routine for the coupled calculation is written as a shell script program that calls the codes and the Python programs processing the code's outputs and preparing the input files. The data flow shown schematically in Fig. 14 consists of the following steps:

1. Create a *SAS-SFR input file*, using an existing (initially prepared) *SAS-SFR input template* and a *SAS-SFR power data file*. For input preparation the TSP tool [93] is used at each iteration step. For the first run some initial guess is to be taken (e.g. uniform or cosine for the axial power shape).

2. Run the SAS-SFR code and write the relevant parameters calculated for each axial node of each channel to the *SAS-SFR parameters output file*. Depending on the logic of considering them in the neutron physics model, different treatment can be considered. The selected node parameters for the neutron physics model are height, masses of fuel, clad and sodium and their average node temperatures[18].

3. Process the new data and obtain corresponding *MCNP parameters input file* with data to be read by TSP and PIRS [94] tools used for preparation of the MCNP input[19].

4. Create an *MCNP input file* with the help of TSP and PIRS based on the initially prepared *MCNP input template*. Generally, all relevant data (axial height, components densities and their temperatures) are updated at each iteration step for the core regions important for neutron physics (e.g. fissile height, upper sodium plenum etc.).

5. Run MCNP and obtain power data calculated at given iteration (as a part of the original code output).

[18] These data are described in more details in the Appendix I and summarized in the second column of the Table A-I.1 of the Appendix

[19] These data are described in more details in the Appendix I and summarized in the third column of the Table A-I.1 of the Appendix

6. Process power data in accord with a relaxation scheme (described hereafter in more details) and obtain node and channel power data suitable for SAS-SFR input format, store it as a new *SAS-SFR power data file*.

7. Check convergence criteria (fuel temperature change, relative change of node power).

The idea behind the use of the TSP and PIRS tools is that they are processing programs to compute the necessary data and insert them into a template file (input file), which is prepared in advance. Thus some parts of the input file have been written manually to the template, and generation of the rest has been coded in Python. In addition, the PIRS tool transfers the material data, such as physical densities and temperatures, calculated by the processing subroutines of the coupled scheme at every iteration step to the format of atomic number densities, which can be used by MCNP, including the processing of temperature data.

The steady state SAS-SFR results are sensitive to variations of node power values in input, and they are the only relevant data for SAS-SFR to be provided from a neutron physics code with a certain level of accuracy. The relaxation technique implemented in MCNP to minimise statistical fluctuations influence results of power values as described in [95]. The only difference introduced within the scope of this work is after preliminary tests that the statistics and weight of the iteration value are not modified from one iteration to another.

Here, it is worth mentioning that in [89] another scheme is used for a similar problem, considering the MC method in neutron physics evaluations. In particular, the convergence of the coupled solution (between MCNP and COBRA) is achieved in [89], when the relative temperature difference between the previous step and the actual is smaller than the established ε criterion, thus, without a relaxation scheme, while a relatively high statistics is used for the MCNP simulation[20]. This leads to a situation that the required convergence for the considered problem is achieved in only a few iterations.

The computation time of the iterative procedure is fully determined by MCNP runs, because SAS-SFR calculations are relatively fast. The simulation starts from a uniform power distribution (identical power density in all core regions). For all studied cases 50 iterations are calculated with 5 million particles in active cycles of each MCNP run. The standard deviation of the criticality eigenvalue K (K-effective) for one MCNP run is 20 pcm, while the standard deviations of node power values depend on the location and total volume of the concerned region where the statistics are observed: typical error values varies for different channels and axial node positions from less than 1% up to 10%. In the last iterations the maximum iteration variation of relaxed node power is observed to remain below 0.02%. The fuel temperature iteration variation normally remains below 0.3 K, but due to a SAS-SFR fuel-clad gap model peculiarity a prompt jump of 3-6 K may occur at some nodes[21].

[20] 2 million particles per cycle and 150 criticality cycles

[21] The peculiarity of the larger spread of fuel temperatures is related to the fact that in some conditions dependent on burn-up or linear rating the fuel to clad gap may become just closed which results in a rather large gap heat transfer coefficient and thus a small temperature difference between the inner clad temperature and the outer fuel surface temperature. If now in the sequence of an iterative determination of the relaxed linear power value a slightly reduced linear rating in this axial node is calculated it may occur that the fuel pin mechanics calculation predicts a slightly open fuel to clad gap. Under these conditions the fuel to clad heat transfer coefficient becomes

3.2 ANALYSIS OF AN SFR CORE WITH THE NEW COUPLED CODE SYSTEM SAS-SFR/MCNP

The ESFR Reference Oxide core design has been selected to demonstrate the prediction capability of the new coupled system SAS-SFR/MCNP. In this part the used core models and other data are given, which are relevant for the establishment of the coupled simulation.

The 10 channel core representation described above has been applied in the SAS-SFR and the MCNP models of the core. The case with three cooling groups (3 CG) has been considered, which is characterized by large differences of power-to-flow ratios between the channels. This resulted in considerable differences of the sodium heat-up and outlet temperatures of the different coolant channels. It is worth to mention, that this set-up provides an unusual core thermal state at SS and for transient conditions, as result of a strongly non-uniform radial power shape, reasonably well suitable for practical exercises but not really fully representative of a realistic core configuration for BOL conditions. The outer row of CRs is inserted by 30 cm into fissile core height in order to reach a critical core state, what slightly mitigates the power density peaking factor. The CRs insertion impact will be demonstrated in the analysis of results.

3.2.1 THE SAS-SFR CORE MODEL

For every channel the following axial sections from bottom to top of a subassembly (SA) containing fuel are simulated within SAS-SFR as shown in Fig. 15:

- SA thimble insert into the grid plate;
- transition section from the thimble to the lower fuel pin support plate;
- pin section:
    - lower gas expansion plenum section of the fuel pin (LGP);
    - lower axial steel blanket section (LAB);
    - fissile height of the fuel pin;
    - upper axial steel blanket section (UAB);
    - upper gas expansion plenum section of the fuel pin (including upper pin plugs) (UGP);
- sodium plenum between fuel pin and upper neutron shielding pins section;
- upper neutron shielding pins section (19 shielding pins) (UNS);
- SA outlet section.

The subdivision in axial nodes of different sections of pin and SA, which are relevant for the neutron physics domain, is listed in Table 7. Those of interest for the proposed coupled calculations depend on the considered SFR design. In this study, the fissile height, upper axial blanket (UAB), upper gas plenum (UGP) merged with pin plugs (UPP) and upper sodium plenum are treated accurately.

---

reduced when compared to the closed gap conditions. As a result the temperature drops between fuel and clad increases more strongly. This effect may lead to the mentioned values of 3 to 6 K.

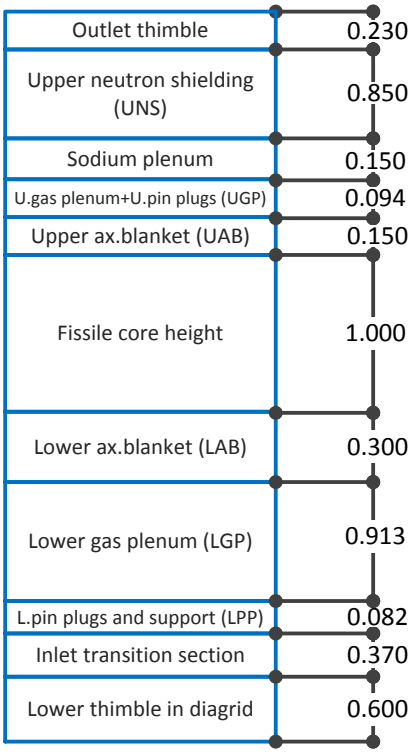

Fig. 15. Axial representation of a subassembly of the ESFR Reference Oxide core and corresponding dimensions [m] for "as fabricated" geometry

Dimensions in Table 7 are given for the average hot geometry, except for the blanket and fissile region, where SAS-SFR expects the values of the cold geometry as input data. The conditions at nominal operation temperatures are determined within the SAS-SFR code consistent with the fuel, clad and coolant heat-up of the individually simulated SA groups as well as with the impact of the different power operation histories i.e. the clad swelling and its stress – strain behaviour in case of a long term power operation. Axial section lengths of reflector regions are the ones at nominal operation temperatures.

Reference for determination of the input data for the representative coolant channel cross section and the hydraulic diameter is the geometry of the SA unit cell at nominal operation conditions. As coolant channel cross section only the cross section within the hexcan is considered. The transient behaviour of the inter-wrapper coolant is not explicitly evaluated. It is assumed that its temperature follows the one of the coolant within the hexcan structure. The mass and volume of the wires are added to the hexcan structure thickness along fuel pin height, not to violate the clad thickness important for the appropriate calculation of the stress – strain behaviour of the fuel pin clad. Thereby it is insured that the wires contribute to the thermal inertia within the transients at least approximately correct. The upper shielding pins section is simulated as a reflector with a two slab structure geometry having a thickness representing the clad and the in-pin structure material appropriately.

Table 7. Heights of coupled axial nodes of SAS-SFR/MCNP coupled scheme

Calculation node height [m]		Description of axial zone
"as fabricated" geometry	"Reference Expanded" geometry	
0.075	0.07550	Sodium plenum
0.075	0.07550	
0.094	0.09460	Upper gas expansion plenum and pin plugs (UGP)
0.075	0.07550	Upper axial blanket (UAB)
0.075	0.07550	
0.070	0.07095	Fissile core height
0.080	0.08109	
0.080	0.08109	
0.080	0.08109	
0.080	0.08109	
0.080	0.08109	
0.060	0.06082	
0.080	0.08109	
0.080	0.08109	
0.080	0.08109	
0.080	0.08109	
0.080	0.08109	
0.070	0.07095	
0.100	0.10047	Lower axial steel blanket (LAB)
0.100	0.10047	
0.100	0.10047	

The diameter of the inner fuel pellet hole is not explicitly specified in the given data sheets. However, starting from the theoretical density of 88.8% for a circular pellet with an as fabricated pellet porosity of 5%, it can be evaluated to about 2.4 mm (cold).

The PRIMAR-4 model of the SAS-SFR code calculates coolant and gas pressures, coolant flow rates and component temperatures in the primary and intermediate circuits. As it has been mentioned already it is a rather simplified representation of the primary circuit but appears sufficient for the purpose of considering transient responses of the primary circuit in case of a ULOF accident with a coolant mass flow halving time constant of 10 s (see Fig. 6).

The initial coolant inlet temperature has been set to 668.15 K, as well as the pressure at the coolant outlet plenum and the flow rates. A coolant heat-up of 150 K between coolant inlet and outlet plenum is specified. Considering the coolant mass flow through control rod and shut down rod positions as well as through reflector assemblies' positions this leads to a coolant mass flow through the core of 18453 kg/s, which is 97.5% of the total mass flow of 18926 kg/s. The calculated pressure drop over the core is 4.8 bar including contributions from SA inlet throttling and the pressure drop along the grid plate flow path.

3.2.2 THE MCNP CORE MODEL

The level of details in the MCNP model influences the neutron transport calculation. Therefore, a rather detailed geometry model has been set-up to depict the most relevant regions mentioned above. The fissile core geometry is represented in a detailed way,

considering the structures of fuel and clad, pin bundle and hexcan, allocated within the SA unit cell cross section. The upper pin part (UAB, UGP and UPP) is treated in a similar manner. The sodium plenum is represented by hexcan and sodium. Other regions are treated as homogeneous mixtures and their parameters are not updated in the course of a coupled calculation. A sketch of the model is given in Fig. 16.

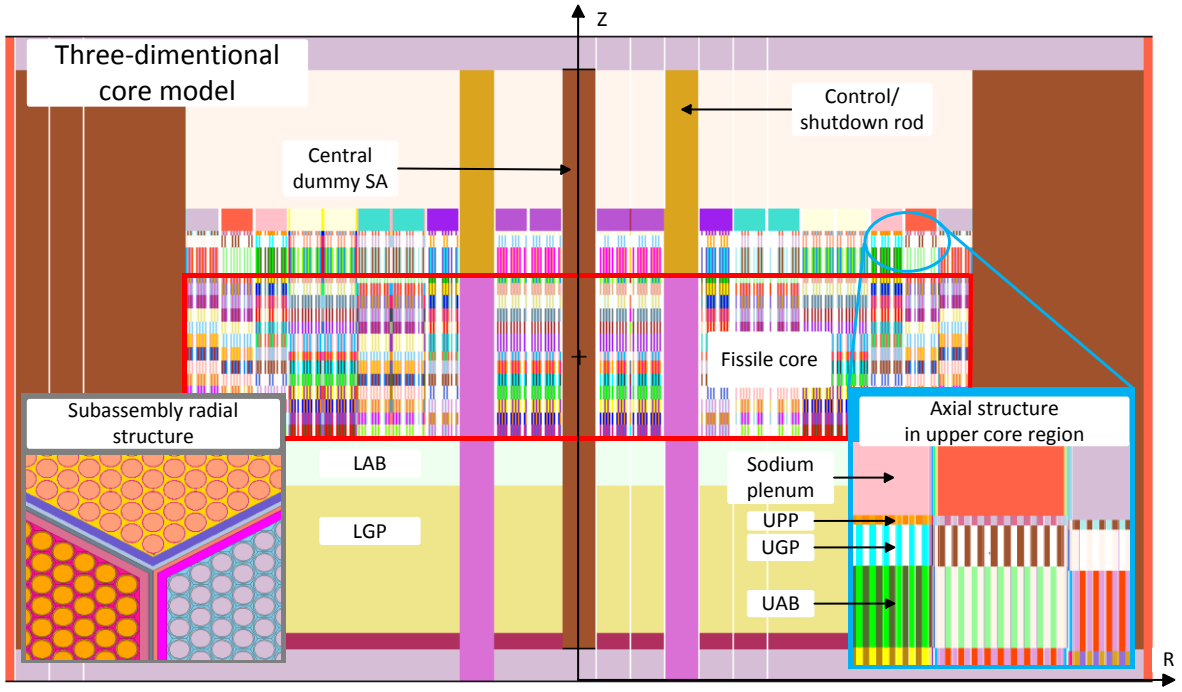

Fig. 16. Vertical cross-section overview of MCNP model of the ESFR Reference Oxide core and examples of representation of the radial SA structure (bottom left) and detailed upper pin and SA structure (bottom right)

Some reference pre-calculated averaged expanded radial dimensions for SA elements, which are clad inner and outer radius and hexcan size (available, for instance in CP-ESFR project) have been considered for the model. This allows on the one side to keep the heterogeneity description of the SA and on the other side to minimise the amount of data to be transferred to the neutron physics calculation. The MCNP input allows defining individual axial height for nodes and to supply the node with updated material component masses and temperatures. Among the geometry parameters of the neutron physics model, for all calculation segments, the variation of individual node axial height is treated directly during the coupled calculations. The applied method to transfer core state parameters for a particular MCNP model with heterogeneous pin and SA structure is given in Appendix I.

The MCNP input creation procedure includes isotope atomic fractions for fuel and construction steel. A special procedure is used to generate temperature dependent cross sections in the MCNP model, which is realised in the PIRS tool [94]. Namely, cross sections temperature dependence in MCNP is modelled by mixing cross sections at two different temperatures within one material, following [96]. In particular, the multi-temperature set of

cross sections [66] has been used (it provides cross sections at 300, 400... 1000, 1200 and 1800 K) together with own-prepared sets at few other temperatures of interest. If a material temperature T is close (within 10 K) to one of the cross section temperatures T_{XS}, it is chosen for the material representation in the MCNP model. Otherwise, two cross sections are chosen with temperatures T_{XS}^1 and T_{XS}^2 closest to T, so that $T_{XS}^1 < T < T_{XS}^2$, and the material represented by a mixture of the cross sections with the fractions f_1 and f_2, defined as follows:

$$f_1 = \frac{\sqrt{T} - \sqrt{T_{XS}^2}}{\sqrt{T_{XS}^1} - \sqrt{T_{XS}^2}}, f_2 = 1 - f_1.$$

3.2.3 RESULTS OF THE SAS-SFR/MCNP STEADY STATE CORE ANALYSIS

Results of different calculations with the new coupled scheme are discussed below and compared with results obtained with a conventional procedure. Thus results for two basic cases are discussed first:

Case 1 – "Reference Expanded" (RE): The results of steady state characterization have been obtained using the conventional procedure. The SAS-SFR model uses the power data obtained from neutron physics simulations on basis of a model, which employs some averaged expanded geometry and temperature in the core. According to Table 3, average fuel, steel and sodium temperatures in the MCNP model amount to 1500 K, 750 K and 750 K respectively. With regard to the core geometry, the MCNP model employs a detailed core geometry while a uniform average axial expansion of nodes is used as given in Table 7. A similar case set-up has been considered within the CP-ESFR project for the Beginning Of Life (BOL) core analysis based on power data, calculated with the KANEXT code [41]. For the transfer of data to SAS-SFR two options have been evaluated:

- case A1, which uses one average axial power profile, i.e. averaged over all SAs with different radial location, and
- case A2, which uses individual channel dependent axial power profiles in SAS-SFR.

Case 2 – "Fully Coupled" (FC): The results are obtained using the developed coupling code system SAS-SFR/MCNP. The core configuration in the MCNP model uses detailed distributions of the core state parameters, while SAS-SFR uses individual channel dependent axial power profiles as calculated by MCNP. The channel powers are also corrected because spatial distributions of material densities and temperatures influence the local power generation.

After a general overview of results of coupled simulations, first the results of calculation cases are used to analyse the influence of power profile input in SAS-SFR steady state simulations on spatial distribution of core parameters at steady state, what is given in §3.4.1. Second, the consequences of the choice of different power spatial distributions on ULOF transient results are discussed in §3.4.2.

Several core configurations have been calculated with MCNP in order to evaluate safety parameters, which are given in Table 8 in comparison to available data. The results show a reasonably good agreement, because several evaluations documented in [97] include also MCNP calculations for a similar core (namely, "Working Horse") and use similar JEFF3.1-based libraries.

Table 8. Comparison of Doppler coefficient and Sodium Void Effect (SVE) for ESFR Reference Oxide core for a MCNP and a coupled SAS-SFR/MCNP simulation.

Safety parameter	Calculation tool	
	MCNPX [97]	SAS-SFR/MCNP
Doppler constant, pcm	-1044	-1110
SVE in fissile core, pcm	1500	1583

Fig. 17 illustrates the evolution of the K-effective value dependent on the number of iterations. The red line shows the evaluated K-effective value in coupled calculations for a given number of iterations, while the blue markers (dots) denote K-effective values obtained at each iteration step. Particularly, since the same statistics is used in all iterations, this scheme allows determining a simple mean value on the basis of the K-effective values obtained at each iteration. The variation of the power data transferred to SAS-SFR between the two last iterations is negligibly small, as well as the evaluated K-effective change.

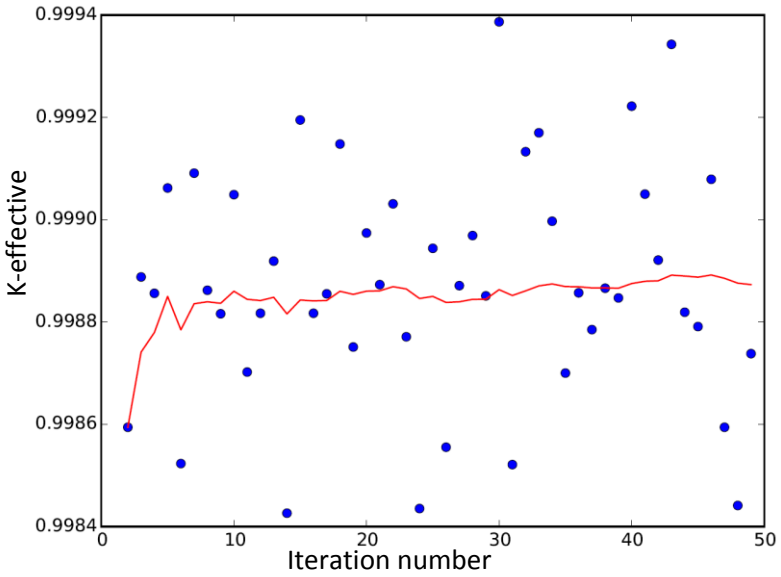

Fig. 17. Calculated K-effective value versus iteration number in SAS-SFR/MCNP coupled calculations for the FC case

The radial power distribution, represented by channel relative powers (or peaking factors), for the case FC is shown in Fig. 18. Channel relative power is defined as:

$$p_{ch}^{i} = \frac{\bar{P}_{SA}^{i}}{\bar{P}_{SA}},$$

where $\bar{P}_{SA}^{i}$ – average subassembly power in channel i, $i = 1..N_{ch}$, $\bar{P}_{SA} = \frac{1}{N_{SA}} \sum_{k=1}^{N_{SA}} P_{SA}^{k}$ – average subassembly power in the core, P_{SA}^{k} – power of subassembly k, N_{SA} and N_{ch} – number of subassemblies in the core and number of channels.

The most power-loaded SAs belong to channel #5 (six SAs all together, see Fig. 12 and Table 6). Different distributions of the power radial distribution in the inner and outer sub-cores (channels #1–4 and channels #5–10, respectively) are observed, as a result of the BOL core fuel load. The channels fissile heights calculated for the FC case to be passed to MCNP model are also shown in Fig. 18, demonstrating correspondence between calculated channel's axial expansion and channel power level. The Fig. 18 also illustrates the channel fissile heights for the RE case, which are all identical, in contrast to the FC case, where they exhibit a radial distribution. One can see that average expansion of the fissile height (used for the Reference Expanded geometry) is underestimated by about 25% with respect to the average value. This in turn leads to a new evaluation result with the coupled solution. Concerning the relative channel powers a maximum difference of about 2% between FC and RE cases is observed for inner core channel #1, while for the other channels it does not exceed 1.5%. It is demonstrated in [98] that these differences are caused mainly by the simultaneous consideration of the fuel temperature distribution and the node wise axial expansion in the neutron physics model of the coupled solution.

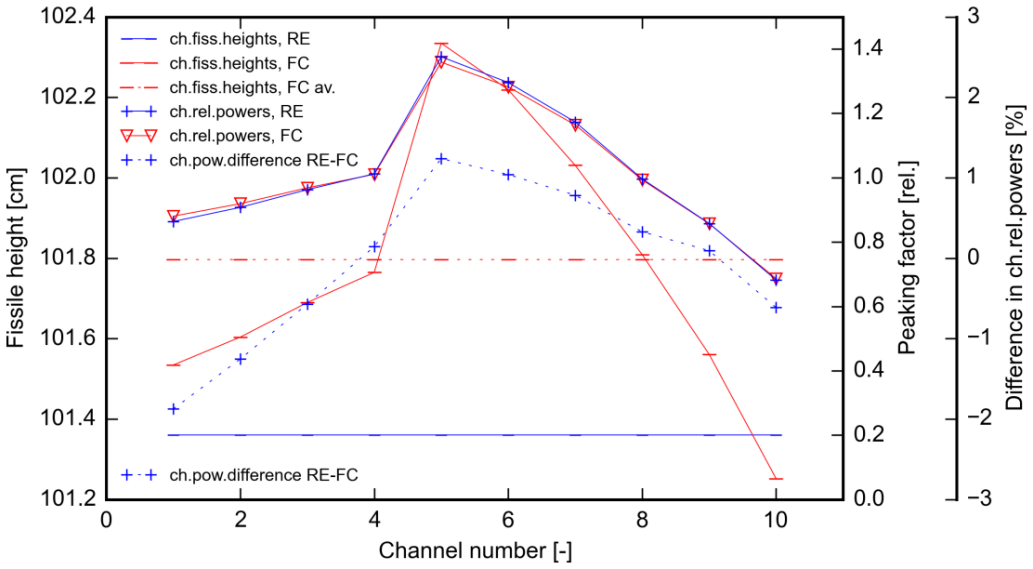

Fig. 18. Computed relative channel power (channel peaking factor) and channel fissile height for the Reference Expanded (RE) and Fully Coupled (FC) case

The Fig. 19 illustrates the spatial distribution of the node linear power rating (left) and the node fuel temperature (right) in a fissile nodes of the computational domain. The node linear power rating is normalized with the mean linear power rating averaged over the fissile core. All channels exhibit maxima in the axial nodes #6 and #7, close to the fissile core's mid-plane. Slightly higher values are observed for the lower part of the core, below mid-plane (compare axial nodes #1 and #13). The maximum value of the shown distribution is the core's

volumetric power peaking factor, which amounts to 1.68 and is obtained in the axial node #7 of channel #5, which is close to core mid-plane.

The corresponding node wise fuel temperature distribution is shown on the right hand side of the map in Fig. 19. It is almost congruent with the node power distribution, except that it is slightly shifted to the upper part of the core. The maximum node fuel temperature of 1915 K is found in axial node #7 of channel #5. The minimum value of 1126 K is found at inlet of channel #10 which includes SAs near the core outer boundary, see Fig. 19.

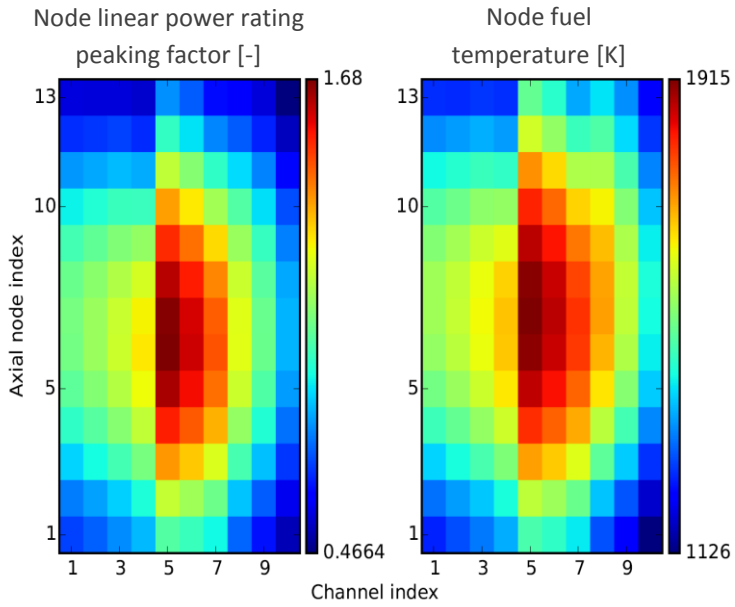

Fig. 19. Computed spatial (node-wise and channel-wise) distribution of linear power rating peaking factor (left) and fuel temperature (right) in fissile core height nodes for Fully Coupled (FC) case

The Fig. 20 depicts the axial fuel, clad and sodium density distribution along the fissile core height for the most power-loaded channel #5. The fuel density follows a cosine-like temperature profile, while clad and sodium density axial distributions are driven by the sodium temperature, that increases from inlet to outlet. One should note that these are "effective" densities used in the neutron physics model, where the radial expansion of clad and hexcan is not modelled, but accounted for in density calculations. Thus they slightly differ from realistic density values, which can be obtained with the use of material masses and dimensions, calculated by SAS-SFR considering clad radial expansion.

The Fig. 21 shows the differences of the node linear power rating and fuel temperature between the cases RE-A1 and RE-A2 and the fully coupled (FC) solution. In case RE-A1 only one average power profile for all channels is used for the SAS-SFR calculations, while in case RE-A2 the individual power profiles for every channel are employed in the SAS-SFR calculations. One can see that using one average power profile (left map in Fig. 21) leads to high differences for the steady state case; the nodal linear power rating and fuel temperature values differ by up to 17% and 64 K to the FC solution. This deviation can be attributed to the

specificity of the initial core configuration, where the control rods (CRs) are inserted in the outer row. The case RE-A2 which uses individual profiles, exhibits considerably lower differences to the FC case, namely up to 2.6% and 15 K for nodal linear power rating and fuel temperature.

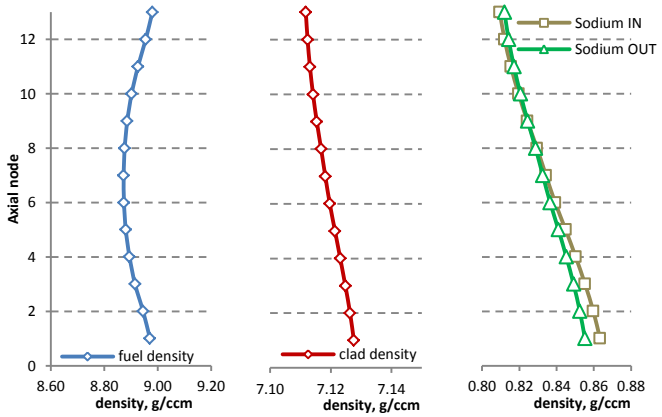

Fig. 20. Computed "effective" density axial distribution along the core fissile height of fuel, clad and sodium (inner and outer) densities along the core fissile height in channel #5 (11.0MW) at steady state

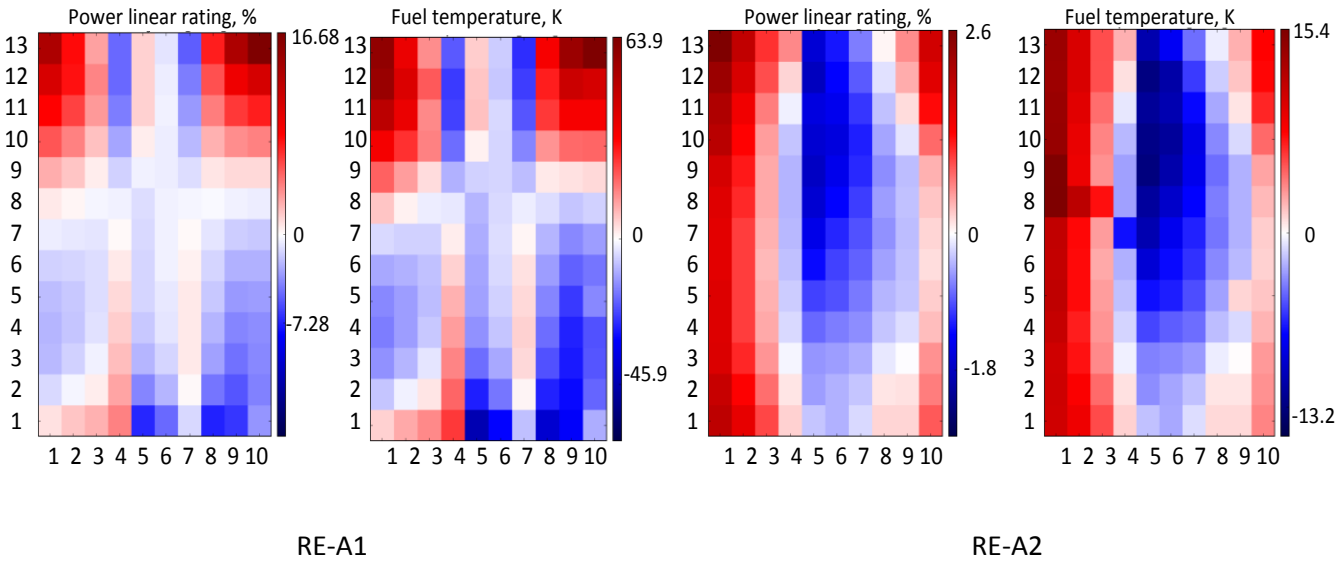

Fig. 21. Computed relative differences of nodal linear power and fuel temperature spatial distribution (node-wise and channel-wise) for the fissile nodes between the two Reference Expanded cases A1 and A2 and the Fully Coupled solution

3.3 PARAMETRIC STUDY ON IMPORTANCE OF DISTRIBUTED CORE PARAMETERS

The coupling has been implemented in such a way to control what parameters being determined in the thermal-hydraulic (TH) calculation are fed back into the neutron physics model. Several calculations have been performed, which differ by TH parameters that are fed back into the neutron physics model. A description of the parametric study is given in Table 9. Results of this work were presented in [98] with the aim to investigate the influence of different distributed core state parameters on the power distribution and the associated SS characterization of the core.

The cases RE-A1 and RE-A2 are discussed already above. They represent the conventional approach that is the one-way calculation, when the core power computed by the neutron physics model is passed to the TH model, and the results of the TH model calculation are considered as final. The other cases – B, C, D – are iteratively coupled calculations, in which the results of TH are feed back into the neutron physics model. The resulting power distribution then passed again to the TH model in each iteration step and it is composed of all previous neutron physics calculations according to the convergence acceleration scheme (see §3.1.2). In the case B, only fuel temperature distribution looped back into the neutron physics model (see Table 9). The case C additionally considers also the fuel temperature and the node-specific axial expansion by changing geometry (namely, the node height) of each fissile node as well as the fuel density in the neutron physics model. Finally, case D additionally takes into account the node-specific distribution of the sodium density. The differences between case D and case FC (Fully Coupled) are due to the fact that the node-specific steel density of both clad and hexcan are taken into account in the neutron physics model.

Table 9. Description of calculation cases for parametric study with SAS-SFR/MCNP

Case ID		Case RE-A1	Case RE-A2	Case B	Case C	Case D	Case FC
Parameter \ Case description		Reference Expanded	Reference Expanded improved	RE +fuel temperature	RE +fuel temp. +exp.	RE +fuel temp. +exp. +sodium density	Fully Coupled
Axial power profile		A*	D*	D	D	D	D
Node height		A	A	A	D	D	D
Temperature:	Fuel	A	A	D	D	D	D
	Steel	A	A	A	A	A	D
	Sodium	A	A	A	A	D	D
Density:	Fuel	A	A	A	D	D	D
	Steel	A	A	A	A	A	D
	Sodium	A	A	A	A	D	D

* A – average, D – distributed

Results of the parametric study are summarized concerning reactivity variations dependent on the individually modified parameter coupling procedures. K-effective values for different calculation cases (see Table 9) are listed in Table 10 together the differences to the

FC case. The results show distinct sensitivities with respect to the incorporation of different parameters into the model. K-effective values for the cases RE-A1 and RE-A2 are identical, because the same neutron physics model is used to obtain them (remind that cases A1 and A2 do not assume any TH feedback). One can see that the cumulative effect of inclusion of all possible TH feedbacks to K-effective amounts to 130 pcm. An accurate representation of the fuel temperature in the neutron physics model by means of the coupled scheme leads to a decrease of the resulting K-effective value by 65 pcm. This is caused by several physical effects:

At first it arises from a reduced core average fuel temperature from 1500 K in case RE to 1470 K in case B with a contribution of about 20 pcm and to re-distribution of the Doppler effect leading to a correction by of about 25 pcm.

The consideration of the individual axial expansion in the neutron physics model (from case B to C) provides a shift of the K-effective value by -105 pcm. It is composed of two fractions. The increase of the average fissile height in the neutron physics model in case C by about 0.4 cm contributes to a shift of the corresponding reactivity effect by about -50 pcm. The other contributions, which are together evaluated to amount to about -55 pcm, are caused by a reduced average fuel density in the neutron physics model, the introduction of an additional amount of steel and sodium coolant within the increased fissile height of the core and finally the effect of a relative insertion of absorber of CRs in the outer row.

The consideration of the sodium density variation (from case C to D) leads to further reduction of K-effective by -40 pcm. This originates from the correction of the total mass of the sodium within the fissile height as result of calculation of nodal sodium mass in SAS-SFR accounting for also the radial clad expansion.

The K-effective differences between case D and fully coupled case FC amounts to 60 pcm. It is attributed to the appropriate consideration of the nodal clad and hexcan steel density.

Nonetheless, the overall variation of the evaluated K-effective for the different cases remains in a threshold of 190 pcm only for the considered configuration. It therefore reflects the accuracy of the prediction of the core reactivity, calculated with a neutron physics model, which uses only some average core parameters (as the RE case).

Table 10. K-effective value for different calculation cases and difference with regard to FC case

Option	Case RE-A1	Case RE-A2	Case B	Case C	Case D	Case FC
K-effective value	1.00020	1.00020	0.99975	0.99870	0.99830	0.99890
Difference of K-effective with case FC, pcm	130	130	85	-20	-60	n.a.

The relative differences of the calculated channel power peaking factors compared to the FC case are shown in Fig. 22. The consideration of fuel temperature and fuel density distributions (cases B and C) causes the most significant corrections in the radial power shape. However, the channel powers are modified here only by about 2%, while it is expected to become larger for a larger number of channels. The channel arrangement scheme typically

uses the maximum SA power deviations in between channels as criteria for deciding on the channel grouping scheme. The scheme adopted for the power distribution, which was obtained with neutron physics model employing average core parameters (like case RE) or "as fabricated" geometry, may not fit to the power distribution, obtained with a coupled solution. In case of transient simulations with PK the more accurate channel power values can be provided considering the SS coupled solution. If required it must be evaluated together with the overall accuracy of the power prediction for the considered level of details in the selected models.

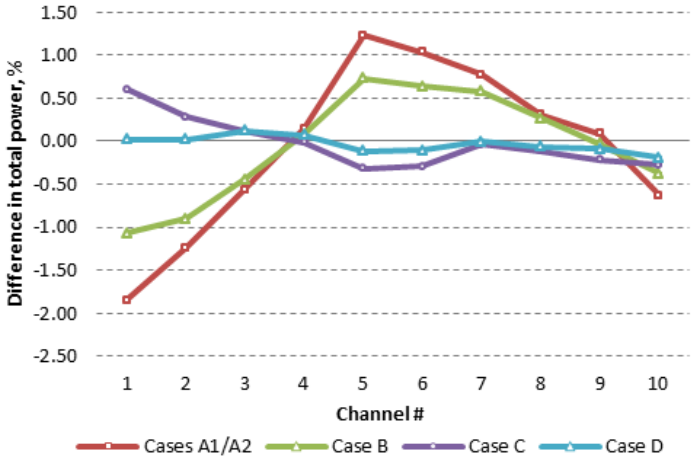

Fig. 22. Evaluated relative channel power difference in [%] for the different calculation cases of Table 9 compared to the FC solution

3.4 INFLUENCE OF THE ACCURACY OF STEADY STATE SIMULATIONS ON TRANSIENT RESULTS

3.4.1 STEADY STATE PREDICTION ACCURACY

For transient simulations of nuclear reactors it is important to depict the plant and core steady state accurately. This can be demonstrated by a systematic comparison of the main parameters predicted by the numerical code using a specific plant and core model. The prediction accuracy of steady state simulation with coupled neutron physics and thermal hydraulics (TH) codes depends not only on the "code capability" but also on the ability of the user to present the nuclear power plant or core in a proper manner regarding the spatial discretization of the computational domains, the model selection, the familiarization with the numerical features of the code, etc. In case of coupled neutron physics and TH simulations, the results will depend additionally on how the mapping and grouping of the subassemblies is done for the description of the feedbacks mechanisms.

Different benchmark exercises for SFRs [99], [100] and [44] have demonstrated that the use of different neutron physics codes (which employ different deterministic or MC methods) results in differences of node power values of up to 1-5%. The biggest deviations

are normally observed for the boundary nodes, where the specific power is lower. Monte Carlo methods supplied with appropriate neutron cross section libraries are usually considered as reference calculations. SA-wise radial power shapes are also calculated with an accuracy of about 1-2% and this is the accuracy of evaluated total channel powers. Modelling core neutron physics at the End Of Cycle (EOC) state (or other configuration with burnt fuel) normally increases the level of inaccuracies. Approximations have to be taken already during modelling of the irradiation history, where the burnup history and burnup representation scheme play an important role. The evaluation of the SFR cores with axial heterogeneity (in particular, with inner fertile breeder zones) also provides a source of additional inaccuracies, since the normalized axial power shape changes considerably with burnup.

With regard to the burnup simulation, the current methodology of SAS-SFR doesn't consider an axial power profile change during the modelling of fuel irradiation. For conventional designs the node power at EOC state can be evaluated with a few percent of accuracy. Thus, the accuracy of burnt core configurations corresponds to the accuracy of the above mentioned Case RE-A2 with individual profiles, or lower. For instance, the approach of case RE-A2 seems to be sufficient for the evaluation of the EOC core state, since considerations of distributed core parameters give a correction of node powers and corresponding fuel temperatures within 2-3% and 15 K, respectively.

Hence, the conclusions given below as a result of the consecutive inclusion of different parameters into the calculation scheme should be addressed mainly to BOL core conditions. In the current study, the SA power deviations from the channel average value are mainly of the order of 1-2% and reach 5-7% for only a few SAs. This inaccuracy can be effectively decreased at BOL conditions by increasing the number of channels and modifying the SA grouping scheme. Ultimately, both codes applied in the coupled calculations allow for a representation of each SA by its own channel.

The account for individual profiles appears to be mandatory for the actual level of details for BOL core configurations. In the studied design it halved the discrepancies of maximum values of power and fuel temperature, when applying the fully coupled solution. Here no feedback on neutron cross sections is accounted for because results are obtained on basis of only one neutron physics model. Including of distributed fuel temperature resulting in a locally calculated Doppler effect introduces non-negligible corrections of node powers with regard to case RE-A2 with individual profiles: up to 0.5-1% in total channel power (see Fig. 22). Due to correction of spatial power distribution (axial and radial) the sodium heat-up differences become negligibly small (within 1 K), and become smaller for other cases. Furthermore considerations of fuel non-uniform expansion gives more uniform differences of the power distribution along axial height (within 0.5-0.7% for node power) when compared to the fully coupled calculation, while channel powers differ by less than 1% in comparison to the ones obtained with the coupled calculation.

Differences in the maximum nodal fuel temperatures for cases B and C (where fuel temperature and density are accounted for consequently) are mainly coherent with differences in total channel power values and evaluated as 10 K/%-of-power for this core. Starting from case B for all cases the differences in maximum power nodes for all channels are within 1%, what is reflected in maximum node fuel temperature differences of about 7 K for case B and

below 5 K for all other cases, Fig. 23. The next two components, sodium density and steel density, have only a relatively moderate influence on the power profile and parameters distribution.

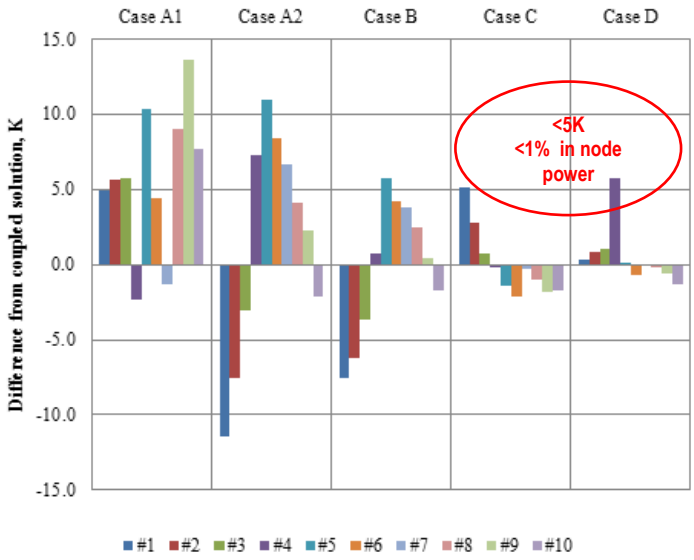

Fig. 23. Evaluated maximum nodal fuel temperatures in [K] for the different calculation cases of Table 9 compared to the FC solution

In case FC all relevant TH parameters calculated by SAS-SFR are fed back to the neutron physics model. Basically there are no approximations in the neutron physics model for important nodes (in fissile height and above-core regions) and for material data supplied to the nodes. For the TH side, certain approximations are included in the SAS-SFR models, which consider the whole SA as one representative pin per SA (in comparison to other TH codes, which are able to model SA at pin level, for instance, SAS4A [53] or SUBCHANFLOW [101]).

3.4.2 INFLUENCE OF INITIAL POWER SHAPE ON TRANSIENT RESULTS WITH POINT KINETICS

It is worth to evaluate the influence of using two different power distributions on ULOF transient results as calculated with the original PK model of SAS-SFR on basis of two cases for steady state (SS) characterization considered above – namely the Fully Coupled (FC) and the Reference Expanded (RE) case. The power spatial distribution, corresponding to SS, is the only difference in this comparison exercise. Below an overview of the transient phenomenology is given for the two cases and the differences are discussed.

Results of the ULOF calculations with PK neutron physics models are discussed hereafter covering the following three time intervals:

(1) the time period up to boiling onset;
(2) the boiling time period up to the first onset of clad melting in a SA group (channel);
(3) the post clad melting onset time period lasting up to the time when first sub-criticality has been achieved and beyond.

During the first phase of the investigated ULOF accident scenario, the net reactivity stays at a value of nearly zero and attains a slightly negative value (about -0.01 $) at the time of boiling onset as shown in Fig. 24. For characterization of the core transient behaviour the time dependent behaviour of the following quantities are plotted in two parts in the following Figures:

- in the upper part of the figure the normalized power, the net reactivity and its components for the PK solution (the Doppler reactivity, the sodium density reactivity, the reactivity related to the axial core expansion, clad and fuel relocation reactivity) and fuel average enthalpy are plotted versus the transient time;
- in the lower part of the figure the sodium mass in the fissile core region and the one in the above-core regions of upper pin plugs, upper steel blanket and sodium plenum in relation to the steady state values are plotted together with transient variations of the fissile core height and the core averaged fuel temperature.

Three reactivity effects determine the transient behaviour prior to the material relocation onset: the Doppler effect, the fuel pin axial expansion and the coolant reactivity effect. The rapid decrease of sodium mass flow results in an increased sodium heat-up and thereby in the insertion of a positive reactivity. This is counterbalanced by the Doppler effect and the axial core expansion introducing negative reactivity contributions. As result of a marginal variation of the net reactivity, the power stays close to the nominal value.

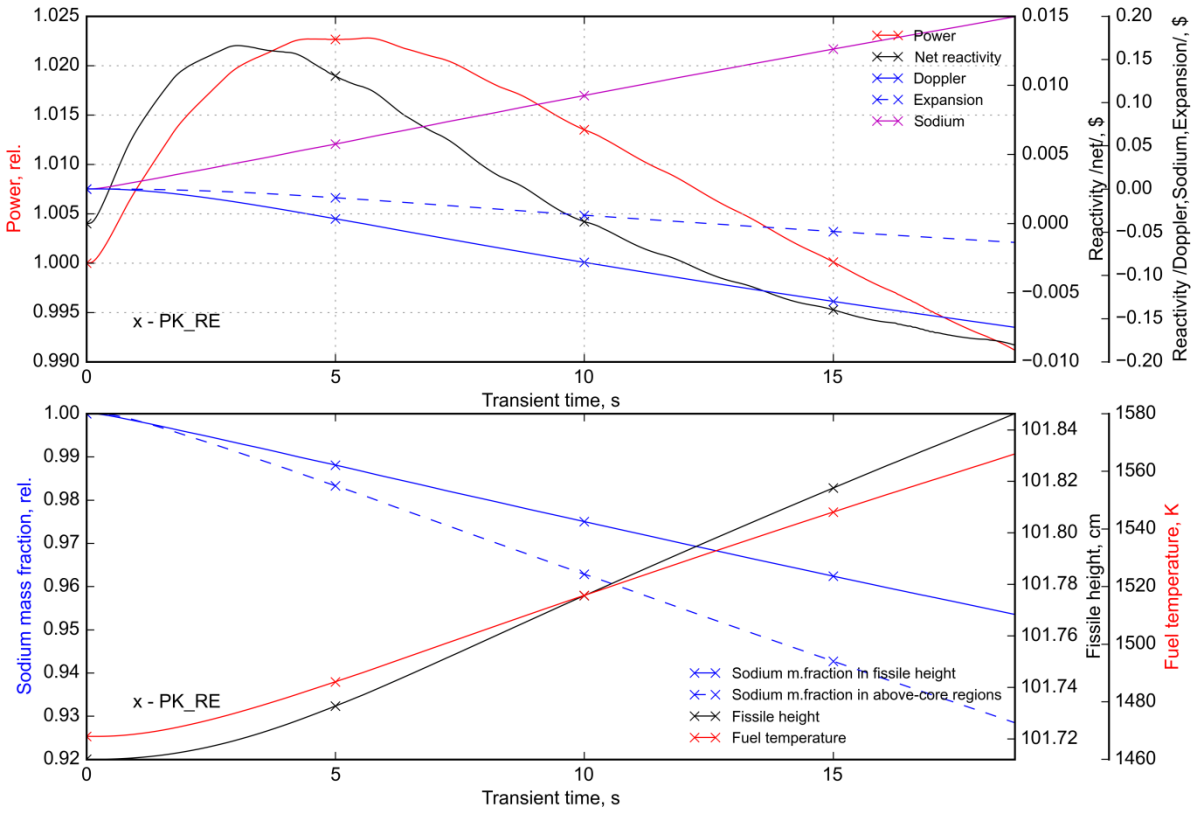

Fig. 24. Temporal evolution of the normalized power, net reactivity and reactivity contributions (top) and sodium mass fraction, fissile height and fuel temperature (bottom) in a ULOF sequence before boiling onset as computed for the Reference Expanded case using PK model

In Fig. 25 comparison of the temporal evolution of characteristic core parameters in a ULOF sequence before boiling onset for two PK cases – Fully Coupled (FC) and Reference Expanded (RE) cases – is presented. The two calculations demonstrate almost identical results for this phase. The boiling starts in the uppermost node of channel #8 with the highest power-to-flow ratio (see Table 6, 3 CG configuration) in both cases at 18.2 s after the start of the transient.

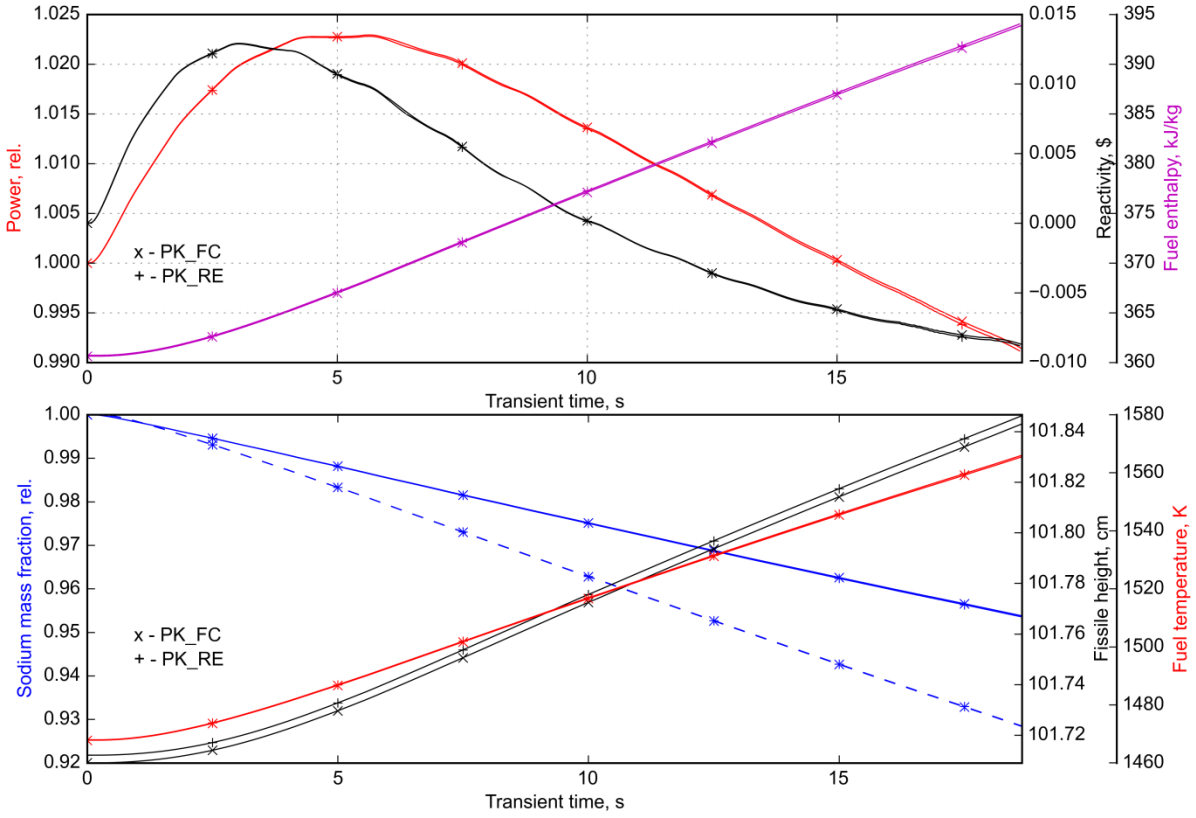

Fig. 25. Temporal evolution of the normalized power, net reactivity and fuel average enthalpy (top) and sodium mass fraction, fissile height and fuel temperature (bottom) in a ULOF sequence before boiling onset as computed for the Reference Expanded and Fully Coupled cases using PK model

The second part of the transient depicted in Fig. 26 is characterized by the development of boiling. The evolution of power transients during the boiling time phase up to and beyond molten clad relocation onset is determined to a large extent by the transient variation of the sodium void reactivity and by the dynamics of the extension of the two-phase flow regions along SAs height. The sodium void propagation front moves not only in the upward direction into the sodium plenum but also in downward direction towards core mid-plane. The dynamic of the boiling propagation is characterized by the sodium mass fraction parameter, which is plotted in the bottom of the figure. It is defined as the ratio between the actual mass of sodium in the fissile core (solid blue line) or in the above core axial regions (blue dotted line) and the respective mass calculated at steady state. In Fig. 26 further voiding of the above core structures causes insertion of a negative reactivity (blue dotted line), while

further voiding of the fissile core (solid blue line) results in an insertion of a strong positive reactivity, which drives the transient. The net reactivity starts to increase noticeably after 2 s into the boiling time period, while the overall dynamics of the boiling propagation is evaluated to be rather slow. The boiling phase takes about 10 s and the power does not exceed 1.5 times the nominal value during first 6.5 s after boiling onset. The mismatch of the power generation and the availability of a convective thermal-hydraulic heat sink causes boiling onset also in other channels.

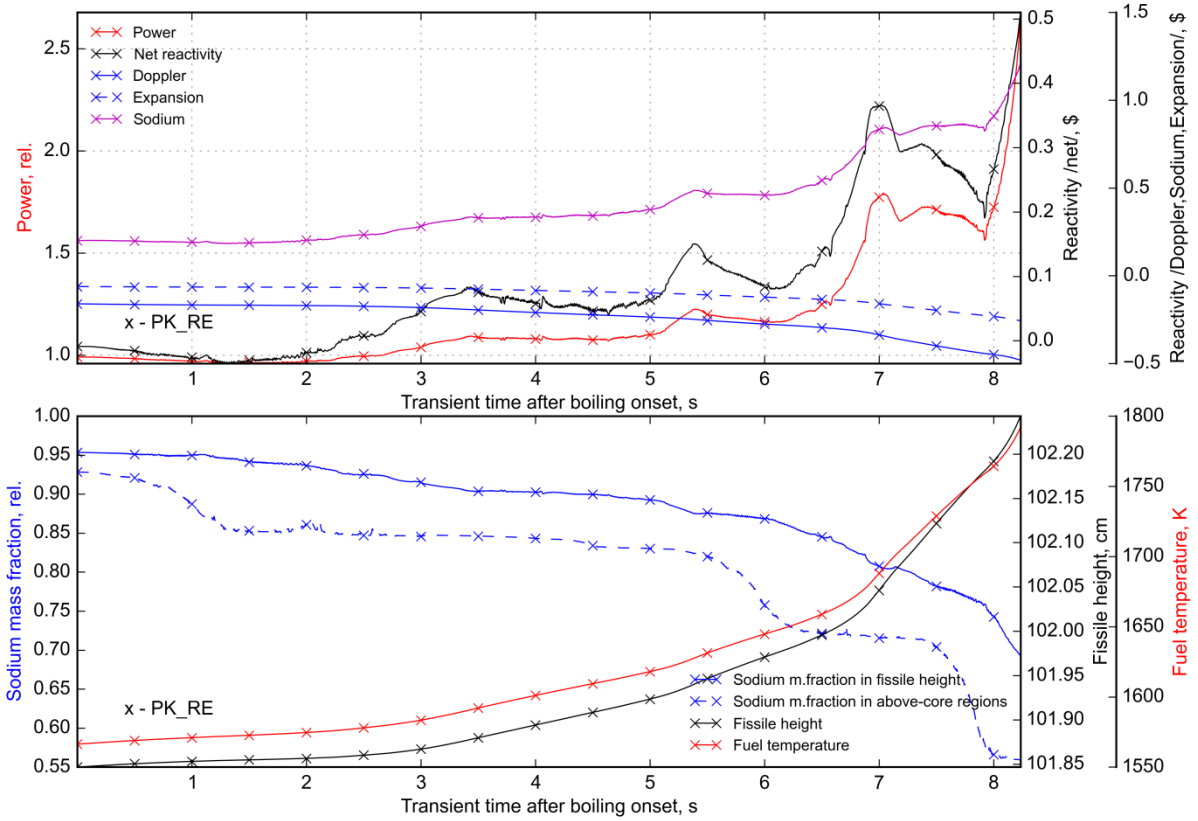

Fig. 26. Temporal evolution of the normalized power, net reactivity and reactivity contributions (top) and sodium mass fraction, fissile height and fuel temperature (bottom) in a ULOF sequence after boiling onset as computed for the Reference Expanded case using PK model

The comparison of the boiling phase of the transient between FC and RE cases is depicted in Fig. 27. Again, it demonstrates a very similar behaviour of power and reactivity for the two cases, as well as the intensity of the core voiding, which is characterized by the sodium mass fraction parameter, shown for every phase in the lower part of the Figures.

The last phase illustrated in Fig. 28 starts after clad melting onset and is characterized by an energetic power excursion, which results in pin failures and discharge of fuel from the fissile core height. The reactivity components of fuel and clad relocation become in effect as shown in the upper part of Fig. 28. The fuel relocation yields here a negative reactivity insertion, which amounts to about 3 $ at the moment of first sub-criticality at t = 1.55 s after clad melting onset. Thus it is fuel relocation which temporary mitigates this ULOF.

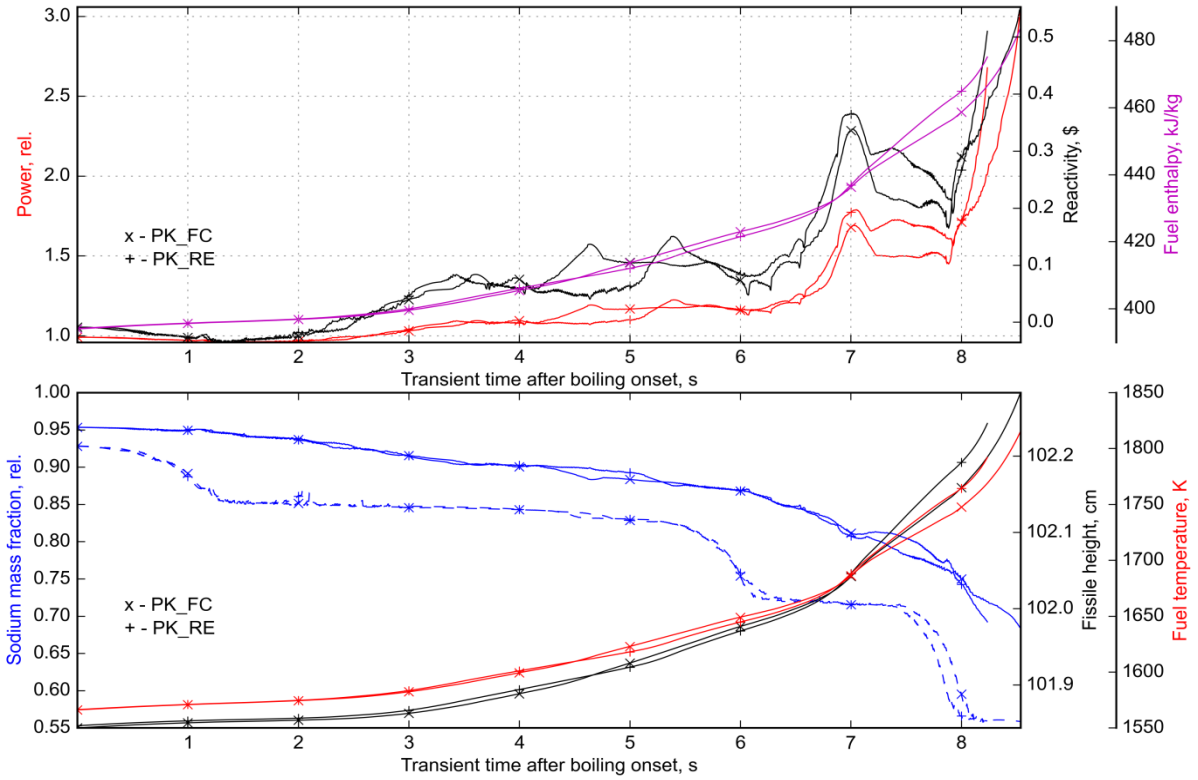

Fig. 27. Temporal evolution of the normalized power, net reactivity and average fuel enthalpy (top) and sodium mass fraction, fissile height and fuel temperature (bottom) in a ULOF sequence after boiling onset as computed for the Reference Expanded and Fully Coupled cases using PK model

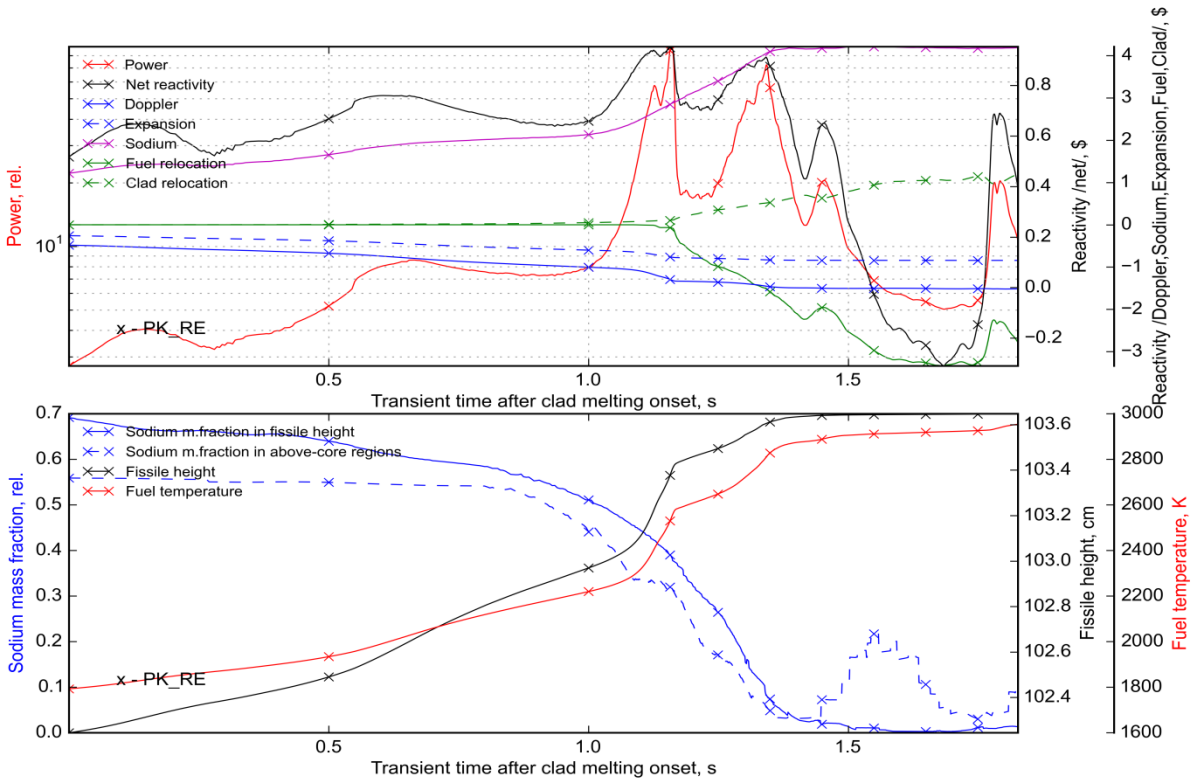

Fig. 28. Temporal evolution of the normalized power, net reactivity and reactivity contributions (top) and sodium mass fraction, fissile height and fuel temperature (bottom) in a ULOF sequence after clad melting onset as computed for the Reference Expanded case using PK model

More noticeable differences between FC and RE cases are observed in this phase of the transient (Fig. 29). Using the power spatial distribution data from the FC solution leads to a slightly more energetic power excursion, than for the RE case, which is characterized by three successive reactivity and power peaks, caused by the sodium void reactivity with a higher amplitude, in contrast to only two peaks for the RE case (while the third peaky variation of the net reactivity is driven by the fuel relocation contribution, see Fig. 28). Nevertheless, as result of the fuel relocation, the core reactivity drops to negative values in a similar manner for both cases.

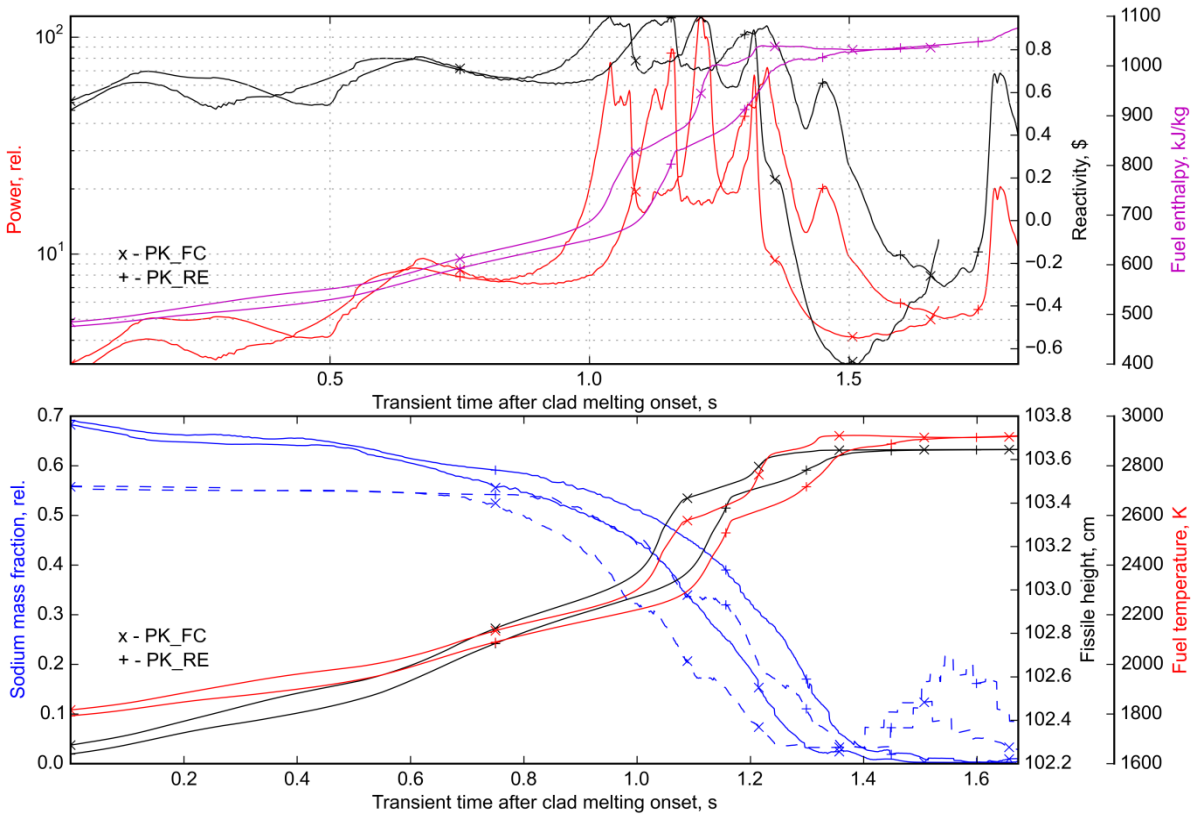

Fig. 29. Temporal evolution of the normalized power, net reactivity and average fuel enthalpy (top) and sodium mass fraction, fissile height and fuel temperature (bottom) in a ULOF sequence after clad melting onset as computed for the Reference Expanded and Fully Coupled cases using PK model

The dynamic of the fuel discharge from the fissile height which characterizes to a large extent the transient phenomenology is illustrated in Fig. 30, where fuel mass fraction within the fissile core height is plotted together with the normalized power and net reactivity for two PK cases. The parameter of the fuel mass fraction within the fissile core height is defined as a ratio of actual total fuel mass within fissile core boundaries to the fuel mass at steady state. At the moment of first sub-criticality the fraction of fuel ejected out of the fissile core amounts to about 0.7% in both FC and RE cases. The fuel mass fraction ejected out of the fissile core increases further during the transient and exceeds 1% at the end of these calculations.

For this scenario it can be concluded, that the overall phenomenology is very similar for the two cases. The difference, which is essentially caused by only slightly different local power conditions in the core between the RE and the FC case, is characterized by a slight time delay of about 0.15 s for the traces of the first power peak and the core averaged fuel enthalpy for the RE case. Subsequently the first sub-criticality also occurs in the RE case calculation by 0.2 s later. After the power excursion the core states are characterized by overheated fuel with a core average fuel temperature of 2900 K, an identical level of the fuel enthalpy and completely voided conditions. Correspondingly, this cannot be qualified as a noticeable difference in results of a ULOF calculation applying different power spatial distribution data. It implies that for a given core configuration and transient set-up the scenario is defined by the reactivity feedback data used by the PK model, which are identical in the two calculations, while the local differences in core power conditions (within few percent's of the node power) are not of a high importance. Subsequently both calculations require modelling of the Transition Phase. The core characterizations at the end of the IP simulation are almost identical.

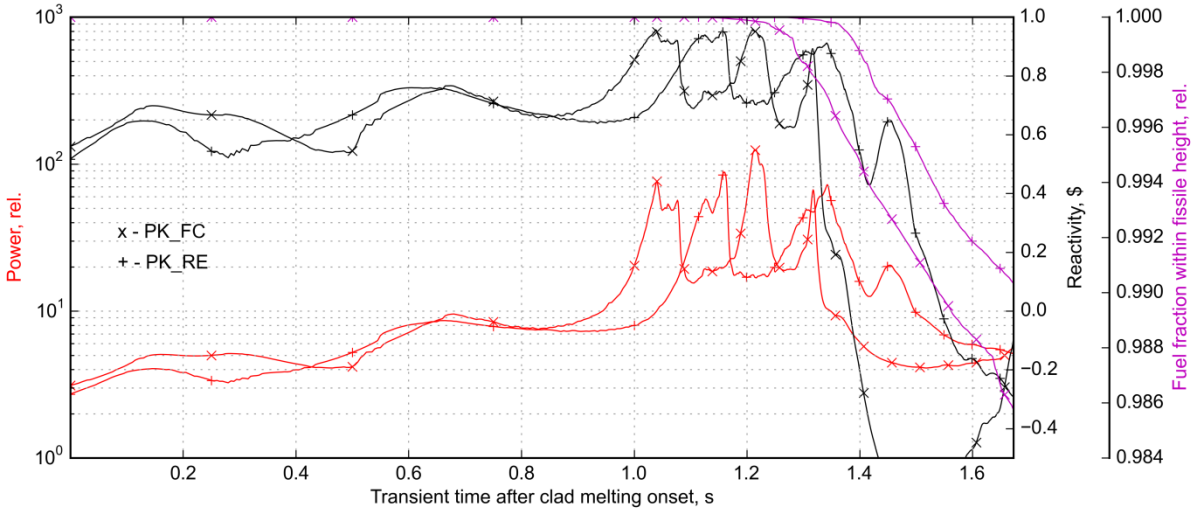

Fig. 30. Temporal evolution of the normalized power, net reactivity and fuel mass fraction within the fissile core height in a ULOF sequence after clad melting onset as computed for the Reference Expanded and Fully Coupled cases using PK model

3.5 CONCLUDING REMARKS RELATED TO CHAPTER 3

A coupled code system SAS-SFR/MCNP has been developed for an accurate prediction of the steady-state parameters of an SFR core as an alternative to the conventional scheme using stand-alone codes. This introduces the capability to treat the core geometry and spatial distributions of important thermal hydraulics (TH) parameters in the neutron physics calculation for accurate prediction of power distribution in the core.

The new calculation route is used to evaluate the BOL core state, but it can also be applied for EOC conditions with some approximations and assumptions. The importance of

accounting for different distributed parameters for accurate SAS-SFR calculations has been demonstrated in this study. The coupled code system showed a high sensitivity of calculated TH parameters to the details of the use of the neutron physics model and depicts the physics of the involved phenomena. The appropriate consideration of fuel temperature and density distribution together with a realistic axial pin expansion in the neutron physics model ensures a considerably more accurate steady state solution in the SAS-SFR calculation, while consideration of sodium and steel density distributions can provide non negligible corrections of the spatial core power distribution and thus influence the resulting core TH characterization at steady state. The latter is of importance for further transient simulations.

Moreover, the new tool provides the basis for the evaluation of core reactivity changes corresponding to the change of operating condition parameters such as core power level, mass flow rate, sodium inlet temperature and for determination of the reactivity balance. In spite of the fact that some distributed parameters don't strongly influence the SAS-SFR results related to the thermal-hydraulics of the core, they may become relevant to evaluate reactivity changes as a result of a change of power or coolant mass-flow rate. The consideration of the axial profile of pin expansion can be of importance for some cases, such as the transition from one power level to another.

The test calculations using the PK approximation for the transient analyses of a ULOF accident indicated that a very accurate steady state representation does not lead to considerably different results for the phenomenology of severe transients leading rapidly to total core destruction for considered ESFR Reference Oxide core configuration with three cooling groups. Consequences may be of more importance when investigating operational transients with accident and incident initiators belonging to the design basis domain of transient analyses. However, analyses of such transients are not the target of this work.

4 EXTENSION OF SAS-SFR WITH A SPATIAL NEUTRON KINETICS OPTION FOR TRANSIENT ANALYSIS OF SFRS

Coupled space-time neutron physics and thermal-hydraulics simulation is one of the most challenging problems in reactor physics for several reasons – physical and mathematical. Common issue for both neutron physics and thermal-hydraulics domains of reactor core simulations is the relatively high level of computation time, which is due to the necessity of a detailed description in time of the complex and fast physical processes. A comprehensive overview of multi-physics nuclear reactor analysis can be found e.g. in [102].

Application of spatial neutron kinetics to the simulation of the Initiation Phase of an accident, like a ULOF, is rather limited as discussed already above. The SIMMER code family, which is normally used to model the Transition Phase, uses a two-dimensional R-Z and a three-dimensional (3D) spatial kinetics solution, while the necessary calculation time rises considerably for cases with a 3D core representation. An application of the SIMMER code for the IP analysis can be found in [32].

One of the most efficient methods for the solution of the 3D time-dependent neutron balance equation is the quasi-static method, [79] and [103]. Its main peculiarity is the consideration of two time step levels: the coarse one for recalculation of the spatially dependent flux shape function and the fine one for calculation of the flux amplitude as it is done by means of a PK solution. Nevertheless direct methods have been and are developed recently, providing diffusion and transport deterministic solutions with an appropriate computation time. In this work, the PARCS code has been selected as the 3D neutron kinetics solver to be coupled with SAS-SFR based on the promising experience gained with PARCS within the FAST code system and its application for sodium boiling transients .

The multi-physics coupling for a transient problem always requires a time discretization, or hierarchy, for the individual physics domains. They are solved each individually on their own most appropriate time scale. The operator splitting technique is considered to couple several existing specialized numerical solutions or codes. In practice it is realized by an explicit time coupling strategy, where the domains exchange data at the end of a main time step, while the output data from one domain is used as input data for the other domain in the next time step. One of the key issues is the definition and handling of the mapping of the involved neutron physics and thermal hydraulics and pin mechanics domains for the data transfer performed during the SS and TS simulation.

More advanced and rigorous solutions could be expected for tightly coupled systems with an implicit time coupling strategy, where one needs to apply nonlinear iterative schemes for the main time step. The detailed discussions on the peculiarities of both methods for application in the reactor physics can be found in literature, [104] and [71]. Hereafter, the details of the implemented coupling approach will be described.

4.1 OVERVIEW OF THE COUPLED SOLUTION

The overall structure of the coupled code system SAS-SFR/PARCS is shown in Fig. 31. In this coupling scheme, the Interface is implemented on Python to provide services for the management of calculation, functionalities for data exchange, data processing and visualization.

The calculation route is defined in a way of a sequence of functional calls, where each code performs the calculation of one time step in case of a transient simulation (TS) or one iteration in case of the steady state simulation (SS). The SS and TS coupled calculations are similar from the viewpoint of data processing and exchange between the two domains. The peculiarities of codes that facilitate such an implementation are listed hereafter:

- modular structure of the PARCS code, which allows to establish a one-call procedure for main functional elements;
- use of the explicit time step scheme, which doesn't require considerable modifications of the stand-alone PARCS neutron physics routines;
- structure of the SAS-SFR code, where the iterative algorithms (loops) related to SS and TS simulations can be separated and used as functional elements.

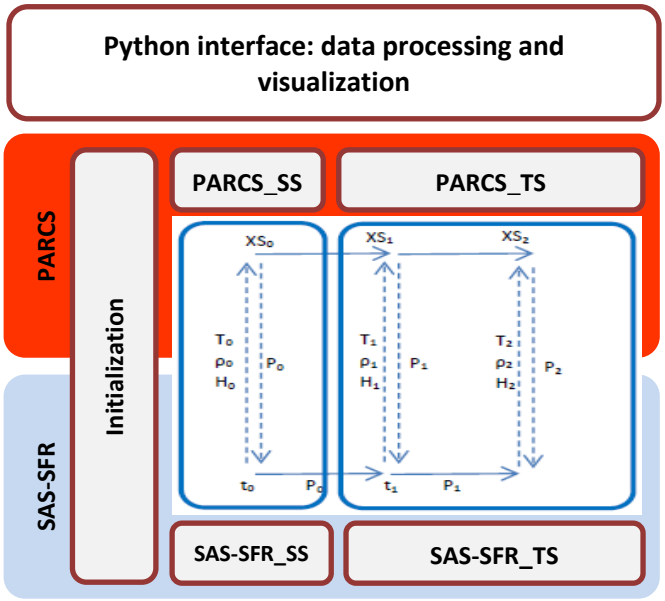

Fig. 31. Schematic structure of the SAS-SFR/PARCS coupled solution

The explicit coupling method in time has been evaluated to be very suitable for coupling of the SAS-SFR code with other neutron physics solution. In the original calculation route of SAS-SFR the PK model calculation is called at every main time step, i.e. at the largest time step, while several levels in the time step hierarchy are considered in the code to treat the primary loop, coolant dynamics, pin heat transfer and material dynamics. Practically, a relatively small main time step size is used in the PK solution, which is solved by the Kaganove method [105], since the latter ensures robust and quick solutions for the power amplitude and reactivity. This point has been considered as an advantage for the

implementation of the coupling approach. SAS-SFR also provides advanced algorithms for evaluation of the main time step, which also can be suitable for the new neutron physics model. On the other side, PARCS provides a high level of flexibility with regard to the choice of the time step size, which has been demonstrated in SFR simulations using the FAST system, where the TRACE thermal hydraulics code provides the time step control for the PARCS neutron physics solver [22].

4.2 IMPLEMENTATION OF COUPLED SAS-SFR/PARCS SOLUTION

4.2.1 SOLUTION STRUCTURE AND PROGRAM DRIVER

The main data processing and the control of the calculation sequence are performed at the Interface level, and are realized in the Python programming language. The FORTRAN code compiled as a Dynamic-link library (DLL) contains all subroutines and modules of both codes and represents a "low" level, which provides functions for routine calculations. In order to build a new coupled calculation route, the program flow (call sequence) of each code has been split into three logical blocks: initialization (INIT) of task, performance of steady state (SS) calculations and performance of transient calculations (TS). Additionally data processing and exchange between the codes on the FORTRAN level is performed. The Python driver program has access to the main functional elements like SS and TS run and to the particular low level memory locations, and provides overall control of the calculations.

The first step of a calculation is the initialization of tasks for both codes. The subroutines intended to read and analyse the input, to establish the task variables dimensions etc. are combined together in one INIT block of each code (one subroutine) on the FORTRAN level. In the Python environment the corresponding function imported from DLL is called. This step is done for each code individually as a part of the initialization of a simulation problem and its control parameters at the Interface level. In practice, each code reads its own input and establishes the calculation route options.

After initialization, the Python driver switches to the SS calculation. The subroutines of the codes related to one SS iteration sequence are combined together as one subroutine on the FORTRAN level and imported from DLL as a function to the Interface. This approach allows having a SS loop in the driver, which calls the SAS-SFR and PARCS SS-related blocks (one steady state iteration) one after another. At each SS iteration SAS-SFR performs calculation starting from the same as fabricated conditions, while in PARCS the original iterative scheme of the SS calculation is adapted. The loop SS calculations run up to a state where convergence criteria are fulfilled. The SS calculation route and control are discussed in more details in §4.5.1 hereafter.

After the SS is converged, the TS loop is organized. In case of the SK option the TS-related blocks of the two domains are called one after another performing the transient time step calculations. In case of the PK option, only the SAS-SFR code performs transient step calculations, which are controlled also by the Interface. For both kinetics options transient data storage logic and processing for plot and analysis at Interface are unified within the

coupled system. TS calculation scheme and control in case of the SK option used are discussed in more details in §4.5.2 hereafter.

Necessary data exchange between the codes is organized on two levels: "low" FORTRAN level, via calls of new subroutines within SS- or TS-related sequence and "top" Python Interface level. Newly written subroutines on the FORTRAN level provide data processing and storage in dedicated locations (newly introduced FORTRAN modules) for the use at Interface level and/or by the other code, i.e. explicit code-to-code data transfer. On the top level the relevant data are read, processed and new data are written to the FORTRAN level memory, i.e. for use at next function call. In particular, on the top level the mapping between the two domains and corresponding processing capabilities are realized, such as node data transfer on basis of the "smeared geometry" model.

Such component structure combined with data exchange at linking points (iteration steps in steady-state and time points at transient) has demonstrated a good performance. Every code is provided with its own input and creates its own output flow, written on different output files. There are other data output and plotting capabilities organized at the Interface level. Important core state parameters, such as power, reactivity or node fuel temperature can be plotted at the end of the calculation or "on-line" (updated plot after every or certain number of time steps during the simulation). Additional printed output is provided for effective monitoring of the calculation results.

4.2.2 MODIFICATIONS OF PARCS

Modifications related to the PARCS code include extensions of original subroutines and providing new ones, which are necessary for the exchange of new data with the TH domain as well as for reading of new input deck blocks and processing of these data. The modifications implemented in the original code structure are realized in such a way, that a specific key (SASSFRPARCS=True) defines the new kinetics simulation coupled to the thermal hydraulics solution algorithms of SAS-SFR. The modifications of the code include:

(1) a new structure of the program call sequence providing the calls of the SS iteration and TS simulation step;
(2) new processing subroutines and modules with dedicated data storage;
(3) implementation of the XS generation model;
(4) modification for allowing an axial expansion of the core geometry and
(5) modification of routines for reading the updated input deck.

With regard to specific data needed in case of coupled simulations, a few new input blocks have been introduced in PARCS considering input for the XS and the used library and for the core material content. Input blocks use a similar structure, as originally employed in the FAST code for the option of the "Sigma-zero" XS model, but with a few modifications. With regard to the "Sigma-zero" XS option, the new input deck provides information on the microscopic cross sections library content, its energy group structure and the interpolation meshes. This input deck has been originally implemented for the coupled simulations with code TRACE. For this work, the input deck related to the calculation node dependent material content has been modified in order to represent the individual components as fuel, clad, sodium and hexcan, associated with the reference "as fabricated" core geometry, in accord

with the used methodology of data transfer (see Appendix II). Additional channel description and calculation route options are provided in the PARCS input by the new input block CH_DATA, while the original input of PARCS is suitable for a detailed description of the SFR core geometry (input block GEOMHEX).

4.2.3 MODIFICATIONS OF SAS-SFR

The SAS-SFR code uses the original input deck. No modifications are required. The specific key (SASSFRPARCS=True) defines the calculation route, corresponding to the coupled simulation sequence. The specific key (SSONLY=True) defines the coupled calculation, where after converged SS the PK option is used for a transient simulation. Basically modifications are related to three main points:

(1) new structure of the program call sequence able to realize the SS and TS simulation steps;
(2) capability of deactivation of the PK model (in case of the SK option used) and
(3) data processing for supply of the needed core state parameters to the neutron physics part of the coupled code system.

It is mentioned in §2.2.1, that in the original version of the code not all core state parameters for the coupling are calculated explicitly and available for the use at the end of each calculation step for the entire transient time. This has been incorporated in the code by introducing new program lines and variables in existing SAS-SFR subroutines and new subroutines.

4.3 GEOMETRY AND CORE EXPANSION APPROACHES

The geometry expansion model is realized on the Interface level and provides the capability to transfer the information of the expanded node calculated in SAS-SFR to the PARCS model and the node power values from PARCS to the SAS-SFR code. The specificity of the approach allows accounting for the individual axial expansion of pin and hexcan of the SAS-SFR node into the neutron physics model, which uses identical axial mesh lengths in plane for all channels. Different (arbitrary) number of axial nodes can be used in the SAS-SFR and the PARCS models, respectively. Consideration of the radial expansion of the core geometry is currently not implemented for the considered ULOF and/or UTOP transients.

Radial mapping between two domains is performed in a straight-forward manner. Sub-assemblies are allocated to channels according to the map given by the PARCS input. The map defines the associated channel number for subassemblies in a similar way, as given in Fig. 12 above. This input is supported by the original PARCS input deck (input block GEOMHEX) defining the subassembly type (i.e. channel type) in core cross section and corresponding material content.

Axial mapping between the fissile nodes of the two domains is provided by the “smeared geometry” model. For other coupled nodes the approach provides the equivalence of nodes in TH and neutron physics models, respecting the peculiarities of the code input. Processing of node data is described in Appendix II.

The axial expansion is modelled on basis of a "smeared geometry" approach [70], which is schematically illustrated in Fig. 32. In the current implementation it considers (1) uniform expansion of the neutron physics model meshes according to the evaluated expanded average core fissile height and (2) a treatment in a "smeared" way of the individual channel dependent expansion of axial nodes as calculated in SAS-SFR.

The average fissile height of the core in the neutron physics model is derived as follows:

$$H_{fiss}^{av} = \sum_{i=1}^{N_{ch}} H_{fiss}^{i} \cdot w_i,$$

where H_{fiss}^{av} – average fissile height in neutron physics model, H_{fiss}^{i} – fissile height of SA group *i* (channel *i*), calculated by SAS-SFR and w_i is the corresponding weight factor. The weight factor defines the contribution of the given channel for derivation of the average fissile height by accounting for the number of SAs in the concerned SA group and its power level and is derived as follow

$$w_i = \frac{N_{SA}^{i}}{N_{SA}^{tot}} \cdot p_i,$$

where N_{SA}^{i} and N_{SA}^{tot} are the number of SAs in given the concerned SA group i and the total number of SAs in the core, respectively, and p_i is the power peaking factor calculated for the average SA power value in the concerned *i*-th SA group.

After the average core fissile height is defined, the transfer of node data from the N_{th} axial nodes of SAS-SFR to the N_n nodes of PARCS is performed SA group-wise in order to calculate homogenized isotopic number densities for every node of the neutron physics model. For every SA group the procedure is organized as follows:

1. First the isotopic number densities are calculated corresponding to the SAS-SFR nodes individually for 5 components in accord to the data transfer approach, given in §2.2.1. Starting from the homogenized isotopic composition for the "as fabricated" conditions, required by input, the number densities are calculated based on variation of component material mass and the axial node height (see Appendix II).

2. The transfer function is constructed for every component, which provides transfer of "expanded" homogenized number densities of a given component to the other axial mesh, namely from N_{th} axial nodes of SAS-SFR to N_n nodes of PARCS, assuming a flat distribution of the nuclide number density within one axial mesh and conservation of the component mass in the new mesh.

3. The homogenized number density of isotope *i* of the unit cell for XS calculation is derived as the sum over all components:
$\rho_i = \sum_k \rho_i^k$, where *k = {fuel, clad, inner sodium, hexcan, outer sodium}*.

In similar way as for the number densities, the isotope temperatures, which are calculated on the thermal hydraulic mesh, are processed in the "smeared geometry" model. An isotope temperature of a given component in the neutron physics node is derived with mass weighting of the component temperatures of the thermal hydraulics nodes, smeared in a given neutron physics node. Examples of temperature profiles of different components on neutron physics and thermal hydraulic meshes are shown in section 5.1.

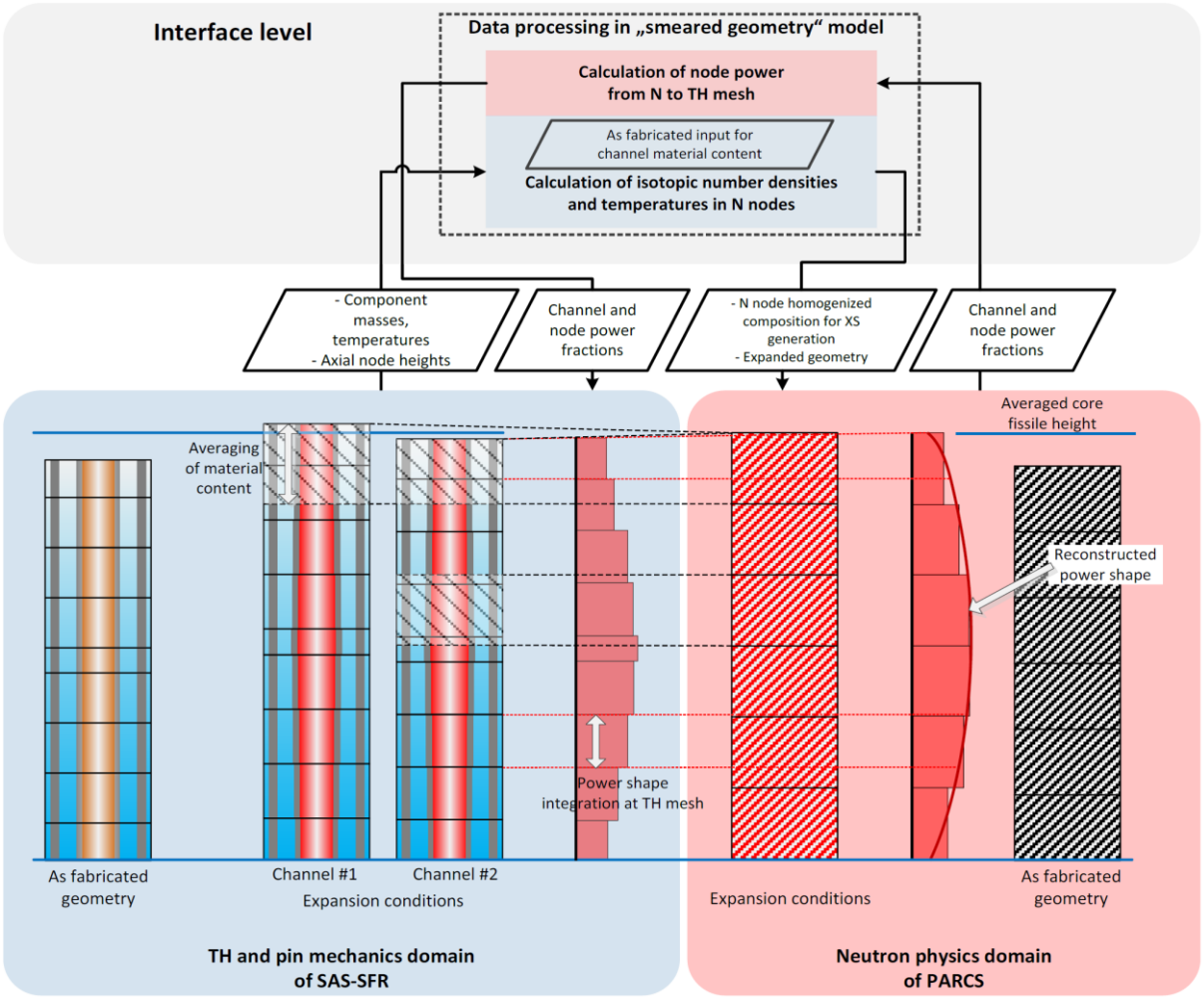

Fig. 32. Principal scheme of "smeared geometry" model with the corresponding coupling to the individual physics domains and the relevant data exchange

The node power data, obtained for the mesh of the neutron physics model, are interpolated in a similar way from the neutron physics to the thermal-hydraulic mesh as follows:

$$\overrightarrow{p_i^{th}} = f(\overrightarrow{\Delta H_i}, \overrightarrow{\Delta H_k}, \overrightarrow{p_k^n}),$$

where $\overrightarrow{p_i^{th}}$ and $\overrightarrow{p_k^n}$ – power fraction values and $\overrightarrow{\Delta H_i}$ and $\overrightarrow{\Delta H_k}$ – axial node heights for the thermal hydraulics and neutron physics models, and i and k are corresponding node indexes ($i = 1, N_{th}, k = 1, N_n$). Two interpolation options have been implemented for this transformation, considering a flat power shape within one calculation mesh or a smoothed power axial shape, constructed as result of a polynomial interpolation.

4.4 NEUTRON CROSS SECTIONS MODEL ("SIGMA-ZERO" MODEL)

The "Sigma-zero" (σ_0) XS model has been implemented as a part of the PARCS code (new modules and subroutines) and is called prior to neutron transport calculations, namely first time at the initialization of neutron physics calculations and then in the beginning of every call for neutron physics code modules.

The “Sigma-zero” methodology is based on the use of a microscopic cross sections library for XS calculation during transient simulations. Its implementation in the FAST code provides fast XS recalculation in spatial kinetics simulations and it has demonstrated robustness and improvements with regard to other approaches, for instance, to the one based on XS derivatives to some state parameters [73]. Practically it is stated that the XS model is able to account for considerable perturbation of physical properties in a region, in particular due to sodium voided conditions and fuel and clad relocation, while a fast iteration algorithm allows calculating effective macroscopic cross sections “on-the-fly”.

The main idea behind the proposed approach is that several sets of microscopic multi-group cross sections for the considered core design are prepared. The multi-isotopic library consisting of data tables in ASCII format is generated based on the ECCO cell code of ERANOS [78] for a suitable range of temperatures and background cross sections on a common grid. Therefore, one fully relies on methods used by ECCO for homogeneous and heterogeneous configurations to assess the specific resonance shielding of the various cross sections. These methods include e.g. accurate homogenization procedures in energy and space, which can be used in conjunction with collision probabilities as well as dedicated capabilities for estimating the diffusion coefficient by considering streaming effects in empty channels (Benoist method).

The temperature-dependent self-shielded data of the new library for PARCS includes total, transport, fission, absorption (equal to capture, i.e. the sum of (n,γ), (n,α), (n,d), etc. plus *fission*), and total scattering matrix cross sections including elastic, inelastic and (n,xn) reactions. The temperature-dependent, unshielded data include number of fission neutrons ν, which is used for calculating the neutron production cross section, and thermal scattering matrix cross sections.

For the physical regions of the core (calculation nodes) at each time step of the transient simulation, a set of PARCS subroutines and input specifications enable to explicitly calculate average macroscopic cross sections. These macroscopic cross sections are generated by interpolating microscopic cross sections from the pre-generated tables, by using, for each time step, region-averaged values for the individual isotopic densities, pre-computed temperatures (from thermal hydraulics domain), and associated background cross sections. Changes of the state variables, e.g. coolant density, fuel temperature, core dimensions etc., leading to perturbations of the neutron spectrum, are caught in their interrelations through corresponding σ_0 variations.

A similar methodology serves as a basis for the cross section generation scheme available in the transient code SIMMER and is used in LOOP2 [106] and in the Los Alamos code TRANSX [107]. However, the sets of multi-group microscopic cross sections are prepared with the NJOY modular system [108] instead on basis of a cell code. The proposed scheme with ECCO in conjunction with dedicated NJOY based data additionally guarantees the excellent treatment of resonance overlapping effects for different situations. The broad use of the TRANSX code worldwide, and the adequacy of LOOP2 for the neutron physics analysis of fast-spectrum systems, which has been successfully demonstrated on the basis of the MUSE-4 benchmark [109] by comparison with MASURCA experimental data and also

with analytical predictions of other codes including stochastic values, clearly support the current choice of implementing a background cross section methodology in PARCS.

The temperatures considered in current transient analyses of the Generation IV SFR range from 300 to 3000 K in steps of 300 K, and also the systematic 20-point σ_0-grid assuming piecewise equal logarithmic spacing comprises the values given in this previous section. This grid is the result of a series of preliminary optimization calculations performed in PSI. In particular, the use of more refined values was found so far not to significantly alter the computational results. However, the associated computational time and especially the overall storage requirements of the PARCS code system would remarkably increase.

A complete data library of 33 neutron group cross sections has been generated for the SFR, including 6 pseudo fission products for U-235, U-238, Pu-239, Pu-240, Pu-241, and Pu-242, allowing transient analyses also for irradiated fuel compositions. These data are based on the adjusted JEF-2.2 cross sections available in the ERANOS 2.1 package, while 33 energy groups and their boundaries are recommended as reference for fast-neutron spectrum applications [77].

4.5 CALCULATION SCHEME AND CONTROL

The steady state and transient simulations require quite similar data exchange between calculations of the two domains. Below a short description is given for steady state and transient simulations.

4.5.1 STEADY STATE COUPLED SIMULATION

The calculation is organized as a loop (Fig. 33) between the neutron physics and the thermal-hydraulics (TH) domains, which is controlled by convergence criteria. Calculation starts with PARCS, which performs its first step on basis of some preliminary nominal core state parameters and provides power data, which are processed in the smeared geometry model and used for the first step of the TH calculation. After the TH step of SAS-SFR, the calculated TH state parameters and geometry data are processed in the smeared geometry model to calculate the node parameters required for the XS generation and geometry expansion of the PARCS core model. The performance of an XS update for coupled nodes of neutron physics model is controlled at the Interface level prior to start of each PARCS calculation by criteria of maximum relative change of (1) fuel temperature (for the fissile nodes only) and (2) sodium density. Corresponding node XS update flags are saved at FORTAN level and used by PARCS XS-related subroutines.

The convergence of SS is reached, when no more XS update is needed for all coupled nodes at next neutron physics iteration step. The value of 0.005 has been found as appropriate for both criteria with convergence reached in 4-6 iterations for the considered ESFR core. After convergence is reached, the last neutron physics calculation is performed on basis of the last obtained core state parameters together with the call for the solution of the adjoint problem in order to initiate the reactivity value calculations in PARCS, which is required for the management of coupled transient simulations.

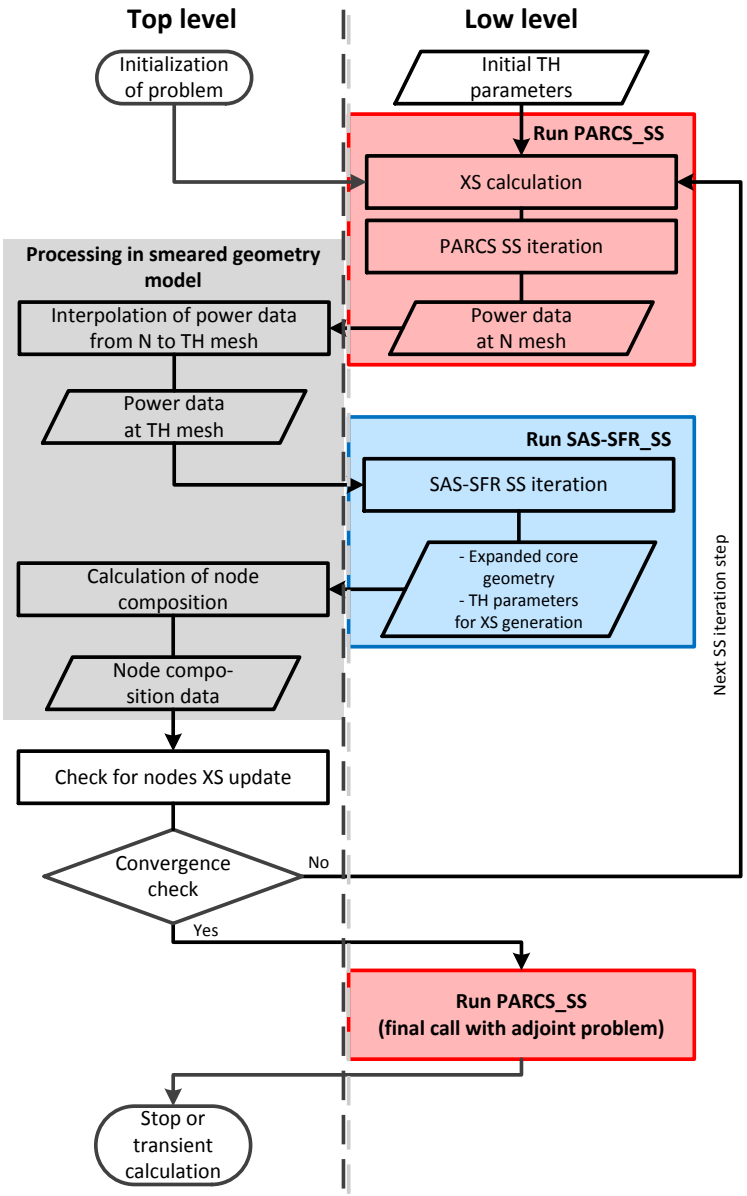

Fig. 33. Principal logical execution scheme of a coupled steady state calculation of SAS-SFR/PARCS code system

4.5.2 TRANSIENT COUPLED SIMULATION

The transient simulation may be run in new coupled system either with use of original PK model of the SAS-SFR code or with spatial kinetics option of the PARCS solver, as defined by user. In the first case, the power data (channel relative power fractions and axial profiles), obtained as result of the converged steady state, are saved and used by the PK model, while necessary reactivity feedback data must be provided by the SAS-SFR input. With the SK option a dedicated input block TRAN in the PARCS input is required.

The calculation logic of the SK option is illustrated in Fig. 34, while the exchange of data between the two domains is organized in the same way as for the SS calculation (see Fig. 33), using the same processing routines at the Interface level. The first transient step starts with a SAS-SFR calculation, which means that the transient characterization on basis of

calculation results obtained in the TH domain is preceding the first transient calculation step in the neutron physics domain. Following the ULOF definition, the perturbation of the core state is imposed by a coolant flow rate decrease, defined by the SAS-SFR input, which causes the transient response of the core state parameters. In case of SK, the corresponding XS update in conjunction with the set criteria leads to reactivity transient variation. The call for the performance of an XS update for a given node is controlled by one of the following criteria for the whole transient simulation time (typical values used for calculations are provided here)[22]:

1) relative change of the average node fuel temperature(0.003-0.005);
2) relative change of the sodium density (0.003-0.005);
3) relative change of the fuel mass (0.001-005);
4) relative change of the clad mass (0.001-005).

The last two criteria related to the fuel and clad mass are necessary in the time period, where a material motion occurs. A specific algorithm is introduced, which allows using smaller criteria for relative changes of the fuel temperature and the sodium density at the start of a simulation (first 100 calculation steps) in order to obtain a better "smeared out" reactivity response during this initial time period.

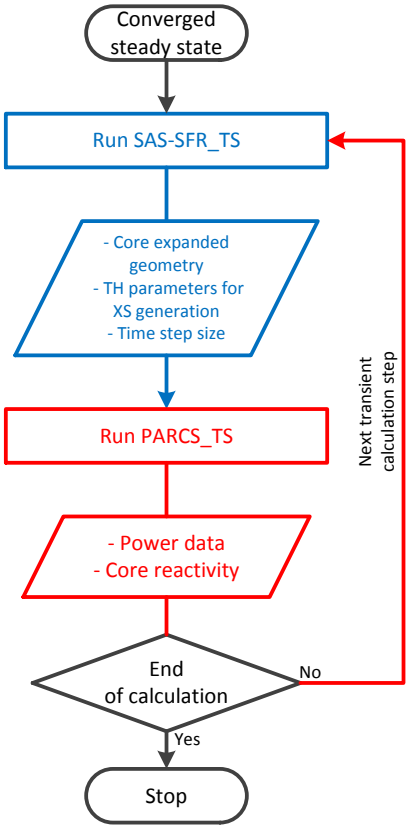

Fig. 34. Principal logical execution scheme of a coupled transient calculation of SAS-SFR/PARCS code system using the space kinetics option

[22] An update of all XS at every time step is possible as well, but it is more time-consuming. The values given are evaluated as an appropriate compromise to treat the changes of core state parameters in XS calculation.

The original SAS-SFR approach contains a sophisticated scheme to determine an appropriate main time step size adjusted to the peculiarities of the considered transient and the explicit forward directed solution algorithm.

The stand-alone PARCS code uses a relatively simple approach with regard to the time step selection. It is defined in the input by the user.

In contrast to that, the SAS-SFR code with its point kinetics model provides specific algorithms to evaluate the transient calculation time step size with a "multiple level" choice, considering a large number of factors, such as core reactivity level, in particular, how close the reactivity approaches a prompt-critical state, and physical phenomena occurring during transient, such as sodium boiling or fuel and clad motion. A new time step is calculated always "on-the-fly", considering the range from a relatively large one of about 0.05 s in the beginning of a transient down to values of the order of $1 \cdot 10^{-4} - 10^{-6}$ s, when prompt criticality is approached or exceeded. The calculation of a new main time step is done at every time step by SAS-SFR (subroutine DTMFND). The original time step "hierarchy" logic and calculation mechanism have been evaluated as reasonable and effective for the new development of this work as well. Practically, the algorithm implemented in DTMFND requires the core reactivity level as input along with parameters, which are representative for specific phenomena. The actually established core reactivity value is provided by the PARCS code when the adjoint problem is solved. In order to compute the dynamic reactivity during the transient calculation the adjoint solution of the initial eigenvalue problem is obtained at the end of the SS, while at any time point during a transient, the dynamic reactivity is defined [75] as:

$$\rho = \frac{(\varphi_0^*, A\varphi)}{(\varphi_0^*, F\varphi)},$$

where A is the net production operator, defined as $A = F - M$, F – the fission source operator, M – migration and loss operator of fixed source problem, φ – neutron flux, and φ_0^* – the solution of adjoint eigenvalue problem (adjoint flux) for the initial stationary conditions. The changes of the core conditions are expressed and determined as perturbations to the net production operator.

5 APPLICATION AND VALIDATION OF THE COUPLED CODE SYSTEM SAS-SFR/PARCS

5.1 CORE MODELS

For this study, both representations of the ESFR core with 60- and 120-degree symmetry as described in §2.4.2 have been used, see Fig. 12. The 60-degree symmetry representation in the neutron physics problem allows reducing the computation time. Both flow gagging options – with three and nine cooling groups (see Table 6) – have been applied for this part of the study, in particular, because it provides an efficient basis for a comparison with results of the CP ESFR project [41], [27]. In addition it allows evaluating consequences of different sequences of boiling propagation across the core cross section on the comparison between results using either a PK solver or a SK solver in case of a ULOF accident.

All physical regions relevant for the neutron physics solution, are represented in PARCS in a similar manner as in the MCNP model, see §3.2.2. An overview of the axial cross-section of the core model is given in Fig. 35. Different to MCNP, in PARCS the upper gas expansion and upper pin plugs sections are represented by one homogenized physical region. All dimensions of non-fuel zones are given in the PARCS input as specified for the Reference Expanded conditions corresponding to the nominal operation conditions, while the fissile core height is updated according to the fuel pin expansion, predicted by SAS-SFR in steady state and transient simulations.

An overview of the SAS-SFR model of the ESFR Reference Oxide core is provided in §3.2.1. The same axial representation of the pin and SA is used, which considers 13 axial meshes within the fissile core height (Table 7). As it is allowed by the "smeared geometry" model, the PARCS model may employ arbitrary number of axial meshes. Examples of an interpolation of the nodal power distribution (from PARCS to SAS-SFR) and node-wise fuel temperatures (from SAS-SFR to PARCS) are shown in Fig. 36 for a 10- and 15-mesh representation of the fissile height in the neutron physics model of PARCS. The nodal specific power values plotted are normalized to 1 within fissile height and are given as coloured edge bars with the width which is equal to the node height (Fig. 36, top). For the fuel temperature interpolation curves (Fig. 36, bottom), the node temperatures are given at node mid-points; the blue mesh corresponds to nodes of SAS-SFR and the red one – to PARCS nodes.

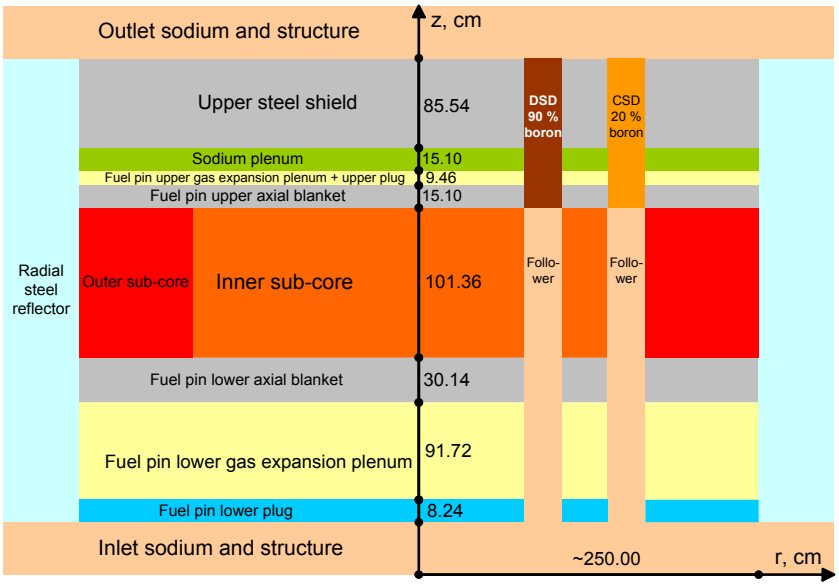

Fig. 35. Schematics of the axial cross-sectional cut of the ESFR Reference Oxide core model and control and shutdown rods structure

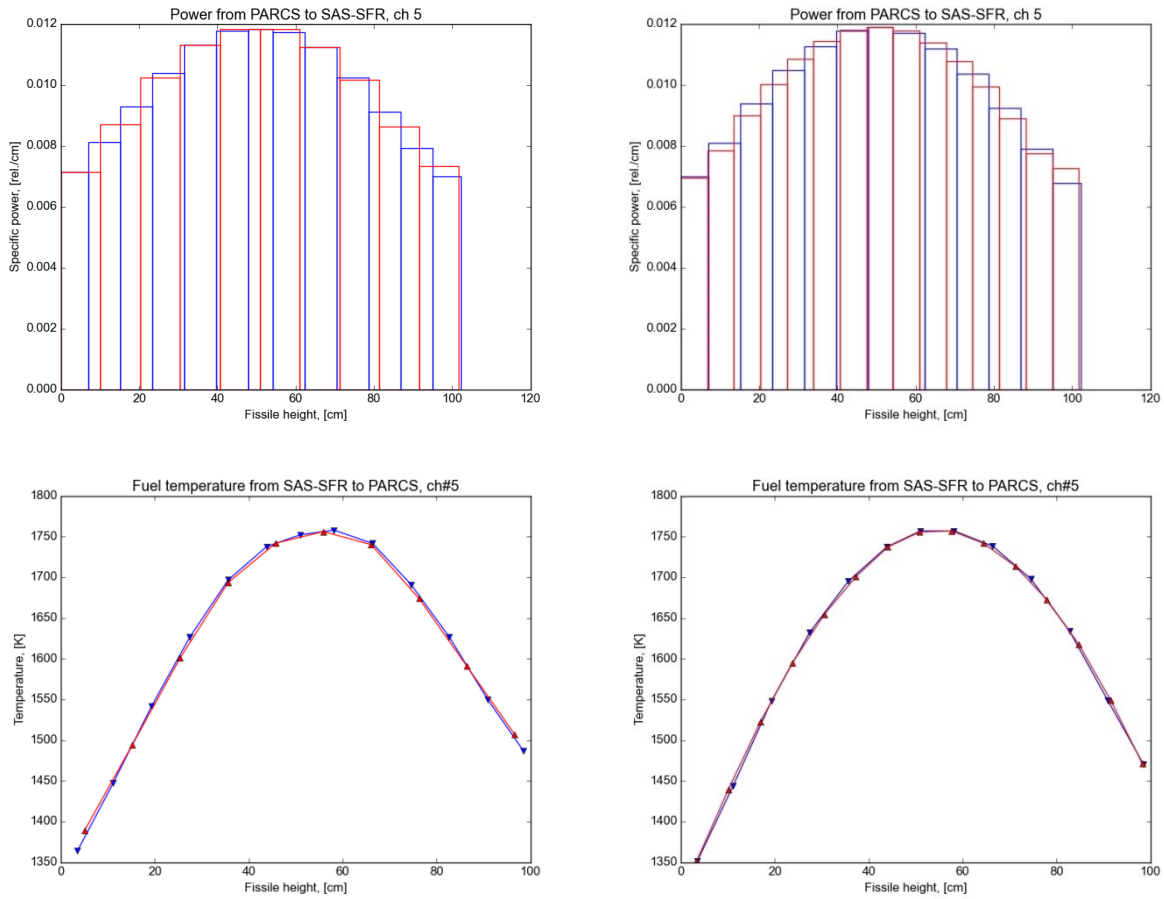

10 axial meshes in PARCS 15 axial meshes in PARCS

Fig. 36. Interpolation of node power fractions (top) and fuel temperature (bottom) for two different axial nodalisation (blue mesh – SAS-SFR, red mesh – PARCS)

5.2 APPLICATION FOR STEADY STATE CONDITIONS

5.2.1 COMPARISON OF SAS-SFR/PARCS AND SAS-SFR/MCNP CALCULATIONS

The steady state configuration of the ESFR Reference Oxide core has been analysed with the new SAS-SFR/PARCS code system and the obtained results are compared with the ones of SAS-SFR/MCNP for code system validation purposes. Both PARCS and MCNP codes use the same 120-degree symmetry core representation and utilise 360-degree three-dimensional core models. The gagging scheme with three cooling groups (3 CG) has been selected for the comparison. All control rods are withdrawn for this comparison exercise and located at the top of sodium plenum. This configuration allows excluding the reactivity effect, related to CRs, resulting from a relative movement of the CRs in relation to the fissile height, when an axial pin expansion is modelled.

Resulting K-effective values obtained with use of the new tools are given in Table 11. The K-effective value, obtained with the code system KANEXT [47] for a core model, corresponding to the Reference Expanded conditions, is also provided for comparison. Appropriate agreement can be stated between the deterministic solution of PARCS and the Monte Carlo solution of MCNP (each with a corresponding approach for the neutron cross sections). A series of calculations has been performed for the evaluation of safety parameters – Doppler constant and Sodium Void effect (SVE). An acceptable agreement can be stated for all safety parameters, listed in Table 11. The SVE values predicted by the deterministic calculations with PARCS (in conjunction with "Sigma-zero" XS model) and KANEXT are slightly higher (about 150-200 pcm) for the core fissile height compared to the MCNP calculation. Also the SVE in the above-core regions (the regions of upper steel blanket, upper gas plenum and pin plug, and sodium plenum) is evaluated similar for all calculation cases and amounts to a value of about -(100-120) pcm. Additionally, deviations of the Doppler constants as calculated for the three cases are in a threshold level of less than 100 pcm.

Table 11. Safety parameters of ESFR Reference Oxide core as calculated with different neutron physics tools

Parameter	Calculation tool		
	SAS-SFR/MCNP	SAS-SFR/PARCS	KANEXT
K-effective (all CRs withdrawn)	1.0124	1.01195	1.01167
Doppler constant, pcm	-1114	-1198	-1094
Doppler constant at voided configuration, pcm	-858	-892	-860
SVE in fissile height, pcm	1581	1753	1784
SVE in fissile height and upper zones, pcm	1475	1623	1656

The channel relative powers and corresponding fissile heights calculated with both new solutions are shown in Fig. 37. Both calculations exhibit the same shape in terms of the radial fissile height distribution and the channel relative power. The differences in channel relative powers (peaking factors) are smaller than 2% for most of the channels; differences

being similar to the ones observed between the two cases – RE and FC – of the SS analysis with the SAS-SFR/MCNP coupled scheme. A maximum difference of about 4% is observed for channel #10, which represents SAs at the core radial boundary, where PARCS over-predicts the power level, while for the central channel #1 the relative power is under-predicted by PARCS by about 3%. Generally, an appropriately good agreement can be stated between deterministic and MC solutions for the channel power and fissile height values.

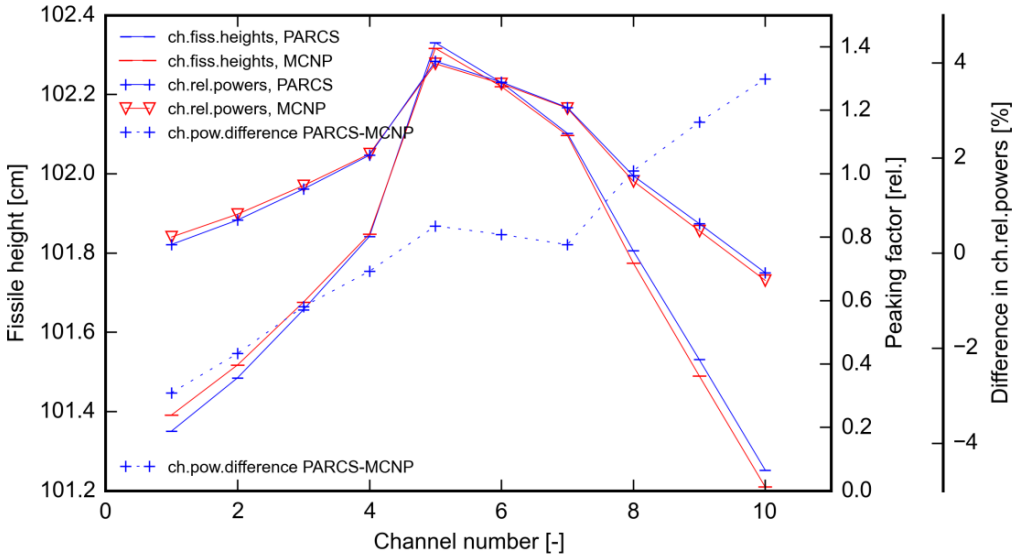

Fig. 37. Channel relative powers (peaking factors) and channel fissile heights for PARCS and MCNP calculation cases (3 CG core configuration, all CR withdrawn)

Withdrawal of CRs in the outer row influences the radial power distribution in the core and leads to a decrease of the power fraction in the inner sub-core. This can be evaluated by a comparison of the calculation results for the two core configurations. The most influenced channels are channels #1 and #2 (inner sub-core), for which the power decreases by about 9% and 5% and channels #4 (inner sub-core) and #7 (outer sub-core), for which the power increases by about 5% and 4%, respectively, since the latter two represent SAs in vicinity of CRs outer row. Maximum SA peaking factors (corresponding to channel #5) for the core configurations, when CRs in outer row are inserted and withdrawn, are evaluated to be similar and amount to about 1.35. In Fig. 38 a SA power peaking factor map is presented as calculated by SAS-SFR/PARCS for the core configuration when all CRs are withdrawn. The subassembly power peaking factor is defined as:

$$p_{SA}^{i} = \frac{P_{SA}^{i}}{\bar{P}_{SA}},$$

where P_{SA}^{i} – power of the subassembly i and $\bar{P}_{SA} = \frac{1}{N_{SA}} \sum_{k=1}^{N_{SA}} P_{SA}^{k}$ – average subassembly power in the core, N_{SA} – number of subassemblies in the core.

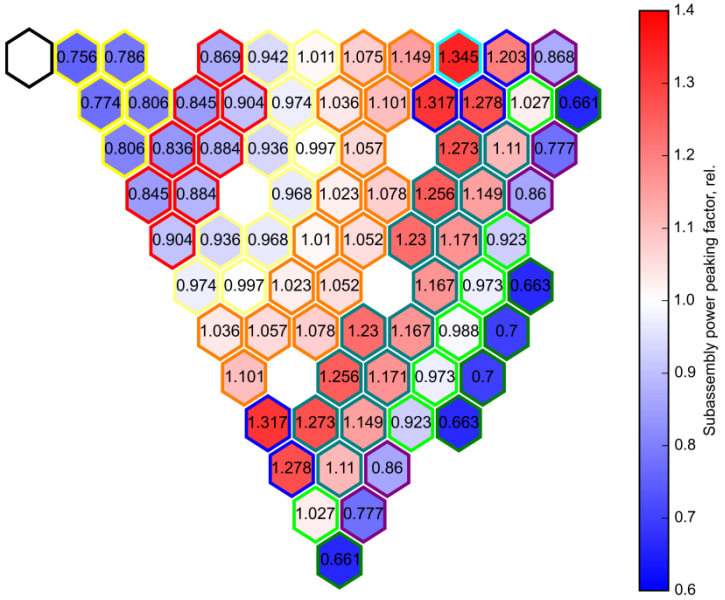

Fig. 38. Sub-assembly power peaking factors for coupled solution with PARCS (all CRs withdrawn, 3 CG configuration)

Differences in node normalized powers (normalized individually for every channel) obtained for both coupled solutions are shown in Fig. 39. These node normalized powers are used at the last SS iteration by thermal hydraulic models of SAS-SFR and define the final SS characterization of the core. For the SAS-SFR/MCNP solution, these power values are obtained at last SS iteration using a relaxation technique (see §3.1.2), while for the SAS-SFR/PARCS these values are calculated in the "smeared geometry" model for the thermal hydraulics mesh on basis of power data calculated in PARCS and given on meshes of the neutron physics model.

On the left side of Fig. 39 the differences are shown for the option of the "smeared geometry" model, which considers a flat linear power axial shape in all nodes. On the right side of Fig. 39 the results are shown for an option with the improved approach, which considers a smooth axial power shape by a reconstruction of the node linear powers axially with polynomials and corresponding interpolation of power data on the thermal hydraulics axial mesh. Maximum differences in the node powers, which are observed at axial boundaries of the fissile height, do not exceed 4% for the first option (left hand side of Fig. 39), while for most of the nodes the difference is below 2%. For the second option with polynomial interpolation the differences are considerably smaller (see Fig. 39, right). This confirms the applicability of this improved approach, since the power distribution is a smooth function in space. The maximal differences of about 1.5% only are also observed in the nodes at the fissile core axial boundaries, while for most of the nodes the difference is not exceeding 0.5%. This coherence of results demonstrates also a good agreement of deterministic and Monte Carlo solutions. For both options a slight overestimation of power release at the fissile core axial boundaries is observed for the PARCS calculations.

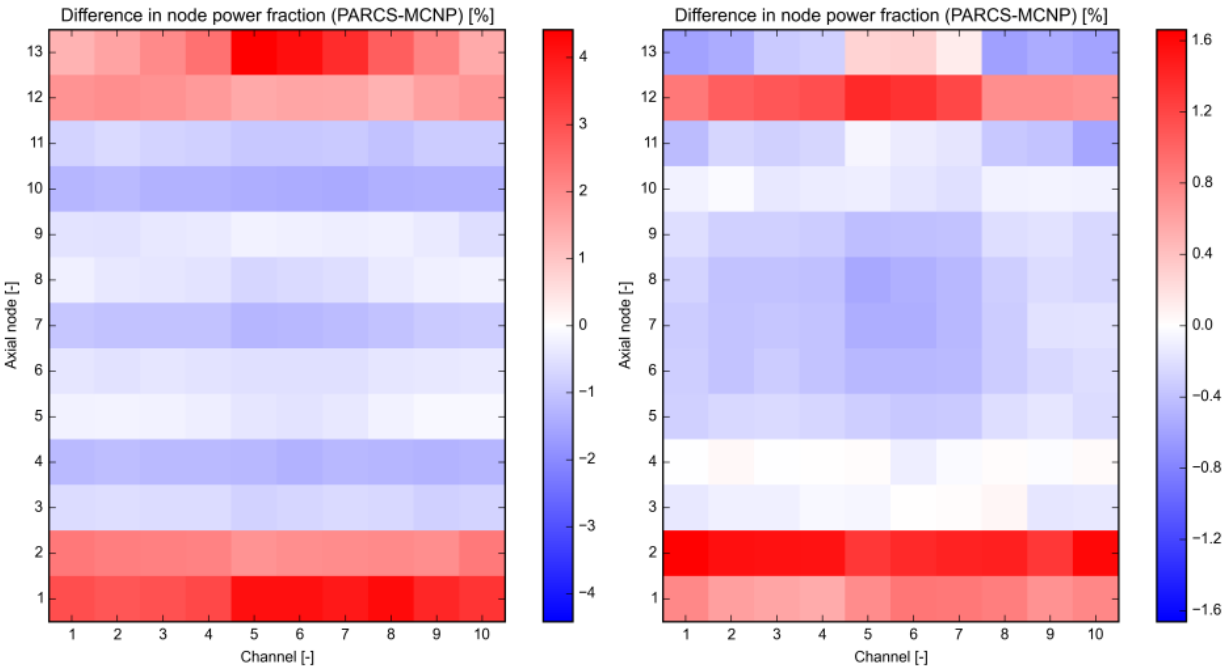

flat linear power axial shape in the node

polynomial interpolation of linear power axial shape

Fig. 39. Differences in node power fractions between PARCS and MCNP solutions (all CRs withdrawn, 3 CG configuration)

Node-to-node comparison of fuel and sodium temperatures, calculated with the new solutions at SS is given in Fig. 40. The "smeared geometry" model option of flat linear power axial shape in the node is used here for the results comparison. The distributions are given axially for 13 axial nodes of the fissile height used in the thermal hydraulics model of SAS-SFR (see Table 7) and "radially" for 10 channels. The differences in node fuel temperatures, caused mainly by differences in node powers, are relatively small (within about 30 K) and correspond well to the correlation of 10 K/%-of-power, formulated above in §3.4.1 for this core.

The inner-sub-core channels #1, #2, #3 have slightly lower node powers and relative power, which results in lower node fuel temperatures for these channels. The channel relative power of channel #1 predicted by both coupled codes differs from each other by around 3% and leads to a difference in the node fuel temperatures of about 20-30 K for most of the nodes. In a similar way, differences in the relative power of outer sub-core channels #8, #9 and #10 lead to slightly higher node fuel temperatures in these channels when calculated with SAS-SFR/PARCS in comparison to the reference SAS-SFR/MCNP calculations. The map of node dependent sodium temperatures shown in Fig. 40 (bottom left) for the PARCS solution exhibits a strongly non-uniform heat-up of the sodium in different channels as result of application of the 3 CG flow gagging scheme. The sodium node temperature values show good agreement as well, because they are defined mainly by the node power. The differences in the sodium temperatures at core outlet (which is calculated in the uppermost axial node) are consistent with differences in the channel powers.

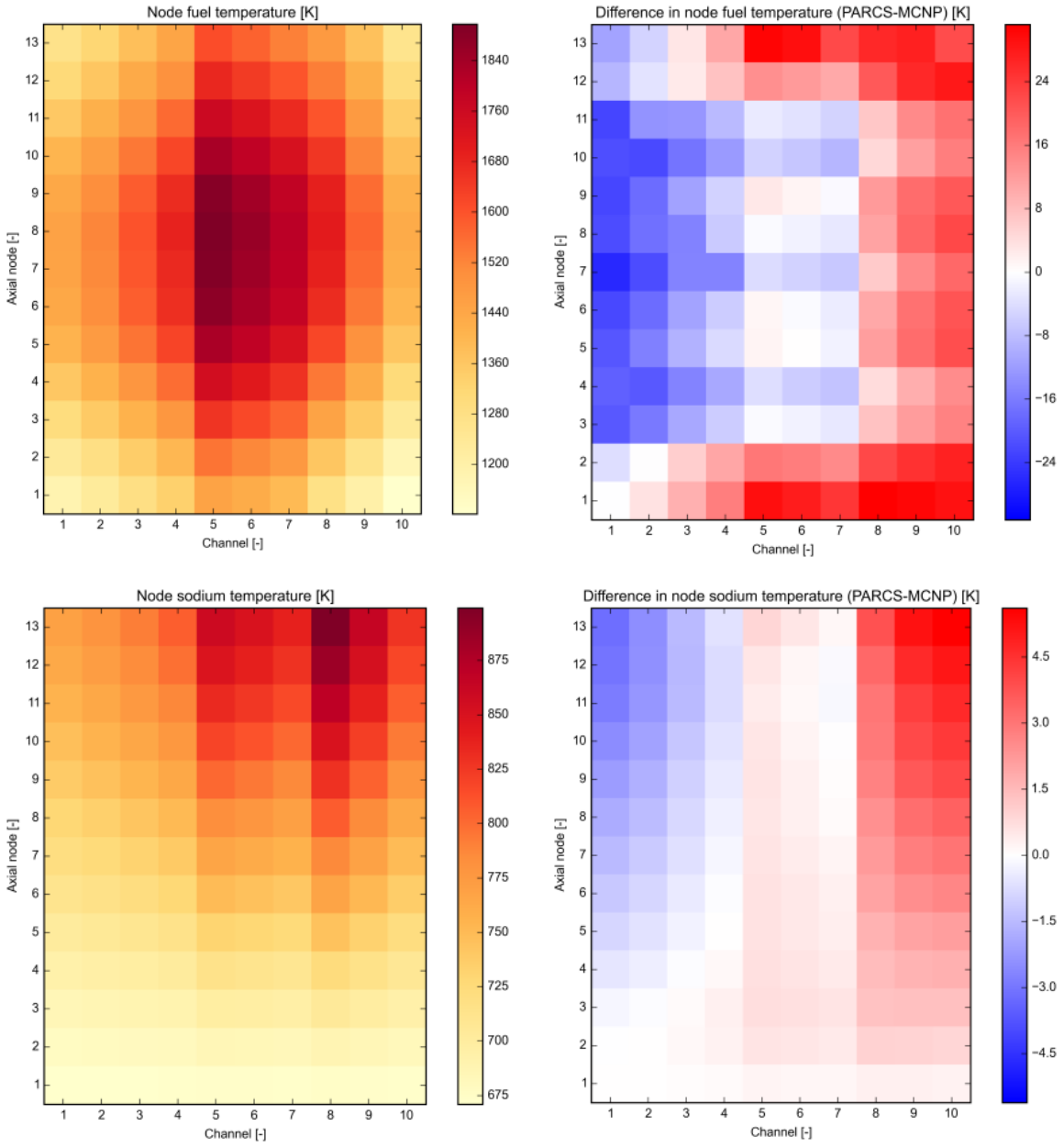

Fig. 40. Fuel and sodium node temperatures computed with PARCS coupled solution for the fissile nodes and their differences with results of the MCNP coupled solution (all CRs withdrawn, 3 CG configuration)

5.2.2 REACTIVITY PREDICTION WITH RESPECT TO CORE POWER LEVEL

The newly developed solution scheme has been validated by a comparison of steady state results of test cases against corresponding ones on the basis of a MC method. The selected test cases correspond to the reactivity transitions due to power level changes for SS core conditions. Varying the power of the core at SS different reactivity values are calculated, due to the change of the XS and the geometry. The power has been varied between 50% and

150% of the nominal value, while the coolant mass flow has been kept constant. Differences due to the Doppler effect, thermal core expansion and sodium heat-up in every case influence the reactivity balance and result in different SS reactivity values. The static reactivity values for different power levels as modelled in SS simulations for both solution approaches are given in Table 12.

Table 12. Core reactivity for different steady-state power level calculated with PARCS and MCNP coupled solutions

Power level, [%nom]	Reactivity [pcm]		
	SAS-SFR/MCNP	SAS-SFR/PARCS	Difference
50	1682.2	1599.9	-82.3
75	1427.0	1370.2	-56.8
100	1207.6	1180.7	-26.9
125	1041.0	1024.2	-16.8
150	926.3	898.9	-27.4

The deterministic neutron physics solution with the "Sigma-zero" XS model is close to the SAS-SFR/MCNP solution demonstrating the correctness of the data transfer methodology realized for the different neutron physics solutions. The core reactivity varies with the power level (see Fig. 41), mainly due to a strong negative reactivity component of the Doppler effect (evaluated to amount to -(500-600) pcm for the transition from 50 to 150% of nominal power) and less pronounced by the cumulative contributions of the components of axial core expansion (about 30-40% of Doppler effect), which are counterbalanced by a relatively small positive contribution of the sodium density effect (about 70 pcm for given transition of power). This conclusion is supported as well when comparing the calculated power reactivity coefficients which are calculated for both solutions at nominal power. The power reactivity coefficient is defined as the incremental change of the reactivity per percent of power change. The data of the reactivity coefficients are listed in Table 13 and illustrated in Fig. 41. In the last column of Table 13 the value is given as calculated with the SIM-SFR code [23]. The code employs a PK model with pre-specified input values for the reactivity feedback effects. The SIM-SFR code has been comprehensively validated for this particular ESFR core configuration within the CP ESFR project [110].

Table 13. Power reactivity coefficient calculated with use of different code systems

Power level [%nom]	Power reactivity coefficient [pcm / %nom.power]		
	SAS-SFR/MCNP	SAS-SFR/PARCS	SIM-SFR
100.0	-7.72	-6.92	-7.01

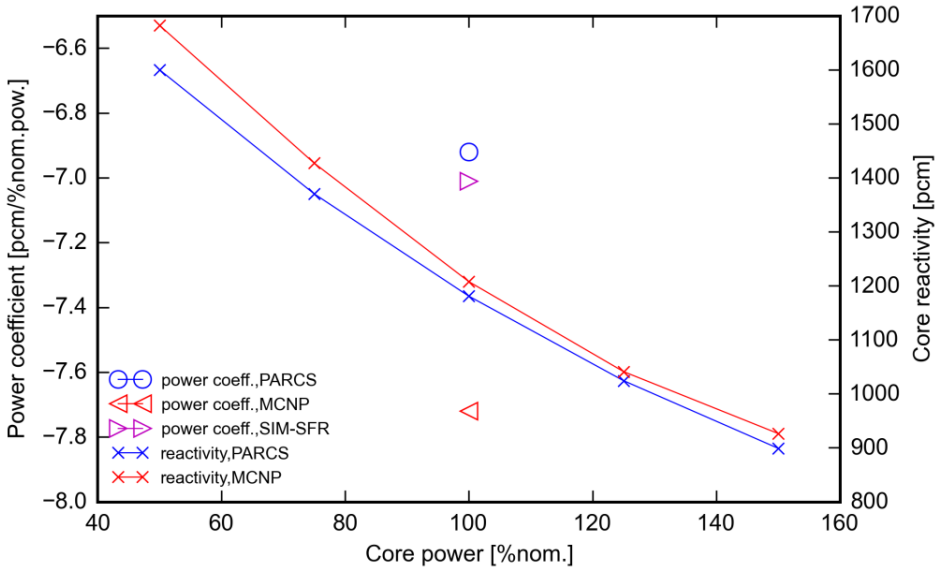

Fig. 41. Reactivity versus core power level and power reactivity coefficient at nominal power at steady state for coupled PARCS and MCNP solutions

5.3 ANALYSIS OF A ULOF TRANSIENT FOR A CONVENTIONAL SFR

The new coupled code system SAS-SFR/PARCS shall simulate the ESFR Reference Oxide core behaviour in case of a ULOF transient. Results obtained using the SK option are compared to the ones obtained using the PK option. For the thermal hydraulics part of the problem the gagging options with three and nine cooling groups has been considered in the analysis (see Table 6). This approach allows it to evaluate consequences of different sequences of boiling propagation across the core cross section on results using either a PK solver or a SK solver.

With regard to the PK simulation case, the transient starts from the same converged SS core configuration, obtained by coupled simulations with PARCS, thus the difference with the SK option is demonstrated.

However, prior to the performance of calculations for such a complex problem several transient tests have been performed to qualify the developed calculation scheme regarding reliability, numerical stability, robustness, consistency on data transfer and physics.

5.3.1 TRANSIENTS DEFINITION AND TESTS

To test the overall capabilities of the coupled code system, two test case set-ups have been defined to be evaluated with the spatial kinetics option, namely:

- Zero transient test and
- Control rod movement tests.

For this purpose, the core is represented by 10 channels using 3 cooling groups. In the following paragraphs the main results obtained for each test case will be discussed.

"Zero" transient test

To check the stability of calculations a so-called "zero" transient test has been performed, which considers a transient simulation with a constant nominal coolant mass flow and inlet temperature, i.e. without any external perturbation. The original SAS-SFR code has always been tested in such a way for consistency of the numerical solution algorithms, as well as for the sensitivity of results to the used hardware and different compiler options, respectively. For the latest code version a typical calculation of an SFR is characterized by negligibly small variations of the reactivity and normalized power over a time period of up to 600 s, which remain on a level smaller than $2 \cdot 10^{-4}$ for the normalized power variation and a value of $5 \cdot 10^{-5}$ \$ for the reactivity variation. Practically, the variations appear due to the fact that the differencing scheme and the solution algorithm for calculation of the coolant temperatures in the subroutines used for the transient and the ones used for the steady state pre-transient power operation differ from each other.

For the coupled code system, additional numerical inaccuracies appear, in particular as result of the switch of the neutron physics solution from fixed to time-dependent neutron source calculations. The stand-alone PARCS code solution with typical source convergence options demonstrates an appropriate stability of the transient solution for the case, where no XS update is considered during the simulation time. For the coupled system a zero transient test has been performed for the 10 channels core representation with the XS update criteria identical to the target simulation case, namely, the XS update for the calculation node is called, if fuel or sodium temperature transient relative change exceeds the level of 0.005.

The plots of the normalized power, reactivity and maximum fuel and sodium temperatures transient variations for the calculated zero transient over a time period of 25 s is given in Fig. 42. An XS update is not necessary during this time period. Smoothed transient variations of power and reactivity are observed. The variations of maximum fuel (< 5 K) and sodium (< 0.1 K) temperature are marginal. The initial reactivity is slightly positive ($5 \cdot 10^{-5}$ \$), what defines the trend of the power variation. The power change reaches the level of $1 \cdot 10^{-3}$ in 25 s transient time. This stability of the calculation is considered sufficient for the time framework of the considered ULOF transient.

Control rod movement tests

A set of transient tests have been performed simulating CR movements as an externally imposed initiator of a Transient Over-Power (TOP) type transient. A study on step-wise movement of all CRs in the outer row of control rod positions which employs a 2 channels core representation is given in Appendix III. As result of the power excursion, the change of fuel temperatures leads to a reactivity feedback due to the Doppler effect, while other reactivity effects have not been considered in these test case exercises. The core power is stabilized at a new level within 10-15 s.

In order to evaluate three-dimensional effects during the power excursion an additional print-out for every transient time step has been introduced into the code of the subassembly normalized integral fluxes and their relative change in comparison to SS values. Subassembly normalized integral flux is defined as:

$$\varphi_i^{norm} = \frac{\varphi_i}{\sum_{i=1}^{N_{SA}} \varphi_i},$$

where φ_i – integral neutron flux in subassembly i (integrated over axial fissile height and over neutron energies) at given time step and N_{SA} – number of subassemblies in the core.

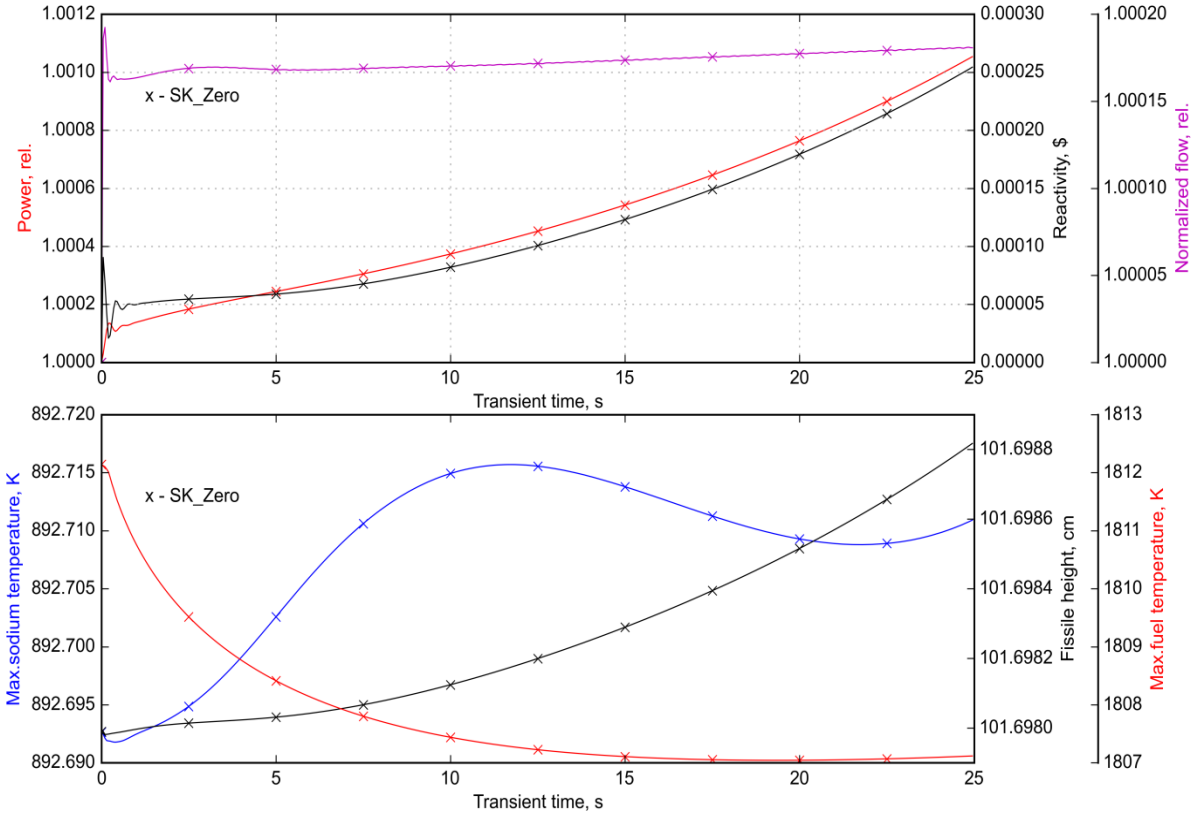

Fig. 42. Temporal evolution of the normalized power, net reactivity and normalized sodium mass flow (top) and maximal fuel and sodium temperatures and fissile height (bottom) in "zero" transient test simulations

In Fig. 43 and Fig. 44 results of the prompt critical transient are demonstrated, which is performed on basis of the 10 channel core model with 3 cooling groups. The core has reached prompt-criticality with an insertion of a dynamic reactivity of about 2 $ within 30 µs as consequence of a step-wise withdrawal of CRs in the outer row by 2 calculation meshes (from core fissile top). In Fig. 43 the normalized power, reactivity, average fuel enthalpy (top), sodium mass fraction in fissile height and in above-core structures, fissile height and fuel temperature (bottom) are shown for the first part of the transient, which includes the prompt critical power excursion. The power reaches a maximum value of 4440 times nominal in 2 ms after onset of the reactivity insertion. The initial dynamic reactivity is evaluated by PARCS at a level of 2.09 $. During the first 0.5 ms time period practically no reactivity feedback is available, but the dynamic reactivity is mitigated by about -0.3 $ as result of the prompt neutron flux redistribution in space.

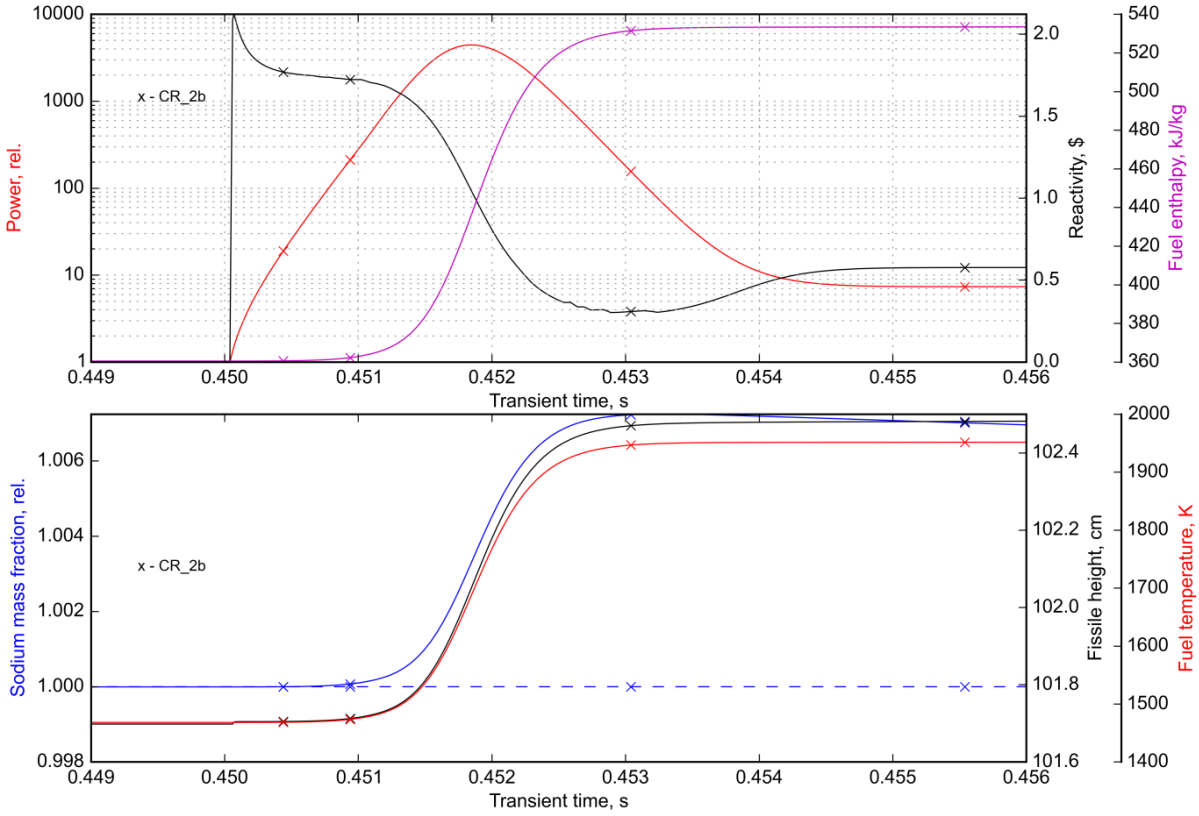

Fig. 43. Computed normalized power, net reactivity and average fuel enthalpy (top) and sodium mass fractions in fissile height and in above-core structures, fissile height and fuel temperature (bottom) for a prompt-critical (2 $) power excursion initiated by an artificial withdrawal of outer row of CRs

The normalized SA flux changes after this redistribution (in 0.2 ms after the reactivity insertion) are given in Fig. 44 for the different SA positions. The difference between the static reactivity values for the two converged SS core configurations – with and without CRs inserted – is equal to 1.88 $, what demonstrates good agreement with the evaluations above.

These results demonstrate clearly the influence of the redistribution of the normalized flux in a radial core cross-section. Fewer neutrons are absorbed near the boundary between inner and outer sub-core after CRs are withdrawn and the multiplicative capability is increased in the vicinity of CR positions. The changes in SA powers are very close to the ones of the flux (Fig. 44). For the second part of the transient, the Doppler reactivity is the most effective mechanism to mitigate this power excursion. The reactivity decreases during this part of the transient due to the rapidly activated Doppler Effect and, in addition, axial expansion reactivity effect, as result of the rapid fuel thermal expansion. The average fuel temperature rises from 1470 K to 1970 K (by 500 K) within a time period of about 3 ms inserting a strong negative reactivity of about -0.9 $. The additional negative reactivity is inserted as result of fuel axial expansion, which is evaluated to amount to about -0.3 $[23], what results in a total reactivity level of 0.55 $ within 5 ms after the onset of the transient. The core

[23] The fuel axial expansion reactivity effect is evaluated to amount to 0.2 pcm/K for this core, what results in negative reactivity response of 0.2 pcm/K x 500 K = 100 pcm or about 0.3 $. The clad and hexcan expansion contributes with positive reactivity, but is practically delayed in time for this exercise.

configuration after this prompt critical excursion is characterized by a slightly larger sodium mass fraction in the fissile height (Fig. 43, bottom), which is due to the increase of the fissile core height while the sodium density has not changed yet due to its thermal inertia. Such a variation of the calculated sodium mass within fissile height demonstrates the consistency of the data transfer from SAS-SFR to neutron physics model of PARCS. In the upper core structures the sodium mass fraction stays equal to 1, since no variation of the outlet sodium temperature occurred during the considered part of the transient.

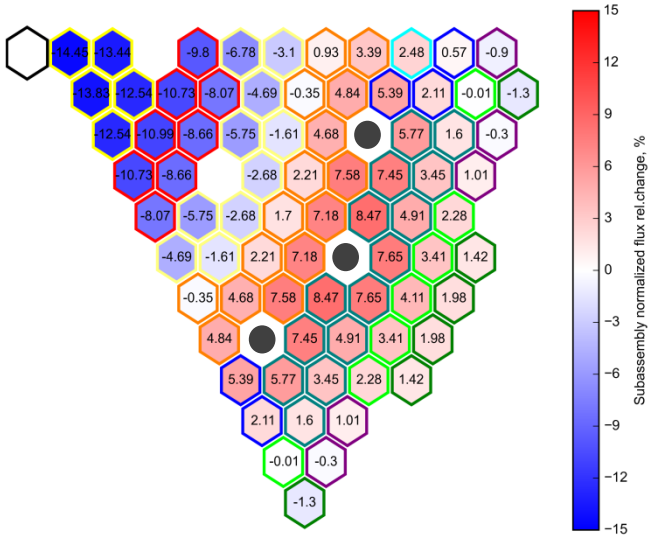

Fig. 44. Changes in normalized neutron flux of subassemblies at t = 0.2 ms after step-wise insertion of 2 $ positive reactivity by withdrawal of outer row of CRs (marked by dark dots), hexagon edge colours correspond to channel colours of map in Fig. 12

5.3.2 Simulation of a ULOF accident with SAS-SFR/PARCS

The ULOF calculations presented hereafter contain three studies which help to discuss the phenomenology of the transient and specific differences between results of the PK and SK solutions. First the three cooling groups (3 CG) case is described. Next a specific study on reactivity components acting during the pre-boiling phase is presented. And last paragraph includes the results and discussions for the nine cooling groups (9 CG) case setup.

5.3.2.1 Comparison of ULOF simulations using PK and SK option for the three cooling groups core configuration

Results of the two ULOF calculations with PK and SK neutron physics models are discussed hereafter covering the following three time intervals:

(1) the time period up to boiling onset;
(2) the boiling time period up to the first onset of clad melting in a SA group (channel);
(3) the post clad melting onset time period up to the first achievement of sub-criticality and beyond.

As it has been demonstrated at §3.4.2, the specific non-uniform sodium heat-up in the different channels of 3 CG core configuration has significant influence on the transient development, in particular resulting in a relatively long boiling phase.

The temporal evolution of the characteristic core parameters before boiling for the PK and SK options is given in Fig. 45. During this phase the total reactivity is mainly defined by three contributions, i.e. due to the Doppler effect, the axial expansion of fissile core height and the sodium density variation, as discussed in §3.4.2. Sodium boiling occurs for both considered cases relatively early at 18.72 s for the PK and at 18.52 s for the SK option in the uppermost fissile node of channel #8 with the highest power-to-flow ratio (see Table 6, marked by red colour). The SK solution predicts a slightly higher power, by 4.2%, at boiling onset, caused by a slightly higher reactivity level up to the time of boiling onset, while the reactivity variations during the first 5 s are very similar for the SK and the PK calculations. At boiling onset, the difference in the net reactivity between SK and PK is rather small, about 1.5 cent or 6 pcm. The reasons of this difference will be discussed in §5.3.2.2.

Characteristic data of the core states at the time of boiling onset are listed in Table 14. As result of the slightly higher core power during this period the average and maximum values of fuel and sodium temperatures are also slightly higher for the SK calculation at this moment (see Fig. 45 and Table 14) compared to the PK model.

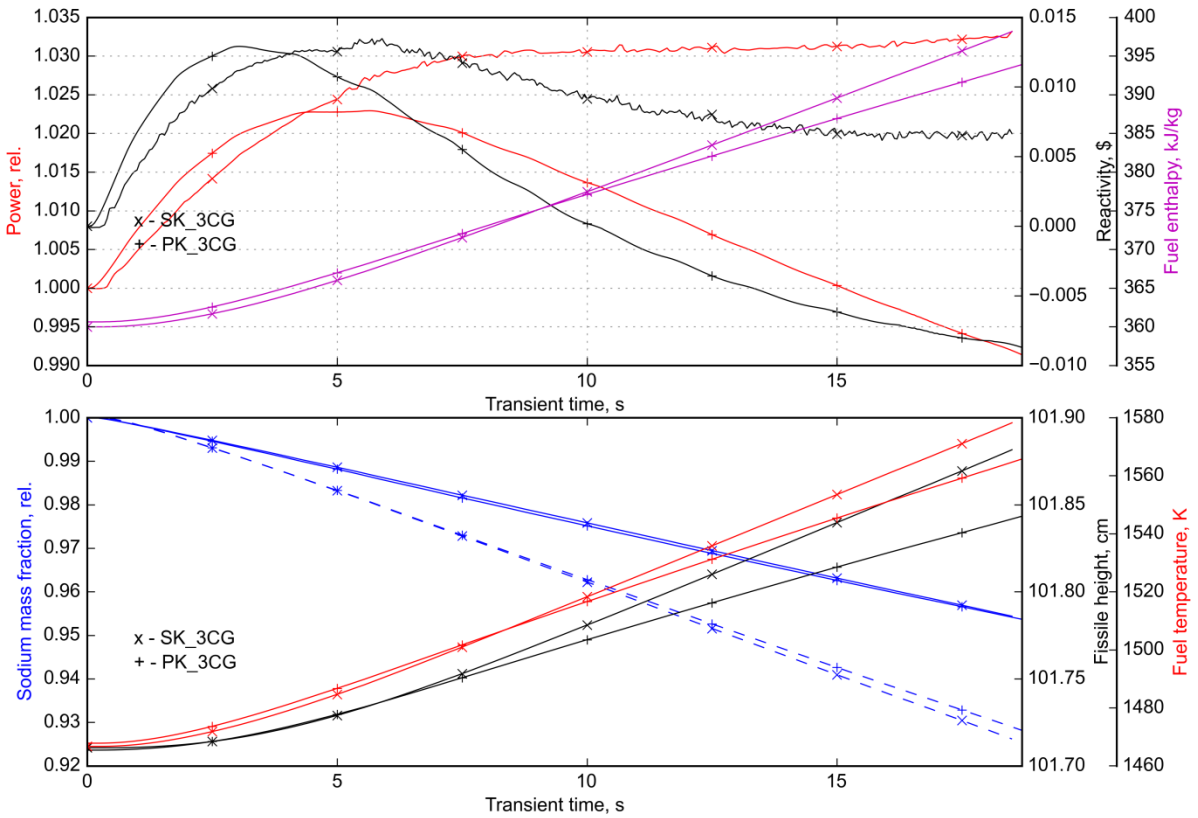

Fig. 45. Temporal evolution of characteristic core parameters in a ULOF as calculated with PK and SK options before boiling onset (3 CG configuration)

Table 14. Characteristic core parameters at the boiling onset in a ULOF as computed with different neutron kinetics options for 3 CG configuration

Parameter	PK	SK
Time of boiling onset, s	18.72	18.52
Total core power, % nom.	99.1	103.3
Normalized mass flow, %	34.3	34.5
Total reactivity, $	-0.009	+0.0066
Doppler, $	-0.160	n.a.
Sodium, $	+0.199	n.a.
Axial expansion, $	-0.062	n.a.
Core-average fuel temperature, K	1565.8	1578.2
Maximal node fuel temperature, K	1977.3	1984.6
Core-average sodium temperature (within fissile height), K	885.2	881.1

The relative change (distortion) of the normalized integral SA fluxes in comparison to the SS values (in %) is given in Fig. 46. For the pre-boiling phase the flux and power distribution distortions are very limited, not exceeding 0.3%, and are caused by the prevailing local fuel Doppler feedback effect.

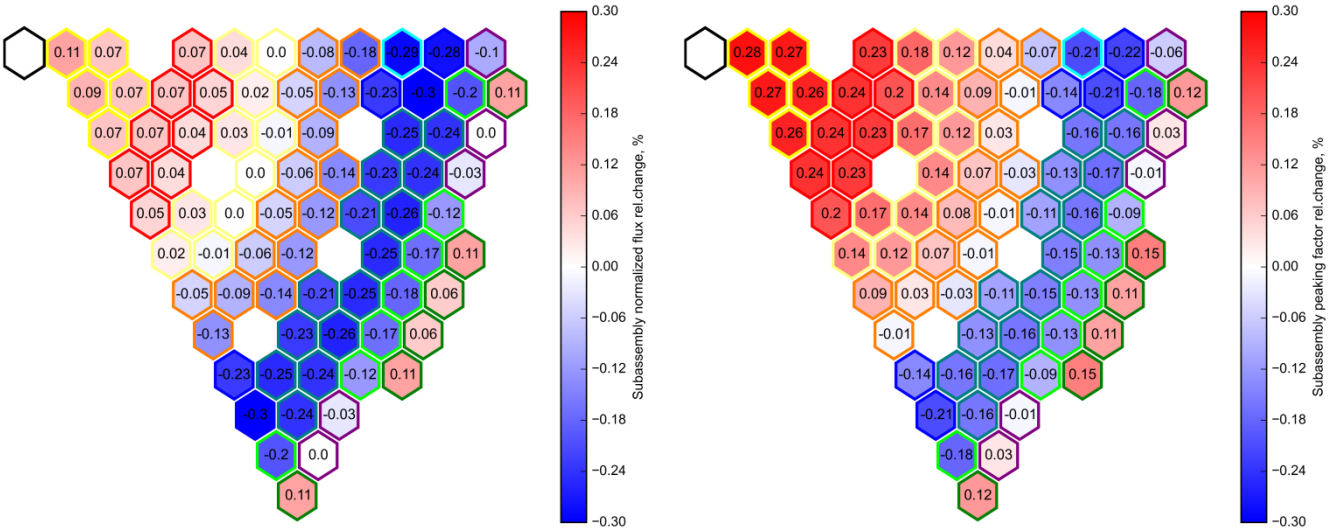

Fig. 46. Subassembly normalized neutron flux (left) and power peaking factor (right) relative change with regard to steady state value as computed with SK option at boiling onset (*t* = 18.52 s) for 3 CG configuration

The development of the transient after boiling onset for the PK and SK options is illustrated in Fig. 47. It has been demonstrated in §3.4.2 (see Fig. 26), that the transient is determined to a large extent by the transient variation of the sodium void reactivity. Moderate negative contributions of Doppler and axial core expansion accompanied by a slight negative sodium void reactivity from the above-core structures are not sufficient to counterbalance the positive reactivity caused by the voiding of part of the fissile core zone. The reactivity starts to increase considerably after 2 s in the boiling time period for both PK and SK solutions.

The boiling onset times for other channels computed by the PK and SK models are given in Table 15 and Table 16 and are illustrated in Fig. 48 up to the moment, when cladding melting occurs firstly. Prior to the start of clad melting the same channels are involved in boiling as well as similar boiling onset times are observed in both considered cases. The duration of the boiling phase is almost identical for the PK and SK solutions (8.57 s and 8.36 s). The boiling of the channels #6, #7, #8 and #9, located in the outer sub-core defines the development of the second part of the boiling phase before clad melting onset. Overall transient behaviour is also very similar and hence also the other core characteristic parameters like core-average fuel temperature and enthalpy, core fissile height expansion and sodium mass fraction (see Fig. 47) exhibit an almost similar temporal behaviour.

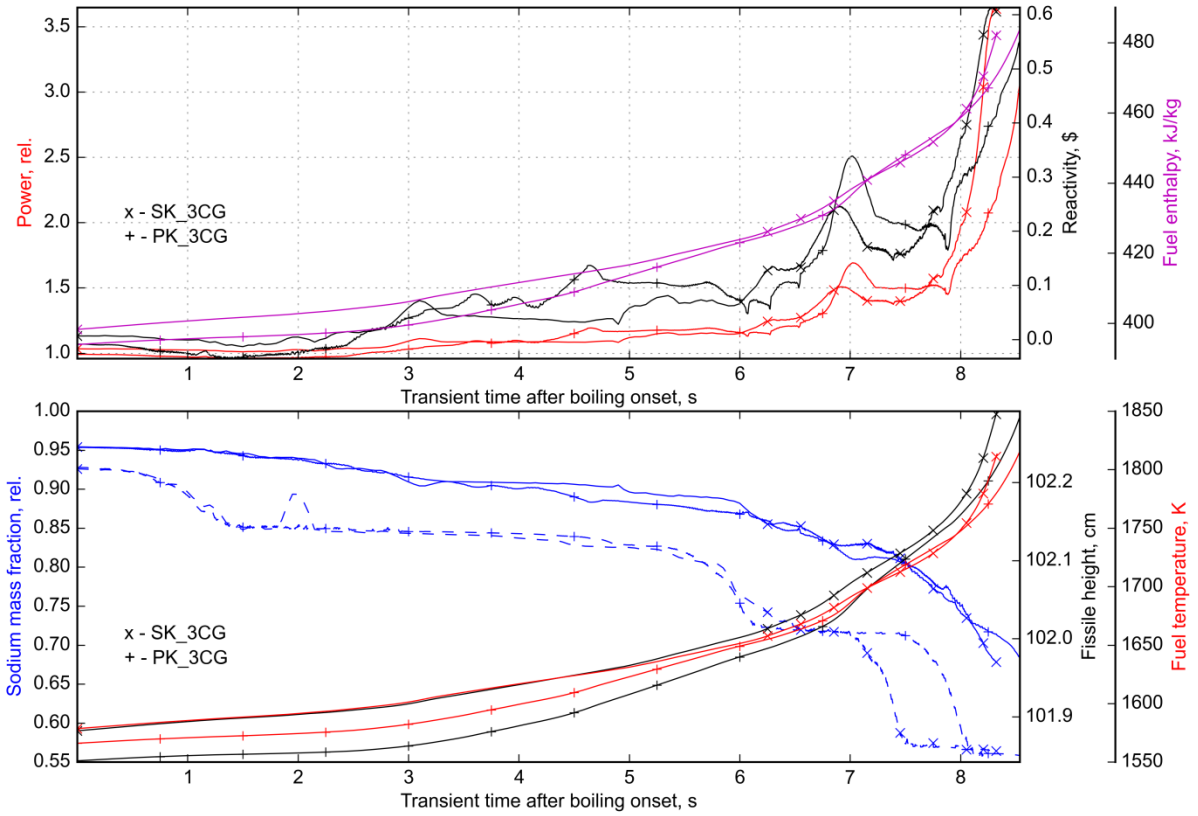

Fig. 47. Temporal evolution of characteristic core parameters in a ULOF as calculated with PK and SK options after boiling onset (3 CG configuration)

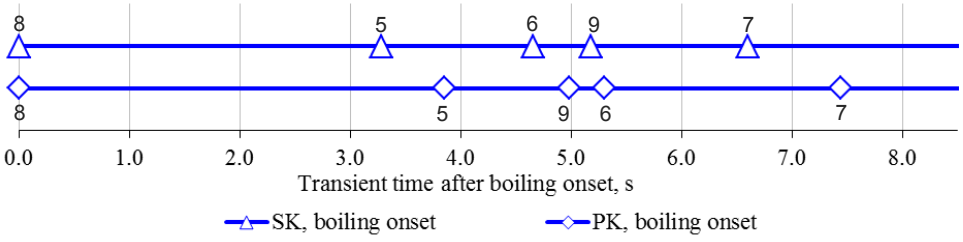

Fig. 48. Channel boiling onset times during boiling phase before clad melting onset as calculated with PK and SK options for 3 CG configuration

Table 15. Event sequence in the ULOF calculation before clad melting onset for 3 CG core configuration computed with the PK option

Channel #	Time, s	Time after boiling onset, s	Event type
8	18.72	0.0	Boiling onset
5	22.57	3.85	Boiling onset
9	23.70	4.98	Boiling onset
6	24.02	5.30	Boiling onset
7	26.16	7.44	Boiling onset

Table 16. Event sequence in the ULOF calculation before clad melting onset for 3 CG core configuration computed with the SK option

Channel #	Time, s	Time after boiling onset, s	Event type
8	18.52	0.0	Boiling onset
5	21.80	3.28	Boiling onset
6	23.18	4.66	Boiling onset
9	23.70	5.18	Boiling onset
7	25.12	6.60	Boiling onset

Core parameters at the time of clad melting onset (activation of the CLAP model in SAS-SFR) are given in Table 17. At this point in time the nominal core power reaches 306% and 363% for the PK and the SK case respectively, while the voided sodium fraction remains relatively low. The boiling patterns of the core for PK and SK cases at the moment of clad melting onset can be evaluated from Fig. 49, where the maps of relative changes of node sodium mass of the fissile core with respect to the steady state value are given channel-wise radially and node-wise in axial direction (for 13 nodes of SAS-SFR model). The sodium mass fractions with respect to the SS values in the fissile height and above-core structure are almost identical for the PK and SK solution, namely 0.68 and 0.56, and 0.67 and 0.56. As a consequence of this low integral sodium void fraction the total reactivity reaches only small values of 0.60 $ and 0.55 $, respectively, which is considerably below prompt critical.

Distortion of normalized integral SA fluxes and subassembly power peaking factors with regard to SS values at the moment of clad melting onset is shown in Fig. 50. Core voiding leads to more noticeable changes in subassembly fluxes and power release predicted with the SK option if compared to those at the time of boiling onset. High voided fraction of the channels #5, #6, #7, #8 and #9 causes increase of the normalized flux and relative power in subassemblies, located in the outer sub-core, as result of neutron spectrum hardening. Largest changes are observed in the core centre (up to -8%) and at its radial boundary (up to 7%). This observation demonstrates a coherency with the results of work [42], discussed in section 1.4 for a similar large SFR core ULOF analysis.

Temporal evolution of characteristic core parameters in the ULOF as calculated with PK and SK options after start of clad melting are given in Fig. 51. Note, that the relative power level is plotted on a logarithmic scale. The boiling onset, clad melting onset and pin failure times for different channels in this phase of the transient for the PK and SK options are listed in Table 18 and Table 19 and illustrated in Fig. 52.

Table 17. Characteristic core parameters at clad melting onset in the ULOF as computed with different neutron kinetics options for 3 CG configuration

Parameter	PK	SK
Time of clad melting, s	27.29	26.88
Total core power, % nom.	305.8	363.3
Normalized mass flow, %	15.5	15.1
Total reactivity, $	+0.55	+0.60
Doppler, $	-0.51	n.a.
Sodium, $	+1.30	n.a.
Axial expansion, $	-0.28	n.a.
Core-average fuel temperature, K	1815.3	1813.2
Maximal node fuel temperature, K	2464.6	2450.4
Core-average sodium temperature (within fissile height), K	971.2	960.5
Sodium mass fractions within fissile height, rel.	0.68	0.67
Sodium mass fractions within upper core regions, rel.	0.56	0.56

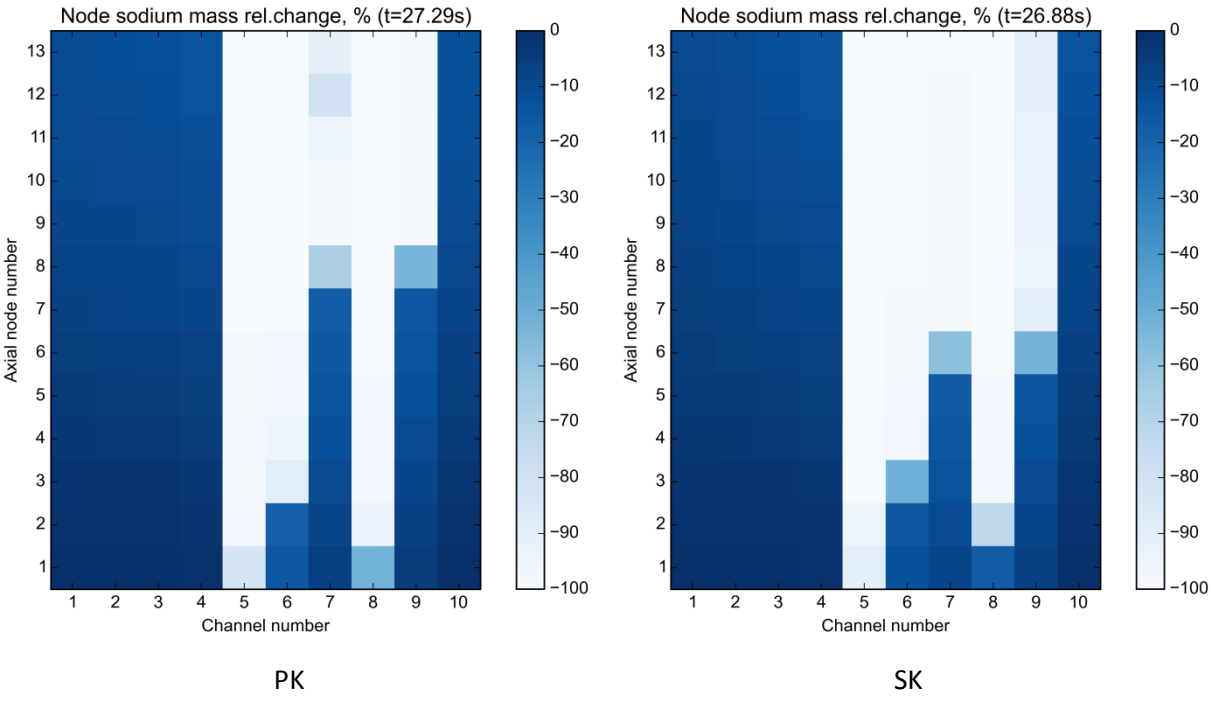

Fig. 49. Relative changes of node sodium mass of the fissile core with respect to the steady state value computed with the PK and SK options at the clad melting onset for 3 CG configuration

Clad melting occurs in channel #5 for the both solutions. From this moment on the liquid clad material relocation reactivity begins contributing to the total reactivity balance. The transient is further driven by the sodium void reactivity, while the fuel relocation reactivity becomes of importance shortly after the first pin failure (as illustrated in Fig. 28 of §3.4.2). One can observe that from the moment of the clad melting onset, the PK and SK solutions start to deviate noticeably in terms of normalized power and net reactivity and the PK model predicts a more energetic material relocation phase. Shorter boiling onset time is observed for channels #3, #2 and #1 in the PK solution. The void reactivity in this case leads

to a more rapid power increase, which in turn intensifies the sodium boiling, as a self-escalating process. Resulting power excursion is characterized by three subsequent power peaks with an amplitude of 70-130 times the nominal power occurring within a time period of less than 0.5 s. First peak is essentially driven by the void effect reactivity. Amplifying this effect clad relocation contribution is very limited before first pin failure occurred in channel #5 (see Fig. 28). The reactivity level reaches 0.96 $, which is attributed to a further core voiding and molten clad relocation towards the upper core boundary. The second power peak in the PK solution is mainly determined by a further void front progression in the initially only partly or non-voided core regions and counter-balanced by a strong negative reactivity feedback due to fuel relocation.

Table 18. Event sequence in the ULOF calculation after clad melting onset for 3 CG core configuration computed with the PK option

Channel #	Time, s	Time after clad melting onset, s	Event type
5	27.29	0.00	Clad melting onset CLAP
8	27.33	0.04	Clad melting onset CLAP
10	27.84	0.55	Boiling onset
4	27.95	0.66	Boiling onset
6	28.00	0.71	Clad melting onset CLAP
3	28.06	0.77	Boiling onset
2	28.21	0.92	Boiling onset
5	28.29	1.00	Pin failure PLUTO2/LEVITATE
1	28.31	1.02	Boiling onset
6	28.33	1.04	Pin failure PLUTO2/LEVITATE
7	28.37	1.08	Pin failure PLUTO2/LEVITATE
8	28.38	1.09	Pin failure PLUTO2/LEVITATE
4	28.50	1.21	Pin failure PLUTO2/LEVITATE
3	28.52	1.23	Pin failure PLUTO2/LEVITATE
9	28.52	1.23	Pin failure PLUTO2/LEVITATE
2	28.57	1.28	Pin failure PLUTO2/LEVITATE
1	28.61	1.32	Pin failure PLUTO2/LEVITATE
10	29.12	1.83	Clad melting onset CLAP

The SK model predicts a slightly less energetic power evolution during the first second after clad melting onset, followed by a relatively moderate power excursion, which does not show any “distinct” peaks of reactivity changes. This implies that boiling progression localized in the outer sub-core results in a somewhat slower release of the sodium-related reactivity, assuming boiling in part of the outer sub-core has propagated further downward up to the time of clad melting onset in case of the calculation with the SK option (see Fig. 49). Within the simulation approach of the PK calculation the transient increase of the void reactivity becomes determined by the linearization assumption of the void reactivity for every node between a not voided and a voided state. The SK behaviour exhibits fundamentally different characteristics, since the actually established core void pattern and spatial interference between neighbour voided regions are basically accounted in neutron transport resulting in a

different cumulative voiding feedback effect as a simple sum of the individual region contributions, in contrast to the PK feedback model. Due to the low void state of the core configuration at the time of clad relocation onset, further void reactivity increase is predicted as slower in case of SK model. The maximum value of the net reactivity does not exceed 0.87 $ during the considered time period, what is 0.09 $ lower as the one for the PK solution.

Table 19. Event sequence in the ULOF calculation after clad melting onset for 3 CG core configuration computed with the SK option

Channel #	Time, s	Time after clad melting onset, s	Event type
5	26.88	0.00	Clad melting onset CLAP
8	27.06	0.18	Clad melting onset CLAP
4	27.38	0.50	Boiling onset
10	27.51	0.63	Boiling onset
6	27.72	0.84	Clad melting onset CLAP
3	27.84	0.96	Boiling onset
5	28.02	1.14	Pin failure PLUTO2/LEVITATE
6	28.09	1.21	Pin failure PLUTO2/LEVITATE
2	28.12	1.24	Boiling onset
7	28.17	1.29	Clad melting onset
7	28.18	1.30	Pin failure PLUTO2/LEVITATE
1	28.27	1.39	Boiling onset
8	28.27	1.39	Pin failure PLUTO2/LEVITATE
4	28.40	1.52	Pin failure PLUTO2/LEVITATE
9	28.46	1.58	Clad melting onset CLAP
3	28.56	1.68	Pin failure PLUTO2/LEVITATE
9	28.65	1.77	Pin failure PLUTO2/LEVITATE

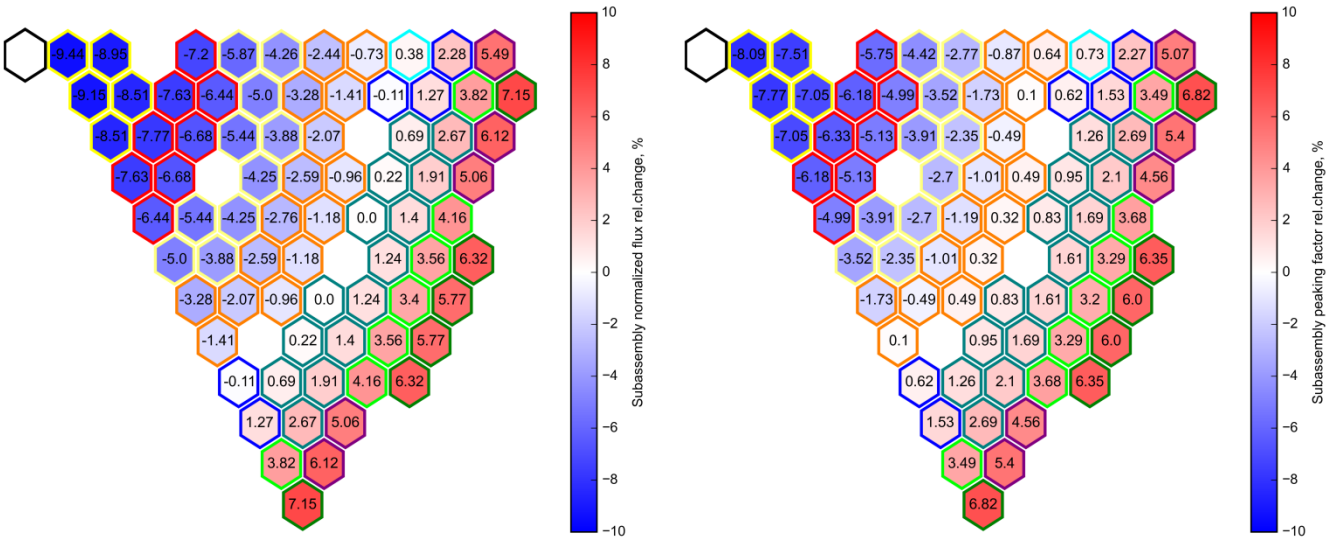

Fig. 50. Subassembly normalized neutron flux (left) and power peaking factor (right) relative changes (in %) with regard to steady state value as computed with the SK option at clad melting onset (t = 28.66 s) for 3 CG configuration

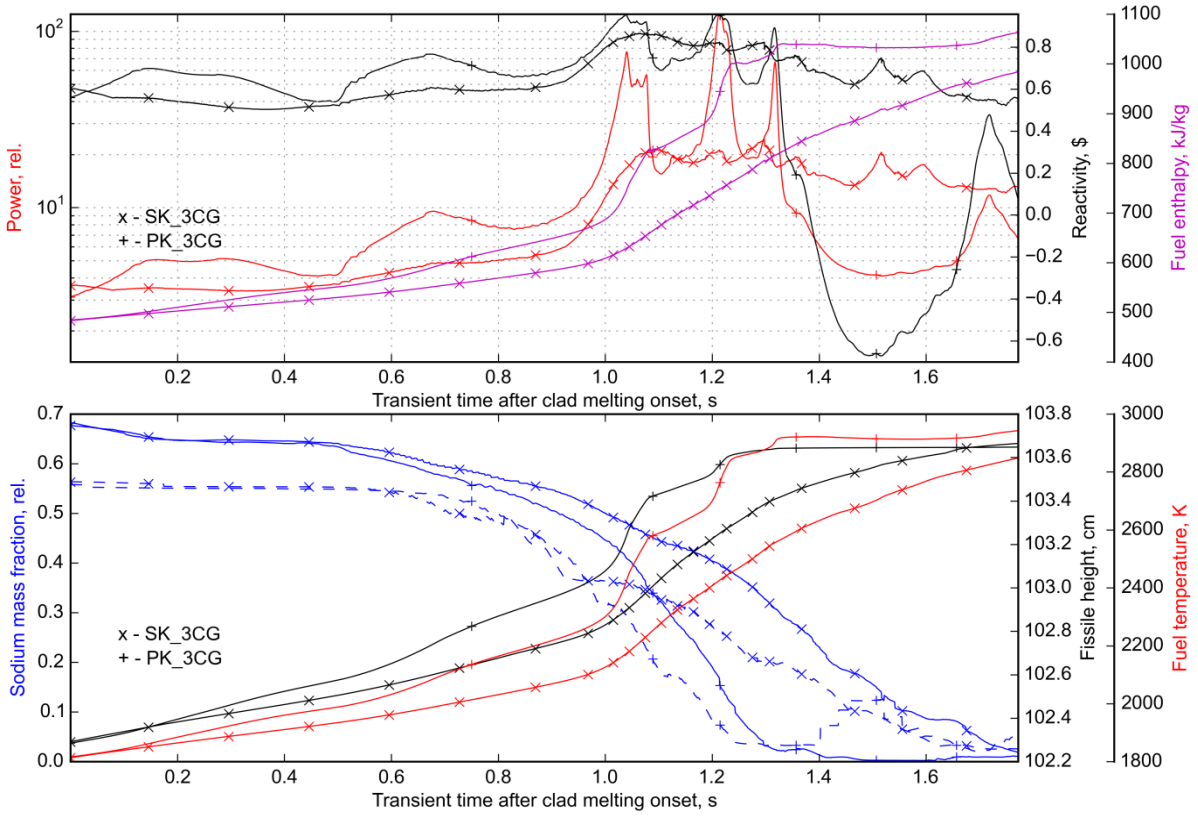

Fig. 51. Temporal evolution of characteristic core parameters in a ULOF as computed with PK and SK options after clad melting onset (3 CG configuration)

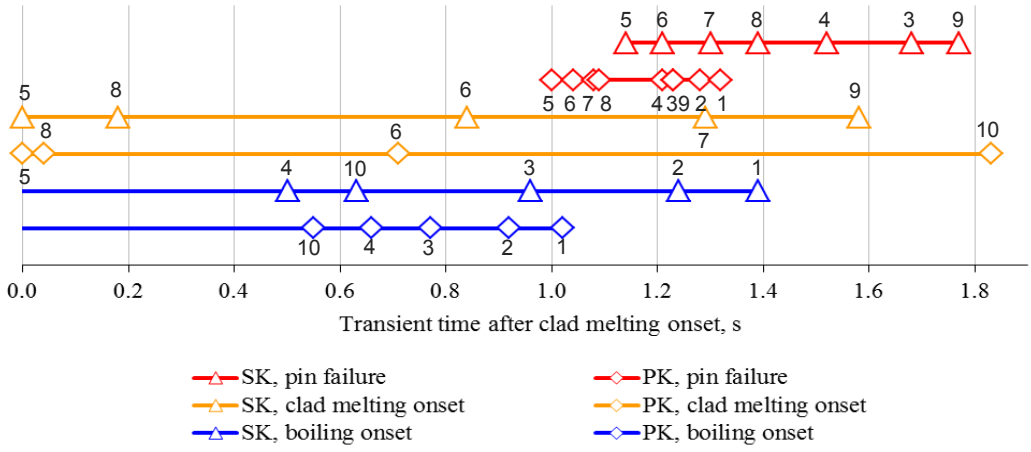

Fig. 52. Channel boiling onset, clad melting onset and pin failure times for the transient phase of a ULOF after clad melting onset

The first pin failure occurred in channel #5 in both solutions, while more rapid power increase prior to this moment in the PK solution resulted in a step-wise increase of the average fuel enthalpy which defines mobility of clad and fuel material during the relocation phase. The map of node clad mass change with respect to the steady state value is given in Fig. 53. The dynamic of the clad relocation in channels #5, #6 and #7 is more energetic prior

to the first pin failure in the PK solution. At the moment of the first pin failure the clad relocation reactivity amounts to 0.08 $, what is a rather small contribution to the positive reactivity, which is driving the transient at this moment.

Core states at the moment of first pin failure are characterized by almost identical fuel average and maximal temperatures of about 2300 K and 2960 K, respectively. Map of node sodium mass fraction with regard to the SS value is given Fig. 54.The sodium mass fraction in fissile height and upper core structures are almost identical as well (0.44, 0.43 and 0.32, 0.32 for the PK and SK solutions), while the power level is slightly higher in the PK solution (23.0 of nominal in PK and 19.0 in SK). Distortion of normalized integral SA fluxes and subassembly relative powers at the moment of first pin failure is given in Fig. 55. Core voiding leads to more noticeable changes in subassembly fluxes and power release if compared to those at the time of clad melting onset as predicted with the SK option. Voided fraction in the fissile height increases what causes further increase of the normalized fluxes and relative power in subassemblies, located in the outer sub-core (up to -12% in the core centre). Relative power release in the inner sub-core thus is higher in the PK solution, what facilitates further boiling of channels #1, #2 and #3 and deviations of the two solutions.

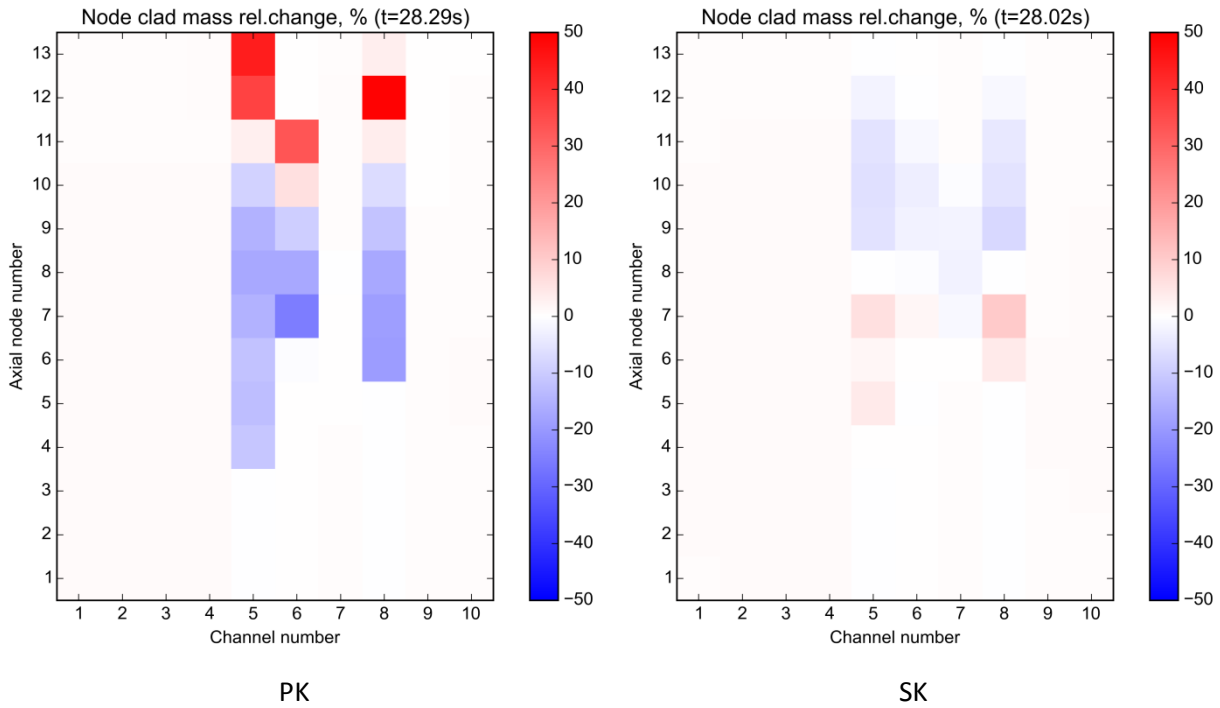

Fig. 53. Relative changes of node clad mass in the fissile core with respect to the steady state value computed with the PK and SK options at the moment of pin failure of channel #5 for 3 CG configuration

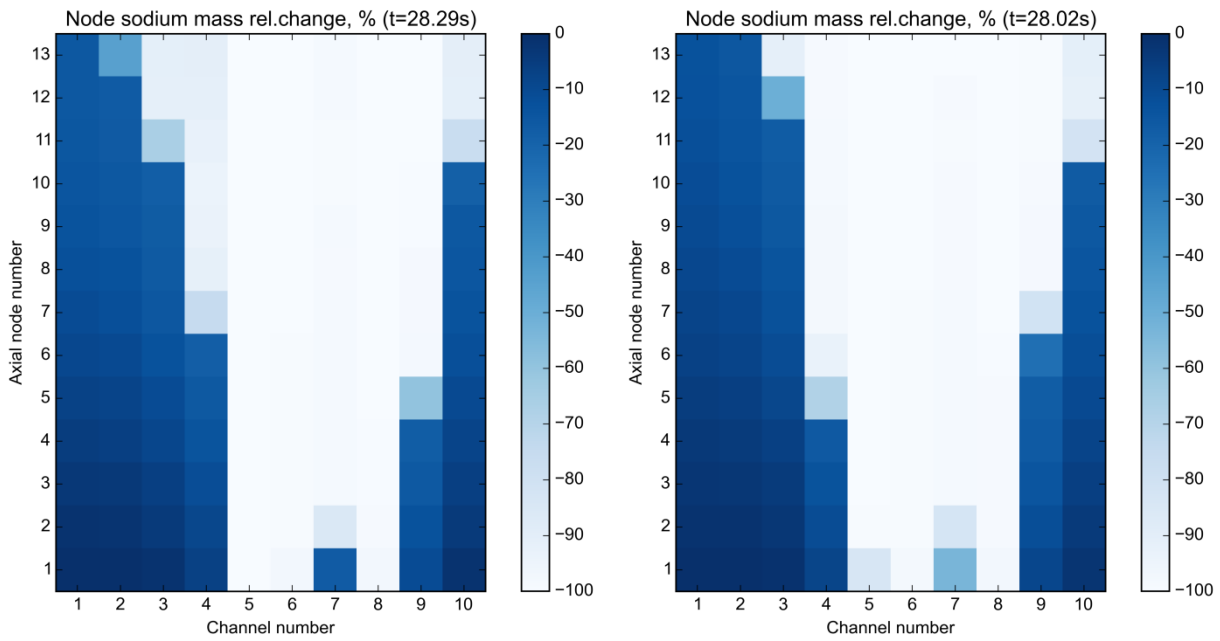

Fig. 54. Relative changes of node sodium mass of the fissile core with respect to the steady state value computed with the PK and SK options at the moment of pin failure of channel #5 for 3 CG configuration

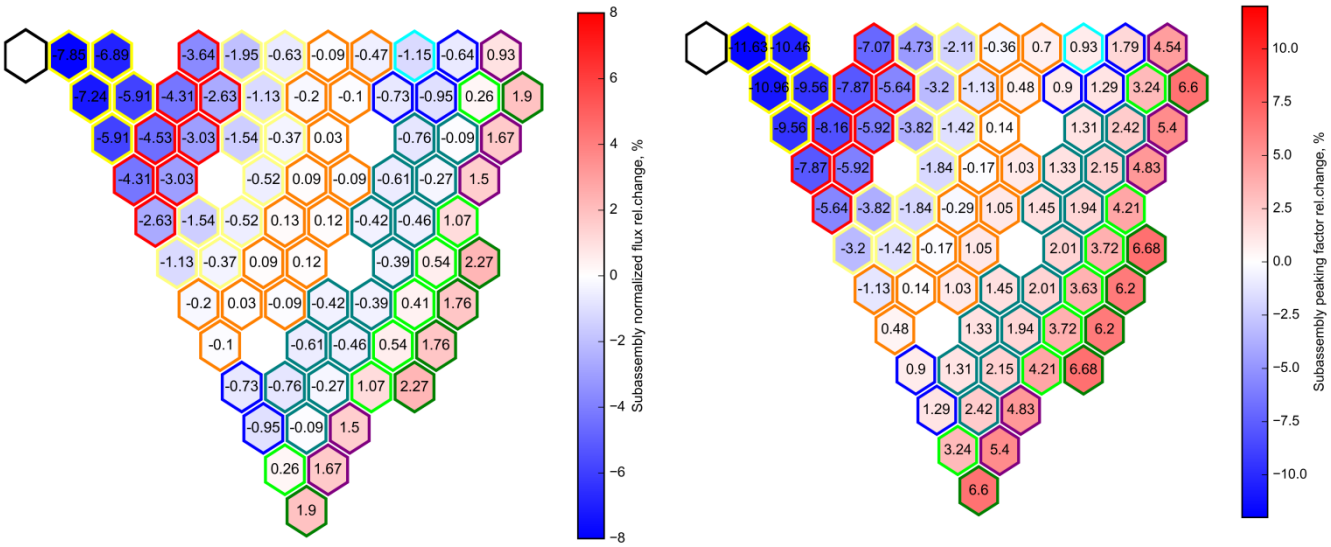

Fig. 55. Subassembly normalized neutron flux (left) and power peaking factor (right) relative change (in %) with regard to steady state value as computed with SK option at pin failure of channel 5 (t = 28.02 s) for 3 CG configuration

Further progression of the transient in PK calculation is characterized by pin failures in other most over-heated channels #6, #7, and #8 and by acting fuel relocation reactivity.

More axial nodes meet into pin failure conditions and thus more fuel within channels #5, #6 and #7 becomes mobile and becomes relocated axially in both upward and downward direction away from core mid-plane. In Fig. 56 the temporal evolution is shown of the fuel mass fraction within fissile height as calculated with PK and SK options in a ULOF after clad melting onset together with the normalized power and net reactivity. One can observe that fuel relocation dynamic is more energetic in the PK solution. During first 0.2 s after the first pin failure the relocation of fuel within the fissile height is the main mechanism to mitigate further insertion of sodium void reactivity and increasing clad relocation reactivity. Further the relocation of fuel beyond axial boundaries of fissile height becomes noticeable, and corresponding fuel-related reactivity becomes much more efficient to mitigate the sodium reactivity, which is approaching its maximum value as result of almost complete core voiding. Third power peak observed in the PK solution is driven by in-core fuel relocation reactivity at fully voided conditions.

For the SK solution the in-core fuel relocation phase takes a time of about 0.3 s (a halve longer than in the PK solution), as result of a slower development of the transient. The same sequence of fuel pin failures in channels (#6, #7, #8) is observed for the SK solution. The moment of pin failure in channel #4 is characterized by in-core fuel relocation, which causes a noticeable decrease of SA normalized fluxes and peaking factors (up to 5-6%) for the core region, where pin failures occurred (channels #5, #6, #7, #8), as depicted in Fig. 57. Basically one observes more moderate fuel relocation feedback on net reactivity predicted by the SK model for this core configuration, characterized by local damages only.

Fuel discharge from fissile height in the PK solution causes rapid decrease of the net reactivity. Sub-criticality of the core is achieved at t = 1.4 s after the clad melting onset, shortly after the third power peak and is characterized by 0.46% of total fuel mass discharged from the fissile core. In Table 20 the parameters of the core are listed at the time when first sub-criticality has been achieved in the PK calculation. The core during calculated material relocation phase in case of SK developing in a less energetic manner does not approach sub-criticality on the time axis adjusted to the clad melting onset time , while on the absolute time scale an almost similar core state is attained (see Table 20), characterized by a slightly lower average fuel enthalpy. Fully voided conditions are achieved at t = 1.8 s for the SK solution and even a larger fraction (about 1.0%) of the fuel is transported beyond fissile height boundaries for the SK model. This core configuration is characterized by a strong distortion of both SA normalized fluxes and power peaking factors as it is demonstrated in Fig. 58 for the moment of pin failure in channel #9. Nevertheless, the net reactivity stays relatively high, at a level of about 0.5 $ at this point in time, what keeps the core power high and further core material relocation could be expected to reach a negative value of the net reactivity. It implies that the material relocation phase for such a perturbed core configuration is also characterized by more moderate negative fuel relocation feedback effect evaluated by the SK solution, as it has been observed for the in-core fuel relocation phase. Compared to PK in the SK approach a variation of the local neutron multiplicative properties is accounted, caused primarily by variation of local fuel content in the core and resulting in a change of axial and radial neutron flux shape.

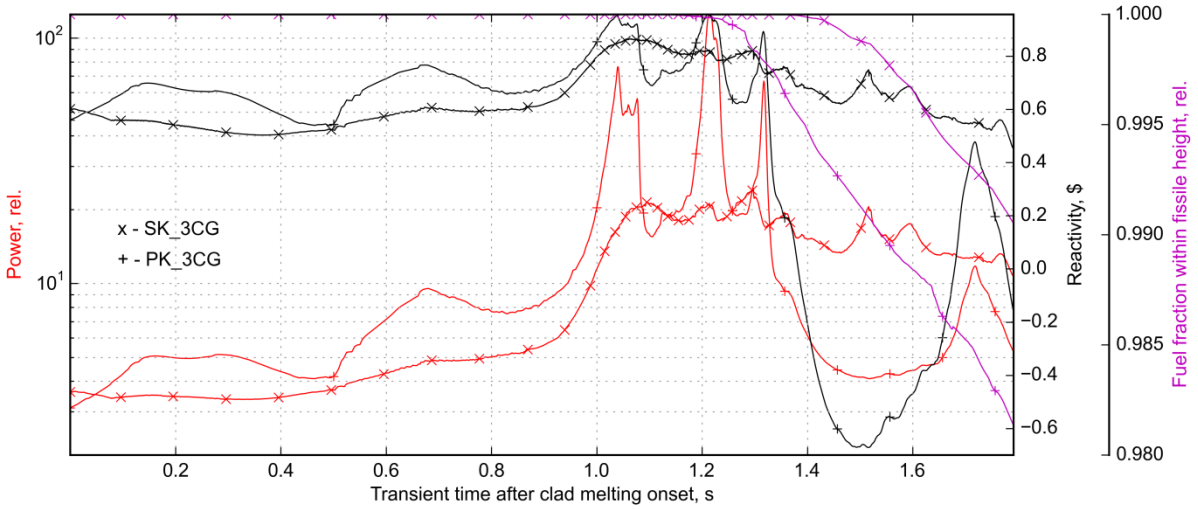

Fig. 56. Temporal evolution of normalized power, net reactivity and fuel mass fraction within fissile height in a ULOF as calculated with PK and SK options after clad melting onset (3 CG configuration)

Table 20. Characteristic core parameters at time moment of first sub-criticality in a ULOF as computed with PK and SK options for 3 CG configuration

Parameter	PK at 28.67 s at first sub-criticality	SK (sub-criticality not reached)	
		at 28.26 s as with adjusted material relocation phase onset	at 28.67 s on absolute transient time scale
Total core power, nom.	7.43	15.39	10.57
Normalized mass flow, %	oscillations around zero	oscillations around zero	oscillations around zero
Total reactivity, $	+0.0	+0.69	+0.44
Doppler, $	-1.50	n.a.	n.a.
Sodium, $	+4.16	n.a.	n.a.
Axial expansion, $	-0.84	n.a.	n.a.
Clad relocation, $	+0.86	n.a.	n.a.
Fuel relocation, $	-2.81	n.a.	n.a.
Core-average fuel temperature, K	2921.8	2616.4	2855.0
Maximal node fuel temperature, K	3621.3	3114.8	3409.0
Core-average sodium temperature (within fissile height), K	1239.6	1097.4	1231.3
Sodium mass fractions within fissile height, rel.	0.02	0.26	0.02
Sodium mass fractions within upper core regions, rel.	0.03	0.17	0.03
Fraction of fuel out of the fissile height, %	0.46	0.0046	0.95

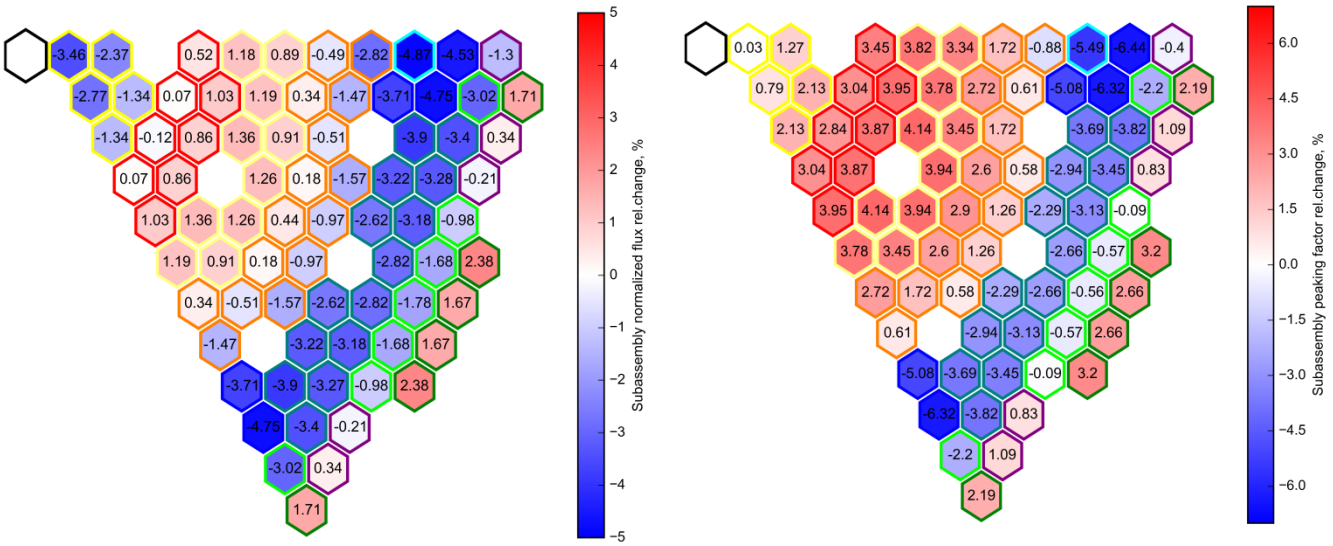

Fig. 57. Subassembly normalized neutron flux (left) and power peaking factor (right) relative change with regard to steady state value as computed with SK option at pin failure in channel 4 (t = 28.40 s) for 3 CG configuration

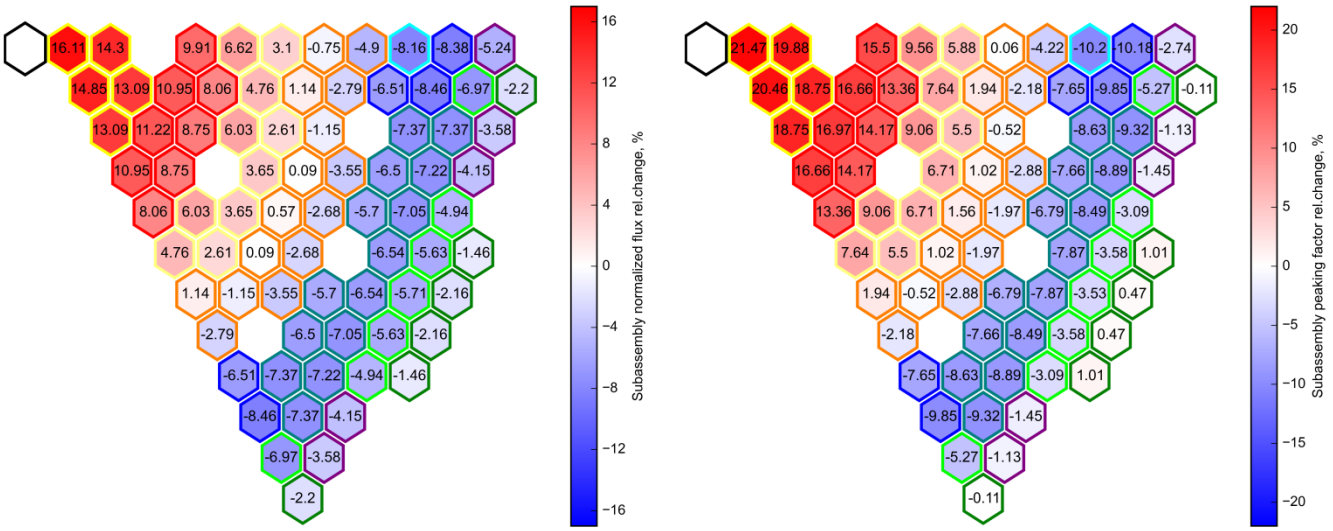

Fig. 58. Subassembly normalized neutron flux (left) and power peaking factor (right) relative change with regard to steady state value as computed with SK option at pin failure in channel 9 (t=28.65 s) for 3 CG configuration

Concluding remarks to §5.3.2.1

Concluding this study, the more important differences in prediction of the net reactivity and corresponding evolution of the transient are observed in the transient phase after clad melting onset. The PK and SK solutions prior to this point in time demonstrate similar behaviour, while at the pre-boiling phase characterized by very small net reactivity variations in both calculations a noticeable different net reactivity evolution is observed. The reason of it will be studied hereafter in §5.3.2.2. During the boiling phase after clad melting onset and before first pin failure the net reactivity variations in the two calculations are

considerably different as result of different sodium void reactivity feedback and a different development of sodium boiling localized primarily within outer sub-core and characterized by a low sodium void fraction of about 0.3 in the fissile core and maximum sodium void reactivity in the PK calculation of only about 1.3 $ at the time of clad melting onset. Further boiling progression starting from this core configuration causes power excursion in the PK calculation, while the SK model predicts a rather slow, not energetic scenario of sodium void reactivity release involving the boiling in the residual part of the core. After first pin failure, this phase is characterized by the strong negative reactivity feedback related to the fuel relocation in the PK calculation, which is not reproduced by the calculation with the SK model in a similar manner, signifying a lower reactivity feedback related to materials motion. This observations will be complemented by the study of 9 CG core configuration, presented hereafter in §5.3.2.3, and only then final conclusions are drawn.

5.3.2.2 MAIN REASONS FOR DIFFERENCES BETWEEN PK AND SK CALCULATIONS DURING THE PRE-BOILING PHASE OF THE TRANSIENT

In order to identify the reasons for differences between the calculations with the PK and SK solutions during the pre-boiling phase of the transient a few calculations of hypothetical ULOF simulations have been performed treating individually three reactivity components, which act during the pre-boiling phase. These are the Doppler effect, the core axial expansion and the sodium density.

In case of the PK calculation, the input worth maps are modified for every case by setting the reactivity data (maps) to zero, which are not relevant for the intended evaluation. In contrast to this the SK solution introduces specific options to switch off the transfer of the data after the converged SS is obtained. The transient initiator, which is the sodium mass flow reduction, is selected identical for all subsequently investigated cases.

Isolated impact of the Doppler effect

In the first transient exercise, for evaluation of the reactivity response, the fuel temperature change is the only considered effect to influence the transient reactivity via the Doppler effect. Thus the Doppler constant distribution is the only relevant reactivity data considered in the PK model calculation, while for the SK solution the fuel node temperatures are the only transferred data to the neutron physics solution during the transient calculation. The resulting transient power and reactivity variations for both cases are depicted in Fig. 59. The Doppler effect-driven transient results of the PK and SK calculations almost coincide because the Doppler constants of the PK and SK models are similar.

Isolated impact of the sodium density variation

In the second exercise, the transient power is driven by the sodium density reactivity feedback only. The sodium worth map, given in units of (*dk/k)/kg*, is the only reactivity data used by the PK calculation. For the SK solution the neutron physics model is performed with a fixed expanded geometry and thermal conditions as calculated for SS, while only the sodium number density is updated during the transient calculation. The resulting transient power and reactivity variations for the two cases are given in Fig. 60.

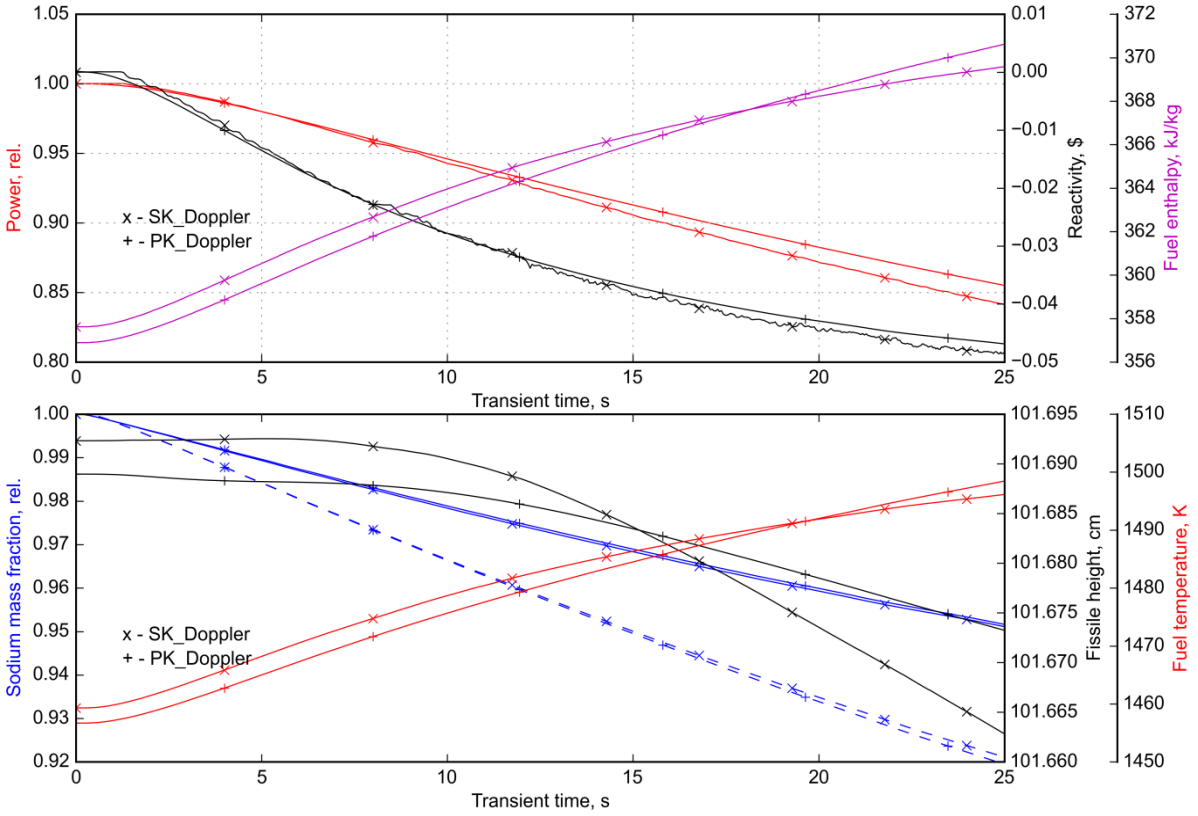

Fig. 59. Temporal evolution of characteristic core parameters in a ULOF transient driven by fuel Doppler effect only as computed with PK and SK options

The power rises quickly in both cases, while it appears that the sodium density reactivity feedback is noticeably larger for the PK calculation. Further sodium heat-up leads to a continuous rise of the difference in the reactivity feedback by about 0.25 cent/s, which is a "self-feeding" process. The reactivity insertion corresponds to the total SVE of about 1750 for the PK model and to 1400 pcm for the SK cases. This means that the SK solution predicts a slightly non-linear dependence of the sodium reactivity feedback on density. This potentially may help to explain the less-energetic power excursions in case of the SK calculation. At the time, when the first power excursion occurs, the sodium mass fraction is still relatively high and a less sodium-related reactivity feedback response is calculated by the SK model. The factor of a separate treatment of the sodium within inter-SA gap also plays a role. The corresponding effect in the PK calculation is determined by using a constant multiplier for the resulting density driven effect of the in-pin-bundle sodium. This accounts for also radial pin expansion and thereby to the additional sodium "ejection" due to the decrease of the coolant flow cross section. In the SK model, however, the outer sodium is treated separately, but with the same temperature as the inner sodium.

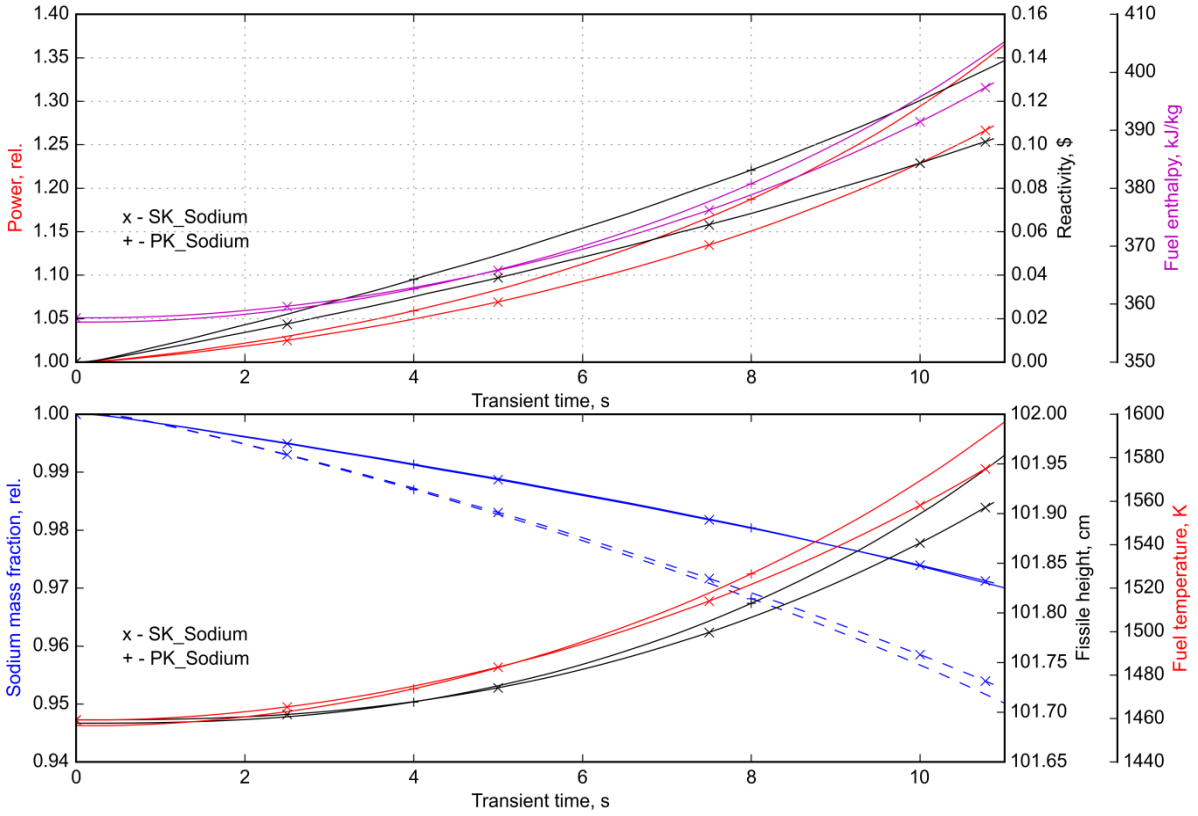

Fig. 60. Temporal evolution of characteristic core parameters in a ULOF transient driven by sodium density effect only as computed with PK and SK options

Isolated impact of the thermal core expansion

The last component studied individually is the reactivity feedback due to axial expansion of the core height. The fuel and clad worth maps, given in units of *(dk/k)/kg*, are the reactivity data used by the PK calculation. For the SK solution, the neutron physics model is performed assuming fixed nodal fuel temperatures and sodium number densities, while the core geometry, fuel, clad and hexcan node masses are updated during the transient calculation at each time step.

The transient normalized power and net reactivity variations for both calculations are denoted in Fig. 61. The traces of the temporal relative power evolution reflect a different impact of the reactivity feedback for the two considered cases. The transient driven by thermal core expansion has a complicated phenomenology. In case of BOL core conditions fuel axial expansion takes place independently from clad and hexcan expansion. As fuel temperatures increase during the initial phase of the transient the fissile core height expands causing a negative reactivity contribution. As result of the clad temperature rise in the initial phase the clad expands in axial direction to a larger extent than the fuel expansion. This leads to a decrease of the clad mass inventory imposing a slightly positive reactivity feedback. A similar response occurs by the heat-up of the hexcan material. The resulting loss of hexcan material along the fissile core height leads to a slightly positive reactivity feedback contribution to the net reactivity. However, it is important here to note that this part of the

reactivity feedback is not considered within the SAS-SFR model properly, but it is considered in the calculation applying the SK neutron physics model.

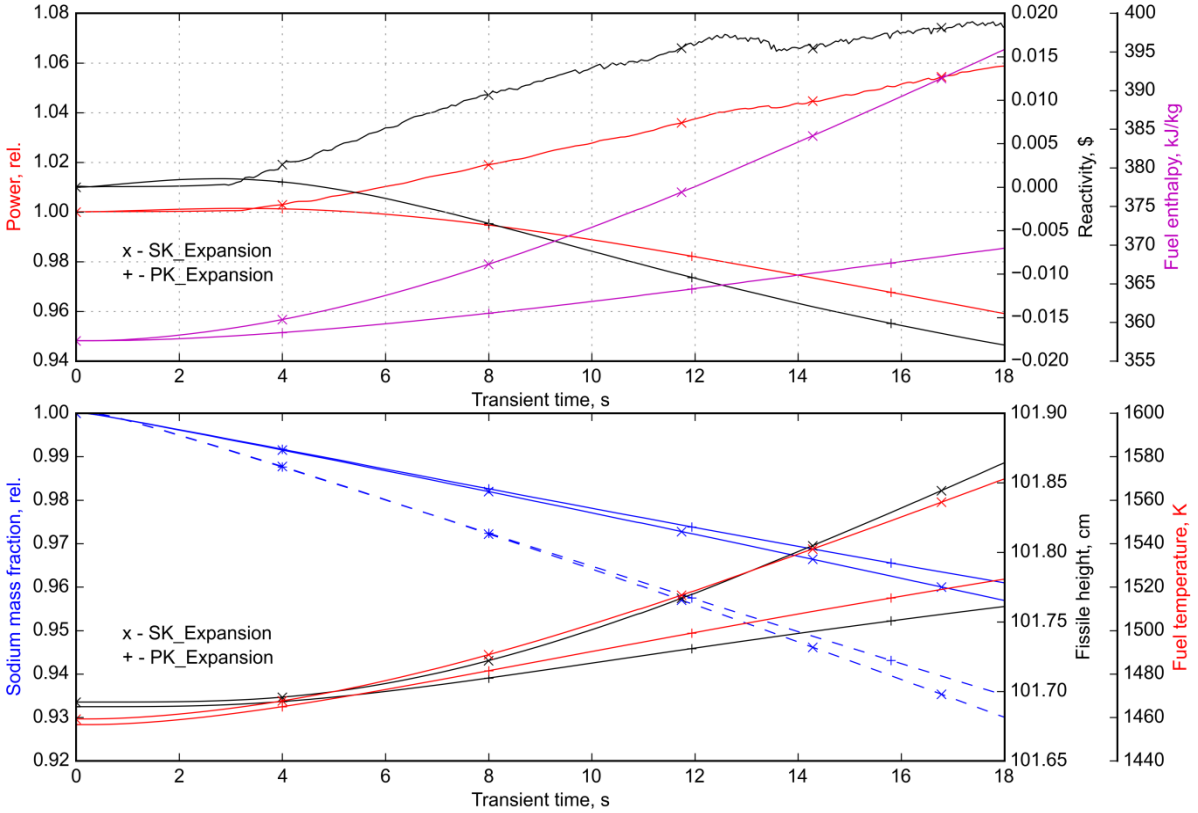

Fig. 61. Temporal evolution of characteristic core parameters in a ULOF transient driven by axial core expansion effect only as calculated with PK and SK options

To summarize the major differences between the SK and PK model simulations during the pre-boiling phase of the transient arise from the more "realistic" representation of the reactivity feedback due to the hexcan expansion in the SK calculation and not due to the application of the SK solution algorithm. Both modelling contain deficits complicating the comparison of this test exercise transient. The PK model of SAS-SFR does not account for the hexcan mass variation in a node, and thus the hexcan related reactivity feedback is not considered during transient calculations. On other side, it is complicated to set-up a SK calculation case in such a manner, that the hexcan-related reactivity response is strictly equal to zero during the entire transient. A nearly negligible influence of the hexcan behaviour on the reactivity feedback could only be expected in a case, where the total hexcan mass within fissile height is conserved in comparison to the SS core configuration.

In order to isolate the effect of the hexcan behaviour on the reactivity feedback, an additional case is analysed assuming that the hexcan temperature remains constant during the transient. In such a case, a marginal increase of the core fissile height leads to an increase of the hexcan mass within the core (small negative reactivity feedback effect from the hexcan, due to an increase of neutron absorption), and vice versa, a decrease of the fissile height will result in a slight positive reactivity feedback contribution, originating from the variation of the

hexcan inventory. The corresponding plots of characteristic core parameters for the SK and PK options are given in Fig. 62. Results of this calculation demonstrate that for the fixed-temperature hexcan assumption the expansion reactivity, calculated by SK, has a very similar tendency, as observed for the PK calculation. In this case the fissile core height increases slightly, due to the fuel heat-up, thus, some negative hexcan contribution is introduced. The resulting negative reactivity of the core axial expansion is somewhat stronger in this test exercise of the SK calculation, than for the PK calculation.

For the first 10 s of this transient exercise the hexcan effect is evaluated to amount to a value of 0.3 $ per 1 cm of fuel pin axial expansion. Considering that the pin expansion is modelled consistently in both calculated cases, the pin axial expansion reactivity can be evaluated from the PK calculation to amount to a value of about 0.25 $/cm (Fig. 61). Thus the reactivity component related to the pin in case, where the hexcan is modelled is about -0.07 $, while the total reactivity is at a level of 0.02 $ at this point in time. Thus the expansion of hexcan provides an insertion of 0.09 $ reactivity at this level of the fuel pin expansion.

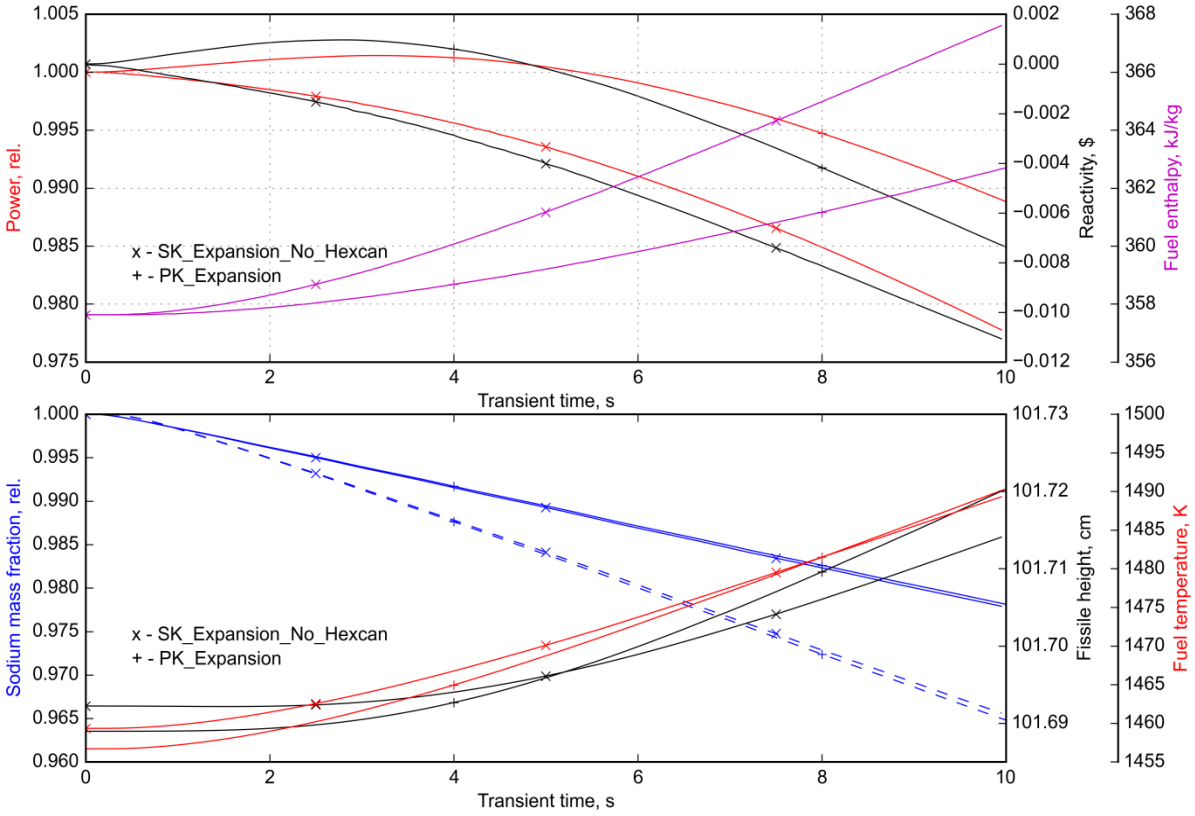

Fig. 62. Temporal evolution of characteristic core parameters in a ULOF transient driven by axial expansion effect only as calculated with PK and SK options (with fixed-temperature hexcan representation in the SK model)

Finally, the case of a constant hexcan temperature has been calculated with all other reactivity feedback effects being activated. The temporal evolution of the characteristic core parameters for first 16 s of transient is illustrated in Fig. 63. The resulting net reactivity and power traces calculated with the use of the SK option are lower during the pre-boiling phase

and stay closer to the PK ones, than in the original hexcan representation in the SK calculation case.

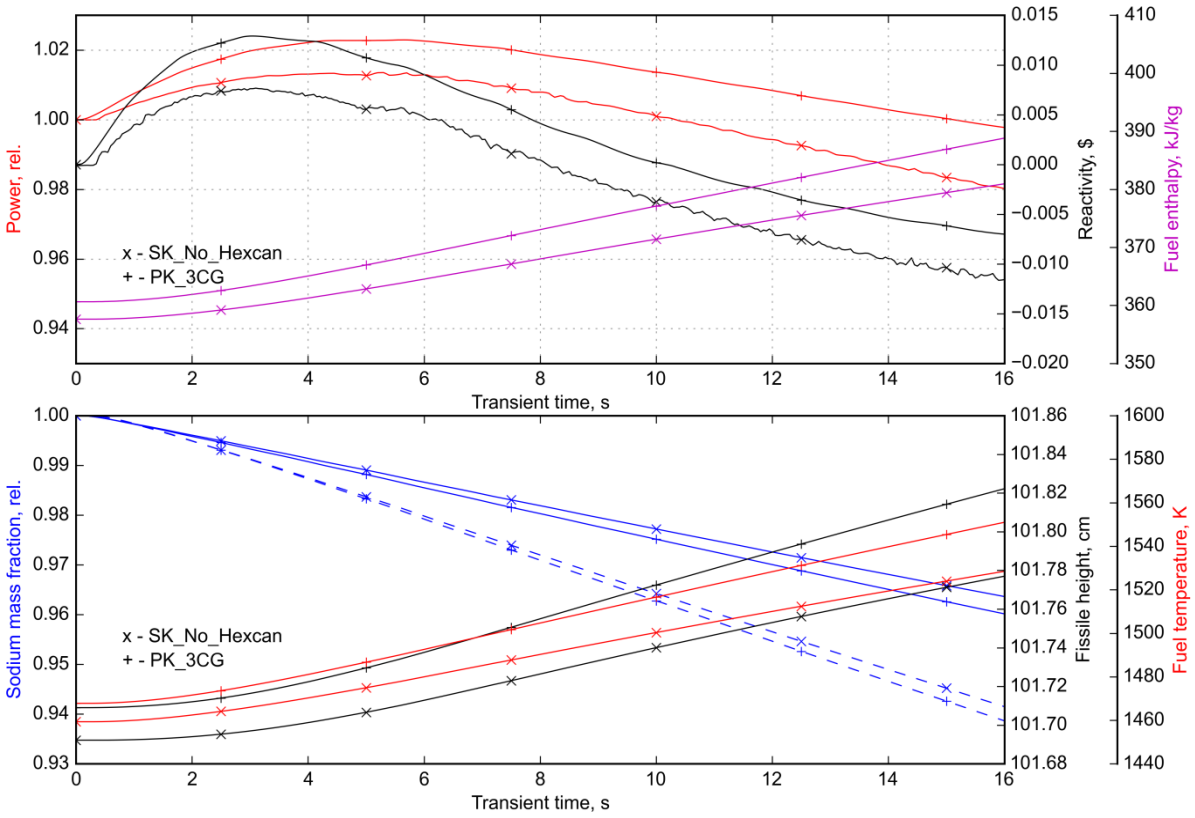

Fig. 63. Temporal evolution of characteristic core parameters in a ULOF transient as computed with PK and SK options with fixed-temperature hexcan representation in the SK model

Concluding remarks to §5.3.2.2

Results of this study demonstrate a high sensitivity of the balance of the reactivity effects during the pre-boiling phase, which finally defines the boiling onset time and the thermal-hydraulics core state achieved up to the time of boiling onset. It has been demonstrated that the hexcan-related reactivity modelling is basically mandatory for the actual level of core details employed in the current study. The hexcan expansion reactivity contribution may contribute in a non-negligible manner for the entire simulation time, contributing with different sign to the net reactivity, depending on the actual thermal conditions of the subassembly elements. Hence, more accurate and detailed comparison of the PK and SK solutions would require introduction of the hexcan-related reactivity feedback component in the PK model of the original SAS-SFR code version.

5.3.2.3 Comparison of ULOF simulations using PK and SK option for the nine cooling groups core configuration

The results presented up to now in §3.4.2 and §5.3.2.1 are influenced by the choice of a thermal hydraulic design option with three cooling groups. Alternatively to that choice a thermal hydraulic design option with nine cooling groups (see Table 6) has been investigated,

where the coolant mass flow is determined such that in each cooling group the same coolant heat-up at steady state is achieved (except 6 SAs of channel #5 having the same flow rate as the neighbour channel #6, see channel map in Fig. 12 and Table 6). In the CP-ESFR project the nine cooling groups (9 CG) gagging scheme has been applied, which results in boiling onset times evaluated to amount to about 26-30 s by different system codes, [41] and [110]. Thus a very similar core configuration has also been studied with the newly developed coupled system. Significant difference with respect to the mentioned studies of [41] and [110] is that the reactivity effect, related to control rod drive lines expansion as well as the diagrid expansion reactivity effect are not modelled in the current study.

Selected results of SS characterization for the 9 CG core configuration are given in Fig. 64 and Fig. 65. The first figure shows node sodium temperature distribution for the 3 CG and 9 CG configuration as well as the corresponding differences. Here, an over-cooling of sodium with regard to the core average sodium heat-up (which amounts to 150 K) in channels of the inner-sub-core can be observed for the 3 CG configuration and an over-heating of sodium in channels of the outer sub-core. In contrast to that the 9 CG case exhibits a uniform sodium heat-up across the whole core cross section.

The SA power peaking factors map as calculated for the 9 CG core configuration and corresponding map of SA peaking factors differences with respect to 3 CG configuration are depicted in Fig. 65. The SA power differences with regard to the 3 CG configuration are mainly caused by different local fuel temperatures and thus can be attributed to the slightly different corresponding local Doppler effect. The differences are evaluated to stay only within a band width of 0.3%.

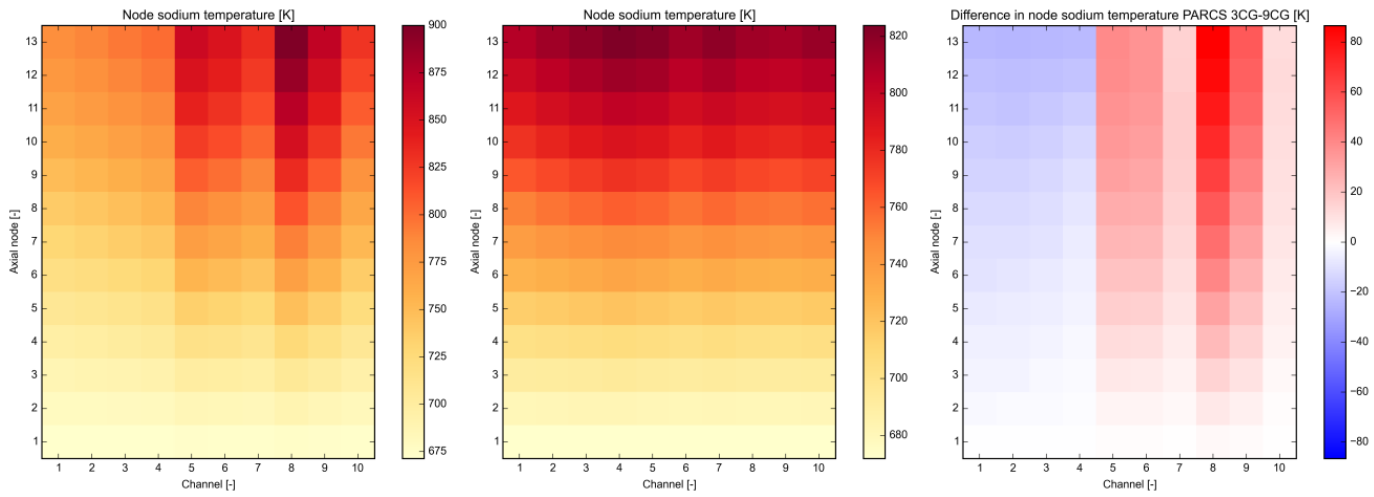

3 CG 9 CG Difference (3 CG-9 CG)

Fig. 64. Node sodium temperature for 3 CG and 9 CG configurations and difference between two configurations as computed with PARCS at steady state

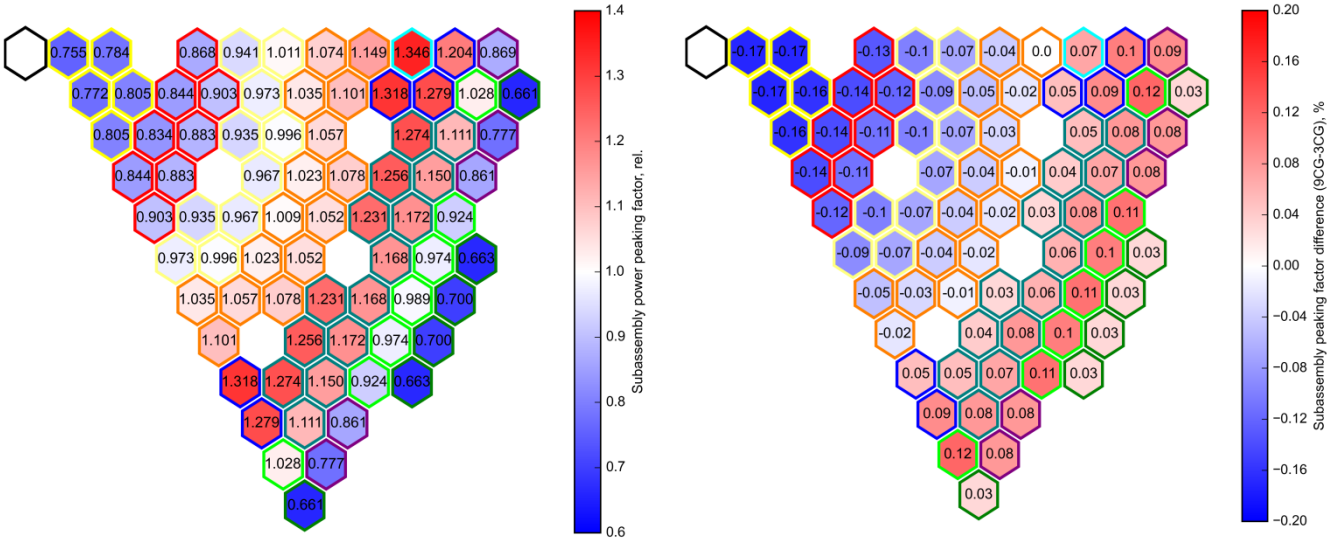

Fig. 65. Subassembly power peaking factors for 9 CG configuration calculated with PARCS (left) and their relative differences from ones for 3 CG configuration (right)

Results of the two ULOF calculations with PK and SK neutron physics models are discussed hereafter covering the already characterised three time phases, in the same manner as in §5.3.2.1. Corresponding temporal evolutions of characteristic core parameters for the three phases of the ULOF transient in the PK calculation with indicated individual reactivity contributions are given in Appendix IV.

In Fig. 66 characteristic core parameters are plotted up to the time of boiling onset for the PK and SK calculations. As it has been demonstrated already before for the 3 CG configuration, mainly three reactivity contributions i.e. the Doppler effect, axial expansion of fissile core height and sodium density effects define the net reactivity for the transient phase before boiling onset (see also Fig. A-IV.1 in Appendix IV). Boiling onset occurs at 29.5 s and 27.5 s into the transient in channel #5 which represents the six most powerful SAs, as predicted by the PK and SK model. The initial sodium heat-up is slightly higher (by about 7 K) in these SAs, than the core average value. Characteristic data of the core states at the time of boiling onset are listed in Table 21. The differences in net reactivity and normalized power variations between the SK and the PK calculation are similar as in the case of the 3 CG core configuration and are caused by the different modelling of the reactivity feedback effect of the hexcan thermal behaviour. However, the resulting differences are more pronounced at the time of boiling onset (7% in nom. power and 0.06 $ in net reactivity), because the pre-boiling phase takes about 10 s longer and, more importantly, because of the more simultaneous coolant and hexcan heat-up in all core channels. On the other side this leads to slightly larger distortions (up to 0.6%) of the SA normalized neutron fluxes and SA power peaking factors (up to 0.7%) at the time of boiling onset shown in Fig. 67, in comparison to the ones calculated for the 3 CG core configuration (see Fig. 58). A relative decrease of the SA normalized flux and power is observed in the SAs of outer sub-core, as result of a stronger local Doppler reactivity.

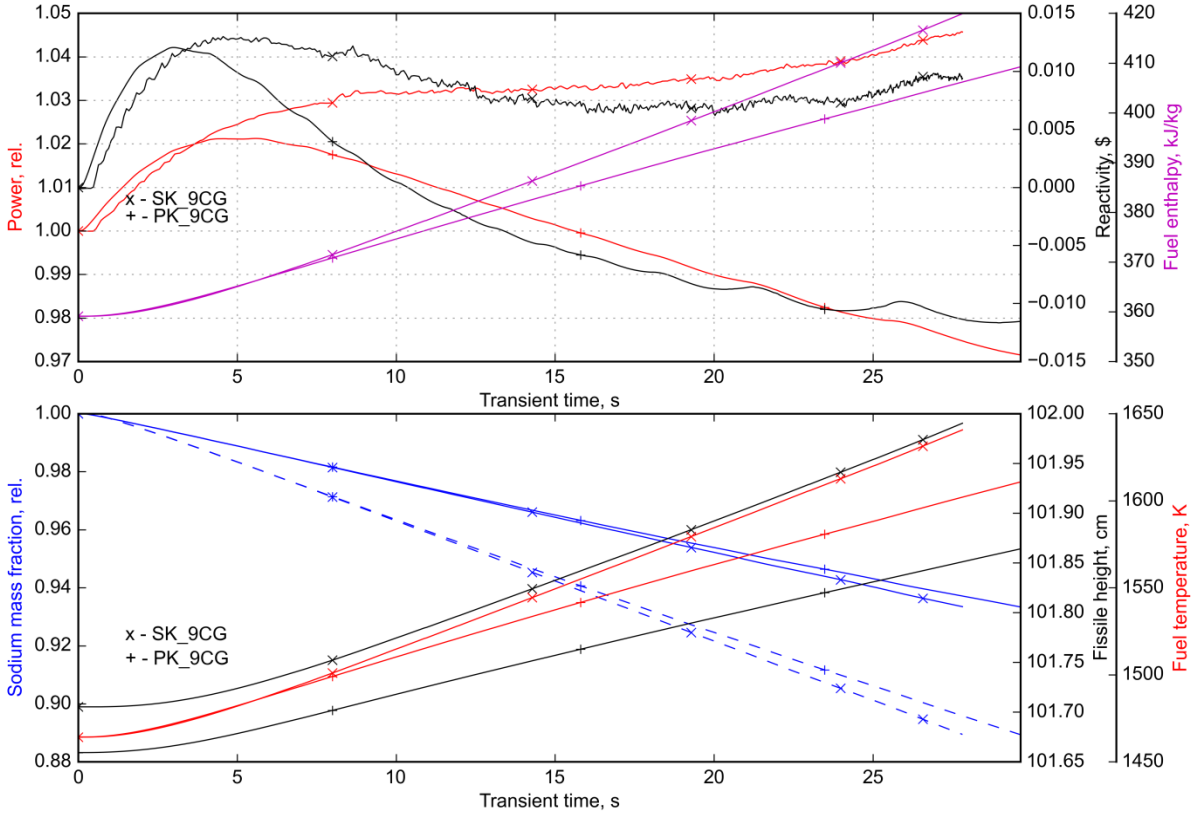

Fig. 66. Temporal evolution of characteristic core parameters in a ULOF as calculated with PK and SK options before boiling onset (9 CG configuration)

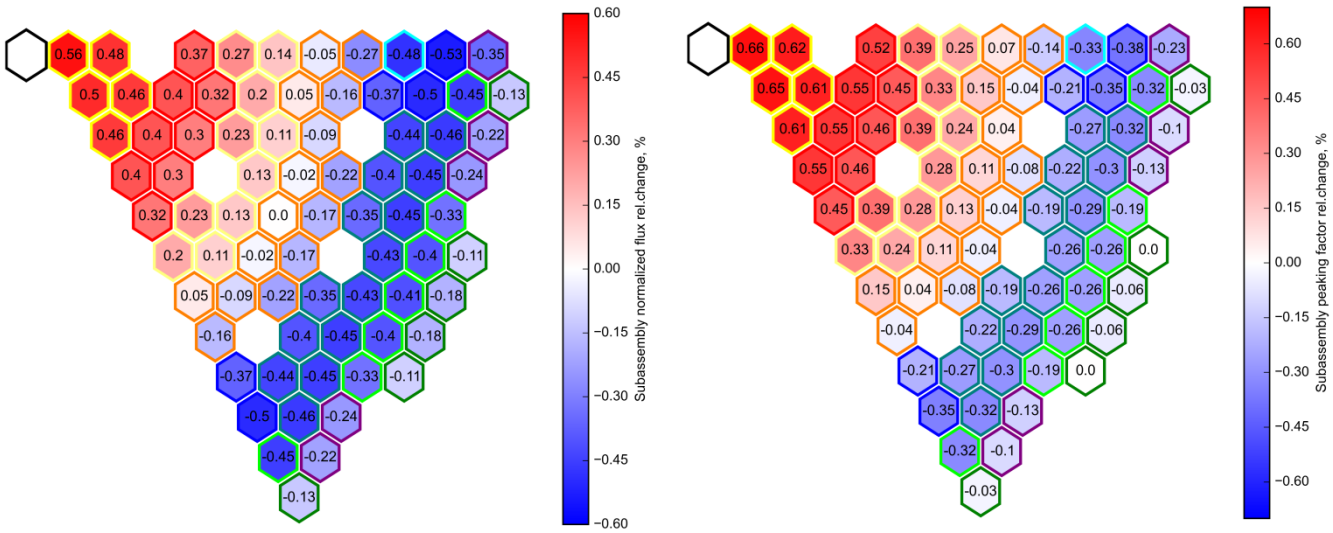

Fig. 67. Subassembly normalized neutron flux (left) and power peaking factor (right) relative change in % with respect to steady state value as computed with the SK option at boiling onset (t = 27.63 s) for 9 CG configuration

Table 21. Characteristic core parameters at the boiling onset in a ULOF as computed with different neutron kinetics options for 9 CG configuration

Parameter	PK	SK
Time of boiling onset, s	29.70	27.63
Total core power, % nom.	97.1	105.2
Normalized mass flow, %	25.1	26.5
Total reactivity, $	-0.011	+0.011
Doppler, $	-0.231	n.a.
Sodium, $	+0.287	n.a.
Axial expansion, $	-0.088	n.a.
Core-average fuel temperature, K	1611.2	1643.3
Maximal node fuel temperature, K	1996.7	2032.6
Core-average sodium temperature (within fissile height), K	939.2	940.7

The temporal evolution of characteristic core parameters for the transient phase after boiling onset is depicted in Fig. 68 for the PK and SK calculations. The boiling phase is slightly more energetic in the SK calculation basically as result of a higher power level at boiling onset taking the time interval of 4.85 s, while it is about 0.4 s longer for the PK calculation (5.21 s). The channel boiling onset times up to the moment, when clad melting occurs (in channel #5 for both cases), are given in Table 22 and Table 23. In Fig. 69 the boiling onset times are illustrated in accord to the temporal evolution of the transient before clad melting onset, which is given in Fig. 68. The transient is also driven by a strong sodium void reactivity in both models during this phase which lasts only about half of the time calculated in case of the 3 CG configuration and involves all channels up to the clad melting onset, as result of the nearly simultaneous coolant heat-up in the different channels.

Selected core parameters at the time of clad melting onset are given in Table 24. Sodium mass fractions in comparison to SS values in fissile height are quite similar for the PK and SK model: 0.55 and 0.53, while for the above-core structure it amounts to 0.34 and 0.25, respectively. Slightly higher sodium void fraction in both fissile and above-core region in case of the SK model at this moment characterizes a slightly more intensive boiling progression predicted by the SK model (see the channel boiling onset times in Fig. 69). A noticeably larger part of the core is voided at the time of clad melting onset in the 9 CG calculation case in comparison to the 3 CG core configuration, as result of a more rapid self-feeding process of sodium void reactivity insertion, driving the net reactivity to a value 0.87 $ in both PK and SK calculations. The sodium-related reactivity contribution is evaluated by the PK model equal to 2.4 $ at this point in time, in contrast to 1.3 $ only in the 3 CG calculation case. As result of this rapid reactivity insertion the core power reaches the values of 23.3 and 19.7 times the nominal power for the PK and the SK cases respectively, while a more heated up core state is attained in terms of average and maximal fuel and sodium temperatures for the calculation with 9 CG compared to the calculation with the 3 CG gagging scheme (see Table 24 and Table 17).

Distortion of the normalized SA integral fluxes and SA power peaking factors with respect to SS values at the time of clad melting onset as computed with the SK model for 9 CG case is shown in Fig. 70. Channels of both inner and outer sub-cores are involved in a boiling

process, thus a less pronounced radial power re-distribution is observed for the 9 CG case when compared to the 3 CG case (see Fig. 50), which is characterized by lower maximal changes of SA normalized fluxes and power peaking factors.

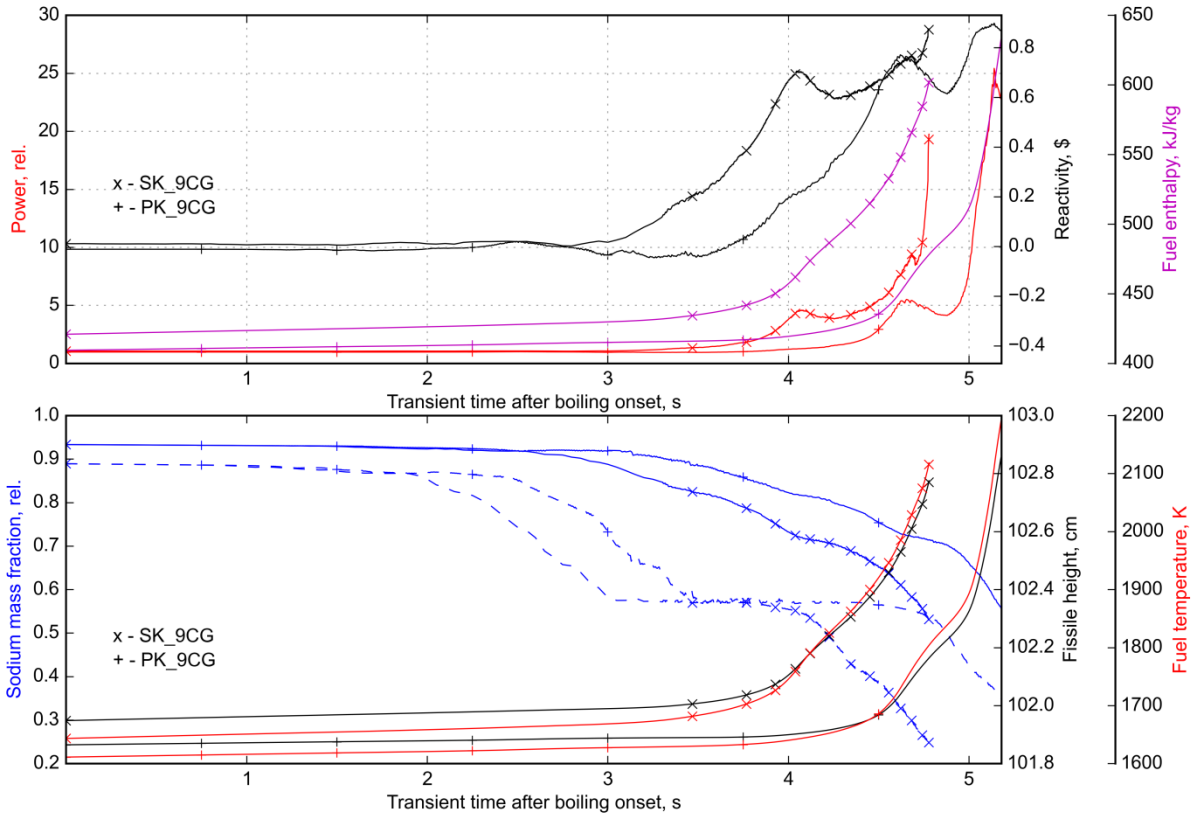

Fig. 68. Temporal evolution of characteristic core parameters in a ULOF as calculated with PK and SK options after boiling onset for 9 CG configuration

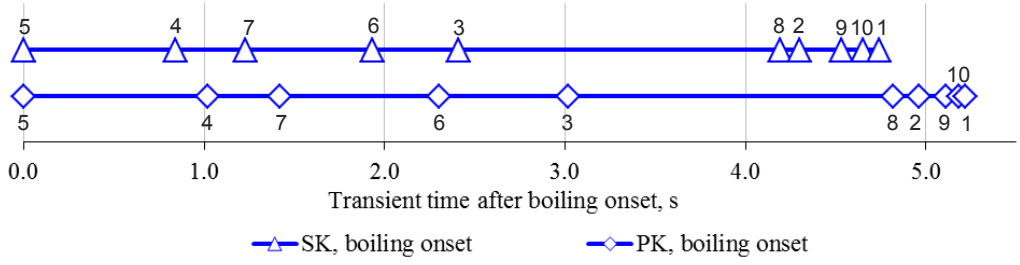

Fig. 69. Channel boiling onset times during boiling phase before clad melting onset as calculated with PK and SK options for 9 CG configuration

Table 22. Event sequence in the ULOF calculation before clad melting onset for 9 CG core configuration computed with the PK option

Channel #	Time, s	Time after clad melting onset, s	Event type
5	29.70	0.0	Boiling onset
4	30.72	1.02	Boiling onset
7	31.12	1.42	Boiling onset
6	32.00	2.30	Boiling onset
3	32.72	3.02	Boiling onset
8	34.52	4.82	Boiling onset
2	34.66	4.96	Boiling onset
9	34.81	5.11	Boiling onset
10	34.88	5.18	Boiling onset

Table 23. Event sequence in the ULOF calculation before clad melting onset for 9 CG core configuration computed with the SK option

Channel #	Time, s	Time after clad melting onset, s	Event type
5	27.63	0.0	Boiling onset
4	28.47	0.84	Boiling onset
7	28.86	1.23	Boiling onset
6	29.56	1.93	Boiling onset
3	30.04	2.41	Boiling onset
8	31.82	4.19	Boiling onset
2	31.93	4.30	Boiling onset
9	32.16	4.53	Boiling onset
10	32.28	4.65	Boiling onset
1	32.37	4.74	Boiling onset

Table 24. Characteristic core parameters at clad melting onset in a ULOF as computed with different neutron kinetics options for 9 CG configuration

Parameter	PK	SK
Time of clad melting onset, s	34.91	32.42
Total core power, % nom.	2325.2	1970.0
Normalized mass flow, %	-0.004	-0.015
Total reactivity, $	+0.87	+0.87
Doppler, $	-1.01	n.a.
Sodium, $	+2.40	n.a.
Axial expansion, $	-0.59	n.a.
Core-average fuel temperature, K	2204.9	2118.8
Maximal node fuel temperature, K	2816.4	2720.3
Core-average sodium temperature (within fissile height), K	1043.7	1060.9
Sodium mass fractions within fissile height, rel.	0.55	0.53
Sodium mass fractions within upper core regions, rel.	0.34	0.25

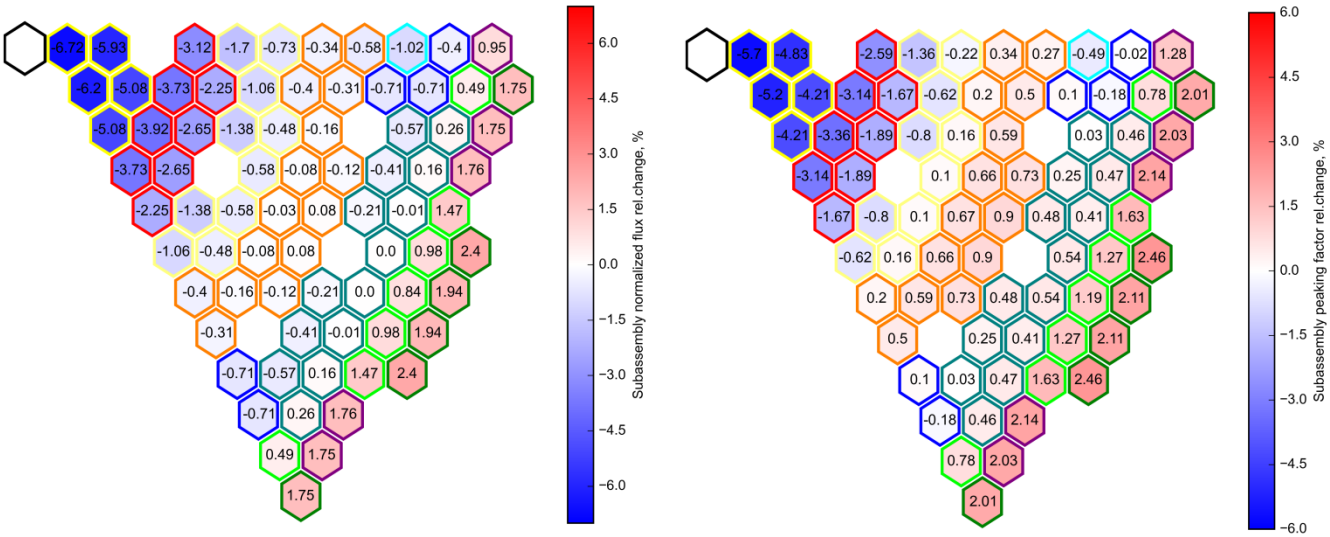

Fig. 70. Subassembly normalized neutron flux and power peaking factor change with regard to steady state value as computed with SK option at clad melting onset (t = 32.43 s) for 9 CG configuration

Transient plots of characteristic core parameters after start of clad melting are given in Fig. 71. The continuing sodium boiling progression leads to a nearly prompt critical power excursion with a peak power value of 70 times nominal in both PK and SK calculation, while the net reactivity approaches a value of 0.9 $ identical for both PK and SK models. This excursion causes a first pin failure in channel #5, which occurs at similar core conditions. The boiling patterns of the core predicted by the PK and SK models at the moment of first pin failure are illustrated in Fig. 73. Basically till the moment of first pin failure the PK and SK solutions demonstrate coherency in terms of sodium void fraction, fuel average temperature, axial core expansion, as well as average fuel enthalpy, which define an almost identical net reactivity and power evolution.

Pin failure times in different channels at this phase of the transient for the PK and SK options are listed in Table 25 and Table 26 and illustrated in Fig. 72. The first pin failure is followed by failures of highly power-loaded channels #6 and #7, within less than 0.1 s in both cases. Essentially similar phenomenology is observed in this phase of transient as compared to the PK calculation for 3 CG core configuration. The fuel relocation reactivity acts with the strong negative contribution shortly after the first pin failure (see Fig. A-IV.3 of Appendix IV). Nevertheless from this time onward the PK and SK solutions start to deviate in terms of net reactivity, resulting in a more energetic material relocation phase as predicted by the SK solution for the given core configuration and the transient set-up. The net reactivity during first 0.4 s after clad melting onset is dominantly defined by further sodium boiling progression and corresponding void reactivity amplified by a slight positive contribution of the clad relocation reactivity which both are counterbalanced by the fuel relocation reactivity feedback. For the SK model it results in a higher net reactivity after the first power peak and more pronounced two subsequent power peaks with an amplitude of 40-50 of the nominal power occurring within a time period of less than 0.5 s. For the PK calculation, only the first

power peak is observed clearly and followed by less pronounced peaky power variations (see Fig. 71).

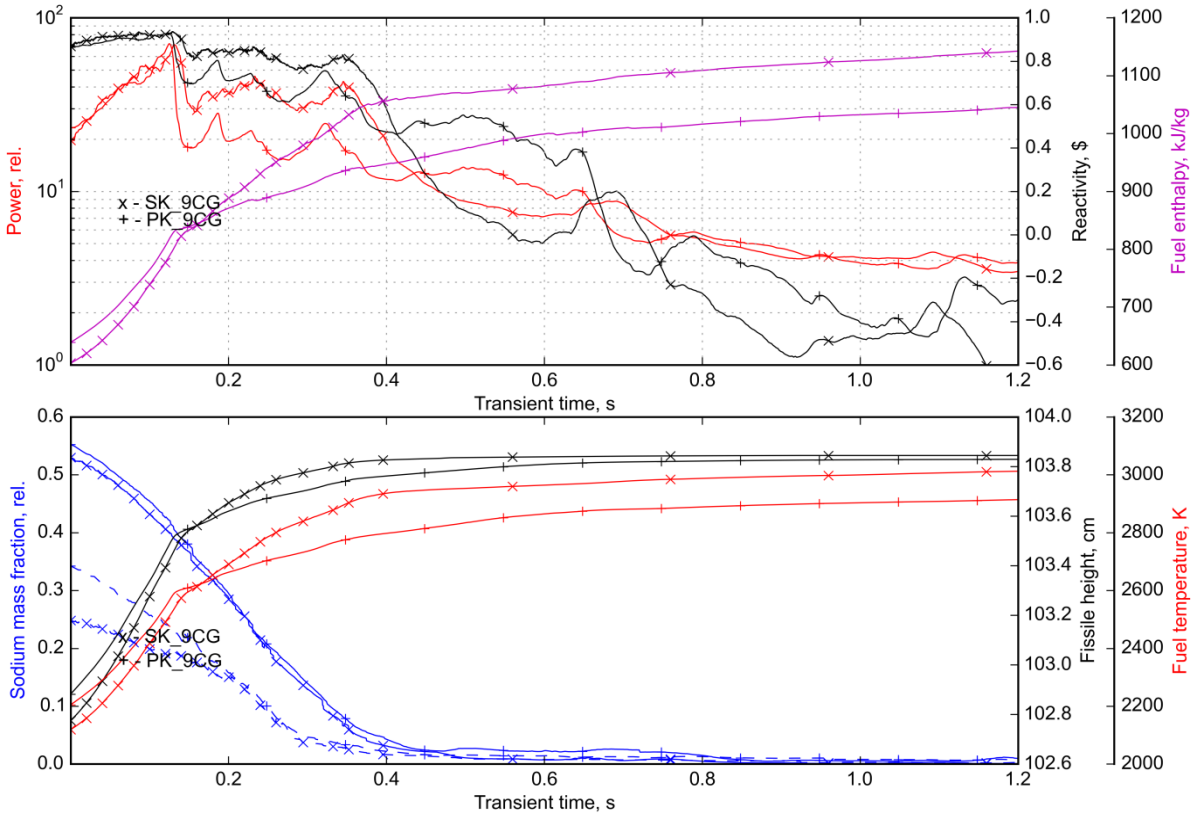

Fig. 71. Temporal evolution of characteristic core parameters in a ULOF as computed with PK and SK options after clad melting onset (9 CG configuration)

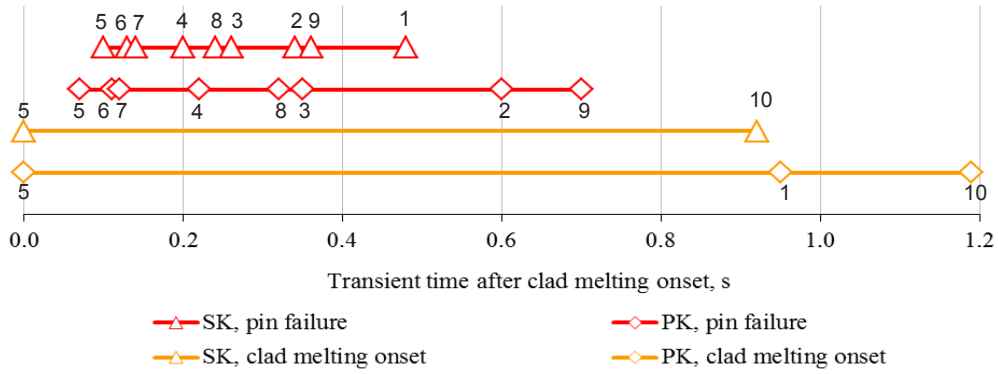

Fig. 72. Channel clad melting onset and pin failure times for the transient phase of a ULOF after clad melting onset (9 CG configuration)

Table 25. Event sequence in the ULOF calculation after clad melting onset for 9 CG core configuration computed with the PK option

Channel #	Time, s	Time after clad melting onset, s	Event type
5	34.91	0.00	Clad melting onset CLAP
1	34.92	0.01	Boiling onset
5	34.98	0.07	Pin failure PLUTO2/LEVITATE
6	35.02	0.11	Pin failure PLUTO2/LEVITATE
7	35.03	0.12	Pin failure PLUTO2/LEVITATE
4	35.13	0.22	Pin failure PLUTO2/LEVITATE
8	35.23	0.32	Pin failure PLUTO2/LEVITATE
3	35.26	0.35	Pin failure PLUTO2/LEVITATE
2	35.51	0.60	Pin failure PLUTO2/LEVITATE
9	35.61	0.70	Pin failure PLUTO2/LEVITATE
1	35.86	0.95	Clad melting onset CLAP
10	36.10	1.19	Clad melting onset CLAP

Table 26. Event sequence in the ULOF calculation after clad melting onset for 9 CG core configuration computed with the SK option

Channel	Time, s	Time after clad melting onset, s	Event type
5	32.43	0.00	Clad melting onset CLAP
5	32.53	0.10	Pin failure PLUTO2/LEVITATE
6	32.56	0.13	Pin failure PLUTO2/LEVITATE
7	32.57	0.14	Pin failure PLUTO2/LEVITATE
4	32.63	0.20	Pin failure PLUTO2/LEVITATE
8	32.67	0.24	Pin failure PLUTO2/LEVITATE
3	32.69	0.26	Pin failure PLUTO2/LEVITATE
2	32.77	0.34	Pin failure PLUTO2/LEVITATE
9	32.79	0.36	Pin failure PLUTO2/LEVITATE
1	32.91	0.48	Pin failure PLUTO2/LEVITATE
10	33.35	0.92	Clad melting onset CLAP

It is worth to discern the phenomenology of the fuel motion within the channels in two phases which are characterized first by in-core fuel relocation (within the fissile height) and second by a relocation of the fuel beyond axial fissile core boundaries.

In Fig. 74 the temporal evolution of the normalized power, net reactivity and fuel mass fraction within fissile height in the ULOF as calculated with PK and SK options after clad melting onset. The transient time $t \leq 0.25$ s after clad melting onset is characterized primarily by fuel relocation within the fissile core height (in-core). Correspondingly, the patterns of the fuel relocation for both cases at the moment of pin failure in channel #4 are very similar as illustrated in Fig. 75, and demonstrate the fuel motion in channels #5, #6 and #7 in both upward and downward directions from the core mid-plane where the failed nodes are evaluated. For the 9 CG case it implies that basically similar core configurations during in-core material relocation phase, essentially after start of fuel motion, result in different

prediction of the net reactivity by the PK and SK approaches, dominantly as result of lower fuel relocation feedback in the SK calculation.

During this in-core material relocation phase a relatively slight distortions of SA normalized flux and power peaking factors are observed as computed by the SK model, as illustrated in Fig. 76 for the moment of pin failure in channel #8, which follows pin failure in channel #4. Similar noticeable distortions (up to -5%), as the ones observed for 3 CG core configuration, occur in the SAs belonging to the failed channels at the moment when out-of-core fuel relocation starts for this rapid scenario (see Fig. 57).

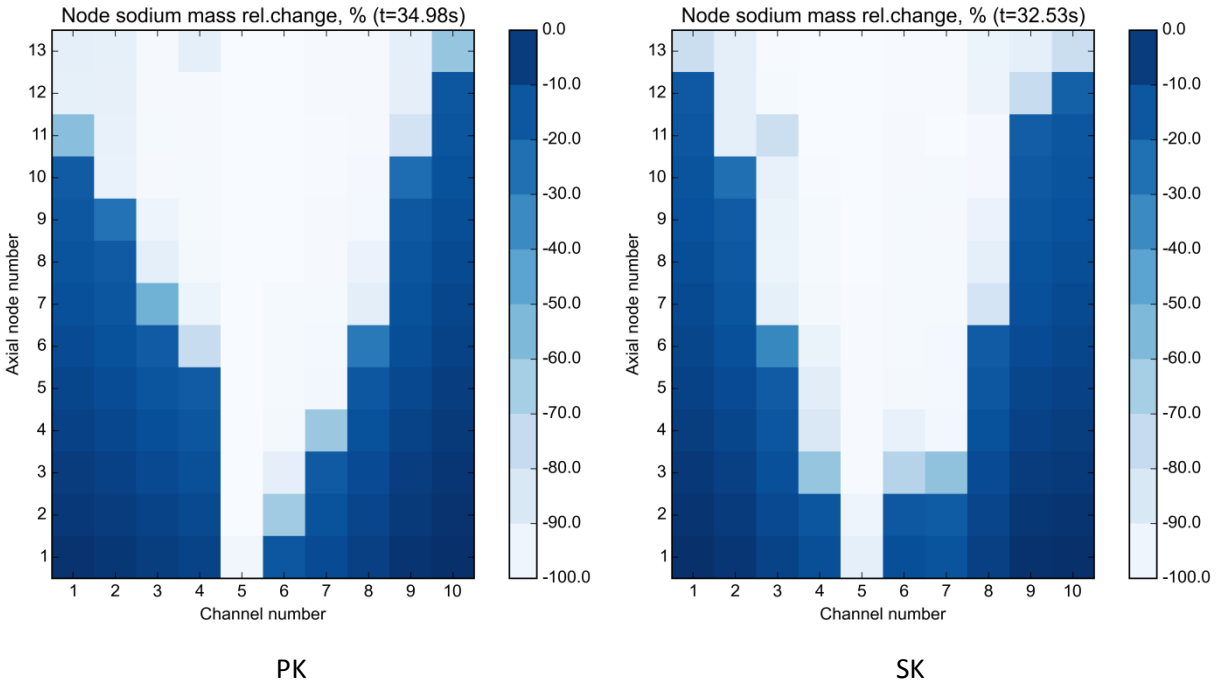

Fig. 73. Relative changes of node sodium mass of the fissile core with respect to the steady state value computed with the PK and SK options at the moment of pin failure of channel #5 for 9 CG configuration

Further transient progression dominated by a strong negative reactivity due to the out-of-core fuel relocation is still influenced by further core voiding during a time period of $t < 0.4$ s after clad melting onset, until fully voided core configuration is achieved in both calculations. For this phase the dynamic of the fuel relocation beyond the axial core boundaries is much stronger by the SK model, as illustrated in Fig. 74. The higher level of power in the SK calculation results in a more rapid subsequent failures in almost all other channels (except #10) and higher molten fuel mobility, which is defined by the fuel enthalpy. Resulting core configuration after the power excursion is characterized by about 10% higher average fuel enthalpy when applying the SK approach as compared to the PK approach, while the average fuel temperature and enthalpy are only slightly lower at the moment of clad melting onset by the SK calculation (see Fig. 68).

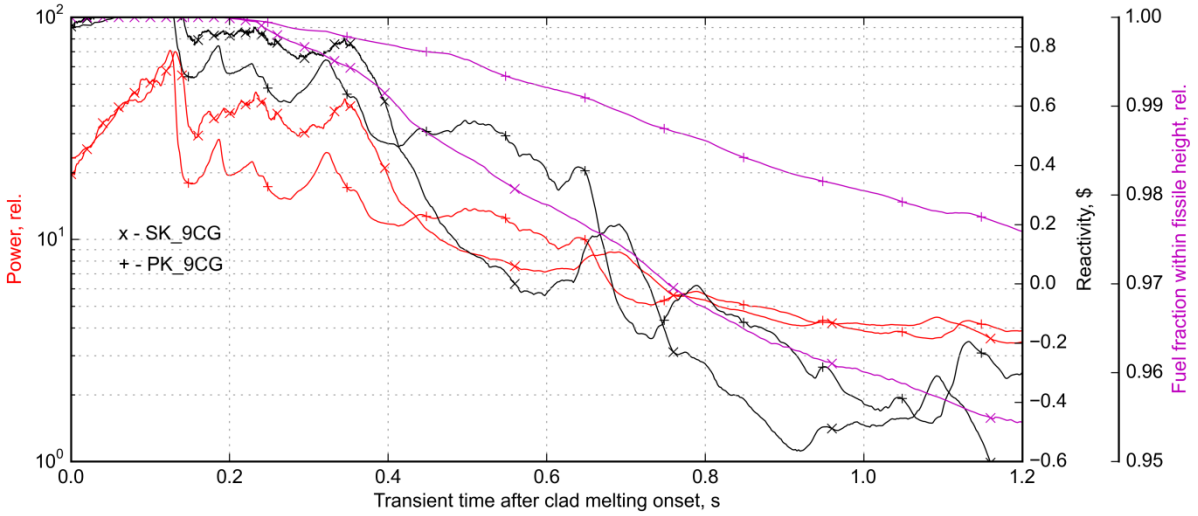

Fig. 74. Temporal evolution of normalized power, net reactivity and fuel mass fraction within fissile height in a ULOF as calculated with PK and SK options after clad melting onset (9 CG configuration)

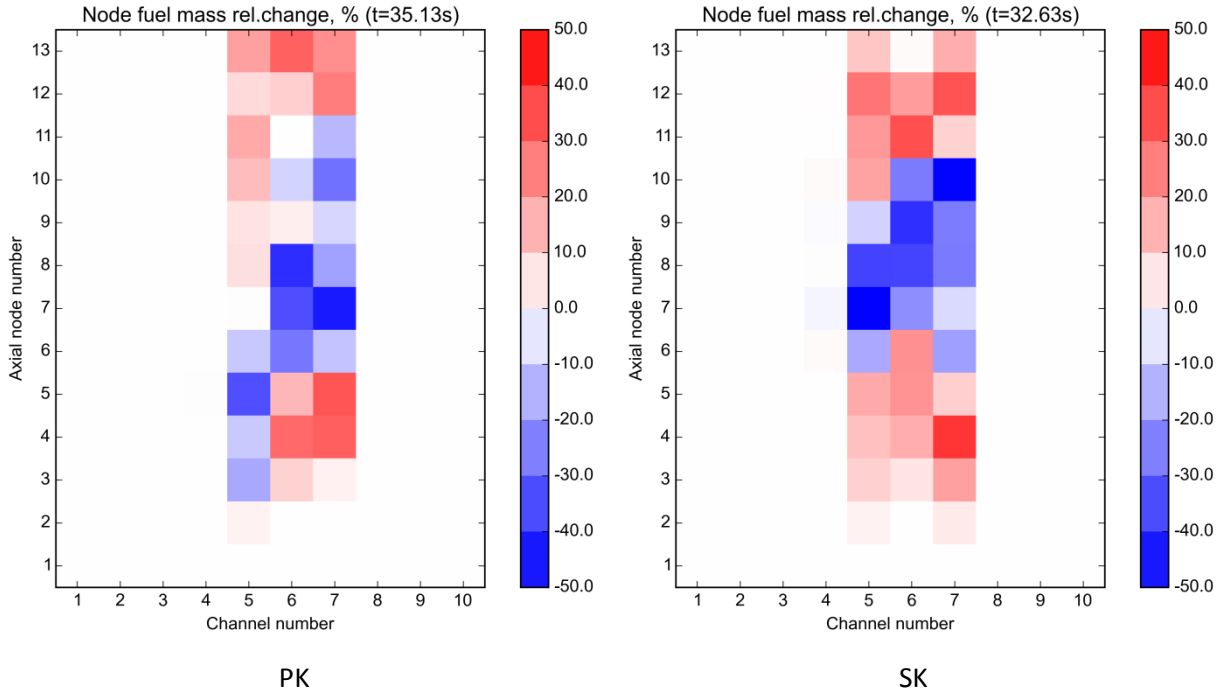

Fig. 75. Relative changes of node fuel mass in the fissile core with respect to the steady state value computed with the PK and SK options at the moment of pin failure of channel #4 for 9 CG configuration

Fuel discharge from the fissile core height leads to first sub-criticality predicted by the PK and SK model at t = 0.7 s and 0.55 s after clad melting onset. Characteristics of critical configurations are listed in Table 27. The power level decreases in a similar way for two models reaching 6.2 and 7.6 of the nominal at this point in time, while fully voided configuration is achieved in both calculations. Higher by about 100 K core average fuel temperature characterises the SK solution as result of a more energetic material relocation

phase. At this moment the fraction of about 1% of fuel mass ejected out of the fissile core corresponds to the total fuel relocation reactivity contribution of about 3 $ in the PK calculation, while the SK calculation predicts an almost 2 times larger amount of the fuel ejected out of fissile height (see Fig. 74 and Table 27).

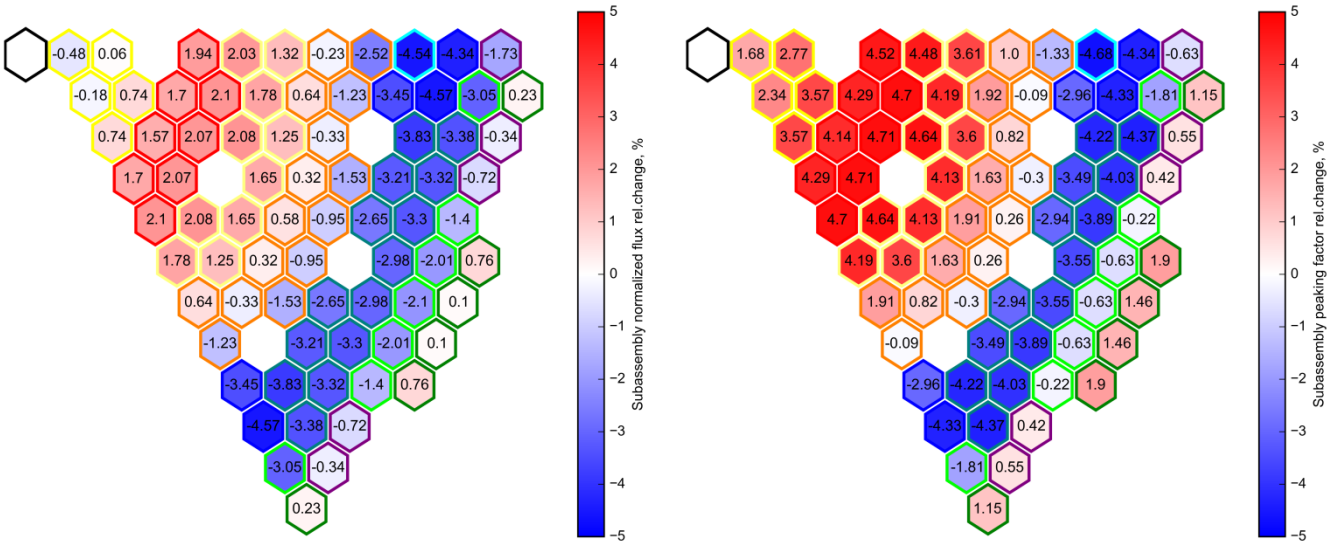

Fig. 76. Subassembly normalized neutron flux and power peaking factor change with regard to steady state value as computed with SK option at pin failure of channel 8 (t = 32.67 s) for 9 CG configuration

The fuel relocation pattern in Fig. 77, left, given as node fuel mass relative change with respect to SS fuel mass value as computed with use of the SK model, illustrates the core configuration at the moment of first sub-criticality. Pin failures occur in nine channels up to this moment, resulting in a strong axial relocation of fuel within the SA height. The corresponding node power changes are given in the right part of Fig. 77. The distortion of SA normalized fluxes and power peaking factors at this moment in time is shown in Fig. 78. A strong spatial distortion of the initial core material content, illustrated at the moment of first sub-criticality, causes considerably different reactivity responses during the relocation phase in comparison to the PK approach, while a basically similar core state is reached in the calculation with the PK model at this moment. Starting from the core configuration with noticeable pin damages, the neutron spatial kinetics describes the transient behaviour of the core in a different manner, deviating stronger for more perturbed configurations in term of the net reactivity, as it has been observed for both 3 CG and 9 CG configurations. In particular, for strong fuel reactivity feedback, it implies that linearization of the effect with the fuel mass inventory in individual axial nodes does not allow to reproduce the fuel relocation reactivity feedback as obtained in the calculation with the SK solution.

Table 27. Characteristic core parameters at time moment of first sub-criticality in a ULOF as computed with PK and SK options for 9 CG configuration

Parameter	PK at first sub-criticality at 35.57 s	SK at first sub-criticality at 32.99 s
Total core power, nom.	6.17	7.58
Normalized mass flow, %	oscillations around zero	oscillations around zero
Total reactivity, $	+0.0	+0.0
Doppler, $	-1.50	n.a.
Sodium, $	+4.20	n.a.
Axial expansion, $	-0.92	n.a.
Clad relocation, $	+0.94	n.a.
Fuel relocation, $	-2.85	n.a.
Core-average fuel temperature, K	2879.3	2960.0
Maximal node fuel temperature, K	3285.3	3273.2
Core-average sodium temperature (within fissile height), K	1223.0	1245.5
Sodium mass fractions within fissile height, rel.	0.026	0.009
Sodium mass fractions within upper core regions, rel.	0.013	0.009
Fraction of fuel out of the fissile height, %	1.02	1.93

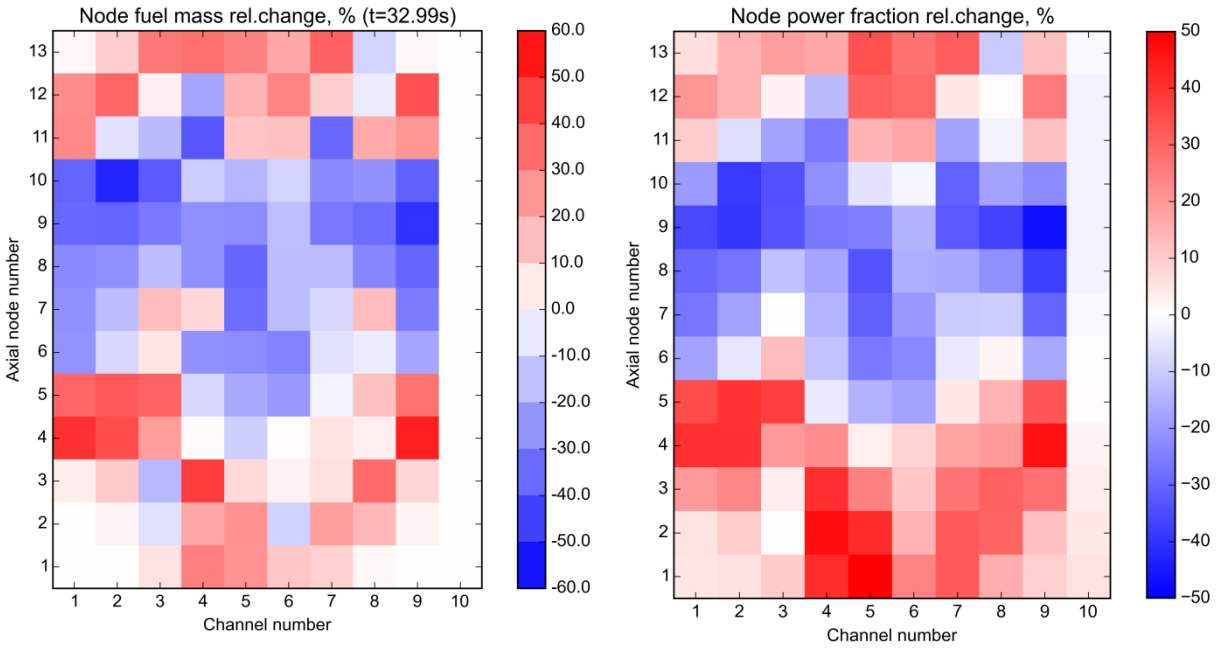

Fig. 77. Relative changes of node fuel mass in the fissile core and node power fraction with respect to the steady state value computed with the SK model at the moment of first sub-criticality (t = 32.99 s) for 9 CG configuration

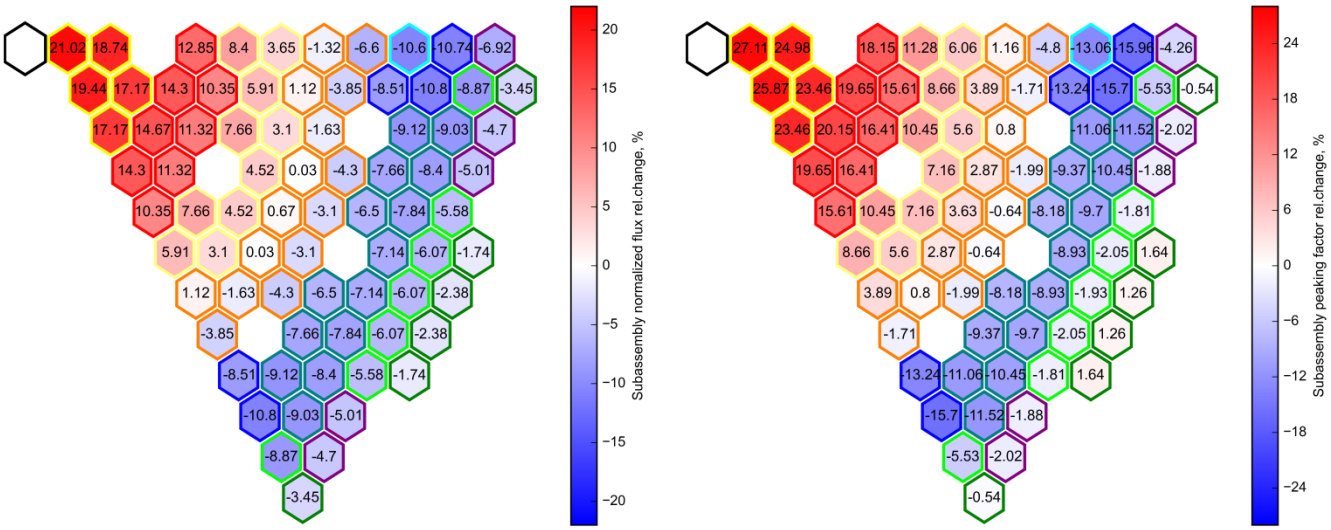

Fig. 78. Subassembly normalized neutron flux and power peaking factor change with regard to steady state value as computed with SK option at first sub-criticality (t = 32.99 s) for 9 CG configuration

Concluding remarks to §5.3.2.3

Comparing these results to the ones discussed in §5.3.2.1 one can formulate common conclusions for both core configurations. First, for the boiling phase it is demonstrated, that taking note of the current level of core details, application of the SK model leads to different ULOF transient scenarios, depending on the cooling groups strategy applied, while for the PK calculations the power excursions with few power peaks and subsequent sub-criticality is predicted similar for both considered cooling group configurations. Material relocation phase is characterized in all calculations by the transient variation of the fuel relocation reactivity feedback which mitigates the transient in such a manner to prevent the achievement of values of a high net reactivity. In case of 9 CG core configuration, almost identical transient evolution is observed for the entire transient for the two solutions, characterized by very similar core conditions at the moment of the first pin failure, which define further progression of the material relocation phase. Nevertheless, in spite of these similar starting conditions, the PK fails to reproduce the material relocation phase in term of net reactivity, primarily due to a more efficient in-core fuel relocation feedback when compared to results obtained when applying the SK model. Taking note of the similar power excursion, the SK solution, even being characterized by a stronger fuel relocation dynamic, predicts higher total energy release before first sub-criticality is achieved, primarily due to a less “efficient” fuel relocation feedback. The new results contribute with similar observations to basic conclusions of the analysis presented in [42] and discussed in section 1.4.

6 SUMMARY AND CONCLUSIONS

This study concentrated on improvements of modelling the accident transient behaviour of Sodium-cooled Fast Reactor. It is devoted in particular to the modelling of the Initiation Phase of severe transients by means of the code SAS-SFR. The study belongs to the domain of applied science, which provides engineering solutions for practical applications based on the currently available scientific knowledge and physical understanding of nature. In this context a new advanced approach for the simulation of tightly coupled phenomena is developed, which is based on qualified models and validated solutions. The study provides a comprehensive description of the modelling of the Initiation Phase with the SAS-SFR code, including existing and newly developed approaches for a more accurate "look" on the modelled phenomena.

Thereby, new neutron physics solutions are developed to depict more accurately the steady state characterization of SFR cores and from there also the evolution during an accidental transient. The capabilities of the new solutions are demonstrated on the basis of the ESFR Reference Oxide core design considering a Beginning Of Life core configuration, for which the analysis of steady state and transient behaviour is broadly presented in literature.

For steady state conditions a coupled simulation scheme is developed using the Monte Carlo neutron transport MCNP code. The coupled solution is established on basis of core state parameters, predicted by the SAS-SFR code, thus providing the best-estimate steady state characterization as result of SAS-SFR thermal hydraulics calculations and Monte Carlo neutron transport calculations with MCNP, which use only minor approximations. The specificity of the new approach is the methodology of the core state parameters transfer to the neutron physics model, which considers treatment of five material components for description of the calculation nodes in the neutron physics solution. The main advantage of the new scheme is its use as the reference for steady state characterization with the SAS-SFR code, which provides an effective basis for cross-comparisons of the results with other system codes. Sensitivity of results dependent on different options of the calculation scheme has been demonstrated by systematic simulations with the new coupled system. The use of the tool is recommended as a basic option for the steady state analysis with SAS-SFR of existing or new SFR designs. Practically the new system allows replacing the conventional calculation route for determination of the steady state characterization by a new more sophisticated approach.

For the transient analysis a coupled simulation system has been developed, which uses the spatial kinetics solution of the PARCS code and aims to overcome the drawback of the PK model, which considers constant normalized spatial distributions of the flux during the entire transient simulation. The coupling is based on the operator splitting technique and an explicit time coupling strategy. For the transfer of the core state parameters to the neutron physics model the same new methodology has been used, as the one for application of the Monte Carlo solution for steady state. In addition, a "smeared geometry" model has been selected and implemented for realisation of the coupling in order to overcome the peculiarity of SAS-SFR to treat the individual expansion of pin and SA elements. And subsequently a suitable cross sections model, the background cross section model σ_0 ("Sigma-zero"), originally available in the FAST code system, has been implemented for neutron physics, which allows

to calculate time-dependent macroscopic cross sections for a wide range of the core state parameter variations. These achievements allow treating all important reactivity effects in a ULOF transient, including the effects of fuel and clad relocation, which play a critical role in evaluation of reactivity and power variations in the later phase of the ULOF transient.

Results of the steady state characterization with the SAS-SFR/PARCS code system show an appropriate agreement with the SAS-SFR/MCNP solution, which demonstrates consistency of the neutron cross sections model in conjunction with the deterministic solution of PARCS compared to the MCNP solution. Results of other study on prediction of core reactivity change with regard to a change of the power level by both solutions have also shown appropriate agreement between the two approaches, demonstrating clearly the consistency of data transfer.

In transient simulations the new SAS-SFR/PARCS tool demonstrates basic agreement with the PK solution for the Reference Oxide core design of the CP ESFR project for the part of the transient prior to clad melting. Detailed analyses revealed the importance of an appropriate simulation of the reactivity feedback related to the transient hexcan behaviour and its thermal expansion prior to steel melting onset. In the SAS-SFR PK model the hexcan material reactivity is modelled only starting from steel melting onset. In contrast to this, for the core configuration with three cooling groups modelled with the SK solution the account for the hexcan thermal behaviour in the neutron physics model leads to a difference in power and reactivity at the time of boiling onset of 3% of the nominal power and 0.015 $ of the total reactivity respectively. The boiling onset occurs slightly earlier, i.e. less than 1 s, in the SK case, while these differences increase noticeably in case of longer pre-boiling phase, as it has been demonstrated for the nine cooling groups core configuration. Subsequently, the hexcan reactivity is evaluated to play a non-negligible role also for the energetic phase of the transient. For instance, at part of the transient, which is characterized by a rapid fuel pin expansion as result of a nearly prompt critical power excursion, an additional negative reactivity may be introduced due to additional neutron absorption as result of delay of the thermal expansion of the hexcan and corresponding increase of the hexcan mass in relation to the increasing fissile core height.

For core design with the relatively high sodium void worth, investigated in this study, observed differences as result of applied spatial kinetics solution as compared to the PK one are not so large in the sense that for the given ULOF framework an energetic power scenario cannot be avoided in both cases which results in a relocation phase and reactivity mitigation by fuel discharge from the fissile core. However, the observed and discussed differences indicate clearly that the basic assumption of the PK solution of SAS-SFR to linearize reactivity feedback contributions with the node wise variation of the mass inventory of sodium, clad material and fuel represents a rather crude and not sufficiently accurate simulation of the real situation. The differences in transient evolution between the PK and SK solutions are expected to be larger starting from the boiling phase when analysing more advanced core design variants with a low or even negative sodium void worth in the next step of future analyses.

The newly developed transient solution algorithms demonstrate new capabilities for modelling of the IP of severe transients which can be summarized as follows:

1) The SK neutron physics model on basis of the PARCS and MCNP code systems in combination with the SAS-SFR code system provides new capabilities to establish a fully consistent representation of a large variety of different core and plant designs of SFR at steady state conditions. In addition the new tool allows it to model asymmetric transients, such as a UTOP initiated by CR movement considering spatial neutron transport effects.
2) The tool structure and inherent flexibility of data exchange and processing models, which has been implemented, provide an effective basis for a detailed analysis of specific reactivity effects in an SFR and could be used efficiently for further developments. The effect of control rod drive line expansion and diagrid expansion may be introduced in the solution without modification of its structure and data exchange.
3) Analysis results for a ULOF transient on basis of different thermal hydraulics cooling conditions i.e. three versus nine cooling groups simulations have shown that the impact of different core and plant design options may lead to larger differences between results than the use of the PK or the SK neutron physics solution algorithm. This conclusion holds mainly for the core characteristics at BOL conditions and needs to be reviewed in detail for other core configurations i.e. EOC core conditions. The flexibility of the newly developed methodology will allow it to investigate respective consequences for different core states in future exercises.
4) As a consequence of results presented in this work it becomes clear that a reliable evaluation of the safety features of a specific SFR core and plant design needs a well balanced approach of the theoretical representation of core design details such as fuel pin design, SA design, core configuration, thermal hydraulic cooling conditions as well as primary and secondary system design specifications. The real advantage of the use of a SK solution algorithm becomes of imminent importance when the level of detail in the representation of all plant characteristics is well balanced and similarly detailed, i.e., at all levels of the simulation.

With the newly developed tools new options have been provided to contribute to SFR safety analyses. The solutions have been qualified to be reliable as demonstrated in this work by code to code comparisons with results of other well established approaches for a variety of test cases.

Recommendations for future work

Validation of results provided in this work for the ULOF simulation is limited to a general level to demonstrate feasibility and advantages of the new SAS-SFR/PARCS code system and coupling methodology. Further comparisons with the PK solution could be foreseen on the basis of the same design and the considered core configurations, involving a larger number of channels for core representation (e.g. one subassembly per channel) and performing a sensitivity analysis of the results to the reactivity feedback input used by the PK model. This could be helpful to better understand in detail differences of the boiling propagation peculiarities in the core for the PK and SK solutions. Additionally, it is of a high

importance to study consequences of a ULOF accident in a low-void SFR core (e.g. ESFR-like core with a large upper sodium plenum introduced) with the new system, where larger differences of results during the boiling phase are expected.

More detailed validation is required for the current version of the SAS-SFR/PARCS code system, in particular, based on available experimental transient benchmarks for SFRs. In this case it becomes of importance to implement a calculation approach to account for in the spatial kinetics solution the control rods axial positions in the core. This then would provide the capability to model accidental reactivity ramp insertions, as well as control rod drive line expansion reactivity feedback effects, which is one of the key issues for accurate representation of the transient phenomenology of ULOF and UTOP transients in case of low void worth core designs. Implementation of the option to account for diagrid expansion is also practically necessary in this case. It then allows evaluating features of innovative SFR designs which aim at the increase of the overall ULOF transient time and essentially of the grace time before boiling onset, where the secondary circuit response becomes not negligible, leading to noticeable changes in the inlet sodium temperature. These two reactivity components can be naturally integrated in the code system without modifications of its structure.

Subsequently, further code application and benchmarking will reveal the peculiarities and potentially drawbacks of neutron physics solution components such as the deterministic diffusion solution of PARCS and the XS generation system “Sigma-zero”. The deterministic diffusion solution may lead to errors in the evaluation of the sodium void reactivity feedback in designs, which are characterized by a large upper sodium plenum and inner breeding zones, as foreseen in the ASTRID core design. Practically for any core design discrepancies between deterministic and Monte Carlo solutions in prediction of reactivity effects may be not negligibly small, because they depend on both the used XS model and the method of solving of the neutron transport equations. The currently implemented method in the PARCS code and with the “Sigma-zero” XS model results in a noticeably larger value of the Sodium Void Effect, i.e. by about 180 pcm, for the ESFR Reference Oxide core than predicted when using the MCNP code. This means that the XS generation method “Sigma-zero” method must be validated by more applications essentially when applied during the material relocation phase. This neutron XS model introduces errors and limitations specific for the Bondarenko method, and in the actual implementation the generated transient XS could be influenced by input and assumptions for preparation of the microscopic cross sections library (number of energy groups, treatment of heterogeneity and method employed in unit cell code).

With regard to a better code performance related to the calculation time, some improvements may be introduced in the microscopic cross sections interpolation calculation scheme. Currently the XS generation assumes recalculation of both micro- and macroscopic cross sections for a given zone by criteria (such as fuel temperature change), while the XS may be recalculated for all zones at every calculation step with low time costs, based on the last calculated self-shielded microscopic cross sections stored for a given zone and an updated nuclide number density, avoiding the time consuming interpolation procedure. Further decrease of the computational time for both XS generation and multi-group neutron transport solution could be achieved decreasing the number of neutron energy groups.

Concerning the neutron physics methods and solutions employed by the current version, further steps of the development work could include implementation of more advanced methods of solving the neutron transport equation, which may become possible due to the rapidly developing capabilities of computation resources, including capabilities of parallel processor calculations (e.g. deterministic transport solutions THREEDANT/PARTISN [119] and [120], SNATCH [58] and [121], TORT-TD [122] and APOLLO3 [123] could be of interest).

With regard to the steady state modelling, one important feature of SAS-SFR to perform pre-irradiation calculations of the fuel pin behaviour before transient analysis was left beyond the scope of this work. Improvements of modelling this feature should consider a coupled simulation of the stationary neutron physics calculations which accounts for the realistic fuel reloading scheme for determination of the local fuel burnup in the core and the fuel irradiation simulation. This would result in a decrease of uncertainties in the characterization of burnt fuel pins at steady state, which significantly influences transient results. Implementation of this option could not be foreseen in this work because it would have needed considerable code modifications and data exchange within the steady state simulation routine packages of SAS-SFR to consider the power operation history during pre-irradiation more accurately then actually foreseen, i.e. including the application of neutron physics solution and cross sections libraries for a detailed modelling of the local core burn-up. However, in a first step the current SAS-SFR/PARCS code system version can be applied for the analysis of transient responses of burnt fuel core configurations, applying the available simplified approach of SAS-SFR for the pin characterization at steady state dependent on burn-up i.e. using constant shape functions of the power distribution during the whole considered power operation time.

BIBLIOGRAPHY

[1] E.P. Velikhov, A.Yu. Gagarinski, S.A. Subbotin, V.F. Tsibulski, "Energy Evolution in the XXI Century", Moscow, IzdAt, 2008

[2] "WENRA Safety Reference Levels for Existing Reactors – Update in relation to lessons learned from TEPCO Fukushima Dai-ichi accident", Report of Western European Nuclear Regulators Association-WENRA RHWG, 2014

[3] "Nuclear Power Reactors in the World", Reference Data Series No. 2, 2016 edition, IAEA-RDS-2/36

[4] "Status of Fast Reactor Research and Technology Development", IAEA-TECDOC-1691, IAEA, Vienna (Austria), 2012

[5] "Fast Reactor Database", IAEA-TECDOC-866, IAEA, Vienna (Austria), February 1996

[6] Generation IV International Forum Web-site, http://www.gen-4.org/

[7] Gen IV Roadmap, 2002 - US DOE Nuclear Energy Research Advisory Committee and the Generation IV International Forum, A technology Roadmap for Generation IV Nuclear Energy Systems, GIF002-00, December 2002

[8] G.L. Fiorini, A. Vasile, "European Commission – 7th Framework programme: The Collaborative Project on European Sodium Fast Reactor (CP ESFR)", Nuclear Engineering and Design, Vol. 241, Issue 9, pp. 3461–3469, September 2011

[9] K. Sun, J. Krepel, K. Mikityuk, S. Pelloni, R. Chawla, "Void reactivity decomposition for the Sodium-cooled Fast Reactor in equilibrium fuel cycle", Annals of Nuclear Energy, vol. 38, pp. 1645-1657, 2011

[10] T. Suzuki, Y. Tobita, K. Kawada, H. Tagami, J. Sogabe, K. Matsuba, K. Ito, H. Ohshima, "A preliminary evaluation of unprotected loss-of-flow accident for a prototype fast-breeder reactor", Nuclear Engineering and Technology, Vol. 47, Issue 3, pp. 240–252, April 2015

[11] I. Sato, Y. Tobita, K. Konishi, K. Kamiyama, J. Toyooka, R. Nakai, S. Kubo, S. Kotake, K. Koyama, Y. Vassiliev, A. Vurim, V. Zuev, A. Kolodeshnikov, "Safety Strategy of JSFR Eliminating Severe Recriticality Events and Establishing In-Vessel Retention in the Core Disruptive Accident", Journal of Nuclear Science and Technology, Vol. 48, No. 4, pp. 556–566, 2011

[12] S. Kondo, "Current R&D status on material motion and interactions relevant to core disruptive accidents", Paper presented at Technical Committee Meeting on Material-Coolant Interactions and Material Movement and Relocation in Liquid Metal Fast Reactors, O-arai, Ibaraki, Japan, June 6-9, 1994

[13] T. Takeda, Y. Shimazu, B. Foad, K. Yamaguchi, "Review of safety improvement on sodium-cooled fast reactors after Fukushima accident", Natural Science, Vol. 4, Special Issue, p. 929-935, 2012

[14] B. Carluec, S. Beils, J.F. Sauvage, P. Mariteau, P. Lo Pinto, “Post-Fukushima lessons and safety orientations for ASTRID”, Proceedings of FR13 (International Conference on Fast Reactors and Related Fuel Cycles: Safe Technologies and Sustainable Scenarios), Paris, France, March 4-7, 2013

[15] M. Schikorr, E. Bubelis, B. Carluec, J. Champigny, “Assessment of SFR reactor safety issues. Part I: Analysis of the unprotected ULOF, ULOHS and UTOP transients for the SFR (v2b-ST) reactor design and assessment of the efficiency of a passive safety system for prevention of severe accidents”, Nuclear Engineering and Design, Vol. 285, pp. 249–262, April 2015

[16] P. Le Coz, J.-F. Sauvage, J.-P. Serpantie, “Sodium-Cooled Fast Reactors: the ASTRID Plant Project”, Proceedings of ICAPP-2011, Nice, France, May 2-5, 2011

[17] M.G. Stevenson, W.R. Bohl, F.E. Dunn, L.L. Smith, “Current status and experimental basis on the SAS LMFBR accident analysis code system”, Proceedings of the Fast Reactor Safety Meeting, CONF-740401, Beverly Hills, California, April 2–4, 1974

[18] U. Imke, D. Struwe et al., “Status of the SAS4A-code development for consequence analysis of core disruptive accidents”, Proceedings of an International Topical Meeting “Sodium Cooled Fast Reactor Safety”, Obninsk, Russia, October 1994

[19] G. Geffraye, O. Antoni, M. Farvacque, D. Kadri, G. Lavialle, B. Rameau, A. Ruby, “CATHARE 2 V2.5-2: A single version for various applications”, Nuclear Engineering and Design, vol. 241, 2011

[20] RELAP5-3D©. Code Manual Volume II: User’s Guide and Input Requirements, INEEL-EXT-98-00834, Revision 2.3, 2005

[21] TRACE v5.0 Theory and User’s manual. Office of Nuclear Regulatory Research, U.S. NRC, Washington, DC, 2007

[22] K. Mikityuk, S. Pelloni, P. Coddington, E. Bubelis, R. Chawla, “FAST: An advanced code system for fast reactor transient analysis”, Annals of Nuclear Energy, vol. 32, pp. 1613-1631, 2005

[23] M. Schikorr, “Assessment of the kinetic and dynamic transient behaviour of sub-critical systems (ADS) in comparison to critical reactor systems”, Nuclear Engineering and Design, Vol. 210, pp. 95-123, December 2001

[24] S. Massara, J. Tommasi, M. Vanier, O. Köberl, “Dynamics of critical dedicated cores for minor actinide transmutation”, Nuclear Technology, Vol. 149, No. 2, pp. 150-174, February 2005

[25] M.M. Stempniewicz, “SPECTRA Sophisticated Plant Evaluation Code for Thermal-hydraulic Response Assessment”, V3.60, Report K5024/10.101640, NRG, Arnhem, April 2010

[26] A. Chenu, “Single- and two-phase flow modeling for coupled neutronics / thermal-hydraulics transient analysis of advanced sodium-cooled fast reactors”, Swiss Federal Institute of Technology, Lausanne (EPFL), doctoral thesis No. 5172, 2011

[27] A. Lázaro, L. Ammirabile, G. Bandini, G. Darmet, S. Massara, Ph. Dufour, A. Tosello, E. Gallego, G. Jimenez, K. Mikityuk, M. Schikorr, E. Bubelis, A. Ponomarev, R. Kruessmann, M. Stempniewicz, "Code assessment and modelling for Design Basis Accident Analysis of the European Sodium Fast Reactor design. Part I: System description, modelling and benchmarking", Nuclear Engineering and Design, Vol. 266, pp. 1–16, January 2014

[28] N. Girault, J. Van Dorsselaere, F. Jacq, G. Brillant, M. Kissane, G. Bandini, M. Buck, J. Champigny, W. Hering, S. Perez-Martin, L. Herranz, P. Raison, N. Reinke, K. Tucek, D. Verwaerde, "The European JASMIN project for the development of a new safety simulation code, ASTEC-Na, for Na-cooled Fast Neutron Reactors", Proceedings of ICAPP-2013, Jeju Island, Korea, April 14-18, 2013

[29] A. Flores y Flores, V. Matuzas, S. Perez-Martin, G. Bandini, S. Ederli, L. Ammirabile, W. Pfrang, "Analysis of ASTEC-Na capabilities for simulating a loss of flow CABRI experiment", Annals of Nuclear Energy, Vol. 94, pp. 175–188, August 2016

[30] S. Kondo, K. Morita, Y. Tobita, N. Shirakawa, "SIMMER-III: An Advanced Computer Program for LMFBR Severe Accident Analysis", ANP'92, No. 40-5, Tokyo, Japan, October 25-29, 1992

[31] Y. Tobita, S. Kondo, H. Yamano, K. Morita, W. Maschek, P. Coste, T. Cadiou, "The development of SIMMER-III, an advanced computer program for LMFR safety analysis, and its application to sodium experiments," Nuclear Technology, Vol. 153/3, pp. 245-255, March 2006

[32] S. Poumerouly, T. Jeanne, J. Lecerf, G. Rimpault, "Comparison of the code systems SAS-SFR and SIMMER-III on the primary phase of an unprotected loss of flow", Proceeding of GLOBAL-2011, Chiba, Japan, December 11-16, 2011

[33] Iu. Shvetsov, Iu. M. Ashurko, I. R. Suslov, K. F. Raskach, L. M. Zabudko, E. E. Marinenko, "The UNICO multi-physics code to analyse transients in Sodium Fast Reactor", Proceedings of FR13 (International Conference on Fast Reactors and Related Fuel Cycles: Safe Technologies and Sustainable Scenarios), Paris, France, March 4-7, 2013

[34] I. M. Ashurko, A. V. Volkov, K. F. Raskach, "COREMELT-2D Code for analysis of severe accidents in a Sodium Fast Reactor, Proceedings of FR13 (International Conference on Fast Reactors and Related Fuel Cycles: Safe Technologies and Sustainable Scenarios), Paris, France, March 4-7, 2013

[35] J. Dadillon et al.,"CABRI – Project (1973 – 1088) – Test facility, Results and Achievements" vol. 1-3, Rapport CEA/IPSN/DERS No. 01/89 (June 1989)

[36] J. Papin et al., "CABRI 2 Project (1986 – 1994) Results and Achievements", Vol. 1-3, Rapport IPSN/DRS No. 5 (December 1994)

[37] J. Papin et al., "CABRI-FAST (1992 – 1997) Results and Achievements", Vol. 1/2 Rapport IRSN/DRS No. 8/2002 (January 2002)

[38] J.M. Frizonnet et al., “CABRI-RAFT (1997 – 2002) Synthesis of the CABRI-RAFT program”, Internal IRSN/JAEA/FZK report, September 2005

[39] H. Yamano, Y. Onoda, Y. Tobita, I. Sato, “Transient Heat Transfer Characteristics between Molten Fuel and Steel with Steel Boiling in the CABRI-TPA2 Test”, Nuclear Technology, Vol. 165, No. 2, pp. 145-165, 2009

[40] S. Perez-Martin, A. Ponomarev, R. Krüssmann, W. Pfrang, “Study of power and cooling criteria for selecting SA groups in the simulation of accidental transients in sodium fast reactors with the SAS-SFR code”, Proceedings of ICAPP-2014, Paper 14050, Charlotte, USA, April 6-9, 2014

[41] R. Krüssmann, A. Ponomarev, W. Pfrang, M. Schikorr, D. Struwe, “Comparison of results of SAS-SFR calculations of the CP-ESFR Working Horse and Optimized Core designs during the Initial Phase of an ULOF accident”, Proceedings of FR13 – International Conference on Fast Reactors and Related Fuel Cycles: Safe Technologies and Sustainable Scenarios, Paris, France, March 4-7, 2013

[42] M. Guyot, P. Gubernatis, R. Le Tellier, “Space–Time Effects in the Initiating Phase of Sodium Fast Reactors and Their Evaluation Using a Three-Dimensional Neutron Kinetics Model”, Annals of Nuclear Energy, Vol. 85, pp. 115-126, November 2015

[43] D. Lemasson, A. Bretault, D. Schmitt, A. Ponomarev, S. Perez-Martin, “New Methodology for Sodium Reactivity Feedback Modeling within the SAS-SFR Code for Fast Reactors Severe Accidents Analysis”, Proceedings of ICAPP-2013, Jeju Island, Korea, April 14-18, 2013

[44] “Evaluation of Benchmark Calculations on A Fast Power Reactor Core with Near Zero Sodium Void Effect”, IAEA-TECDOC-731, 1994

[45] R. Krüssmann, A. Ponomarev, W. Pfrang, D. Struwe, J. Champigny, B. Carluec, D. Schmitt, D. Verwaerde, “Assessment of SFR reactor safety issues: Part II: Analysis results of ULOF transients imposed on a variety of different innovative core designs with SAS-SFR”, Nuclear Engineering and Design, Vol. 285, pp. 263–283, April 15, 2015

[46] A. Lázaro, M. Schikorr, K. Mikityuk, L. Ammirabile, G. Bandini, G. Darmet, D. Schmitt, Ph. Dufour, A. Tosello, E. Gallego, G. Jimenez, E. Bubelis, A. Ponomarev, R. Krüssmann, D. Struwe, M. Stempniewicz, “Code assessment and modelling for Design Basis Accident analysis of the European Sodium Fast Reactor design. Part II: Optimised core and representative transients analysis”, Nuclear Engineering and Design, Vol. 277, pp. 265–276, October 2014

[47] The KANEXT modular code system, http://inrwww.webarchiv.kit.edu/kanext.html

[48] G. Palmiotti, E.E. Lewis, C.B. Carrico, “VARIANT: VARIational Anisotropic Nodal Transport for Multidimensional Cartesian and Hexagonal Geometry Calculation”, Technical report ANL-95/40, Argonne National Laboratory, 1995

[49] “Transient and accident analysis of a BN-800 type LMFR with near zero void effect”, IAEA-TECDOC-1139, 2000

[50] A.E. Waltar, A.B. Reynolds, “Fast Breeder Reactors”, Pergamon Press, New York, 1981

[51] K. Sun, J. Krepel, K. Mikityuk, R. Chawla, “A neutronics study for improving the safety and performance parameters of a 3600 MWth Sodium- cooled Fast Reactor”, Annals of Nuclear Energy, Vol. 53, pp. 464–475, 2013

[52] K. S. Allen, T. W. Knight, C. M. Read Jr., Design of an equilibrium core 1000 MWt Sodium-Cooled heterogeneous Innovative Burner Reactor, Nuclear Engineering and Design, Vol. 242, p. 108–114, 2012

[53] J. E. Cahalan, T. H. Fanning, “The SAS4A/SASSYS-1 Safety Analysis Code System”, ANL/NE-12/4, Argonne National Laboratory, 2012

[54] D. Schmitt, S. Massara, G. Darmet, T. Jourdheuil, P. Tetart, B. Maliverny, “Design of a Sodium-cooled Fast Reactor with Innovative Annular Geometry and Very Low Sodium Void Worth”, Proceedings of ICAPP-2011, Paper 11073, Nice, France, May 2-5, 2011

[55] L. Buiron, Ph. Dufour, G. Rimpault, G. Prulhiere, C. Thevenot, J. Tommasi, F. Varaine, A. Zaetta, “Innovative core design for Generation IV Sodium-cooled Fast Reactors”. Proceedings of ICAPP-2007, Paper 7383, 2007

[56] E.E. Morris, “Impact of Spatial Kinetics in Severe Accident Analysis for a Large HWR”, ARS-94 – International Meeting on Advanced Reactor Safety, ANS, Pittsburgh, PA, USA, April 17-21, 1994

[57] W. A. Bezella, “A Two-Dimensional Fast Reactors Accident Analysis Model with Sodium Voiding Feedback Using the Synthesized Quasistatic Approach”, Ph.D Thesis, Purdue University, 1972

[58] M. Guyot, “Neutronics and Thermal–Hydraulics Coupling: Some Contributions Toward an Improved Methodology to Simulate the Initiating Phase of a Severe Accident on Sodium Fast Reactors”, Ph.D Thesis, Aix-Marseille University, 2014

[59] S. S. Podobed, A. N. Shmelev, V. S. Shkolnik, “Space-Dependent Effects in Fast Reactor Dynamics and Their Analysis Using Three-Dimensional Kinetics Code WIND-3D”, Topical Meeting on Advances in Reactor Physics, Charleston, S.C., March 8-11, 1992

[60] J. Wakabayashi, H. Yoshikawa, “Analysis of Space-Dependent Dynamics in Power Reactors and the Computer Code SPEC-FR”, Proceedings of Specialists Meeting on Reactivity Effects in Large Power Reactors “Space Dependant Reactor Dynamics”, Commission of the European Communities, Ispra (Italy), October 28-31, 1970

[61] D. Struwe, “A Two-Dimensional Model for Fast Reactor Kinetics Analysis with Space-Dependant Feedback”, Proceedings of Specialists Meeting on Reactivity Effects in Large Power Reactors “Space Dependant Reactor Dynamics”, Commission of the European Communities, Ispra, Italy, October 28-31, 1970

[62] J. K. Fletcher, M. A. Perks, “The Spatial Kinetics Program SPARK and Its Application to Fast Reactor Transients”, Proceedings of the Joint NEACRP/CSNI Specialists'

Meeting on New Developments in Three-dimensional Neutron Kinetics and Review of Kinetics Benchmark Calculations, Garching, Germany, January 22-24, 1975

[63] J. E. Cahalan, T. Ama, G. Palmiotti, T. A. Taiwo, W. S. Yang, "Development of a Coupled Dynamics Code with Transport Theory capability and Application to Accelerator-Driven Systems Transients", PHYSOR-2000, Pittsburgh, USA, May 7-11, 2000

[64] A. Travleev, "An approach to assess reactivity changes due to core thermal expansion", Annual Meeting on Nuclear Technology KTG-2010, Berlin, Germany, May 4-6, 2010

[65] S. Massara, D. Schmitt, A. Bretault, D. Lemasson, G. Darmet, D. Verwaerde, D. Struwe, W. Pfrang, A. Ponomarev, "Behavior of an heterogeneous annular FBR core during an Unprotected Loss of Flow accident: Analysis of the primary phase with SAS-SFR", Proceedings of ICAPP-2012, Paper 12213, Chicago, USA, June 24-28, 2012

[66] "Processing of the JEFF-3.1 cross section library into continuous energy Monte Carlo radiation transport and criticality data library", NEA/NSC/DOC (2006)18, http://www.nea.fr/abs/html/nea-1768.html

[67] H.R. Trellue, R.C. Little, M.C. White, R.E. MacFarlane, A.C. Kahler, "ENDF70: A continuous energy MCNP neutron data library based on ENDF/B-VII.0", Nuclear Technology, Vol. 168, No. 3, pp. 832-836, 2009

[68] X.-N. Chen, A. Rineiski, F. Gabrielli, L. Andriolo, R. Li, W. Maschek, "SIMMER-III parametric studies of fuel-steel mixing and radial mesh effects on power excursion in ESFR ULOF transients", Proceedings of ICAPP-2015, Nice, France, May 3-6, 2015

[69] J. T. Goorley, et al., "Initial MCNP6 Release Overview – MCNP6 version 1.0", LA-UR-13-22934, 2013

[70] A. Ponomarev, V. Sanchez, "Modeling of reactivity effects and non-uniform axial expansion of SFR core on basis of neutronics model with constant calculation mesh", Proceedings of ICAPP-2014, Charlotte, USA, April 6-9, 2014

[71] K. Ivanov, M. Avramova, "Challenges in coupled thermal–hydraulics and neutronics simulations for LWR safety analysis", Annals of Nuclear Energy, Vol. 34, Issue 3, pp. 501–513, 2007

[72] J. Watson, K. Ivanov, "Improved cross-section modelling methodology for coupled three-dimensional transient simulations", Annals of Nuclear Energy, Vol. 29, Issue 8, pp. 937–966, May 2002

[73] S. Pelloni, K. Mikityuk, "A new cross-section generation model in the FAST code system and its application to gas- and sodium-cooled Generation IV fast reactor", Annals of Nuclear Energy, Vol. 38, Issue 1, pp. 1-13, January 2011

[74] A. Chenu, K. Mikityuk, R. Chawla, "A coupled 3D neutron kinetics/thermal-hydraulics model of the Generation IV sodium-cooled fast reactor", Proceedings of ICAPP-2010, Paper 10281, San Diego, California, USA, June 13-17, 2010

[75] T. Downar, Y. Xu, T. Kozlowski. PARCS v2.7 U.S. NRC Core Neutronics Simulator User Manual. Purdue University, August 2006

[76] J. T. Murgatroyd, “Optimisation of the CO2 Cooled Fast Reactor for Plutonium and Minor Actinide Management”, Proceedings of the ENS-2002, World Nuclear Expo, Lille(France), 2002

[77] J. M. Ruggieri, J. Tommasi, J. F. Lebrat, C. Suteau, D. Plisson-Rieunier, C. De Saint Jean, G. Rimpault, J. C. Sublet, “ERANOS 2.1: International Code System for GEN IV Fast Reactor Analysis”, Proceedings of ICAPP-2006, Paper 6360, Reno, Nevada, June 4-8, 2006

[78] G. Rimpault, D. Plisson, J. Tommasi, R. Jacqmin, J.-M. Rieunier, D. Verrier, D. Biron, “The ERANOS code and data system for fast reactor neutronic analyses”, Proceeding of PHYSOR-2002, Seoul, Korea, October 7-10, 2002

[79] A. Rineiski, J. Y. Doriath, “Time Dependent Neutron Transport with Variational Nodal Method”, Proceedings of Joint International Conference on Mathematical Methods and Supercomputing for Nuclear Applications, p. 1661, Saratoga Springs, NY, October 5-9, 1997

[80] S. Pelloni, E. Bubelis, K. Mikityuk, P. Coddington, “Calculations of reactivity-initiated transients in gas-cooled fast reactors using the code system fast”, Annals of Nuclear Energy, Vol. 33, Issue 6, pp. 499–509, April 2006

[81] A. Chenu, K. Mikityuk, R. Chawla, “A coupled thermal-hydraulics/ 3D kinetics TRACE/PARCS model of the 3600 MW Gen-IV Sodium-cooled Fast Reactor: benchmark against ERANOS model”, Proceedings of ICAPP-2010, San Diego, California, USA, June 13-17, 2010

[82] R. Rachamin, C. Wemple, E. Fridman, “Neutronic analysis of SFR core with HELIOS-2, Serpent, and DYN3D codes”, Annals of Nuclear Energy, Vol. 55, pp. 194-204, May 2013

[83] A. Ivanov, V. Sanchez, R. Stieglitz, K. Ivanov, “High fidelity simulation of conventional and innovative LWR with the coupled Monte-Carlo thermal-hydraulic system MCNP-SUBCHANFLOW”, Nuclear Engineering and Design, Vol. 262, pp. 264–275, September 2013

[84] SHARP Assembly-Scale Multiphysics Demonstration Simulations. Argonne Report ANL/NE-13/9, 2013

[85] M. Daeubler, A. Ivanov, B. L. Sjenitzer, V. Sanchez, R. Stieglitz, R. Macian-Juan, „High-fidelity coupled Monte Carlo neutron transport and thermal-hydraulic simulations using Serpent 2/SUBCHANFLOW“, Annals of Nuclear Energy, Vol. 83, pp. 352–375, August 2015

[86] N. Guilliard, W. Bernnat, J. Lapins, I. Pasichnyk, Y. Perin, K. Velkov, W. Zwermann, “Analysis of large core neutronics by the Monte Carlo method coupled with thermal hydraulics”, PHYSOR-2016, Sun Valley, ID, May 1-5, 2016

[87] J.E. Hoogenboom, A. Ivanov, V. Sanchez, C. Diop, “A flexible coupling scheme for Monte Carlo and thermal-hydraulics codes”, Proceedings of International Conference on Mathematics and Computational Methods Applied to Nuclear Science and Engineering (M&C 2011), Rio de Janeiro, Brazil, May 8-12, 2011

[88] V. Seker, J.W. Thomas, T.J. Downar, “Reactor simulations with coupled Monte Carlo and computational fluid dynamics”, Proceedings of Joint International Topical Meeting on Mathematics & Computation and Supercomputing in Nuclear Applications (M&C + SNA 2007), Monterey, California, April 15-19, 2007

[89] M. Vazquez, H. Tsige-Tamirat, L. Ammirabile, F. Martin-Fuertes, “Coupled Neutronics Thermal-Hydraulics Analysis Using Monte Carlo and Sub-Channel Codes”, Nuclear Engineering and Design, Vol. 250, pp. 403–411, 2012

[90] C.L. Wheeler, C.W. Stewart, R.J. Cena, D.S. Rowe, A.M. Sutey, “COBRA-IV-I: An Interim Version of COBRA for Thermal-Hydraulic Analysis of Rod Bundle Nuclear Fuel Elements and Cores”, BNWL-1962, March 1976

[91] R. Bonifetto, S. Dulla, P. Ravetto, L. Savoldi Richard, R. Zanino, “A full-core coupled neutronic/thermal-hydraulic code for the modeling of lead-cooled nuclear fast reactors”, Nuclear Engineering and Design, Vol. 261, pp. 85–94, August 2013

[92] J. Leppänen. PSG2/Serpent – A Continuous-energy Monte Carlo Reactor Physics Burnup Calculation Code (User’s Manual). Version September 5, 2011

[93] A. Travleev, “TSP: Python Package to Facilitate Preparation of Input Files”, Internal report INR 31/13 – NUKLEAR 3462, KIT, Karlsruhe, Germany, November 2013

[94] A. Travleev, R. Molitor, V. Sanchez, “Python-based framework for coupled MC – TH reactor calculations“, Joint International Conference on Supercomputing in Nuclear Applications and Monte Carlo 2013 (SNA + MC 2013), La Cité des Sciences et de l’Industrie, Paris, France, October 27-31, 2013

[95] J. Dufek, W. Gudowski, “Stochastic approximation for Monte Carlo calculation of steady-state conditions in thermal reactors“, Nuclear Science and Engineering, Vol. 152, No. 3, pp. 274-283, March 2006

[96] St.C. Van der Marck, R. Klein Meulekamp, A. Hogenbirk, “New temperature interpolation in MCNP”, Proceedings of M&C 2005 Conference, Avignon, France

[97] L. Ammirabile, H. Tsige-Tamirat, „Pre-conceptual thermal-hydraulics and neutronics studies on sodium-cooled oxide and carbide cores“, Annals of Nuclear Energy, Vol. 60, pp. 127-140, 2013

[98] A. Ponomarev, A. Travleev, W. Pfrang, V. Sanchez, “Coupled MCNP – SAS-SFR Calculations for Sodium Fast Reactor Core at Steady-State”, Proceedings of ICAPP-2015, Nice, France, May 3-6, 2015

[99] L. Buiron, G. Rimpault, B. Fontaine, T.K. Kim, N.E. Stauff, T.A. Taiwo, A. Yamaji, J. Gulliford, E. Fridmann, I. Pataki, A. Kereszturi, A. Tota, T. Kugo, K. Sugino, M.M. Uematsu, R. Lin Tan, T. Kozlowski, C. Parisi, A. Ponomarev, “Evaluation of

large 3600MWTh Sodium-Cooled Fast Reactor OECD neutronic benchmarks", PHYSOR-2014, Kyoto, Japan, September 28 – October 3, 2014

[100] J. Krepel et al, "Working Horses" ESFR core concept characterization: neutronics and thermal hydraulics characteristics", Deliverable CP ESFR SP2.1.2.D2, 2010

[101] U. Imke, V. Sanchez, "Validation of the subchannel code SUBCHANFLOW using the NUPEC PWR test (PSBT)", Science and Technology of Nuclear Installations, August 2012

[102] A.G. Mylonakis, M. Varvayanni, N. Catsaros, P. Savva, D.G.E. Grigoriadis, "Multi-physics and multi-scale methods used in nuclear reactor analysis", Annals of Nuclear Energy, Vol. 72, pp. 104–119, 2014

[103] S. Dulla, E.H. Mund, P. Ravetto, "The quasi-static method revisited", Progress in Nuclear Energy, Vol. 50, pp. 908–920, 2008

[104] V.S. Mahadevan, E. Merzari, T. Tautges, R. Jain, A. Obabko, M. Smith, P. Fischer, "High-resolution coupled physics solvers for analysing fine-scale nuclear reactor problems", Philosophical Transactions of Royal Society, 2014

[105] J. J. Kaganove, "Numerical solution of the one-group space-independent reactor kinetics equations for neutron density given the excess reactivity", ANL report (ANL-6132), February 1960

[106] K. Mikityuk, A. Vasiliev, P. Fomichenko, P. Alekseev, "LOOP2: Comprehensive transient code for advanced nuclear reactors", Proceedings of International Conference on the New Frontiers of Nuclear Technology: Reactor Physics, Safety and High-Performance Computing (PHYSOR-2002), Seoul, Korea, 2002

[107] R.E. MacFarlane, "TRANSX 2: A code for interfacing MATXS cross-section libraries to nuclear transport codes," Technical report, LA-12312-MS, Los Alamos, USA, 1992, http://t2.lanl.gov/codes/transx-hyper/TRANSX.html

[108] R.E. MacFarlane, D.W. Muir, "The NJOY nuclear data processing system Version 91," Technical report, LA-12740-M, Los Alamos, USA, 1994

[109] "Benchmark on Computer Simulation of MASURCA Critical and Subcritical Experiments: MUSE-4 Benchmark", Technical report, NEA/NSC/DOC (2005)23, Paris, France (2006), http://www.nea.fr/html/science/docs/2005/nsc-doc2005-23.pdf

[110] A. Lázaro, "Development, Assessment and Application of Computational Tools for Design Safety Analysis of Liquid Metal Cooled Fast Breeder Reactors", Doctoral Thesis, Universitat Politècnica de València, Departament d'Enginyeria Química i Nuclear, 2014

[111] K.O. Ott, R.J Neuhold, Introductory Nuclear Reactor Dynamics, American Nuclear Society, LaGrange Park, Illinois, USA (1985) 69

[112] T. A. Taiwo, E. E. Morris, J. E. Calahan, "SAS-DIF3DK Spatial Kinetics Capability for Thermal Reactor Systems", Proceedings of the Joint International Conference on

Mathematical Methods and Super-computing for Nuclear Applications, Saratoga Springs, New York (USA), American Nuclear Society, 1997

[113] K. Mikityuk, S. Pelloni, P. Coddington, E. Bubelis, "Development of an Advanced Code System for Fast Reactor Transient Analysis", Proceedings of the 11th International Topical Meeting on Nuclear Reactor Thermal-Hydraulics (NURETH-11), Avignon, France, 2005

[114] P. Sciora, L. Buiron, G. Rimpault, F. Varaine, E. Hourcade, A.C. Scholer, D. Ruah, D. Verrier, S. Massara, D. Lecarpentier, T. Jourdheuil, "A break even oxide fuel core for an innovative French Sodium-cooled Fast Reactor: neutronic studies results", Proceedings GLOBAL-2009, Paper 9528, Paris, France, September 6-11, 2009

[115] W. P. Barthold, J. C. Beitel, P. S. K. Lam, Y. Orechwa, S. F. Su, R. B. Turski, "Low Sodium Void Cores", In Proceedings of the Int. Conf. ENS/ANS Topical Meeting on Nuclear Power Reactor Safety, Brussels, Belgium, October 16-19, 1978

[116] J. Bouchard, "Generation IV advanced nuclear energy systems", Nuclear Plant Journal, Vol. 26, No. 5, Vermont Yankee, USA, 2008

[117] A. Rineiski, B. Vezzoni, D. Zhang, X. N. Chen, F. Gabrielli, M. Marchetti, "Sodium Void Effect reduction and minor actinide incineration in ESFR", In Proceedings of the Int. Conf. ANS Annual Meeting 2011, Hollywood, USA, June 26-30, 2011

[118] B. Vezzoni, F. Gabrielli, A. Rineiski, M. Marchetti, X.-N. Chen, M. Flad, W. Maschek, C.M. Boccaccini, D. Zhang, "Safety-related optimization and analyses of an innovative fast reactor concept", Sustainability, ISSN 2071-1050, 4(6):1274-1291, 2012

[119] "DANTSYS 3.0, one-, two- and three-dimensional, multigroup, discrete ordinates transport code system", RSICC Computer Code Collection, Los Alamos National Laborator, 1995

[120] R.E. Alcouffe, R.S. Baker, J.A. Dahl, S.A. Turner, R. Ward, "PARTISN: A Time-Dependent, Parallel Neutral Particle Transport Code System", Los Alamos National Laboratory, LA-UR-08-07258, 2008

[121] R. Le Tellier, L. Gastaldo, C. Suteau, D. Fournier, J.M. Ruggieri, "High-order discrete ordinate transport in hexagonal geometry: a new capability in ERANOS", Il Nuevo Cimento, 2010

[122] A. Seubert, K. Velkov, S. Langenbuch, "The time-dependent 3D discrete ordinates code TORT-TD with thermal-hydraulic feedback by ATHLET models", International Conference on the Physics of Nuclear Reactors Nuclear Power: A sustainable Resource (PHYSOR-2008), Interlaken, Switzerland, September 2008

[123] B. Roque, P. Archier, P. Bourdot, C. De-Saint-Jean, F. Gabriel, J.-M. Palau, V. Pascal, D. Schneider, G. Rimpault, J.-F. Vidal, "APOLLO3® Roadmap for a new generation of simulation tools devoted to the neutronic core calculation of the ASTRID prototype", Proceedings of FR13 (International Conference on Fast Reactors and Related Fuel Cycles: Safe Technologies and Sustainable Scenarios), Paris, France, March 4-7, 2013

APPENDICES

APPENDIX I – CORE STATE PARAMETERS TRANSFER FROM SAS-SFR TO MCNP

The treatment of five core material components, as described in section 2.2, is implemented for the coupled simulations with the MCNP code taking into account the peculiarities of its core model. Pins and hexcan structures are modelled with fixed dimensions in plane ($R_{in}^{(RE)}$, $R_{out}^{(RE)}$– inner and outer radius of the clad, $F_{s,in}^{(RE)}$ – inner sodium flow cross-section and $\varepsilon_{s,out}^{(RE)}$ – outer sodium volumetric fraction). Subassembly pitch size is also set identical for both SAS-SFR and MCNP models. All dimensions in plane correspond to average "reference expanded" (RE) conditions (parameters marked by index *(RE)*). The height of an axial node (*H*) for the fissile pin section is equal as the node height calculated in SAS-SFR. The initial reference axial node height of the fissile height of the MCNP model amounts to the "as fabricated" value. Heights of the upper axial blanket, gas plenum and pin plugs axial zones of SA are fixed as corresponding to RE conditions. For the axial zone of sodium plenum the expanded height is derived channel-wise, considering expansion of the pins upward, into the sodium plenum. Its upper boundary is defined by the lower pin plugs of the shielding pins section of the SA and is fixed in the model as corresponding to RE conditions. Node parameters for the initial reference conditions have index *(0)* in derivations below. The parameters of the SAS-SFR node for the actual expanded conditions, i.e. calculated at every iteration, are used for preparation of the MCNP input as summarizes in Table A-I.1.

Table A-I.1. Summary of SAS-SFR node data transfer for preparation of the MCNP input

SA axial zone	Node data from SAS-SFR	Node data used for preparation of MCNP input
Fissile height	M_f, $M_f^{(0)}$, T_f, M_c, T_c, $M_{s,in}$, $T_{s,in}$, H, $H^{(0)}$	(γ_f, T_f), (γ_c, T_c), $(\gamma_{s,in}, T_{s,in})$, $(\gamma_h, T_{s,in})$, $(\gamma_{s,out}, T_{s,in})$ H
Upper axial blanket Upper gas plenum Upper pin plugs	$T_{s,in}$	$(\gamma_c^{(RE)}, T_c^{(RE)})$, $(\gamma_h, T_{s,in})$, $(\gamma_{s,in}, T_{s,in})$, $(\gamma_{s,out}, T_{s,in})$ $H^{(RE)}$
Sodium plenum	$T_{s,in}$	$(\gamma_h, T_{s,in})$, $(\gamma_{s,in}, T_{s,in})$, $(\gamma_{s,out}, T_{s,in})$, $H^{(RE)}$*

* the height is derived accounting axial expansion of the fissile pin section

The PIRS interface requires the input of material densities, which are derived for different components as follows:

1. **Fuel:** Considering mass conservation of the fuel in the node the fuel density is derived as follows:

$$\gamma_f = \gamma_f^{(0)} \cdot \frac{H^{(0)}}{H},$$

where γ_f, $\gamma_f^{(0)}$ and H, $H^{(0)}$ – are fuel densities and node heights at the expanded and initial reference conditions, respectively.

The fuel density corresponding to the initial reference conditions is calculated as follows:

$$\gamma_{\mathrm{f}}^{(0)} = \frac{M_f^{(0)}}{\mathrm{H}^{(0)} \cdot \pi \cdot (R_{in}^{(RE)})^2},$$

where $M_f^{(0)}$ – fuel mass in the node (the value for expanded conditions M_f is equal to the one for the initial reference conditions $M_f^{(0)}$), $R_{in}^{(RE)}$– inner radius of the clad (consideration of "smeared" fuel density which takes whole pin inner volume) at the average reference expanded conditions.

2. **Clad:** Clad density for use in preparation of the neutron physics model is derived on basis of the given node clad mass and fixed pin dimensions, as follows:

$$\gamma_c = \frac{M_c}{\mathrm{H} \cdot \pi \cdot ((R_{out}^{(RE)})^2 - (R_{in}^{(RE)})^2)},$$

where $R_{in}^{(RE)}$, $R_{out}^{(RE)}$– inner and outer radius of the clad in the MCNP model, M_c – clad mass calculated at the actual iteration.

3. **Inner sodium:** Sodium density within hexcan is calculated using actual node inner sodium mass $M_{s,in}$ as follows:

$$\gamma_{s,in} = \frac{M_{s,in}}{H \cdot F_{s,in}^{(RE)}},$$

where $F_{s,in}^{(RE)}$– inner sodium flow cross-section in the MCNP model.

4. **Hexcan:** As soon as it is assumed that hexcan also is modelled having fixed average expanded reference dimensions in plane (which are inner and outer flat-to-flat dimensions), hexcan density is derived assuming free hexcan expansion in upward direction driven by its temperature, which is assumed identical to the inner sodium temperature, as follows:

$$\gamma_h = \gamma_{steel}^{(T)} \cdot \frac{(1+2\alpha_L^{(T)}\Delta T)}{(1+2\alpha_L^{(T^{(RE)})}\Delta T^{(RE)})},$$

where $\gamma_{steel}^{(T)}$– hexcan steel density corresponding to given temperature T, while the second term of derivation accounts radial expansion of hexcan which is not modelled explicitly;

$$\gamma_{steel}^{(T)} = \gamma_{steel}^{(T^{(room)})} \cdot \frac{1}{(1+3\alpha_L^{(T)}\Delta T)},$$

where $\gamma_{steel}^{(T^{(room)})}$ is hexcan steel density at room temperature ($T^{(room)} = 293\,K$) given by input, $\alpha_L^{(T)}$ and $\alpha_L^{(T^{(RE)})}$ – linear expansion coefficients for hexcan steel, calculated for $\Delta T = T - T^{(room)}$ and $\Delta T^{(RE)} = T^{(RE)} - T^{(room)}$ and $T^{(room)}$ – room temperature.

5. **Outer sodium:** Simple natural sodium density correlation is used assuming that outer sodium temperature is equal to the one of inner sodium, while the fraction of outer sodium corresponds to average expanded reference geometry and given by input:

$$\gamma_{s,out} = \gamma_{Na}(T_{s,in}) \cdot \varepsilon_{s,out}^{(RE)},$$

where $\varepsilon_{s,out}^{(RE)}$ – outer sodium volumetric fraction, corresponding to the RE conditions, γ_{Na} – sodium density, $T_{s,in}$. – node actual inner sodium temperature, calculated in SAS-SFR.

The last component to be described is a pin wire. Its mass is accounted for in the hexcan component via a multiplying coefficient of the hexcan density. The latter is defined as the ratio of the sum of wire and hexcan masses to the hexcan mass calculated at the average expanded reference conditions. For all values of interest an additional output printing is organized at the end of the iteration.

APPENDIX II – CORE STATE PARAMETERS TRANSFER FROM SAS-SFR TO PARCS

Calculation of macroscopic cross sections for neutron physics node in the "Sigma-zero" model requires homogenized nuclide number densities of a corresponding unit cell and their temperatures as an input. These data are available as output of the "smeared geometry" model, which allows using different axial meshes for the neutron physics and thermal hydraulics domains. The treatment of five core material components, described in section 2.2, is implemented for the coupled simulations with the PARCS code in such a way, that the input of the "smeared geometry" model consists of component-wise homogenized nuclide number densities and temperatures, given for all coupled nodes of SAS-SFR.

Homogenized node number densities, corresponding to the initial "as fabricated" cold conditions (at room temperature) are provided by PARCS input separately for 3 solid components – fuel, clad and hexcan: $\overrightarrow{\rho_f^{(a.f.)}}$, $\overrightarrow{\rho_c^{(a.f.)}}$ and $\overrightarrow{\rho_h^{(a.f.)}}$. In derivations below for calculation of the expanded number densities these values are adjusted in correspondence with the diagrid plate expansion from the "as fabricated" to the reference expanded (RE) conditions by applying the multiplier $\left(\frac{S_6^{(a.f.)}}{S_6^{(RE)}}\right)^2$, where $S_6^{(a.f.)}$, $S_6^{(RE)}$ – SA pitch in diagrid for the "as fabricated" and for reference expanded (RE) conditions, respectively. Adjusted number density uses index *(0)* in the derivations below. State parameters of the SAS-SFR node for actual "expanded" conditions, calculated at every steady state iteration and time step, are used for calculation of the corresponding node number densities as summarized in Table A-II.1.

First homogenized number densities are calculated component-wise as corresponding to the thermal-hydraulic node of SAS-SFR as follows:

1. **Fuel:** The homogenized number density of the fuel component isotope *i* (*i=1, N_f)* is derived as follows:

$$\rho_{i,f} = \rho_{i,f}^{(0)} \cdot \frac{M_f}{M_f^{(0)}} \cdot \frac{H^{(0)}}{H},$$

where $\rho_{i,f}^{(0)}$ – adjusted homogenizes number density of an isotope *i* of the fuel component at cold conditions, *H* and $H^{(0)}$ – are the expanded and cold axial node heights, M_f and $M_f^{(0)}$ – fuel mass in the node at the expanded and cold conditions, respectively.

2. **Clad:** Homogenized number density of clad component isotope (*i=1, N_c*) is derived in a similar way, as the one of the fuel component:

$$\rho_{i,c} = \rho_{i,c}^{(0)} \cdot \frac{M_c}{M_c^{(0)}} \cdot \frac{H^{(0)}}{H},$$

where $\rho_{i,c}^{(0)}$ – adjusted homogenized number density of the isotope i of the clad component at cold conditions, M_c and $M_c^{(0)}$ – clad mass in the node at the expanded and cold conditions.

3. **Inner sodium:** The sodium homogenized number density for inner hexcan volume is derived as follows:

$$\rho_{Na,in} = \frac{M_{s,in}}{H \cdot F_{s,in}^{(RE)}} \cdot \frac{N_{Avog}}{A_{Na}},$$

where $M_{s,in}$ – sodium mass in the node at the expanded conditions, $F_{s,in}^{(RE)}$ – inner sodium flow cross-section at the RE conditions, given by input for the PARCS model, N_{Avog} – Avogadro constant, A_{Na} – sodium atomic mass.

4. **Hexcan:** Homogenized number density $\rho_{i,h}$ of the isotope *i* (*i=1, N_h*) of the hexcan component at expanded conditions is derived assuming free hexcan expansion upward direction driven by its temperature, as follows:

$$\rho_{i,h} = \rho_{i,h}^{(0)} \frac{1}{(1+\alpha_L^{(T)}\Delta T)},$$

where $\rho_{i,h}^{(0)}$– adjusted homogenized number density of hexcan isotope *i* at the cold conditions, $\Delta T = T - T^{(0)}$, T and $T^{(0)}$- hexcan temperature, corresponding to the expanded and cold conditions ($T^{(0)} = 293\ K$) and $\alpha_L^{(T)}$- linear expansion coefficients for hexcan steel, calculated for heat-up ΔT.

5. **Outer sodium:** Outer sodium homogenized number density is derived on basis of simple natural sodium density correlation for steady state and pre-boiling phase, as follows (temperature of outer sodium is considered identical to the one of the inner sodium):

$$\rho_{Na,out} = \gamma_{Na}(T_{s,in}) \cdot \frac{N_{Avog}}{A_{Na}} \cdot \varepsilon_{s,out}^{(RE)},$$

where $\varepsilon_{s,out}^{(RE)}$– outer sodium volumetric fraction, corresponding to the RE conditions, γ_{Na}– sodium density, $T_{s,in}$.– actual inner sodium temperature, calculated in SAS-SFR.

After boiling onset different strategies, defined by the user, may be considered for the treatment of the outer sodium component and corresponding calculation of the number density. For every node boiling factor is calculated at every time step, as follows: $\varepsilon^{boil} = \frac{M_{s,in}}{M_{s,in}^{(0)}}$. If the boiling factor amounts to a value below the boiling criteria ε_{min}^{boil}, defined by user input, the homogenized number density of outer sodium is derived considering identical mass fraction with regard to a SS value, which amounts to ε^{boil}, calculated for inner sodium. The boiling criteria ε_{min}^{boil} may vary from 0 to 1 ($\varepsilon_{min}^{boil} = 0$ corresponds to the case, when no outer sodium boiling is considered), while the value $\varepsilon_{min}^{boil} = 0.5$ has been used for simulations of a ULOF.

The last component to be described is a pin wire. Its mass is accounted for in the hexcan component number densities given by input via multiplying the coefficient for the initial hexcan density. The latter is defined as ratio of the sum of wire and hexcan masses to the hexcan mass.

After the homogenized number densities are processed also component-wise in the "smeared geometry" model, the homogenized number density of isotope *i* in the neutron physics node is derived as a sum along all components as follows:

$\rho_i = \sum_k \rho_i^k$,

where *k = {fuel, clad, inner sodium, hexcan, outer sodium}*.

Table A-II.1. Summary of SAS-SFR node data transfer for calculation of node number densities input for "smeared geometry" model

SA axial zone	Node data from SAS-SFR	Node data provided to "smeared geometry" model
Fissile height	M_f, $M_f^{(0)}$, T_f, M_c, $M_c^{(0)}T_c$, $M_{s,in}$, $T_{s,in}$, T_h, H, $H^{(0)}$	(ρ_f, T_f), (ρ_c, T_c), $(\rho_{Na,in}, T_{s,in})$, (ρ_h, T_h), $(\rho_{Na,out}, T_{s,in})$* H
Upper axial blanket Upper gas plenum Upper pin plugs	$M_{s,in}$, $T_{s,in}$	$(\rho_c^{(RE)}, T_c^{(RE)})$, $(\rho_h^{(RE)}, T_h^{(RE)})$, $(\rho_{Na,in}, T_{s,in})$, $(\rho_{Na,out}, T_{s,in})$* $H^{(RE)}$
Sodium plenum	$T_{s,in}$	$(\rho_h^{(RE)}, T_h^{(RE)})$, $(\rho_{Na,in}, T_{s,in})$, $(\rho_{Na,out}, T_{s,in})$* $H^{(RE)}$

* Additional strategies for boiling conditions in the node

APPENDIX III – CONTROL ROD MOVEMENT TESTS WITH DOPPLER EFFECT REACTIVITY FEEDBACK

The characteristics of the calculated TOP transient cases simulating a CR insertion or withdrawal are given in Table A-III.1. For this purpose, the core is represented by 2 channels (inner and outer sub-core) using 2 cooling groups. A step-wise movement of all CRs in the outer row of control rod positions has been assumed. In accordance with the scenario, the CR absorbers are moved upward to the top of the core or downwards, connected to a pre-specified number of axial meshes. The absorber fraction in the CR has been decreased in order to get the appropriate reactivity response, corresponding to one axial mesh of the model.

Table A-III.1. Core configurations and transient parameters for test simulations of CR insertion/withdrawal

Core configuration (meshes from top)	Insertion/ Withdrawal, cm	Transient dynamic reactivity, $		Beta, pcm
		Positive	Negative	
1 mesh	7.0952	0.0860	-0.0861	249.88
2 mesh	15.2040	0.2542	-0.2544	
3 mesh	23.3128	0.5252	-0.5259	
4 mesh	31.4216	0.8985	-0.9006	

Current code capabilities allow to model control rod movement by input replacing the mixture of axial nodes representing the follower by CR absorber in case of a CR insertion, and vice versa by follower in case of a CR withdrawal.

Transient variations of the relative core power and the reactivity with time are shown in Fig. A-III.1 for different TOP transients. The dynamic reactivity value is calculated at every time step by means of the perturbation theory, available as part of the original calculation route of the PARCS code. As result of the power excursion, the change of fuel temperatures leads to a reactivity feedback due to the Doppler effect. Other reactivity effects have not been considered in these test case exercises. The core power is stabilized at a new level within 10-15 s. The total dynamic reactivity of the core approaches a value close to zero and reaches for all considered cases values below 1-5 cent within the first 20 s of the transient time.

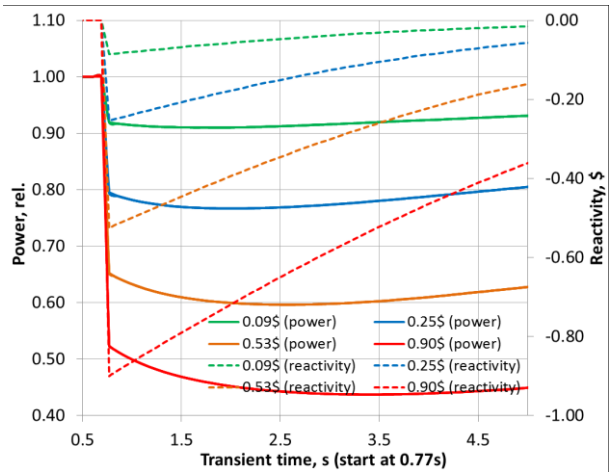

CR insertions, time of 0-5 s

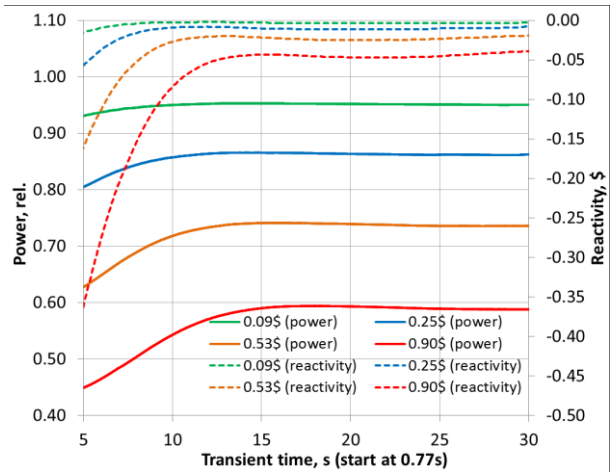

CR insertions, time 5-30 s

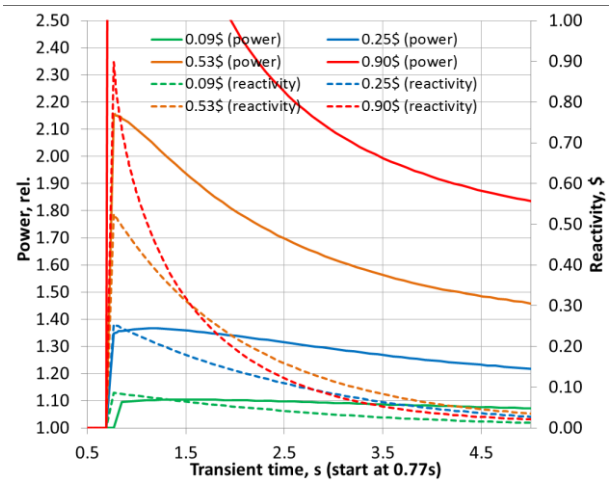

CR withdrawal, time of 0-5 s

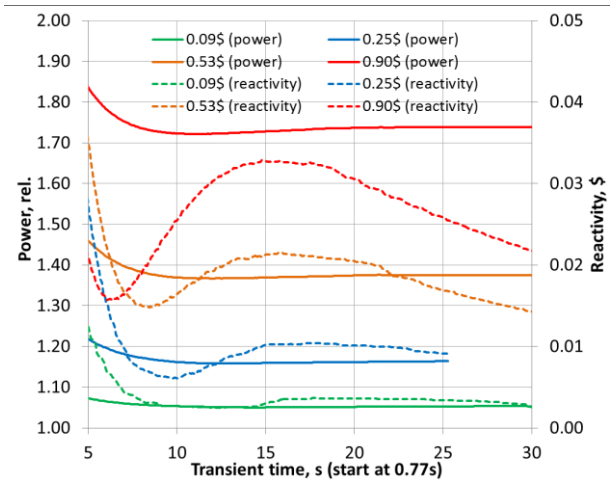

CR withdrawal, time 5-30 s

Fig. A-III.1. Transient variation of the core power and reactivity in CR movement tests

APPENDIX IV – TEMPORAL EVOLUTION OF CHARACTERISTIC CORE PARAMETERS FOR A ULOF CALCULATION WITH THE PK OPTION FOR THE 9 CG CORE CONFIGURATION

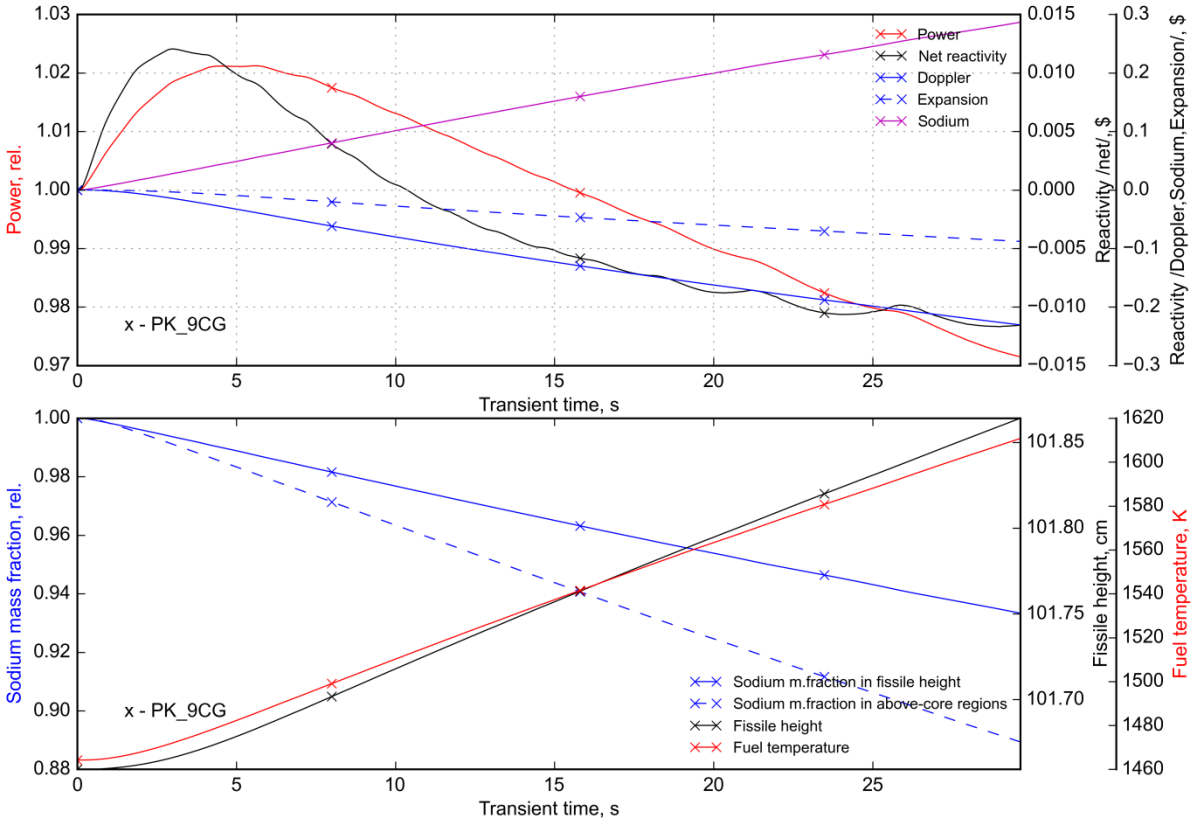

Fig. A-IV.1. Temporal evolution of normalized power, net reactivity and reactivity contributions (top) and sodium mass fraction, fissile height and fuel temperature (bottom) in a ULOF sequence before boiling onset as computed for 9 CG configuration with PK option

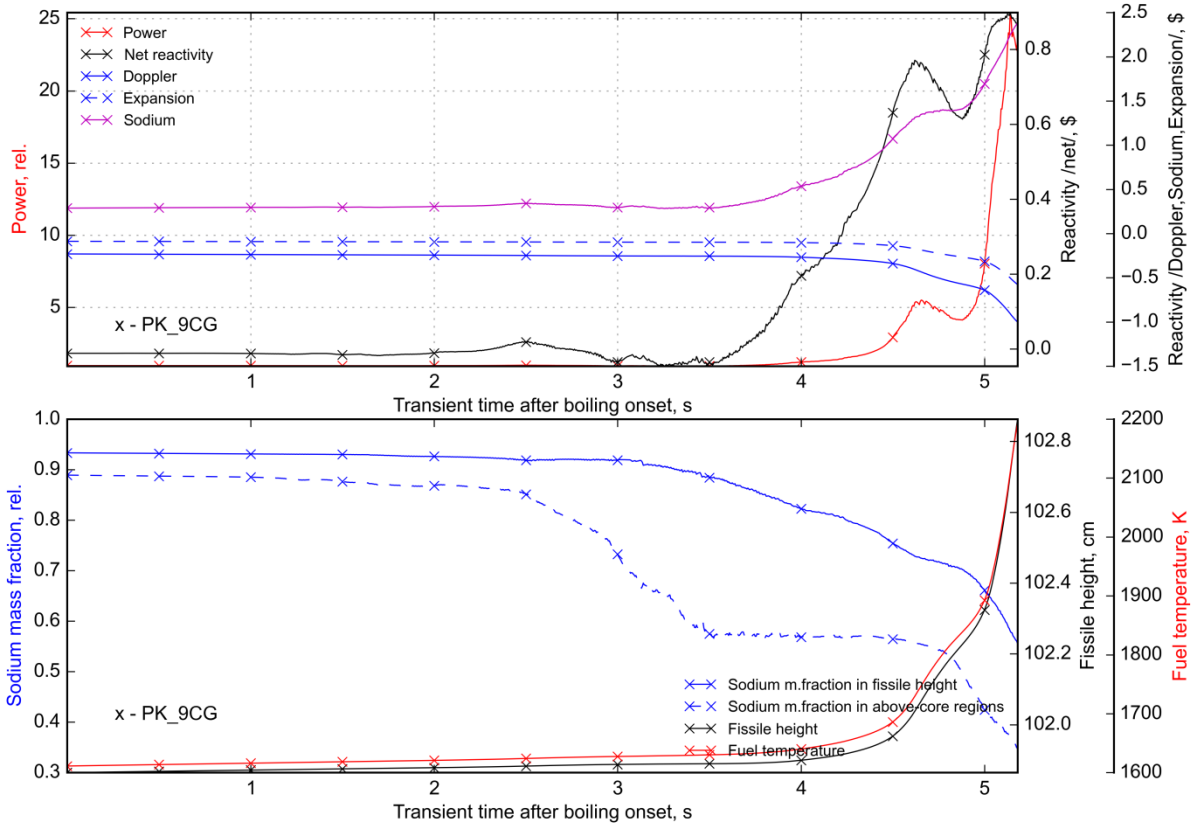

Fig. A-IV.2. Temporal evolution of power, the reactivity contributions, sodium mass fraction, fissile height and fuel temperature in a ULOF sequence before clad melting onset as computed for 9 CG configuration with PK option

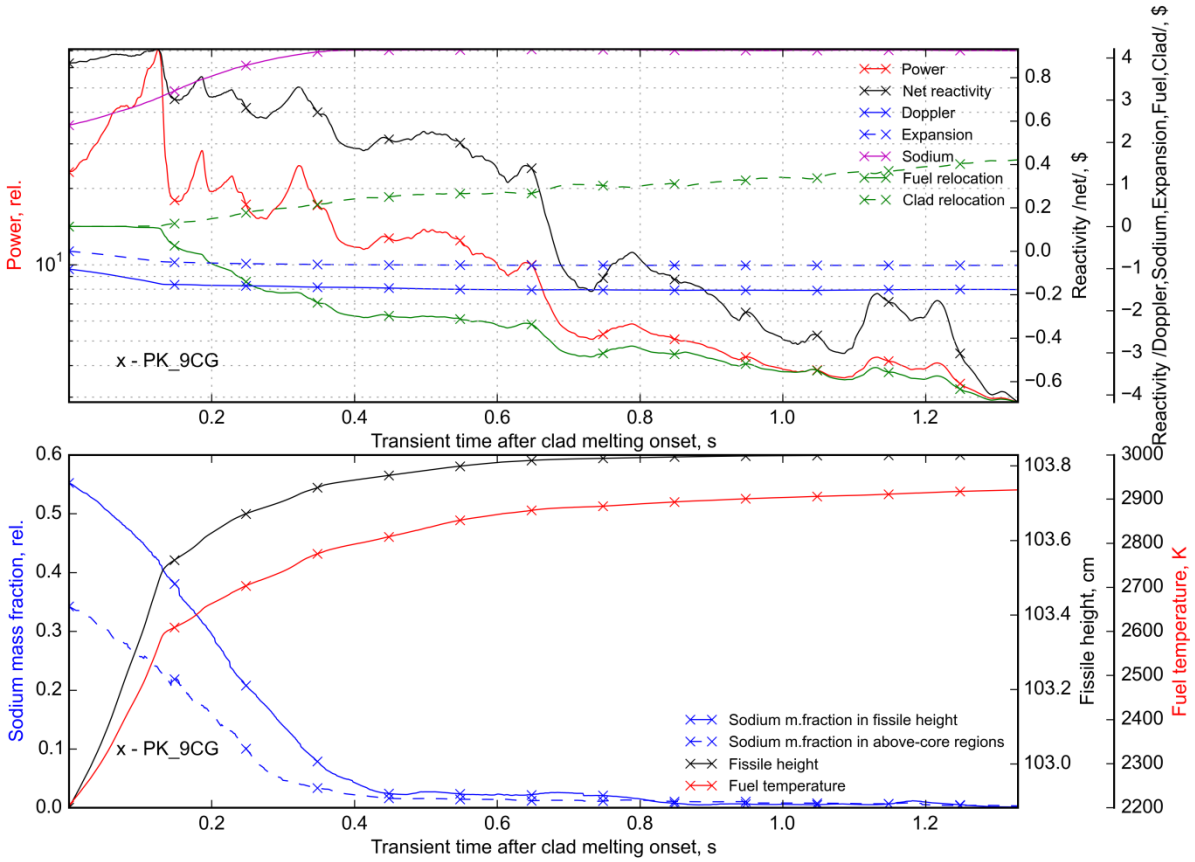

Fig. A-IV.3. Temporal evolution of power, the reactivity contributions, sodium mass fraction, fissile height and fuel temperature in a ULOF sequence after clad melting onset as computed for 9 CG configuration with PK option